ktu
1922

AUKSĖ NAVARUCKIENĖ

SYNTHESIS AND INVESTIGATION OF PROPERTIES OF VANILLIN-BASED CROSS-LINKED POLYMERS

DOCTORAL DISSERTATION

Kaunas
2023

KAUNAS UNIVERSITY OF TECHNOLOGY

AUKSĖ NAVARUCKIENĖ

SYNTHESIS AND INVESTIGATION OF PROPERTIES OF VANILLIN-BASED CROSS-LINKED POLYMERS

Doctoral dissertation
Technological Sciences, Chemical Engineering (T 005)

2023, Kaunas

Scientific Supervisor:
Prof. Dr. Jolita OSTRAUSKAITĖ (Kaunas University of Technology, Technological Sciences, Chemical Engineering, T 005).

Edited by: English language editor Dovilė Blaudžiūnienė (Publishing House *Technologija*), Lithuanian language editor Rozita Znamenskaitė (Publishing House *Technologija*)

Dissertation Defense Board of Chemical Engineering Science Field:
Prof. Dr. Raimundas ŠIAUČIŪNAS (Kaunas University of Technology, Technological Sciences, Chemical Engineering, T 005) – **chairperson**;
Assoc. Prof. Dr. Joana BENDORAITIENĖ (Kaunas University of Technology, Technological Sciences, Chemical Engineering, T 005);
Assoc. Prof. Dr. Vaidas KLIMKEVIČIUS (Vilnius University, Natural Sciences, Chemistry, N 003);
Prof. Dr. Viktorija PLAVAN (Kyiv National University of Technology and Design, Ukraine, Technological Sciences, Chemical Engineering, T 005);
Prof. Dr. Virgilijus VALEIKA (Kaunas University of Technology, Technological Sciences, Chemical Engineering, T 005).

The official defense of the dissertation will be held at 1 p.m. on 15 September, 2023 at the public meeting of the Dissertation Defense Board of Chemical Engineering Science Field in Rectorate Hall at Kaunas University of Technology.

Address: K. Donelaičio g. 73-402, Kaunas, LT-44249, Lithuania.
Phone: (+370) 608 28 527; email doktorantura@ktu.lt

The doctoral dissertation was sent out on 14 August, 2023.
The doctoral dissertation is available on the internet at http://ktu.edu and at the library of Kaunas University of Technology (K. Donelaičio 20, Kaunas, LT-44239, Lithuania).

KAUNO TECHNOLOGIJOS UNIVERSITETAS

AUKSĖ NAVARUCKIENĖ

TINKLINIŲ POLIMERŲ SU VANILINO FRAGMENTAIS SINTEZĖ IR SAVYBIŲ TYRIMAS

2023, Kaunas

Mokslinė vadovė:
prof. dr. Jolita OSTRAUSKAITĖ (Kauno technologijos universitetas, technologijos mokslai, chemijos inžinerija, T 005).

Redagavo: anglų kalbos redaktorė Dovilė Blaudžiūnienė (leidykla „Technologija"), lietuvių kalbos redaktorė Rozita Znamenskaitė (leidykla „Technologija")

Chemijos inžinerijos mokslo krypties disertacijos gynimo taryba:
prof. dr. Raimundas ŠIAUČIŪNAS (Kauno technologijos universitetas, technologijos mokslai, chemijos inžinerija, T 005) – **pirmininkas**;
doc. dr. Joana BENDORAITIENĖ (Kauno technologijos universitetas, technologijos mokslai, chemijos inžinerija, T 005);
doc. dr. Vaidas KLIMKEVIČIUS (Vilniaus universitetas, gamtos mokslai, chemija, N 003);
prof. dr. Viktorija PLAVAN (Kijevo nacionalinis technologijų ir dizaino universitetas, Ukraina, technologijos mokslai, chemijos inžinerija, T 005);
prof. dr. Virgilijus VALEIKA (Kauno technologijos universitetas, technologijos mokslai, chemijos inžinerija, T 005).

Disertacija bus ginama viešame Chemijos inžinerijos mokslo krypties disertacijos gynimo tarybos posėdyje 2023 m. rugsėjo 15 d., 13 val., Kauno technologijos universiteto Rektorato salėje.

Adresas: K. Donelaičio g. 73-402, Kaunas, LT-44249, Lietuva.
Tel. (+370) 608 28 527; el. paštas doktorantura@ktu.lt

Disertacija išsiųsta 2023 m. rugpjūčio 14 d.
Su disertacija galima susipažinti interneto svetainėje http://ktu.edu ir Kauno technologijos universiteto bibliotekoje (K. Donelaičio g. 20, Kaunas, LT-44239).

Contents

LIST OF ABBREVIATIONS

AESO – acrylated epoxidized soybean oil
BAPO – phenylbis(2,4,6-trimethylbenzoyl)phosphine oxide
BDT – 1.3-benzenedithiol
BRC – biorenewable carbon
C13-MA – tridecyl methacrylate
DCM – dichloromethane
DLW – direct laser writing
DMTA – dynamical mechanical thermal analysis
DSC – differential scanning calorimetry
G' – storage modulus
GDMK – glycerol dimethacrylate
PDMS – polydimethylsiloxane
PET – polyethylene terephthalate
PETMP – pentaerythritol tetrakis(3-mercaptopropionate)
SLA – stereolithography
TASHFF – triarylsulfonium hexafluorophosphate salts
$T_{dec-10\%}$ – temperature of 10% weight loss
T_g – glass transition temperature
TGA – thermogravimetrical analysis
t_{gel} – gel point
THF – tetrahydrofurane
TPO – diphenyl(2,4,6-trimethylbenzoyl)phosphine oxide
TPOL – ethyl(2,4,6-trimethylbenzoyl)phenylphosphinate
UV/Vis – ultraviolet/visible
UVB – 2,5-bis(5-tert-butyl-2-benzoxazolyl)thiophene
VD – vanillin diacrylate
VDGE – vanillin alcohol diglycidyl ether
VDM – vanillin dimethacrylate
VHDM – vanillin hydroxypropane dimethacrylate
Vis – visible
μTM – microtransfer molding

1. INTRODUCTION

Substitution of petroleum-derived materials with plant-based materials in polymer synthesis is beneficial due to their low toxicity, reduced dependence on finite fossil resources, and lower greenhouse gas emissions [1]. Natural compounds can be used directly or after chemical modification for the synthesis of polymers [2]. The main resource of bio-based materials is plants as they can produce rapid accumulation of biomass with minimal efforts [3]. Bio-based polymers can replicate mechanical and thermal characteristics of petroleum-based polymers and also add new features, such as antimicrobial activity, biodegradability or shape memory properties. Vanillin is one of a few bio-based and aromatic compounds that are industrially available. In recent years, vanillin and its derivatives attracted a huge interest of scientific community as valuable source of monomers for polymer synthesis [4]. Vanillin-based polymers were obtained by thermal- and photopolymerization [5,6]. However, there are no examples of vanillin-based polymers in dual curing systems.

Dual curing is a process, which combines two different polymerization reactions occuring simultaneously or sequentially. As a result, polymers with unique properties are obtained due to the formation of interpenetrating or semi-interpenetrating networks [7]. The desired properties of synthesized polymers can be easily manipulated by changing the dominant reaction. Both, thermal and photopolymerizations can be used in the dual curing process. However, photopolymerization has huge advantages against thermal polymerization [8]. It is a fast and environmentally friendly curing process, which only needs seconds or minutes to fully polymerize resin, it can be performed at room temperature or even lower temperatures without the need of heating and can be used to cure only the selected areas of the resin [9].

Four commercially available vanillin derivatives, vanillin dimethacrylate, vanillin diacrylate, vanillin hydroxypropane dimethacrylate, and vanillin alcohol diglycidyl ether, were chosen for the synthesis of novel bio-based photopolymers. During this study six series of vanillin-based polymers and one separate resin were synthesized and the influence of vanillin derivative, comonomers and photoinitiator to the properties of the resulting polymers was investigated. The experimental results have been presented in seven publications.

The aim of the work was to develop new vanillin-based photocross-linked polymers for microtransfer molding and optical 3D printing technologies.

The tasks proposed for the achievement of the above-stated aim were as follows:
1. To design vanillin-based photocurable resins and investigate the influence of resin composition on photocuring process and rheological characteristics.
2. To synthesize, new vanillin-based photocross-linked polymers, investigate the influence of composition to the properties of polymers;

3. To investigate the influence of resin composition and process conditions on photocuring kinetics and the properties of resulted polymers in dual-curing systems;
4. To test the suitability of the photocurable vanillin-based resins for microtransfer molding and optical 3D printing.

Scientific novelty
1. Novel vanillin-based photocross-linked polymers have been synthesized; for the first time, the influence of the photoinitiator on the photocuring kinetics and the properties of the resulting polymers was investigated in vanillin-based photocurable systems.
2. For the first time, novel vanillin-based resins were tested in dual curing systems and their photocuring kinetics and the properties of the resulting polymers were investigated.
3. For the first time, vanillin derivatives were used for the synthesis of shape-memory polymers.

Practical value of the work
1. Vanillin diacrylate-based resin and vanillin diacrylate-, tridecyl methacrylate- and 1,3-benzenedithiol-based resins are suitable for application in microtransfer molding.
2. Selected vanillin dimethacrylate-, acrylated epoxidized soybean oil- and pentaerythritol tetrakis(3-mercaptopropionate)-based resin is suitable for application in optical 3D printing technologies.

The main statements of doctoral thesis:
1. Vanillin-based resins are suitable for the synthesis of shape-memory polymers.
2. Vanillin-based photocurable resins are suitable for application in microtransfer molding and optical 3D printing.

Contribution of the author

The author has designed and characterized six different series of vanillin-based photopolymers and one separate resin, investigated photocuring kinetics of the designed resins, thermal, mechanical and shape-memory properties of the resulting polymers, and prepared manuscripts. Prof. Dr. Jolita Ostrauskaitė (Kaunas University of Technology) contributed to conceptualising the initial ideas, advising with the synthesis and characterization of vanillin-based polymers and contributed to the editing of all seven papers. Dr. Sigita Graužėlienė (née Kašėtaitė) (Kaunas University of Technology) advised with regards to the synthesis and characterization of vanillin-based polymers and contributed to the editing of articles. Prof. Dr. Mangirdas Malinauskas (Laser Research Center, Vilnius University) advised with the direct laser writing and microtransfer molding and contributed to the editing of the papers. Dr. Sima Rekštytė and Edvinas Skliutas (Laser Research Center, Vilnius University) performed direct laser writing and microtransfer molding of the selected

resins, analyzed molded structures and contributed to drafting the manuscript of the article. Jurga Jeršovaitė (Laser Research Center, Vilnius University) performed microtransfer molding of the selected resins. Dr. Vita Raudonienė and Dr. Danguolė Bridžiuvienė (Biodeterioration Research Laboratory, Nature Research Center) performed antimicrobial testing of the selected polymer samples. Dr. Egidija Rainosalo (Centria University of Applied Sciences, Finland) conceived and designed the thermomechanical experiments and analyzed the data. Justinas Jaras, Viltė Šereikaitė and Greta Motiekaitytė (Kaunas University of Technology) contributed to the experimental part. Dr. Kristina Kantminienė (Kaunas University of Technology) contributed to the editing of the article. Dimitra Ladika and Dr. David Gray (Institute of Electronic Structure and Laser, Foundation for Research and Technology, Greece) contributed to the investigation of two-beam initiation threshold experiment and writing original draft preparation of manuscript of article. Vaidas Talačka ("AmeraLabs") determined printing parameters for the selected resin and performed digital light processing 3D printing of the selected resin.

List of scientific publications on the topic of the dissertation

1. <u>Auksė Navaruckienė</u>, Sigita Kašėtaitė, Jolita Ostrauskaitė. Vanillin-based thiol-ene systems as photoresins for optical 3D printing. *Rapid prototyping journal*. **2020**, *26* (2), 402-408. JIF: 3.095.
2. <u>Auksė Navaruckienė</u>, Edvinas Skliutas, Sigita Kašėtaite, Sima Rekštytė, Vita Raudonienė, Danguolė Bridžiuvienė, Mangirdas Malinauskas, Jolita Ostrauskaitė. Vanillin acrylate-based resins for optical 3D printing. *Polymers*. **2020**, *12* (2), 397. JIF: 4.329.
3. <u>Auksė Navaruckienė</u>, Danguolė Bridžiuvienė, Vita Raudonienė, Egidija Rainosalo, Jolita Ostrauskaitė. Influence of vanillin acrylate-based resin composition on resin photocuring kinetics and antimicrobial properties of the resulting polymers. *Materials*. **2021**, *14* (3), 653. JIF: 3.748.
4. <u>Auksė Navaruckienė</u>, Danguolė Bridžiuvienė, Vita Raudonienė, Egidija Rainosalo, Jolita Ostrauskaitė. Vanillin acrylate-based thermo-responsive shape memory antimicrobial photopolymers. *Express polymer letters*. **2022**, *16* (3), 279-295. JIF: 3.952.
5. Justinas Jaras, <u>Auksė Navaruckienė</u>, Edvinas Skliutas, Jurga Jeršovaitė, Mangirdas Malinauskas, Jolita Ostrauskaitė. Thermo-responsive shape memory vanillin-based photopolymers for microtransfer molding. *Polymers*. **2022**, *14* (12), 2460. JIF: 4.967.
6. Viltė Šereikaitė, <u>Auksė Navaruckienė</u>, Justinas Jaras, Edvinas Skliutas, Dimitra Ladika, David Gray, Mangirdas Malinauskas, Vaidas Talačka, Jolita Ostrauskaitė. Functionalized soybean oil- and vanillin-based dual cure photopolymerizable system for light-based 3D structuring. *Polymers*. **2022**, 14, 5361. JIF: 4.967.
7. Greta Motiekaitytė, <u>Auksė Navaruckienė</u>, Vita Raudonienė, Danguolė Bridžiuvienė, Justinas Jaras, Kristina Kantminienė, Jolita Ostrauskaitė. Antimicrobial dual-cured photopolymers of vanillin alcohol diglycidyl

ether and glycerol dimethacrylate. *Journal of applied polymer science.* **2023**, *140* (2), e53289. JIF: 3.057.

1.1. Vanillin-based monomers

Vanillin is the main constituent of vanilla (*Vanilla planifolia*), which is one of the most popular natural flavor commonly used in food, beverage and cosmetic industries [10]. About 20% of vanillin is produced from natural sources. It can be extracted directly from plants or produced by chemical modification of lignin [11]. Vanillin, produced by chemical modification of lignin is considered as natural, making lignin the main source of the plant-derived vanillin [12]. Recently vanillin and its derivatives had been used in polymer synthesis due to their aromatic structure and their hydroxyl, phenol and aldehyde groups, which can be modified to obtain new monomers for polymerization [13, 14, 15].

Various attemts to synthesize vanillin-based acrylates were reported in the literature. Wool *et al.* synthesized vanillin methacrylate by the reaction of vanillin and methacrylic anhydride. The reaction was carried out under argon atmosphere at 50°C for 24 h. 4-dimethylaminopyridine was used as a catalyst. The obtained vanillin methacrylate was later used in the synthesis of bio-based thermoset [16]. Abdelaty *et al.* synthesized vanillin acrylate monomer in a one-step reaction of vanillin and acryloyl chloride in the presence of triethylamine. The obtained vanillin acrylate was used to synthesize thermo-responsive functional copolymers using comonomer N-isopropylacrylamide [17]. Mabry *et al.* determined that chemical reduction of vanillin can result in vanillyl alcohol, which can react with methacrylic anhydride and form vanillin dimethacrylate (VDM), which was stated as suitable monomer for polymer synthesis [18].

Vanillin was also successfully used in the synthesis of epoxy monomers. Diglycidyl ether of methoxyhydroquinone was synthesized by using vanillic acid, which is obtained by chemically modifying vanillin. Vanillic acid was mixed with benzyltriethylammonium chloride and epichlorhydrin and stirred for 1 h at 75°C. Next, NaOH was added and mixture was stirred at 25°C for 1 h. As a result, diglycidyl ether of methoxyhydroquinone was obtained and was reported as suitable monomer for the synthesis of thermosets [19]. Sangermano *et al.* synthesized vanillin alcohol diglycidyl ether (VDGE) by two step reaction using vanillyl alcohol, which was obtained by chemical reduction of vanillin. Vanillyl alcohol was mixed with benzyltriethylammonium chloride and epichlorhydrin and the reaction was carried out at 30°C for 4 h. In the second step, the mixture was cooled down to 15°C and NaOH was added. Mixture was stirred at 15°C for 12 h. The resulted VDGE monomer was reported as a promising monomer for cationic photopolymerization [5]. Structures of monomer which can be obtained by the modification of vanillin are presented in Figure 1. These examples show that vanillin is a promising material for monomer, and later, polymer synthesis.
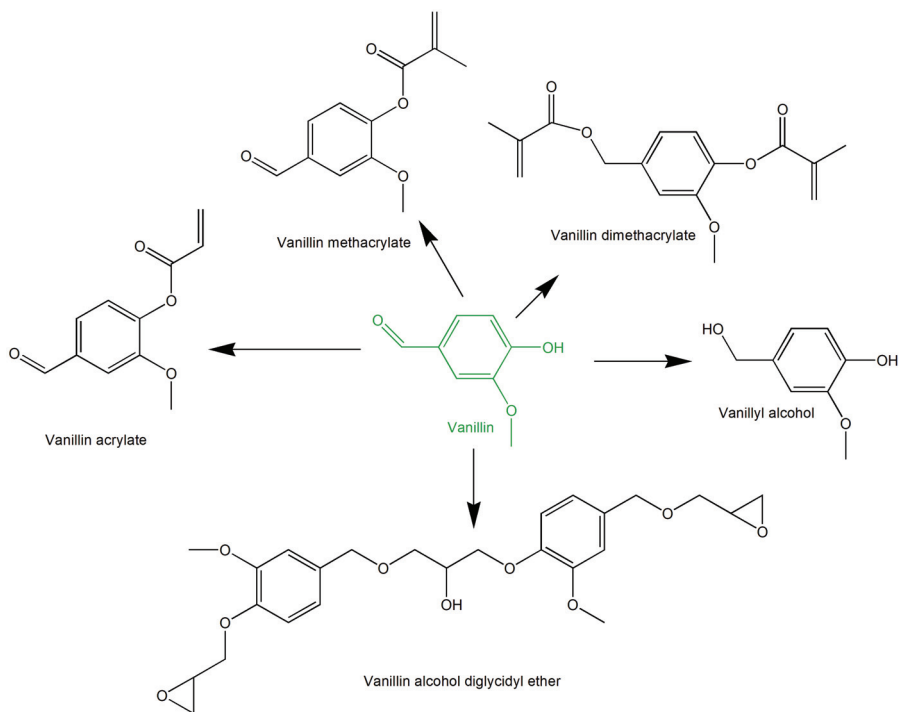
Figure 1. Structures of monomer which can be obtained by the chemical modification of vanillin

1.2. Vanillin-based polymers, their properties and application

In the recent years, there have been various attempts to use vanillin and its derivatives in polymer synthesis [14]. Thermal polymerization has been successfully used for polymer production from vanillin derivatives. VDM-based polymer was synthesized using thermal polymerization by curing resin at 90°C and 130°C for 2 h. The resulted cross-linked polymers showed high glass transition temperature (T_g) of 90.5°C and were considered as promising candidates for polymer composite production [20]. Dai *et al.* used vanillin-based monomer in thermal polymerization to synthesize benzocyclobutane-based polymer. This polymer showed high thermal stability with temperature at 10% weight loss ($T_{dec-10\%}$) higher than 400°C, good mechanical properties and low water absorption [21].

Vanillin-based polymers were also obtained by photopolymerization. Liguori *et al.* successfully designed photocurable resins using methacrylated vanillin and ethylenediamine. Homogenous and uniform cross-linked polymer films with high thermal stability and self healing properties were obtained by UV photocuring of these resins [22]. Abdelaty used free-radical photopolymerization of vanillin acrylates with N-isopropylacrylamide and maleimide to synthesize temperature-responsive polymers. These polymers are considered to be used as biosensor hydrogels for drug-delivery [23]. Xu *et al.* designed photocurable imine-containing methacrylate resins using vanillin methacrylate and di- or

trifunctional amines. The resulted polymers showed vitrimeric properties with chemical recyclability and thermal reprocessability [24].

Various literature sources have reported vanillin and its derivatives as antimicrobial materials. Salmi-Mani *et al.* had developed antimicrobial polyethylene terepthalate (PET) polymer by grafting *N*-(4-hydroxy-3-methoxybenzyl) acrylamide monomer on the surface of the PET. Newly developed polymer demonstrated inhibition against gram-positive strains with a reduction up to 97% [25]. Gonz´alez-Ceballos *et al.* had developed metal-free antimicrobial polymer based on commercially available acrylic monomers with covalently linked vanillin derivatives. The resulted polymers showed inhibition against *Escherichia coli*, *Staphylococcus aureus*, and *Listeria monocytogenes* with reduction up to 99.95%, 99.96%, and 99.02%, respectively. This polymer was tested in the food industry as a package material and was reported to increase the shelf life of a packed meat products by 50% [26].

Vanillin-based epoxy resins were reported as potential candidates to replace vinyl ester-based resins due to their aromatic structure [16]. The incorporation of vanillin derivatives into the resins can increase mechanical strength, thermal stability and resistence of the resulting polymers [27]. Various resourses have reported the use of vanillin derivatives for broad applications such as adhesive, plastic, architecture, food industry, etc.

Vanillin-based vitrimer with self-healing ability was sucessfully synthesized by imidization of dialdehyde monomer. The research showed that mechanical properties of healed sample were restored to 74.5% of the original sample after 1 h healing. These properties are very important for the reprocessability of vanillin-based polymers [28]. Other literature source reported that epoxy vitrimer was synthesized from vanillin and isophorone diamine. It showed high thermal stability and excellent tensile strength and was degradable in an isophorone diamine solution. These properties showed that vanillin-based vitrimers can be easily recycled and used to synthesize new vitrimers [29].

Magnetic microspheres were synthesized via suspension polymerization using vanillin methacrylate and methacrylated Fe_3O_4 nanoparticles and were used as an adsorbent for the removal of pollutants from the wastewater [30]. Another, temperature and pH responsive smart materials were synthesized using vanillin derivatives and showed great potential application as biosensor hydrogels [31]. Various divanillin- and *o*-vanillin-based polymers exhibited good fluorescence effect making them suitable candidates for the production of electro-optic devices. It was reported that halogen free vanillin-based polymers were synthesized and applied as flame retarding materials [4]. Vanillin-based polymers were also applied in biomedical and aerospace industries [27].

In summary, vanillin-based polymers exhibit a wide range of unique properties and their application areas are unlimited. However, there is still a lack of information about vanillin-based cross-linked polymers, their use in dual curing systems and application in high-tech. Due to this, vanillin-based photocross-linked polymers were synthesized using a dual-curing technique and applied in optical 3D printing and microtransfer molding techniques in this work.

### 1.3. Photopolymerization mechanisms used in this study

In this study, different photopolymerization mechanisms were used and compared as well as combined in dual-curing systems (Figure 2). Free-radical photopolymerization is relatively insensitive to impurities and can be run at room temperature or below [8]. It is a rapid process that occurs in a matter of minutes or seconds. The main disadvantage of free radical photopolymerization is the poor control of molecular weight, as well as oxygen inhibition [32]. In this work, free-radical photopolymerization was used to polymerize acrylate monomers. When only one acrylate monomer was used, acrylate homopolymerization took place. However, when two different acrylate monomers were used, homopolymerization of each monomer and copolymerization of two acrylate monomers can take place at the same time.

Thiol-Michael potopolymerization, which is a variant of thiol-ene photopolymerization, can occur when an acrylate monomer reacts with a thiol comonomer (Figure 2). The main difference between these two reactions is that during thiol-ene polymerization thiol reacts with electron-rich alkene (vinyl group), while during thiol-Michael photopolymerization thiol reacts with the electron deficient alkene (acrylate functional group) [33]. Both, thiol-ene and thiol-Michael photopolymerizations are light-activated reactions which proceed rapidly with no side products [34]. The main advantage of these photopolymerizations is that there is no inhibition of oxygen [35].

Cationic photopolymerization was used in the last publication of this study. Vanillin alcohol diglycidyl ether was chosen as monomer for this reaction. The main advantages of this polymerization is high reaction rate, which can be achieved at high and low temperatures and it is not inhibited by oxygen [36]. However, high reactivity leads to undesired side reactions which results in high branching and lower molecular weight [37].

Dual-curing process was used to combine free-radical photopolymerization with thiol-ene (thiol-Michael) and cationic polymerization simultaneously or sequentially. This allows developing the materials with unique thermal and mechanical properties, due to the formation of interpenetrating or semi-interpenetrating polymer networks [38]. The desired properties of synthesized polymers can be easily tuned by changing the dominant reaction [7]. In this study, resins with off-stoichiometric acrylate:thiol content were formulated to obtain dual-curing systems in which free-radical and thiol-ene (thiol-Michael) polymerization mechanisms were combined.

Thiol-ene
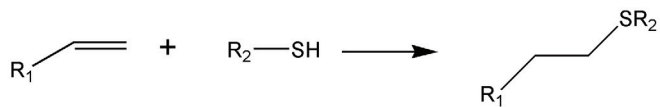
Thiol-Michael
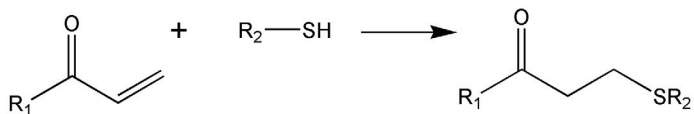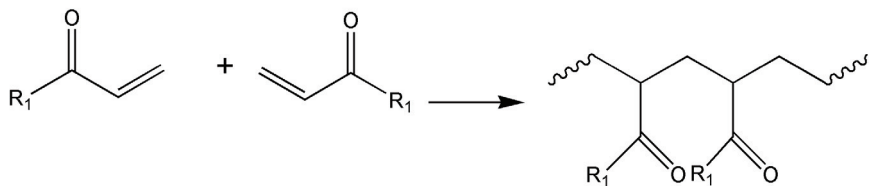
Free-radical

Cationic
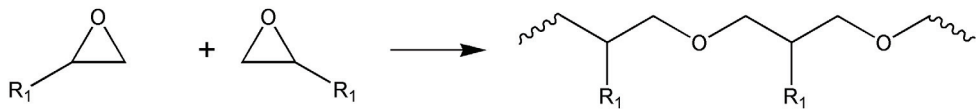
Figure 2. Simplified schemes of thiol-ene, thiol-Michael, free-radical and cationic polymerization

2. REVIEW OF ARTICLES

2.1. Investigation of vanillin-based thiol-ene systems and influence of resin composition on the photocuring kinetics

This chapter is based on published work: *A. Navaruckienė, S. Kašėtaitė, J. Ostrauskaitė. Vanillin-based thiol-ene systems as photoresins for optical 3D printing. Rapid prototyping journal. 2020, 26 (2), 402-408* [39]. *JIF: 3.095. Input: 0.334.*

The aim of this study was to design new bio-based photopolymers using vanillin derivatives and investigate their properties. Vanillin diacrylate (VD) and vanillin dimethacrylate (VDM) were used as main starting materials for the development of new bio-based polymers and 1.3-benzenedithiol (BDT) was used as a comonomer. Two photoinitiators, ethyl(2,4,6-trimethylbenzoyl)phenylphosphinate (TPOL) and diphenyl(2,4,6-trimethylbenzoyl)phosphine oxide (TPO) were used in different quantities in order to determine the influence of photoinitiator and its concentration on polymer properties. Fourteen compositions were designed to determine the influence of solvent and vanillin derivative on photocuring kinetics of the resins (Table 1). Codes **A1**–**A14** used in this chapter correspond to the codes **C1**–**C14** in the published article. The chemical structures of used materials are presented in Figure 3.
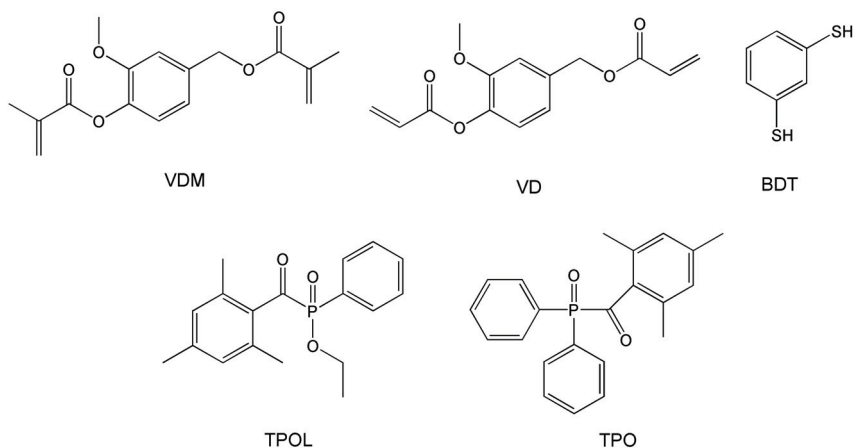
Figure 3. Structures of vanillin dimethacrylate (VDM), vanillin diacrylate (VD), 1,3-benzenedithiol (BDT), ethyl(2,4,6-trimethylbenzoyl)phenylphosphinate (TPOL), and diphenyl(2,4,6-trimethylbenzoyl)phosphine oxide (TPO)

Table 1. Composition of the resins **A1–A14**

Resin	Vanillin derivative	Amount of vanillin derivative, mol	Amount of BDT, mol	Photoinitiator	Amount of photoinitiator, mol.%	Solvent
A1	VDM	1	1	TPOL	1	DCM
A2	VDM	1	1	TPO	1	DCM
A3	VD	1	1	TPOL	1	-
A4	VD	1	1	TPO	1	-
A5	VDM	1	1	TPOL	3	DCM
A6	VD	1	1	TPOL	3	-
A7	VD	1	1	TPOL	3	DCM
A8	VDM	1	1	TPO	3	DCM
A9	VD	1	1	TPO	3	-
A10	VD	1	1	TPO	3	DCM
A11	VDM	1	1	TPOL	5	DCM
A12	VDM	1	1	TPO	5	DCM
A13	VD	1	1	TPOL	5	-
A14	VD	1	1	TPO	5	-

All collected data presented in this dissertation were statistically analyzed using ANOVA for the Microsoft Excel programme. All the experiments were performed five times and the results were assumed as the average values ± standard deviation as described in published articles.

Real-time photorheometry was used to investigate the photocuring kinetics of vanillin-based systems. The composition of the resins had significant influence on photocuring kinetics. The values of storage modulus (G') and gel point (t_{gel}) of the vanillin-based resins are presented in Figure 4. It was determined that more rigid polymers were obtained when VD was used instead of VDM as the storage modulus was increased from 0.73 (**A5**) to 0.81 (**A7**) MPa. The more rigid polymers were obtained from VD-based resins **A4** (20.2 MPa) in comparison to **A3** (17.8 MPa) when TPO was used as photoinitiator instead of TPOL due to the higher reactivity of TPO compared to TPOL [40]. The increased amount of photoinitiator led to the direct reduction of G' values and the reduced rigidity of polymer (series of **A3** (17.80 MPa), **A6** (9.92 MPa) and **A13** (1.96 MPa)). However, by increasing the amount of photoinitiator from 1 mol.% to 3 mol.% the gel point can be reduced up to 8 s indicating the faster photopolymerization process, which is an important parameter for the production of polymers.

After taking all of this into consideration, polymers **A5** and **A6** were selected for further investigation.
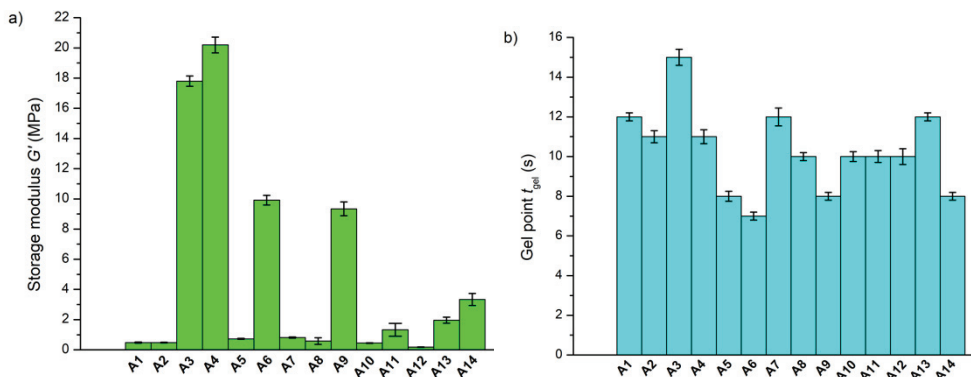
Figure 4. Storage modulus (a) and gel point (b) values of compositions **A1**–**A14**

The cross-linked structure of vanillin-based polymers was confirmed by FT-IR spectroscopy and the Soxhlet extraction. The higher values of insoluble fraction were obtained by VD-based polymer **A6** (92%) in comparison to polymer **A5** (87%) due to the solvent acting as chain transfer agent.

Differential scaning calorimetry (DSC) and thermogravimetrical analysis (TGA) were used to determine the thermal characteristics of polymers. The glass transition temperature (T_g) was very similar for both polymers **A5** (T_g = -4°C) and **A6** (T_g = -5°C), however, the temperature at 10% weight loss ($T_{dec-10\%}$) was different. Polymer **A6** showed higher thermal stability ($T_{dec-10\%}$ = 270°C) compared to polymer **A5** ($T_{dec-10\%}$ = 250°C).

2.2. Synthesis and investigation of vanillin acrylate-based polymers by free-radical photopolymerization

This chapter is based on published work: *A. Navaruckienė, E. Skliutas, S. Kašėtaite, S. Rekštytė, V. Raudonienė, D. Bridžiuvienė, M. Malinauskas, J. Ostrauskaitė. Vanillin acrylate-based resins for optical 3D printing. Polymers. 2020, 12 (2), 397* [41]. *JIF: 4.967. Input: 0.125.*

Vanillin derivatives showed promising results in photocurable systems with comonomer BDT as described in chapter 2.1, however the systems without BDT were not investigated. Vanillin derivatives were chosen as main starting materials for this study without comonomers in order to investigate the influence of vanillin acrylate, solvent and the quantity of the photoinitiator on the properties of the resulting polymers and to test the most promising composition in direct laser writing (DLW) and microtransfer molding (μTM) techniques. Photocross-linked polymers were prepared by radical photopolymerization of VD or VDM, using different amounts of TPOL as photoinitiator (Figure 2). The compositions of the resins are presented in Table 2. Codes **B1**–**B9** used in this chapter correspond to the codes **C1**–**C9** in the published article. Mechanical and rheological characteristics of the designed resins were compared to commercially available resins for optical 3D

printing PR48 and FormLabs Clear FL6PCL02 in order to check their suitability for optical 3D printing.

Table 2. Composition of the resins **B1–B9**

Resin	Vanillin derivative	Amount of vanillin derivative, mol	Solvent	Amount of photoinitiator TPOL, mol.%
B1	VD	1	-	1
B2	VD	1	DCM	1
B3	VDM	1	DCM	1
B4	VD	1	-	3
B5	VD	1	DCM	3
B6	VDM	1	DCM	3
B7	VD	1	-	5
B8	VD	1	DCM	5
B9	VDM	1	DCM	5

The values of G' and t_{gel} of the resins **B1**–**B9** are presented in Figure 5. The fastest photocuring was demonstrated by resins containing 3 mol.% of TPOL and the resulted polymers were the most rigid. The only exception is polymer **B5** ($G' = 11.3$ MPa), the rigidity of which was reduced by the use of DCM in the composition. The photocuring rate of all VD-based resins was lower in comparison to corresponding VDM-based resins. The reason for that is a darker color of VD in comparison to VDM causing the longer photocuring process as light needs more time to reach and cure deeper layers of the resins. Resins **B4**–**B6**, prepared with 3 mol.% of TPOL, were selected as the most promising ones for further investigation.

To determine if these resins are suitable for optical 3D printing, their rheological characteristics were compared to the commercially available petroleum-based resins PR48 and FormLabs Clear FL6PCL02. The photocuring rate of resins **B4** and **B6** was the same or slightly higher than that of commercial resins, the only exception was resin **B5**, the photocuring rate of which was two times lower than that of commercial resins. As for the rigidity, polymers **B4** and **B6** (18.10 and 18.20 MPa respectively) were more rigid than that of Formlabs Clear FL6PCL02 (15.20 MPa), but less rigid than that of PR48 (21.40 MPa).
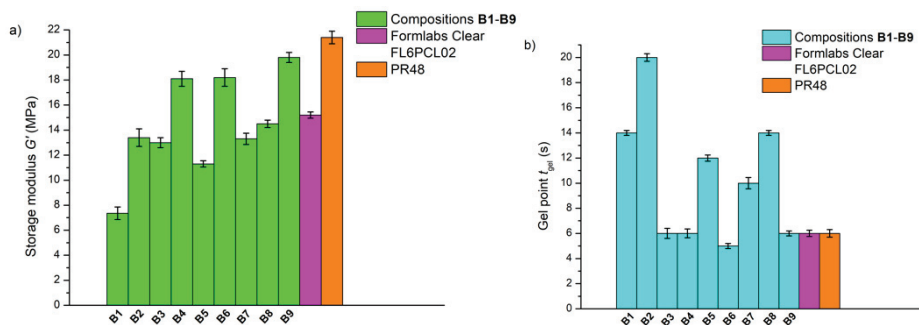
Figure 5. Storage modulus (a) and gel point (b) values of compositions **B1**–**B9**, PR48 and Formlabs Clear FL6PCL02

Soxhlet extraction and swelling tests were performed to confirm the cross-linked structure of the polymers. The highest yield of insoluble fraction was obtained for VD-based polymer **B4** (96%) prepared without solvent. This polymer also had the lowest swelling values in chloroform (49.22%) and toluene (48.62%), which indicated that a denser inner polymer network was formed.

Polymers **B4** and **B6** showed similar glass transition temperatures (87 and 86°C, respectively), while the T_g of **B5** was lower (79°C). Similar values of $T_{dec-10\%}$ (330–350°C) were obtained during thermal decomposition of polymers. The highest thermal stability was showed by polymer **B4**, while the lowest by polymer **B5** and correlated to the values of yield of insoluble fraction (96 and 77%, respectively).

Resin **B4** was tested in DLW technology to determine the optimal fabrication parameters. The testing was performed at the Laser Research Center, Vilnius University. 3D microporous woodpile structures and the figurine of Marvin were manufactured and showed high level of shrinkage during printing process and visible voids on the surface (Figure 6 (a) to (c)). µTM was selected as an alternative method to avoid these obstacles. Acrylated epoxidized soybean oil (AESO) was used to produce a master structure of Marvin and moulds were made from resin **B4** (Figure 6 (d)). In this case, the figurine of Marvin, produced using resin **B4** in prepared mould, had smooth surface and replicated structure of the Marvin (Figure 6 (e)).
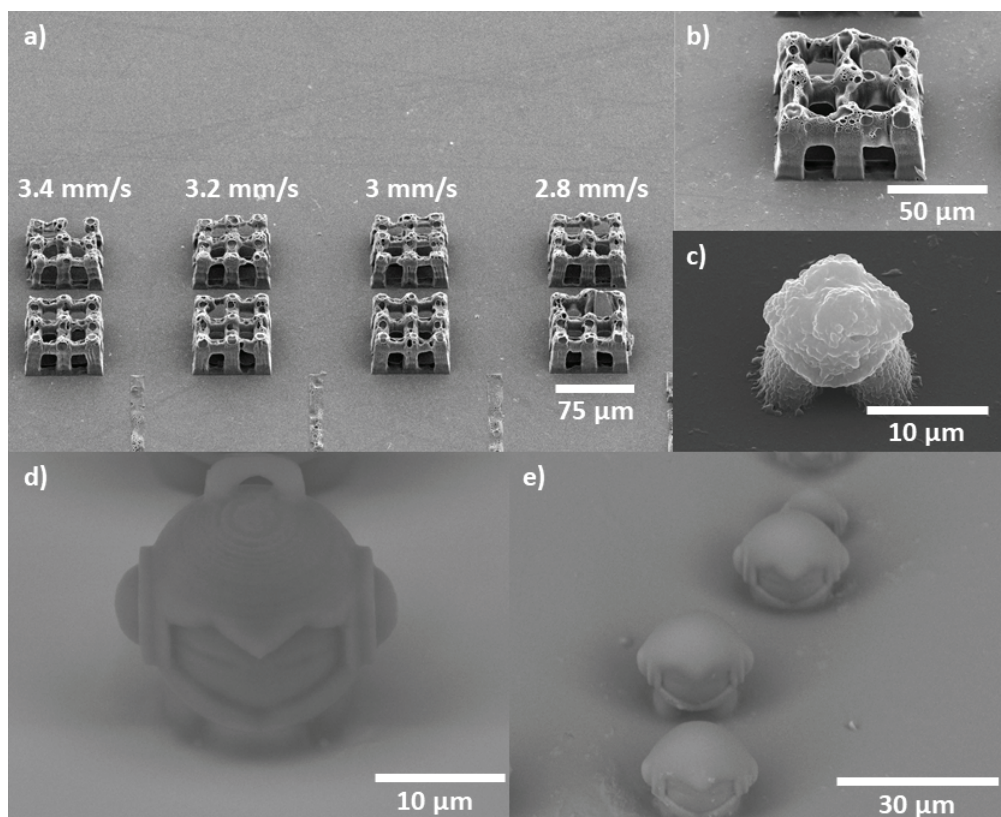
Figure 6. (a) – 75 × 75 µm² size woodpile structures out of **B4** resin: v varies from 2.8 to 3.4 mm/s, (b) – close-up of the 75 × 75 µm² woodpile structure: $v = 1$ mm/s, (c) – Figurine of Marvin out of **B4** resin: $v = 1.8$ mm/s, (d) – Figurine of Marvin out of AESO: $v = 1.2$ mm/s, (e) – Figurine of Marvin out of **B4** resin moulded from the master structure via microtransfer molding, 365 nm wavelength light source was used for curing

2.3. Investigation and comparison of free-radical and thiol-Michael photopolymerization and study of the resulting antimicrobial vanillin-based polymers

This chapter is based on published work: *A. Navaruckienė, D. Bridžiuvienė, V. Raudonienė, E. Rainosalo, J. Ostrauskaitė. Influence of vanillin acrylate-based resin composition on resin photocuring kinetics and antimicrobial properties of the resulting polymers. Materials. 2021, 14 (3), 653* [42]. *JIF: 3.748. Input: 0.200.*

Vanillin derivatives showed promising results in photocurable systems with and without comonomers as described in chapters 4.1 and 4.2. The aim of this study was to compare vanillin-based copolymers with homopolymers. Twenty one different resins were composed to determine the influence of vanillin derivative, thiol and its amount, photoinitiator and its amount, and presence of the solvent to

photocuring kinetics and the rigidity of the resulting polymers (Table 3). VDM and VD were selected for the photopolymerization with BDT and photoinitiator phenylbis(2,4,6-trimethylbenzoyl)phosphine oxide (BAPO) (Figure 7).
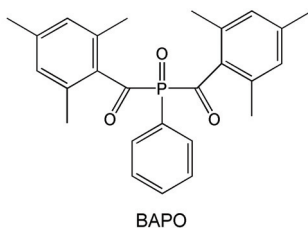
BAPO

Figure 7. Structure of phenylbis(2,4,6-trimethylbenzoyl)phosphine oxide (BAPO)

Table 3. Composition of the resins **C1–C21**

Resin	Vanillin derivative	Amount of vanillin derivative, mol	Amount of BDT, mol	Solvent	BAPO concentration, mol.%
C1	VD	1	1	-	1
C2	VD	1	1	DCM	1
C3	VD	1	-	-	1
C4	VD	1	-	DCM	1
C5	VDM	1	1	DCM	1
C6	VDM	1	-	DCM	1
C7	VD	1	1	-	3
C8	VD	1	1	DCM	3
C9	VD	1	-	-	3
C10	VD	1	-	DCM	3
C11	VDM	1	1	DCM	3
C12	VDM	1	-	DCM	3
C13	VD	1	1	-	5
C14	VD	1	1	DCM	5
C15	VD	1	-	-	5
C16	VD	1	-	DCM	5
C17	VDM	1	1	DCM	5
C18	VDM	1	-	DCM	5
C19	VD	1	0.5	-	3
C20	VD	1	0.5	DCM	3
C21	VDM	1	0.5	DCM	3

A series of the resins with 1, 3 and 5 mol.% of BAPO were investigated by real-time photorheometry to obtain the optimal concentration (Figure 8). Resin with 3 mol.% of BAPO was chosen for further investigation as it resulted in similar or faster photocuring rate comparing to the resins containing 1 mol.% of BAPO. Even though resins with 5 mol.% of BAPO showed higher photocuring rate, they could not be used as undissolved particles of BAPO were visible in the polymer samples. The addition of solvent into composition resulted in lower photocuring rate and reduced the rigidity of the polymers. The t_{gel} increased from 7.0 to 10.0 s and G' was reduced from 12.7 to 12.0 MPa by adding solvent in pure VD-based composition. The rigidity of polymers was also reduced by the addition of thiol, however at this time the photocuring rate was increased. For example, the addition of BDT in VD-based composition reduced the rigidity from 12.7 MPa to 1.57 MPa and the value of t_{gel} from 7.0 to 3.6 s. To better determine the influence of BDT on photocuring rate and rigidity of the obtained polymers, 3 resins with off-stoichiometric amount of acrylate:thiol content were composed. Dual curing process, combining thiol-Michael and free-radical mechanisms, was used for the synthesis of these polymers. The photocuring rate of these resins was slightly lower than that of thiol-Michael photopolymerization, but the resulting polymers were more rigid. For example, VDM-based polymer with 0.5 mol BDT reached t_{gel} after 5.3 s and the final rigidity of 15.2 MPa when VDM-based polymer with 1 mol of BDT reached t_{gel} after 3.6 s and the final rigidity of 2.14 MPa. The rheological characteristics of the selected resins were compared to the commercially available petroleum-based resins for optical 3D printing, PR48 (t_{gel} = 6.0 s, G' = 21.4 MPa) and FormLabs Clear FL6PCL02 (t_{gel} = 6.0 s, G' = 15.2 MPa). Vanillin-based resins showed similar reaction rate as commercially available ones, however the rigidity of the resulted polymers was slightly lower.
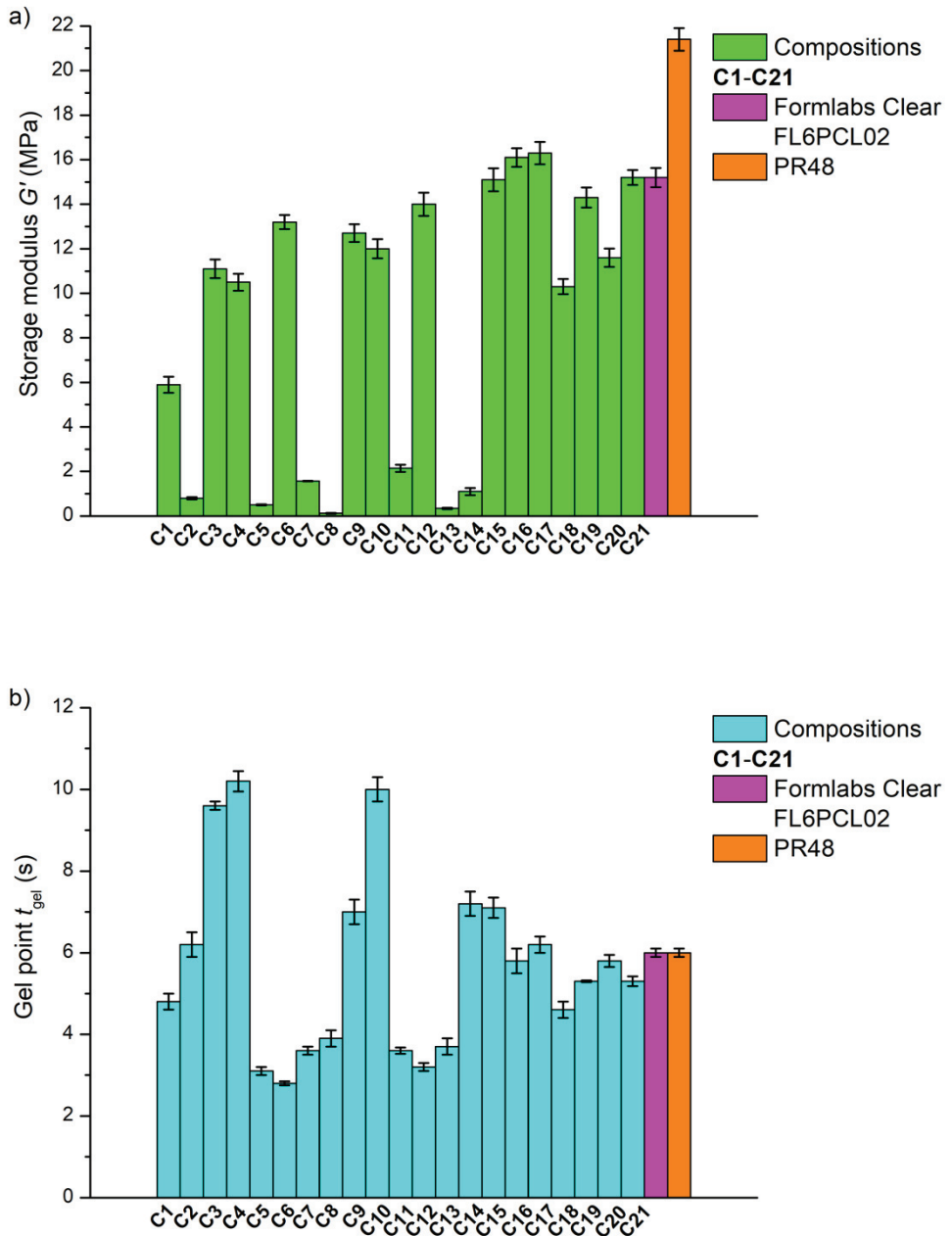
Figure 8. Storage modulus (a) and gel point (b) values of compositions **C1**–**C21**, PR48 and Formlabs Clear FL6PCL02

2.4. Synthesis and investigation of properties of dual-cured antimicrobial vanillin acrylate-based photopolymers

This chapter is based on published work: *A. Navaruckienė, D. Bridžiuvienė, V. Raudonienė, E. Rainosalo, J. Ostrauskaitė. Vanillin acrylate-based thermo-responsive shape memory antimicrobial photopolymers. Express polymer letters. 2022, 16 (3), 279-295* [43]. *JIF: 3.952. Input: 0.200.*

The amount of thiol has significant influence on the photocuring kinetics of vanillin-based photopolymers as described in chapter 4.3. The aim of this study was to determine the influence of vanillin derivative and the amount of comonomer BDT to the properties of the resulting polymers. Six vanillin acrylate-based polymer compositions were developed to achieve this aim. Three commercially available vanillin derivatives, vanillin hydroxypropane dimethacrylate (VHDM) (Figure 9), VDM and VD, were used in dual-curing systems with TPOL.
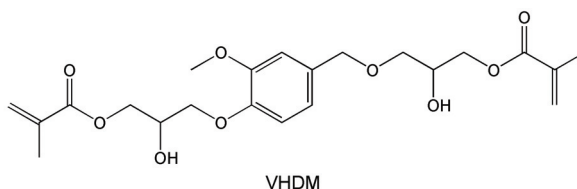
VHDM

Figure 9. Chemical structure of vanillin hydroxypropane dimethacrylate (VHDM).

Compositions of the vanillin-based resins are presented in Table 4. Codes **D1**–**D6** used in this chapter correspond to codes **C1**–**C6** in the published article. Different ratios of acrylate and thiol were chosen to obtain the desired properties of polymers by manipulating dominant reactions in dual-curing systems. During dual-curing process, two main reactions, thiol-acrylate photopolymerization and acrylate homopolymerization, are occurring at the same time. When the ratio of acrylate to thiol is reduced from 1:1 to 1:0.5, acrylate homopolymerization becomes a dominant reaction and the properties of the resulting polymers change.

Table 4. Composition of the resins **D1**–**D6**

Resin	Vanillin derivative	Amount of vanillin derivative, mol	Amount of BDT, mol	Amount of photoinitiator TPOL, mol.%	Solvent
D1	VD	1	1	3	-
D2	VD	1	0.5	3	-
D3	VDM	1	1	3	THF
D4	VDM	1	0.5	3	THF
D5	VHDM	1	1	3	-
D6	VHDM	1	0.5	3	-

Values of *G'*, t_{gel} and polymer shrinkage are presented in Figure 10. In all cases photocuring was faster and more rigid polymers were obtained when 0.5 mol of thiol was used and acrylate homopolymerization was the dominant reaction. For example, the photocuring rate of VD-based resin increased (t_{gel} increased from 6.2 to 4.8 s) and the rigidity of resulted polymers increased (*G'* increased from 8.89 to 11.4 MPa) by reducing the amount of thiol from 1 to 0.5 mol. However, the reduction of thiol amount increased the shrinkage of all polymers up to 4%, as acrylates have tendency to shrink during photopolymerization [44].
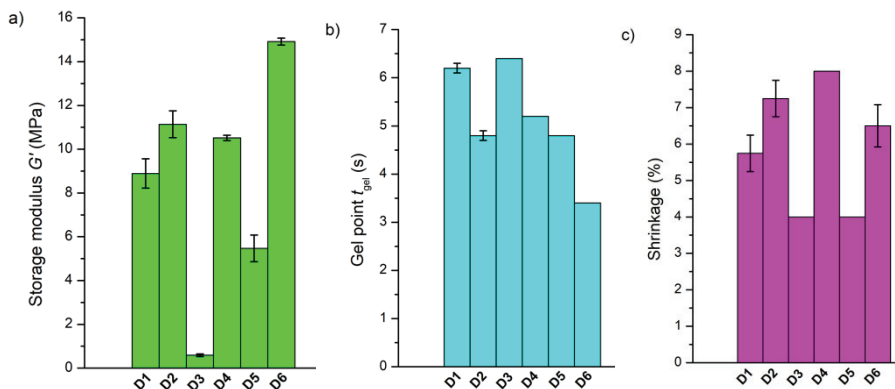
Figure 10. Storage modulus (a), gel point (b) and shrinkage (c) values of compositions **D1**–**D6**

Similar to rheological characteristics, better thermal properties were shown by polymers with lower amount of BDT. $T_{dec-10\%}$ was increased from 327 to 341°C and T_g increased from 17 to 40°C by reducing the amount of thiol in VHDM-based polymer compositions. The lowest values of 10% weight loss were shown by VDM-based polymers (277–294°C). The reason for that is the presence of the solvent THF in the resin, which acts as a chain transfer agent and is responsible for the formation of linear and branched macromolecules during the photopolymerization process [45]. The lower values of T_g and $T_{dec-10\%}$ correlated to the lower amount of the yield of insoluble fraction, which was in the range of 82–87% when 1 mol of BDT was used and increased to 95–99.9% when the amount of thiol was reduced.

The tensile test was performed to investigate the mechanical properties of polymers **D1**–**D6**. Polymers, prepared with 1 mol of BDT, showed low values of Young's modulus and high elongation at break (1.4–3.5 MPa and 19.0–119.7%) in comparison to polymers, prepared with 0.5 mol of BDT (3952.3–11339.4 MPa and 6.8–12.3%). The lowest values of Young's modulus and elongation at break were shown by VDM-based polymers, which were caused by the formation of linear or branched macromolecules in the presence of the solvent [45]. The highest values of Young's modulus and elongation at break were shown by VHDM-based polymers.

26

The reason for that was the longer chains between crosslinking points, which were formed during photopolymerization.

All synthesized polymers showed thermo-responsive shape memory properties. The ability to change their permanent shape and maintain temporary shape was determined by their T_g. The scheme of shape memory properties of polymer D6 ($T_g = 40°C$) is presented in Figure 11. Polymer specimen was heated to the temperature above its T_g (up to 60°C) and deformed to desired shape (coil). After deformation, the specimen was cooled down to temperature below its T_g (25°C). This process is called high-temperature programming. At that temperature the polymer specimen was able to maintain a coil shape with no shape changes in time. Shape memory properties were confirmed by heating polymer specimen again as it was able to return to its permanent shape within seconds. The same tendency was shown by all six vanillin-based polymers of this series.
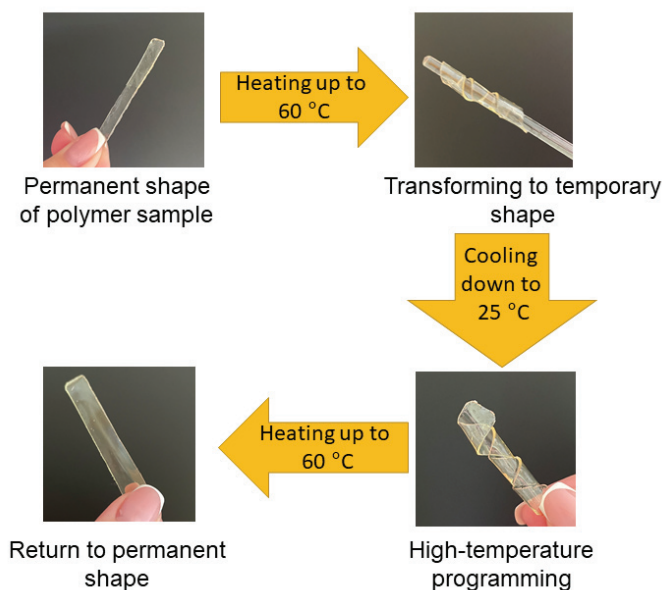
Figure 11. Shape memory behaviour of polymer **D6**

2.5. Synthesis and investigation of properties of vanillin dimethacrylate- and tridecyl methacrylate-based shape memory photopolymers.

This chapter is based on published work: *J. Jaras, A. Navaruckienė, E. Skliutas, J. Jeršovaitė, M. Malinauskas, J. Ostrauskaitė. Thermo-responsive shape memory vanillin-based photopolymers for microtransfer molding. Polymers. 2022, 14 (12), 2460* [46]. *JIF: 4.967. Input: 0.166.*

The main limitation of monomer VDM in polymer synthesis was the need of the solvent in the initial mixture as described in chapter 4.4. To eliminate this limitation tridecyl methacrylate (C13-MA) was chosen as a comonomer, which also

acted as solvent for VDM particles. VDM was mixed with various amounts of C13-MA and BDT, and twelve compositions were developed in order to find efficient system for μTM. Codes **E1**–**E12** used in this chapter correspond to codes **C1**–**C12** in the published article. The amount of C13-MA was increased from 1.5 to 4.5 mol and the amount of BDT was decreased from 1 mol to 0.25 mol, while the amount of VDM remained constant (Table 5). As mentioned in chapter 2.4., two different reactions, thiol-acrylate polymerization and acrylate homopolymerization, occur during dual-curing process. These reactions were manipulated to create unique polymers by changing the amount of C13-MA and BDT.

Table 5. Composition of resins **E1**–**E12**

Resin	Amount of VDM, mol	Amount of BDT, mol	Amount of C13-MA, mol	Amount of TPOL, mol.%
E1	1	1	1.5	3
E2	1	0.75	1.5	3
E3	1	0.5	1.5	3
E4	1	0.25	1.5	3
E5	1	1	3	3
E6	1	0.75	3	3
E7	1	0.5	3	3
E8	1	0.25	3	3
E9	1	1	4.5	3
E10	1	0.75	4.5	3
E11	1	0.5	4.5	3
E12	1	0.25	4.5	3

It was determined that less rigid polymers were obtained and photocuring was slower when the amount of C13-MA increased (Figure 12). For example, the rigidity decreased (G' decreased from 17.343 MPa (**E4**) to 2.930 MPa (**E12**)) by increasing the amount of C13-MA from 1.5 to 4.5 mol. The same results were obtained by changing the amount of BDT. When the amount of BDT increased from 0.25 to 1 mol, the value of G' decreased from 10.148 MPa (**E8**) to 0.031 MPa (**E5**). Even though an increased amount of BDT slowed down the photocuring process and lowered the rigidity of polymers, it also reduced the shrinkage of the polymers. The shrinkage was reduced from 10% (**E12**) to 1% (**E9**) by increasing the amount of thiol from 0.25 to 1 mol.
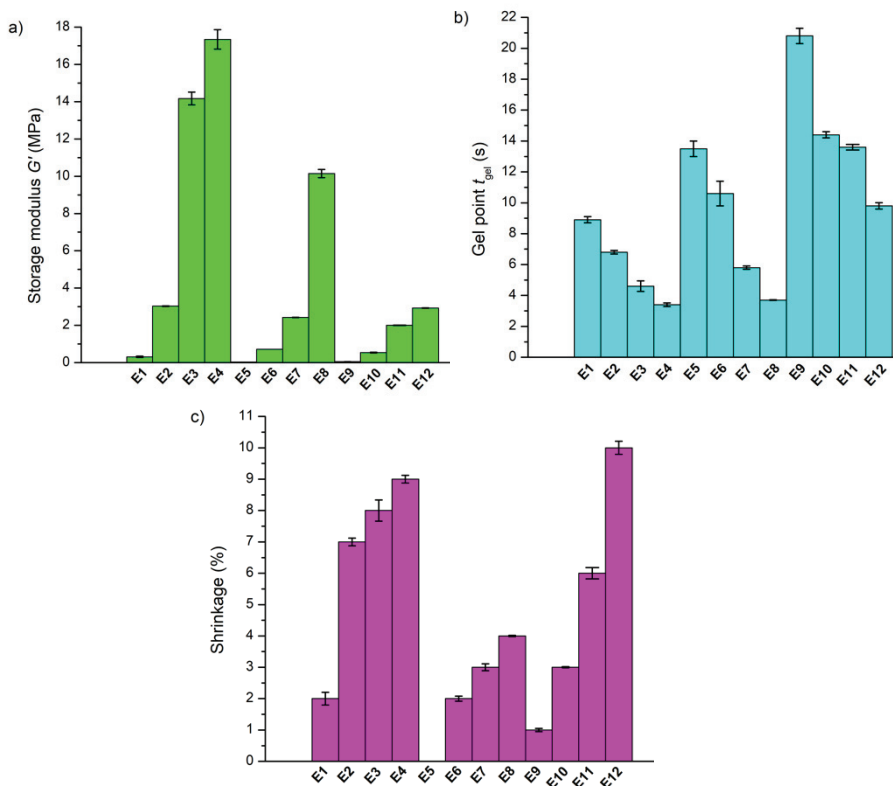
Figure 12. Storage modulus (a), gel point (b) and shrinkage (c) values of compositions **E1**–**E12**

Dynamic mechanical thermal analysis (DMTA) was used to determine T_g of the polymers. T_g of the polymers depended on their composition. The increase in C13-MA amount from 1.5 to 4.5 mol reduced T_g from 54°C (**E4**) to 17°C (**E12**). T_g was also reduced by the increase of the amount of BDT. For example, when the amount of thiol was increased from 0.25 to 1 mol, T_g was reduced from 28°C (**E8**) to -9°C (**E5**). A similar tendency was observed during the TGA test. $T_{dec-10\%}$ was reduced from 332°C (**E4**) to 308°C (**E1**) by increasing the amount of BDT from 0.25 to 1 mol. An increased amount of C13-MA from 1.5 to 3 mol resulted in higher values of $T_{dec-10\%}$, however further increase of C13-MA amount from 3 to 4.5 mol decreased the values of $T_{dec-10\%}$.

Mechanical properties of polymers **E1**, **E2**, **E5** and **E9** were not tested as they were too soft. The highest values of Young's modulus and the lowest values of elongation at break were shown by polymer **E4** (60.05 MPa and 5.47%), which was prepared with the lowest amount of BDT and C13-MA. It was determined that the addition of BDT (polymer **E3**) resulted in an increased value of elongation at break and lower Young's modulus (12.44 MPa and 17.3%). The reason for that was the flexible thioether linkages, which allow polymers to stretch more during the tensile test. The increased amount of C13-MA in the composition had a similar effect as

29

BDT. The value of the Young's modulus decreased from 60.05 MPa (polymer **E4** with 1.5 mol C13-MA) to 5.53 MPa (polymer **E12** with 4.5 mol C13-MA) while elongation at break increased from 5.47% (polymer **E4**) to 8.38% (polymer **E12**). The reason for that was the long carbon chain of tridecyl methacrylate [47].

All synthesized polymers **E1**–**E12** showed thermo-responsive shape memory properties. As explained in chapter 2.4., polymer samples can be heated to the temperature higher than their T_g, deformed to the desired temporary shape which is fixed by cooling the samples below their T_g. Polymers can always return to their permanent shape by heating them to temperature higher than their T_g. A scheme of the shape memory behavior of polymer **E8** is presented in Figure 13. A counterpoise weight was used to show that polymer **E8** is a rigid material. Polymer can easily return to its permanent shape without counterpoise weight.
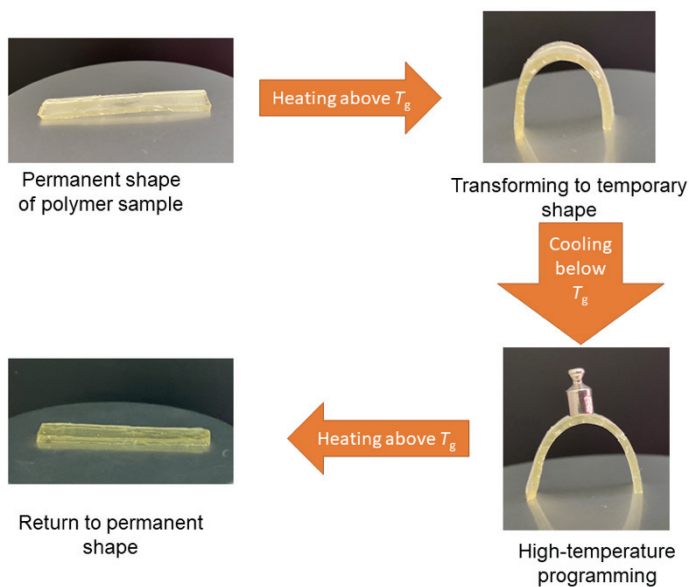
Figure 13. Scheme of shape-memory behaviour of polymer **E8**

Two different photocurable resins, **E1** (forming soft polymer) and **E8** (forming rigid polymer), were selected for testing in μTM. The results are presented in Figure 14. Image (a) shows a 3D printed USAF target and image (b) represents polydimethylsiloxane (PDMS) stamp, prepared by using the 3D printed target. Images (c) and (d) are replicas made of **E1** and **E8** resins. Both resins were able to replicate unique features of the target (shape, letters, numbers and lines). Due to this, both resins have a great perspective for the μTM technique.
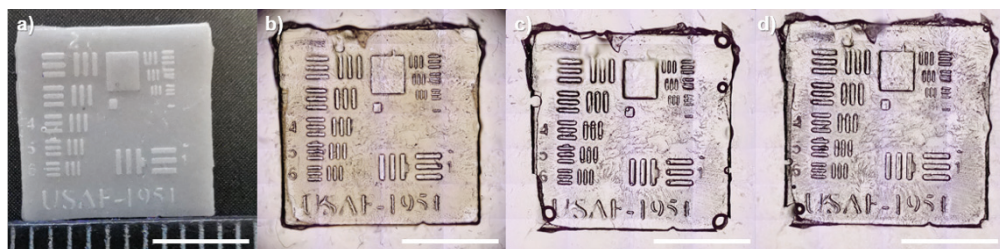
Figure 14. Results of µTM. (a) 3D printed 1951 USAF target (25% of the downloaded vector file size). (b) PDMS soft mold. (c) and (d) are replicas made out of **E1** and **E8** resins, respectively. Scalebars are equal in all the images and represent 5 mm.

2.6. Vanillin dimethacrylate and acrylated epoxidized soybean oil-based dual cure systems. Dependency of polymer properties on polymer composition

This chapter is based on published work: *V. Šereikaitė, A. Navaruckienė, J. Jaras, E. Skliutas, D. Ladika, D. Gray, M. Malinauskas, V. Talačka, J. Ostrauskaitė. Functionalized soybean oil- and vanillin-based dual cure photopolymerizable system for light-based 3D structuring. Polymers. 2022, 14, 5361* [48]. *JIF: 4.967. Input: 0.111.*

All five series of polymers described in chapters 4.1–4.5 showed properties suitable for microtransfer molding, although none of them were good enough for optical 3D printing. After analyzing the previous results and literature, a new composition containing 3 mol of AESO, 1 mol of VDM, 0.25 mol of pentaerythritol tetrakis(3-mercaptopropionate) (PETMP), 2.5 wt.% of TPO, and 0.08 wt.% of UVB was designed (Figure 15). AESO was chosen as a bio-based comonomer to increase the biorenewable carbon content (BRC) of the resulting polymer, reduce the price of polymer, increase printability, and apply it in optical 3D printing. The calculated BRC content of the polymer **VS** was 76.45%.
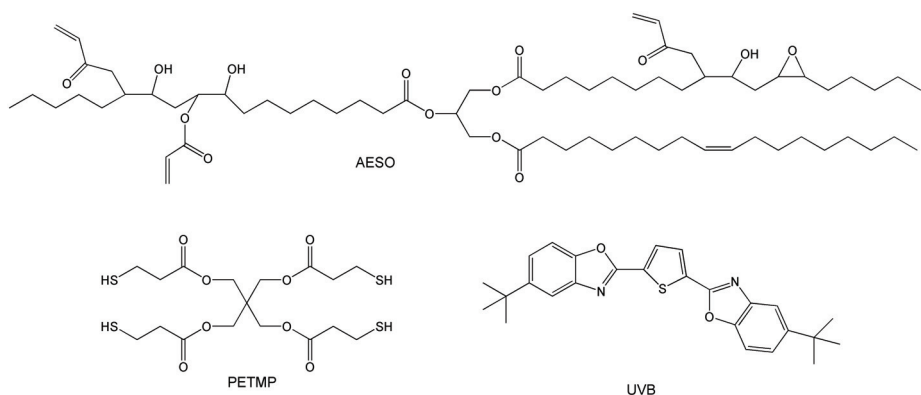
Figure 15. Chemical structures of acrylated epoxidized soybean oil (AESO), pentaerythritol tetrakis(3-mercaptopropionate) (PETMP) and 2,5-bis(5-tert-butyl-2-benzoxazolyl)thiophene (UVB).

AESO was selected as the main component due to its photocuring rate suitable for 3D printing and its biobased origin. Pure AESO polymers are known to be brittle, thus VDM was chosen as a comonomer to improve mechanical and thermal characteristics of resins [16]. PETMP was added to the mixture to provide flexibility to a rigid polymer network, as well as shape memory properties of the resulting polymers [49]. The lower than stoichiometric amount of acrylic and thiol groups was selected to obtain more rigid and mechanically stronger polymers by the domination of acrylate homopolymerization. The discussed influence of the components of the resins to the properties of polymer **VS** is summarized in Figure 16.
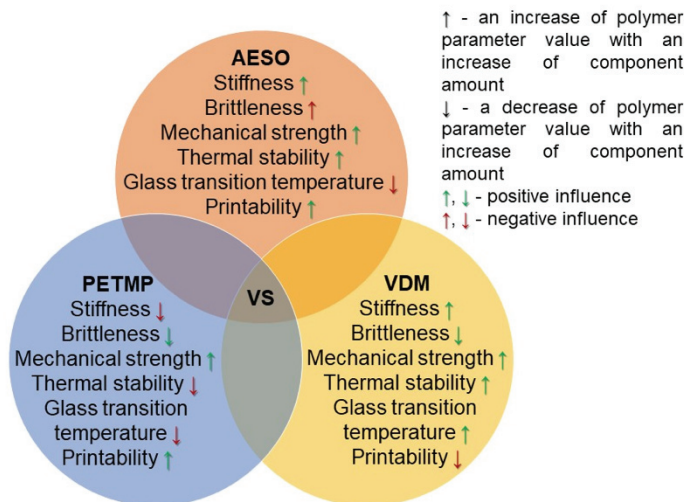
Figure 16. Scheme of the influence of component amounts on some parameters of the polymer **VS**

Real-time photorheometry was used to determine the rheological characteristics of the resin **VS**. It was determined that polymer **VS** is a rigid material as it reached the value of G' (317.66 MPa) which was 20 times bigger than that of vanillin dimethacrylate- and thiol-based polymers [43]. This composition also showed fast photocuring as it reached the gel point after only 1.5 s without an induction period. These results make resin **VS** a promising candidate for optical 3D printing.

Polymer **VS** showed high values of the mechanical characteristics and reached the Young's modulus of 4753.1 MPa and the elongation at break of 4.72%. These parameters show that polymer **VS** is a rigid and stiff material.

The composed resin was tested in SLA 3D printing technology at company Ameralabs. Results showed that the resin was able to obtain even smallest details by maintaining a smooth surface. The images of 3D printed "Ameralabs Town" are presented in Figure 17.
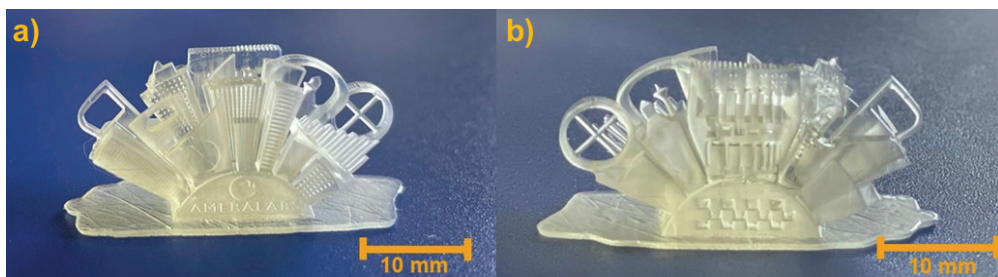
Figure 17. Images of SLA 3D printed polymer structures. The front side is on the left (a), and the back side is on the right (b).

The main limitations for the printing process were high viscosity of the resin, which was increased by the use of AESO, and a relatively slow printing process.

2.7. Synthesis and investigation of properties of sequentially and simultaneously dual-cured vanillin-based polymers

This chapter is based on published work: *G. Motiekaitytė, A. Navaruckienė, V. Raudonienė, D. Bridžiuvienė, J. Jaras, K. Kantminienė, J. Ostrauskaitė. Antimicrobial dual-cured photopolymers of vanillin alcohol diglycidyl ether and glycerol dimethacrylate. Journal of applied polymer science. 2023, 140 (2), e53289* [50]. *JIF: 3.057. Input: 0.142.*

Vanillin-based acrylates showed a great perspective in polymer synthesis and dual curing as was described in chapters 4.1–4.6. Vanillin alcohol diglycidyl ether (VDGE) was chosen as an epoxide monomer to investigate how different types of vanillin derivatives perform in this process and investigate the properties of the resulting polymers. Glycerol dimethacrylate (GDMK) was chosen as a comonomer and two photoinitiators, BAPO and triarylsulfonium hexafluorophosphate salts (TASHFF), were used in this study (Figure 18). Codes **G1**–**G3** used in this chapter correspond to codes **C1**–**C3** in the published article. The composition of the resins is presented in Table 6. A star-shaped figure (*) next to the resin codes indicates that sequential photocuring process was used for that resin.
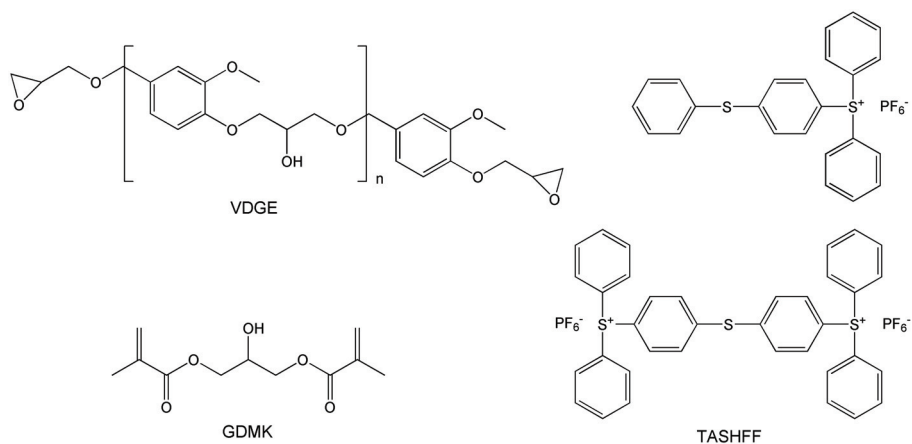
Figure 18. Chemical structure of vanillin alcohol diglycidyl ether, n=0.0-0.2 (VDGE), glycerol dimethacrylate (GDMK) and triarylsulfonium hexafluorophosphate salts (TASHFF).

Table 6. The composition of resins **G1**–**G3**

Resin	Amount of VDGE, mol	Amount of GDMK, mol	Amount of TASHFF, mol.%	Amount of BAPO, mol.%	Amount of DCM, mol
G1	1	0.5	3	3	0.4
G2	1	1	3	3	0.4
G3	0.5	1	3	3	0.2
VDGE	1	0	3	0	0.4
GDMK	0	1	0	3	0

Dual-curing process was performed in two different ways: sequential and simultaneous. During the sequential dual-curing, a light filter was used to manipulate the photocuring process. When the light filter was used, only the free-radical photopolymerization was initiated and when the filter was removed cationic photopolymerization started. The results are presented in Figure 19. Resin **G1*** showed the highest difference in rigidity between the first and the second stages of the curing. The reason for that was the highest amount of VDGE in the resin, which reacts during the second stage of photocuring. The increase in the polymer rigidity from 11.51–23.00 MPa after first stage to 22.63–25.56 MPa after second stage was observed in sequential dual curing. It was determined that the increase in GDMK content increased the photocuring rate and the rigidity of the resulted polymers.
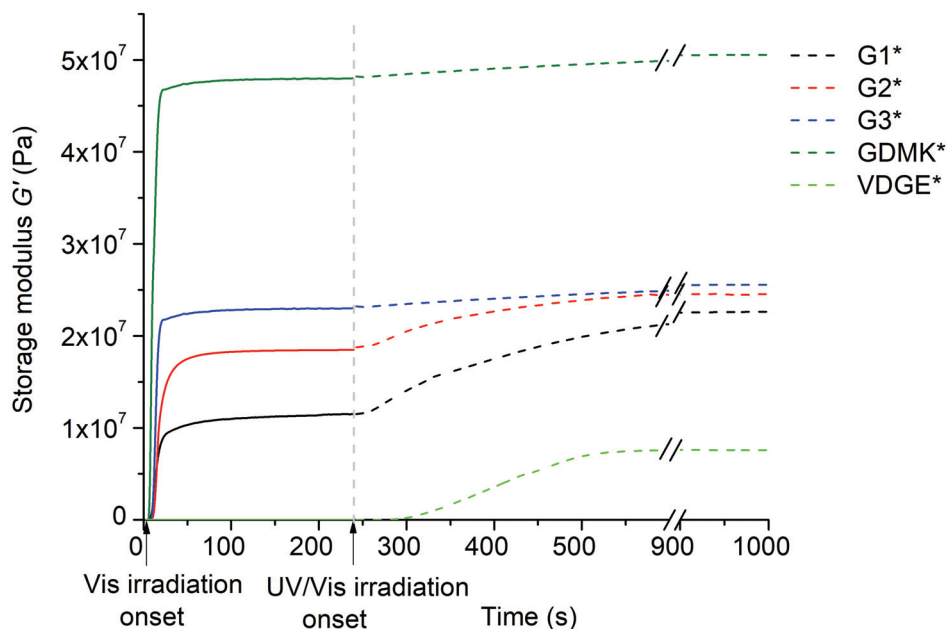
Figure 19. Dependence of the storage modulus G' of the resins on the irradiation time (sequential photocuring). Solid line – wavelength range of 400–450 nm, split line – wavelength range of 250–450 nm.

During simultaneous dual-curing process both reactions started at the same time with no limitations. The results are presented in Figure 20. In this case, the photocuring rate was very similar for all three polymers as t_{gel} was in the range of 12.0–12.5 s. The highest rigidity was showed by polymer **G2**, but it was very similar to the rigidity of polymer **G3** (28.23 and 27.51 MPa, respectively). The same as in the sequential process, the lowest rigidity was shown by polymer **G1** (17.97 MPa) with the lowest amount of GDMK. Polymers prepared by using the simultaneous process were chosen for further investigation due to the similar rheological characteristics in comparison to sequential process and less complicated production process.
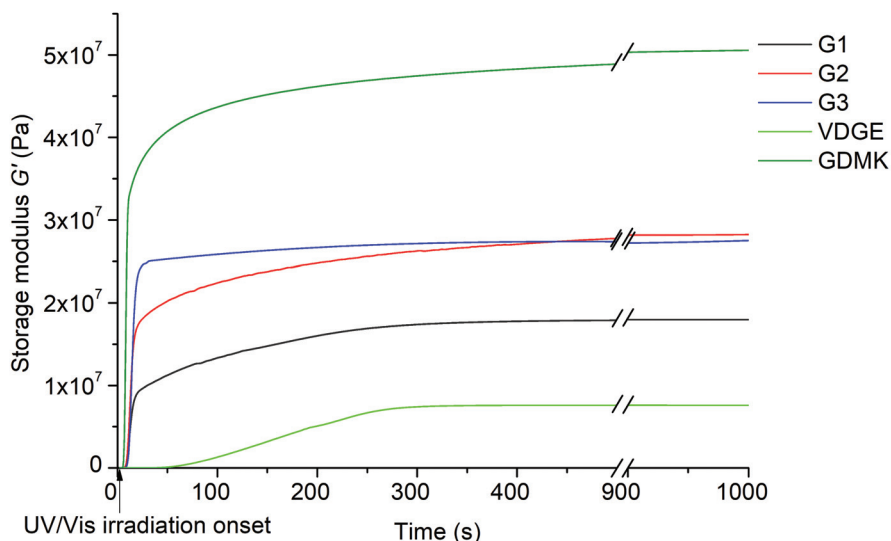
Figure 20. Dependence of the storage modulus G' of the resins on the irradiation time (simultaneous photocuring).

It was determined that the increased amount of VDGE in the polymer composition also increased the T_g of polymers. T_g was increased from 41°C (**G3**) to 57°C (**G1**) by increasing amount of VDGE. However, different results were obtained during the TGA test. The increased amount of VDGE lowered $T_{dec-10\%}$ from 274°C (**G3**) to 227°C (**G1**). These results correlated to the rigidity of the polymers.

Tensile test showed that Young's modulus increased (from 76.64 MPa to 190.71 MPa) and the elongation at break decreased (from 4.75% to 3.41%) when the amount of GDMK in the composition was increased. The reason for that is structures of GDMK and VDGE, as VDGE is a longer molecule compared to GDMK and leads to the formation of longer chains in the polymer structure when higher amount of VDGE is used and the resulting polymer is more flexible [51].

3. CONCLUSIONS

1. The developed photocurable resins with vanillin derivatives have the following features:
   a) More rigid polymers were obtained when vanillin diacrylate was used instead of vanillin dimethacrylate as the storage modulus was increased from 0.73 to 0.81 MPa;
   b) The presence of dichloromethane slowed down the photocuring process and reduced the rigidity of the resulted photopolymers.
   c) 3 mol.% of photoinitiators phenylbis(2,4,6-trimethylbenzoyl)phosphine oxide, diphenyl(2,4,6-trimethylbenzoyl)phosphine oxide and ethyl(2,4,6-trimethylbenzoyl)phenylphosphinate is an optimal amount as it results in the best ratio of photocuring rate and rigidity of the product;
   d) The photocuring rate of vanillin acrylate-based resins and the rigidity of the resulting polymers were similar to commercially available petroleum-based resins for optical 3D printing considering them as suitable candidates for optical 3D printing.

2. Vanillin acrylate-based cross-linked polymers have been synthesized by photopolymerization with and without the addition of comonomers and shows these properties:
   a) Photocuring rate of vanillin diacrylate-based resins was lower than that of vanillin dimethacrylate-based resins; vanillin acrylate-based polymers showed high values of the yield of insoluble fraction (77–99%), confirming that most part of the product is a cross-linked polymer network;
   b) The increased amount of comonomers 1,3-benzenedithiol or tridecyl methacrylate reduced the glass transition temperature and the destruction temperature at the 10% weight loss of polymers;
   c) The increased amount of comonomers 1,3-benzenedithiol, tridecyl methacrylate or acrylated epoxidized soybean oil reduced the values of Young's modulus and increased the values of elongation at break of polymers.
   d) Polymers with vanillin and 1,3-benzenedithiol fragments showed thermos-responsive shape memory properties which are determined by their glass transition temperature.

3. Vanillin epoxide-based photopolymers have been synthesized using sequential and simultaneous dual-curing:
   a) The increase in glycerol dimethacrylate content from 0.5 to 1 mol increased the photocuring rate from 12.5 s to 12.0 s and the rigidity of the resulting polymers from 17.97 to 28.23 MPa in both dual-curing methods;
   b) The increased amount of vanillin diglycidyl ether in the resin composition from 0.5 to 1 mol increased the glass transition temperature of polymers from 41 to 57°C. and lowered the destruction temperature at the 10% weight loss from 274°C to 227°C;

c) The dual-curing of vanillin-based photocurable systems is a simple way to obtain polymers with increased rigidity, as the polymer rigidity was increased from 11.51–23.00 MPa after the first stage to 22.63–25.56 MPa after the second stage in sequential dual curing and more rigid polymers (17.97–27.51 MPa) with the same composition were obtained after simultaneous dual curing.

4. Vanillin-based resins are suitable for application in microtransfer molding and optical 3D printing:

a) Vanillin acrylate-based resin and vanillin dimethacrylate-based resins with tridecyl methacrylate and 1,3-benzenedithiol are suitable for application in microtransfer molding, as they were able to replicate unique features of the target (shape, letters, numbers and lines);

b) Photosensitive dual-curable resin of vanillin dimethacrylate, acrylated epoxidized soybean oil and pentaerythritol tetrakis(3-mercaptopropionate) is suitable for optical 3D printing technology as it showed high printing accuracy and good layer adhesion.

4. SANTRAUKA

ĮVADAS

Iš naftos produktų gautų medžiagų pakeitimas augalinės kilmės medžiagomis polimerų sintezei yra naudingas dėl jų mažo toksiškumo, sumažėjusios priklausomybės nuo ribotų iškastinių išteklių ir mažesnio šiltnamio efektą sukeliančių dujų kiekio [1]. Biopolimerai gali būti sintetinami tiesiogiai arba gaunami chemiškai modifikuojant ir vėliau polimerizuojant gamtinės kilmės medžiagas [2]. Pagrindinė tokių medžiagų žaliava yra augalai, nes jie gali greitai generuoti biomasę ir jiems reikalingi minimalūs ištekliai [3]. Biopolimerų mechaninės bei terminės savybės gali būti panašios į polimerų, gautų iš naftos produktų, savybes, ir jie netgi gali turėti papildomų savybių, tokių kaip antimikrobinis veiklumas, bioskaidumas ar formos atminties savybės. Vanilinas yra viena iš gamtoje aptinkamų antimikrobinių medžiagų. Pastaraisiais metais vanilinas ir jo dariniai pritraukė tyrėjų dėmesį dėl galimybės jį panaudoti gaminti monomerams, kurie vėliau gali būti naudojami polimerų sintezei [4]. Polimerai su vanilino fragmentais gali būti gaunami terminės polimerizacijos ar fotopolimerizacijos būdu [5, 6]. Tačiau šiuo metu dar nėra polimerų su vanilino fragmentais, pritaikytų dvigubojo kietinimo sistemoms.

Dvigubasis kietinimas – tai procesas, sujungiantis dvi polimerizacijos reakcijas, kurios gali vykti nuosekliai arba vienu metu. Šio proceso metu gaunamos medžiagos su persipinančiais ar iš dalies persipinančiais polimerų tinklais, kurie suteikia joms unikalias savybes [7]. Gautų polimerų savybės gali būti lengvai pakeičiamos keičiant dominuojančią polimerizacijos reakciją. Dvigubojo kietinimo procesui gali būti taikoma tiek terminė polimerizacija, tiek ir fotopolimerizacija. Palyginus šias reakcijas galima teigti, jog fotopolimerizacija yra pranašesnė už terminę polimerizaciją [8]. Tai yra greitas ir aplinkai draugiškas bei tvarus procesas, kuris vyksta akimirksniu (dervai sukietinti užtenka kelių sekundžių ar minučių), jam nebūtinas kaitinimas ir jis gali būti vykdomas kambario ar netgi žemesnėje temperatūroje, taip pat gali selektyviai sukietinti tik pasirinktas dervos vietas [9].

Šiame darbe naudoti keturi komerciniai vanilino dariniai: vanilino diakrilatas, vanilino dimetakrilatas, vanilino hidroksipropano dimetakrilatas ir vanilino alkoholio diglicidileteris. Tyrimo metu buvo susintetintos šešios skirtingos fotopolimerų su vanilino fragmentais serijos bei viena atskira derva ir ištirtos jų savybių priklausomybės nuo pasirinkto vanilino darinio, kopolimerų, taip pat fotoiniciatoriaus tipo bei jo kiekio. Tyrimų rezultatai pristatyti septyniose publikacijose.

Darbo tikslas – sukurti naujus tinklinius fotopolimerus su vanilino fragmentais, skirtus mikroįspaudimo litografijai bei optiniam trimačiam (3D) spausdinimui.

Šiam tikslui pasiekti buvo iškelti tokie uždaviniai:

1. Sukurti naujas fotojautrias dervas su vanilino junginiais ir ištirti jų sudėties įtaką fotokietinimo procesui bei reologinėms savybėms.

2. Susintetinti ir charakterizuoti naujus fototinklinius polimerus su įvairių vanilino darinių fragmentais ir nustatyti jų savybių priklausomybę nuo sudėties.
3. Ištirti dvigubojo kietinimo sistemų su vanilino junginiais sudėties ir proceso sąlygų įtaką fotokietėjimo kinetikai, gautų polimerų struktūrai ir savybėms.
4. Ištirti fotojautrių dervų su vanilino junginiais tinkamumą mikroįspaudimo litografijai ir optiniam trimačiam (3D) spausdinimui.

Mokslinis naujumas
1. Susintetinti nauji fototinklinti polimerai su vanilino fragmentais ir pirmą kartą ištirta fotoiniciatoriaus įtaka dervų su vanilino junginiais fotokietinimo kinetikai bei gautų polimerų savybėms.
2. Pirmą kartą nauji tinkliniai polimerai su vanilino fragmentais buvo išbandyti dvigubojo kietinimo sistemose, ištirta jų fotokietinimo kinetika ir gautų polimerų savybės.
3. Pirmą kartą vanilino dariniai panaudoti formos atminties polimerų sintezei.

Darbo praktinė vertė
1. Dervos, sudarytos iš vanilino diakrilato be komonomerų, taip pat dervos, sudarytos iš vanilino diakrilato, tridecilmetakrilato ir 1,3-benzenditiolio, gali būti pritaikytos mikroįspaudimo litografijai.
2. Vanilino dimetakrilato, akrilinto epoksidinto sojų aliejaus ir pentaeritritoltetrakis(3-merkaptopropionato) derva yra tinkama naudoti stereolitografinio trimačio (3D) spausdinimo technologijai.

Ginamieji disertacijos teiginiai:
1. Dervos su vanilino fragmentais yra tinkamos formos atminties polimerų sintezei.
2. Fotojautrios dervos su vanilino fragmentais yra tinkamos mikroįspaudimo litografijai ir optiniam trimačiam (3D) spausdinimui.

Autorės indėlis rengiant disertaciją
Disertacijos autorė sukūrė ir charakterizavo šešias skirtingas fotopolimerų su vanilino fragmentais serijas bei vieną atskirą dervą, ištyrė dervų fotokietinimo kinetiką ir gautų polimerų termines, mechanines bei formos atminties savybes, taip pat parengė straipsnių rankraščius. Prof. dr. Jolita Ostrauskaitė (Kauno technologijos universitetas) prisidėjo prie pradinių idėjų generavimo, rengiant tyrimų idėjas bei tikslus, konsultavo sintetinant bei charakterizuojant polimerų su vanilino fragmentais kompozicijas ir prisidėjo redaguojant mokslinių straipsnių rankraščius. Dr. Sigita Graužėlienė (buv. Kašėtaitė) (Kauno technologijos universitetas) konsultavo sintetinant bei charakterizuojant polimerus su vanilino fragmentais ir prisidėjo redaguojant mokslinių straipsnių rankraščius. Prof. dr. Mangirdas

Malinauskas (Lazerinių tyrimų centras, Vilniaus universitetas) konsultavo atliekant tiesioginį lazerinį rašymą bei mikroįspaudimo litografiją ir prisidėjo redaguojant straipsnių rankraščius. Dr. Sima Rekštytė ir Edvinas Skliutas (Lazerinių tyrimų centras, Vilniaus universitetas) atliko tiesioginį lazerinį rašymą bei mikroįspaudimo litografiją, analizavo gautas struktūras ir prisidėjo redaguojant straipsnių rankraščius. Jurga Jeršovaitė (Lazerinių tyrimų centras, Vilniaus universitetas) atliko atrinktų dervų mikroįspaudimo litografiją. Dr. Vita Raudonienė ir dr. Danguolė Bridžiuvienė (Biodestruktorių tyrimo laboratorija, Gamtos tyrimų centras) atliko atrinktų polimerų antimikrobinius tyrimus. Dr. Egidija Rainosalo (*Centria* taikomųjų mokslų universitetas, Suomija) kūrė termomechaninius eksperimentus ir analizavo rezultatus. Justinas Jaras, Viltė Šereikaitė ir Greta Motiekaitytė (Kauno technologijos universitetas) prisidėjo prie eksperimentinės dalies. Dr. Kristina Kantminienė (Kauno technologijos universitetas) prisidėjo redaguojant straipsnių rankraščius. Dimitra Ladika ir dr. David Gray (Graikijos Elektroninių struktūrų ir lazerių institutas, Tyrimų ir technologijų centras) prisidėjo prie dviejų spindulių inicijavimo tyrimo ir rengiant straipsnio rankraštį. Vaidas Talačka (MB „AmeraLabs") nustatė tinkamus parametrus optiniam trimačiam (3D) spausdinimui, naudodamas dervą, išspausdino trimačius (3D) gaminius.

Publikacijų sąrašas disertacijos tema

1. <u>Auksė Navaruckienė</u>, Sigita Kašėtaitė, Jolita Ostrauskaitė. Vanillin-based thiol-ene systems as photoresins for optical 3D printing. *Rapid prototyping journal*. **2020**, *26* (2), 402-408. JIF: 3.095.

2. <u>Auksė Navaruckienė</u>, Edvinas Skliutas, Sigita Kašėtaite, Sima Rekštytė, Vita Raudonienė, Danguolė Bridžiuvienė, Mangirdas Malinauskas, Jolita Ostrauskaitė. Vanillin acrylate-based resins for optical 3D printing. *Polymers*. **2020**, *12* (2), 397. JIF: 4.329.

3. <u>Auksė Navaruckienė</u>, Danguolė Bridžiuvienė, Vita Raudonienė, Egidija Rainosalo, Jolita Ostrauskaitė. Influence of vanillin acrylate-based resin composition on resin photocuring kinetics and antimicrobial properties of the resulting polymers. *Materials*. **2021**, *14* (3), 653. JIF: 3.748.

4. <u>Auksė Navaruckienė</u>, Danguolė Bridžiuvienė, Vita Raudonienė, Egidija Rainosalo, Jolita Ostrauskaitė. Vanillin acrylate-based thermo-responsive shape memory antimicrobial photopolymers. *Express polymer letters*. **2022**, *16* (3), 279-295. JIF: 3.952.

5. Justinas Jaras, <u>Auksė Navaruckienė</u>, Edvinas Skliutas, Jurga Jeršovaitė, Mangirdas Malinauskas, Jolita Ostrauskaitė. Thermo-responsive shape memory vanillin-based photopolymers for microtransfer molding. *Polymers*. **2022**, *14* (12), 2460. JIF: 4.967.

6. Viltė Šereikaitė, <u>Auksė Navaruckienė</u>, Justinas Jaras, Edvinas Skliutas, Dimitra Ladika, David Gray, Mangirdas Malinauskas, Vaidas Talačka, Jolita Ostrauskaitė. Functionalized soybean oil- and vanillin-based dual cure photopolymerizable system for light-based 3D structuring. *Polymers*. **2022**, 14, 5361. JIF: 4.967.

7. Greta Motiekaitytė, <u>Auksė Navaruckienė</u>, Vita Raudonienė, Danguolė Bridžiuvienė, Justinas Jaras, Kristina Kantminienė, Jolita Ostrauskaitė. Antimicrobial dual-cured photopolymers of vanillin alcohol diglycidyl ether and glycerol dimethacrylate. *Journal of applied polymer science*. **2023**, *140* (2), e53289. JIF: 3.057.

4.1. Vanilino tioleno sistemos ir dervų sudėties įtaka fotopolimerizacijai

Šis skyrius parašytas remiantis publikuotu straipsniu: *A. Navaruckienė, S. Kašėtaitė, J. Ostrauskaitė. Vanillin-based thiol-ene systems as photoresins for optical 3D printing. Rapid prototyping journal. 2020, 26 (2), 402–408* [39]. *JIF: 3.095. Indėlis: 0,334.*

Šio darbo tikslas buvo fotopolimerizacijos būdu susintetinti naujus biopolimerus naudojant vanilino darinius ir ištirti jų savybes. Vanilino diakrilatas (VD) ir vanilino dimetakrilatas (VDM) buvo pasirinkti kaip pagrindinės medžiagos polimerų sintezei, o 1,3-benzenditiolis (BDT) naudotas kaip komonomeras. Siekiant atrinkti tinkamiausią fotoiniciatorių bei jo kiekį buvo pasirinkti du fotoiniciatoriai – etil(2,4,6-trimetilbenzoil)fenilfosfinatas (TPOL) ir difenil(2,4,6-trimetilbenzoil)fosfino oksidas (TPO). Norint ištirti tirpiklio bei jo kiekio ir vanilino darinio įtaką fotokietinimo kinetikai, buvo sukurta keturiolika kompozicijų (1 lentelė). Kompozicijoms suteikti kodai **A1**–**A14**, kurie atitinka straipsnyje vartotus kodus **C1**–**C14**. Naudotų medžiagų struktūrinės formulės pateiktos 1 paveiksle.
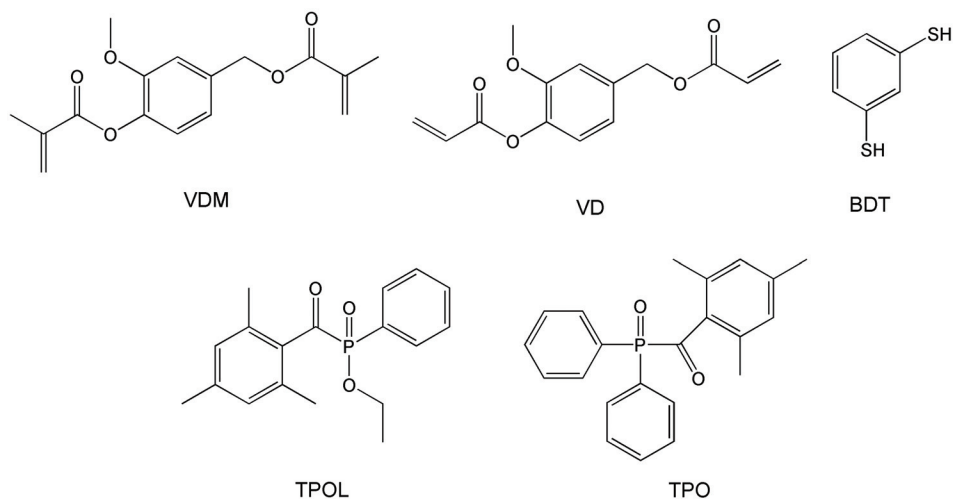
1 pav. Vanilino dimetakrilato (VDM), vanilino diakrilato (VD), 1,3-benzenditiolio (BDT), etil(2,4,6-trimetilbenzoil)fenilfosfinato (TPOL) ir difenil(2,4,6-trimetilbenzoil)fosfino oksido (TPO) struktūrinės formulės

1 lentelė. Dervų **A1**–**A14** sudėtis

Derva	Vanilino darinys	Vanilino darinio kiekis, mol	BDT kiekis, mol	Fotoiniciatorius	Fotoiniciatoriaus kiekis, mol.%	Tirpiklis
A1	VDM	1	1	TPOL	1	DCM
A2	VDM	1	1	TPO	1	DCM
A3	VD	1	1	TPOL	1	–
A4	VD	1	1	TPO	1	–
A5	VDM	1	1	TPOL	3	DCM
A6	VD	1	1	TPOL	3	–
A7	VD	1	1	TPOL	3	DCM
A8	VDM	1	1	TPO	3	DCM
A9	VD	1	1	TPO	3	–
A10	VD	1	1	TPO	3	DCM
A11	VDM	1	1	TPOL	5	DCM
A12	VDM	1	1	TPO	5	DCM
A13	VD	1	1	TPOL	5	–
A14	VD	1	1	TPO	5	–

Visi šioje disertacijoje pateikti tyrimų rezultatai buvo statistiškai išanalizuoti, naudojant *Microsoft Excel* programą ANOVA. Visi eksperimentai buvo atlikti po penkis kartus ir rezultatai išreikšti vidurkiu ± standartinis nuokrypis, kaip aprašyta paskelbtuose straipsniuose.

Fotoreometrija buvo taikoma ištirti dervų su vanilino junginiais fotokietinimo kinetikai. Nustatyta, jog reologinės charakteristikos priklauso nuo dervų sudėties. Dervų su vanilino junginiais tampros (kaupimo) modulio *G'* ir gelio taško (t_{gel}) vertės pateiktos 2 paveiksle.

Standesni polimerai gauti naudojant VD monomerą vietoj VDM. Taip pat standesni polimerai gauti, kai vietoj TPOL naudotas TPO (lyginant **A4** polimerą (20,2 MPa) su **A3** polimeru (17,8 MPa). Tai vyksta dėl didesnio TPO reaktyvumo palyginus su TPOL [40]. Fotoiniciatoriaus kiekio didinimas lėmė *G'* sumažėjimą, kuris reiškė ir gautų polimerų standumo sumažėjimą (**A3** (17,80 MPa), **A6** (9,92 MPa) ir **A13** (1,96 MPa) polimerų serija). Nepaisant to, didinant fotoiniciatoriaus kiekį nuo 1 mol.% iki 3 mol.%, t_{gel} vertė gali sumažėti net 8 s dėl greitesnės fotopolimerizacijos, kurios greitis yra labai svarbus polimerų gamybai.

Įvertinus šiuos duomenis, buvo nuspręsta tolimesniems tyrimams naudoti **A5** ir **A6** polimerus.
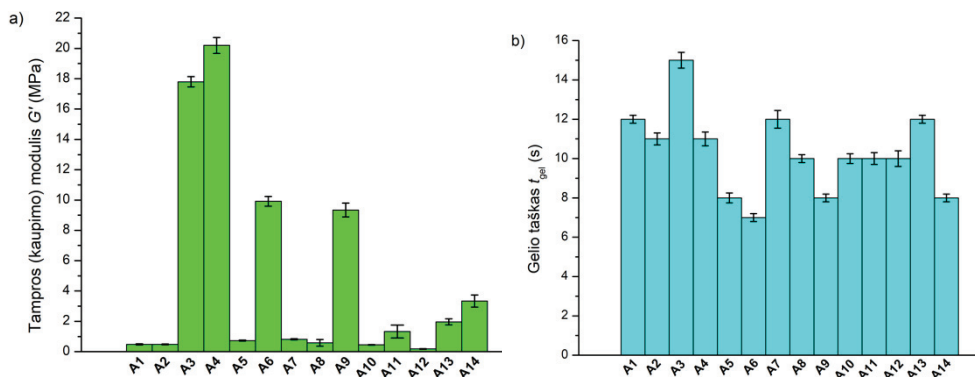
2 pav. Dervų **A1**–**A14** tampros (kaupimo) modulio (a) ir gelio taško (b) vertės

4.2. Polimerų su vanilino akrilatų fragmentais sintezė taikant radikalinę fotopolimerizaciją ir gautų polimerų savybių tyrimas

Šis skyrius parašytas remiantis publikuotu straipsniu: *A. Navaruckienė, E. Skliutas, S. Kašėtaitė, S. Rekštytė, V. Raudonienė, D. Bridžiuvienė, M. Malinauskas, J. Ostrauskaitė. Vanillin acrylate-based resins for optical 3D printing. Polymers. 2020, 12 (2), 397* [41]. *JIF: 4.967. Indėlis: 0,125.*

Vanilino dariniai pritaikyti fotokietinamoms sistemoms naudojant komonomerą BDT, kaip aprašyta 4.1 poskyryje, tačiau sistemose be BDT jie nebuvo išbandyti. Vanilino dariniai pasirinkti kaip pradinės medžiagos nenaudojant komonomerų, siekiant ištirti vanilino akrilato, tirpiklio, fotoiniciatoriaus bei jo kiekio įtaką gautų polimerų savybėms ir pritaikyti pasirinktas kompozicijas tiesioginio lazerinio rašymo (DLW) bei mikroįspaudimo litografijos (µTM) technologijose. Radikalinė fotopolimerizacija pritaikyta polimerų su VD ir VDM fragmentais sintezei, naudojant skirtingus fotoiniciatoriaus TPOL kiekius (1 paveikslas). Dervų sudėtis pateikta 2 lentelėje. Dervoms buvo priskirti kodai **B1**–**B9**, kurie atitinka straipsnyje vartotus kodus **C1**–**C9**. Gautų kompozicijų reologinės ir mechaninės charakteristikos buvo palygintos su komercinių trimačiam (3D) spausdinimui naudojamų dervų, PR48 ir *FormLabs Clear FL6PCL02*, savybėmis.

2 lentelė. Dervų **B1**–**B9** sudėtis

Derva	Vanilino darinys	Vanilino darinio kiekis, mol	Tirpiklis	Fotoiniciatoriaus TPOL kiekis, mol.%
B1	VD	1	–	1
B2	VD	1	DCM	1
B3	VDM	1	DCM	1
B4	VD	1	–	3
B5	VD	1	DCM	3
B6	VDM	1	DCM	3
B7	VD	1	–	5
B8	VD	1	DCM	5
B9	VDM	1	DCM	5

Kompozicijų **B1**–**B9** G' ir t_{gel} vertės pateiktos 3 paveiksle. Fotokietinimas vyko greičiausiai, kai buvo naudojami 3 mol.% fotoiniciatoriaus TPOL. Taip pat, naudojant 3 mol.% TPOL buvo gautos vienos iš didžiausių G' verčių, kurios nusako polimerų standumą. Vienintelė išimtis buvo polimeras **B5** (G' = 11,3 MPa), kurio standumo sumažėjimą lėmė tirpiklio naudojimas kompozicijoje. Visais atvejais fotopolimerizacija vyko greičiau, kai VDM buvo naudojamas vietoj VD. To priežastis yra tamsi VD spalva, kuri trukdo šviesai pasiekti gilesnius dervos sluoksnius ir taip lėtina fotopolimerizacijos procesą. Tolimesniems tyrimams buvo pasirinktos kompozicijos **B4**–**B6**, paruoštos naudojant 3 mol.% TPOL.

Siekiant įvertinti pasirinktų dervų tinkamumą trimačiam (3D) spausdinimui, gauti rezultatai buvo palyginti su komercinėmis dervomis PR48 ir *FormLabs Clear FL6PCL02*. Dervų **B4** ir **B6** fotokietėjimo greitis buvo toks pat arba kiek didesnis nei komercinių dervų. Vienintelė išimtis buvo **B5**, kurios fotokietėjimas vyko dvigubai lėčiau nei komercinių dervų. Polimerai **B4** ir **B6** (G' = 18,10 MPa; 18,20 MPa) buvo standesni nei *FormLabs Clear FL6PCL02* (15,20 MPa), bet minkštesni nei PR48 (21,40 MPa).
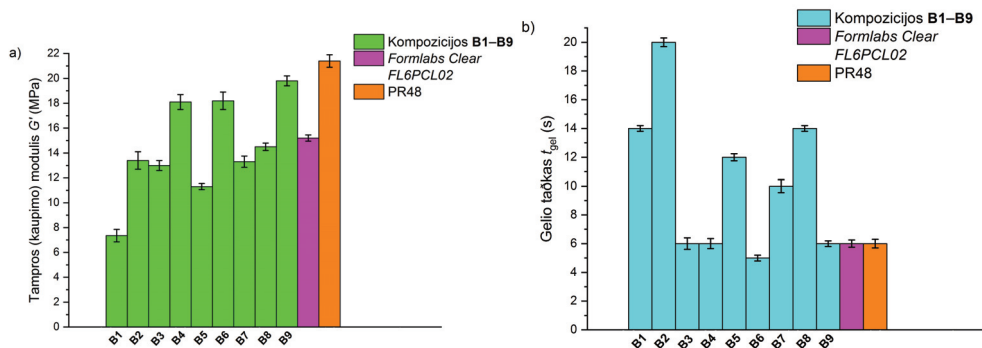
3 pav. Kompozicijų **B1**–**B9**, PR48 bei *Formlabs Clear FL6PCL02* tampros (kaupimo) modulio (a) ir gelio taško (b) vertės

DLW technologija buvo taikoma siekiant parinkti optinio trimačio (3D) spausdinimo parametrus **B4** dervai. Tyrimai buvo atlikti Vilniaus universiteto Lazerinių tyrimų centre. Trimačiai (3D) pagaliukai ir Marvino figūrėlės buvo atspausdintos, tačiau dėl didelio susitraukimo ir matomų ertmių paviršiuje **B4** derva nebuvo tinkama šiam spausdinimo metodui (4 paveikslas (a)–(c)). µTM buvo pasirinkta kaip alternatyva optiniam trimačiam (3D) spausdinimui. Akrilintas epoksidintas sojų aliejus (AESO) buvo panaudotas spausdinti pradinę Marvino struktūrą, pagal kurią vėliau sukurta liejimo forma (4 paveikslas (d)). Taikant šią technologiją buvo gautas lygus **B4** polimero struktūros paviršius, puikiai atkartojantis liejimo formą (4 paveikslas (e)).
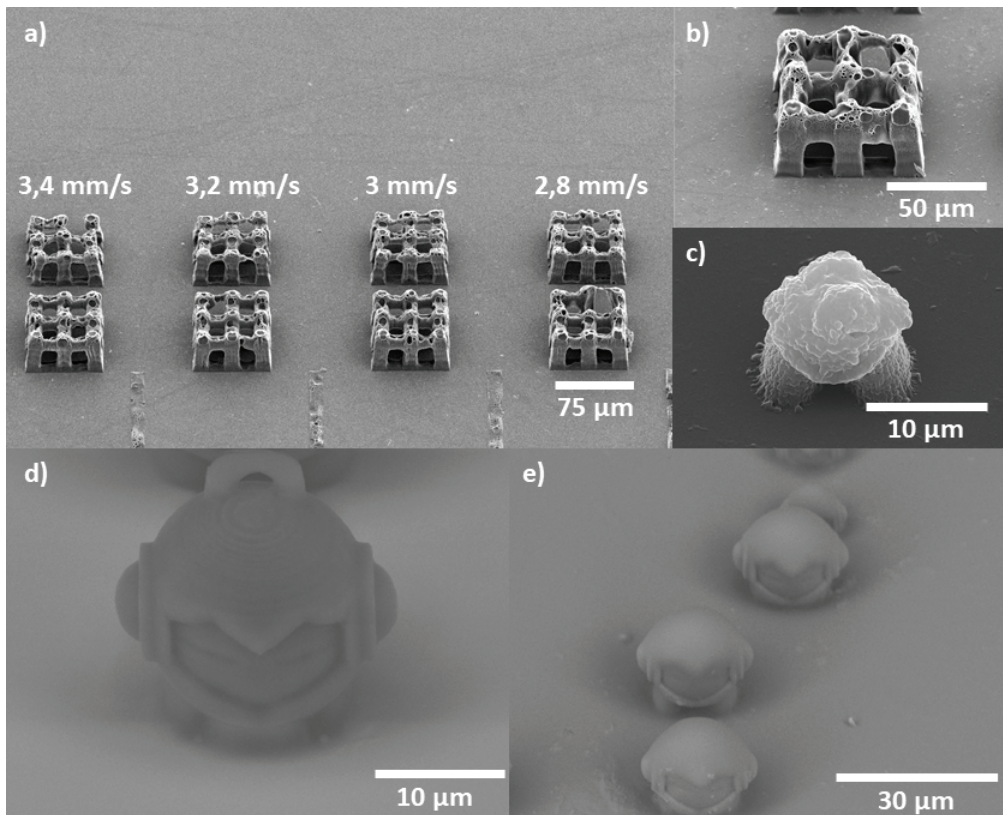
4 pav. (a) – 75 × 75 μm^2 dydžio struktūros iš **B4** dervos: v kinta nuo 2,8 iki 3,4 mm/s; (b) – priartinta 75 × 75 μm^2 figūrėlė: v = 1 mm/s; (c) – Marvino figūrėlė iš **B4** dervos: v = 1,8 mm/s; (d) – Marvino figūrėlė iš AESO: v = 1,2 mm/s; (e) – Marvino figūrėlės iš **B4** dervos taikant štampavimo techniką, fotokietinimui naudotas 365 nm bangos ilgio šviesos šaltinis

4.3. Radikalinės bei tiol-Michael fotopolimerizacijų palyginimas ir gautų polimerų antimikrobinių savybių tyrimas

Šis skyrius parašytas remiantis publikuotu straipsniu: *A. Navaruckienė, D. Bridžiuvienė, V. Raudonienė, E. Rainosalo, J. Ostrauskaitė. Influence of vanillin acrylate-based resin composition on resin photocuring kinetics and antimicrobial properties of the resulting polymers. Materials. 2021, 14 (3), 653* [42]. *JIF: 3.748. Indėlis: 0,200.*

Vanilino dariniai buvo pritaikyti fotokietinamose sistemose naudojant komonomerus ir jų nenaudojant, kaip buvo aprašyta 4.1 ir 4.2 poskyriuose. Šio darbo tikslas – palyginti vanilino fragmentų turinčius homopolimerus su kopolimerais. Siekiant nustatyti dervos sudėties (vanilino darinio, tiolio bei jo kiekio, fotoiniciatoriaus bei jo kiekio ir tirpiklio) įtaką fotokietėjimo kinetikai ir gautų polimerų savybėms buvo sukurta dvidešimt viena skirtingos sudėties derva (3 lentelė). Šiam tyrimui pasirinkti VDM arba VD su arba be BDT ir

fotoiniciatoriumi fenil-bis(2,4,6-trimetilbenzoil)fosfino oksidu (BAPO) (5 paveikslas).
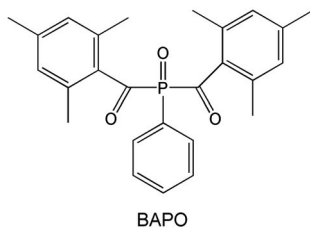
BAPO

5 pav. Fenil-bis(2,4,6-trimetilbenzoil)fosfino oksido (BAPO) struktūrinė formulė

3 lentelė. Dervų **C1**–**C21** sudėtis

Derva	Vanilino darinys	Vanilino darinio kiekis, mol	BDT kiekis, mol	Tirpiklis	BAPO kiekis, mol.%
C1	VD	1	1	–	1
C2	VD	1	1	DCM	1
C3	VD	1	–	–	1
C4	VD	1	–	DCM	1
C5	VDM	1	1	DCM	1
C6	VDM	1	–	DCM	1
C7	VD	1	1	–	3
C8	VD	1	1	DCM	3
C9	VD	1	–	–	3
C10	VD	1	–	DCM	3
C11	VDM	1	1	DCM	3
C12	VDM	1	–	DCM	3
C13	VD	1	1	–	5
C14	VD	1	1	DCM	5
C15	VD	1	–	–	5
C16	VD	1	–	DCM	5
C17	VDM	1	1	DCM	5
C18	VDM	1	–	DCM	5
C19	VD	1	0,5	–	3
C20	VD	1	0,5	DCM	3
C21	VDM	1	0,5	DCM	3

Siekiant nustatyti optimalų fotoiniciatoriaus kiekį, buvo paruošta dervų serija su 1, 3 ir 5 mol.% BAPO (6 paveikslas). Nustatyta, jog naudojant 3 mol.% BAPO fotokietėjimo greitis yra didesnis arba panašus į dervų, paruoštų su 1 mol.% BAPO.

Dervos su 5 mol.% BAPO polimerizavosi greičiau, bet gautuose polimeruose buvo pastebėta neištirpusių BAPO dalelių. Įvertinus šiuos rezultatus, nuspręsta tolimesniems tyrimams naudoti 3 mol.% fotoiniciatoriaus. Nustatyta, jog dervoje naudojant tirpiklį, lėtėja fotopolimerizacija ir gaunami minkštesni polimerai. Pridėjus tirpiklio į VD dervą t_{gel} padidėjo nuo 7,0 s iki 10,0 s, o G' sumažėjo nuo 12,7 MPa iki 12,0 MPa. Minkštesni polimerai gauti ir naudojant tiolį, tačiau, priešingai nei tirpiklio atveju, fotokietėjimas greitėjo. Pavyzdžiui, pridėjus BDT į VD dervą standumas sumažėjo nuo 12,7 MPa iki 1,57 MPa, o t_{gel} sumažėjo nuo 7,0 s iki 3,6 s. Siekiant geriau įvertinti tiolio įtaką fotokietėjimui, buvo paruoštos trys dervos su nestechiometriniu tiolio ir akrilgrupių santykiu. Šių dervų fotopolimerizacijos metu vyko dvigubasis kietinimas, sujungiantis tiol-Michael ir radikalinės polimerizacijos mechanizmus. Gauti polimerai buvo standesni nei tiol-Michael metodu gautieji, tačiau fotopolimerizacijos greitis buvo kiek mažesnis. Pavyzdžiui, VDM polimerai su 0,5 mol BDT pasiekė t_{gel} po 5,3 s, o jų standumas buvo 15,2 MPa, palyginimui, VDM polimerai su 1 mol BDT pasiekė t_{gel} po 3,6 s, o jų standumas buvo 2,14 MPa. Atrinktų dervų (su 3 mol.% BAPO) reologinės charakteristikos buvo palygintos su komercinių dervų, skirtų optiniam trimačiam (3D) spausdinimui PR48 ($t_{gel} = 6,0$ s, $G' = 21,4$ MPa), ir *FormLabs Clear FL6PCL02* ($t_{gel} = 6,0$ s, $G' = 15,2$ MPa) savybėmis. Nustatyta, jog atrinktų dervų su vanilino junginiais fotokietėjimo greitis labai panašus į komercinių, tačiau gauti polimerai yra kiek minkštesni.
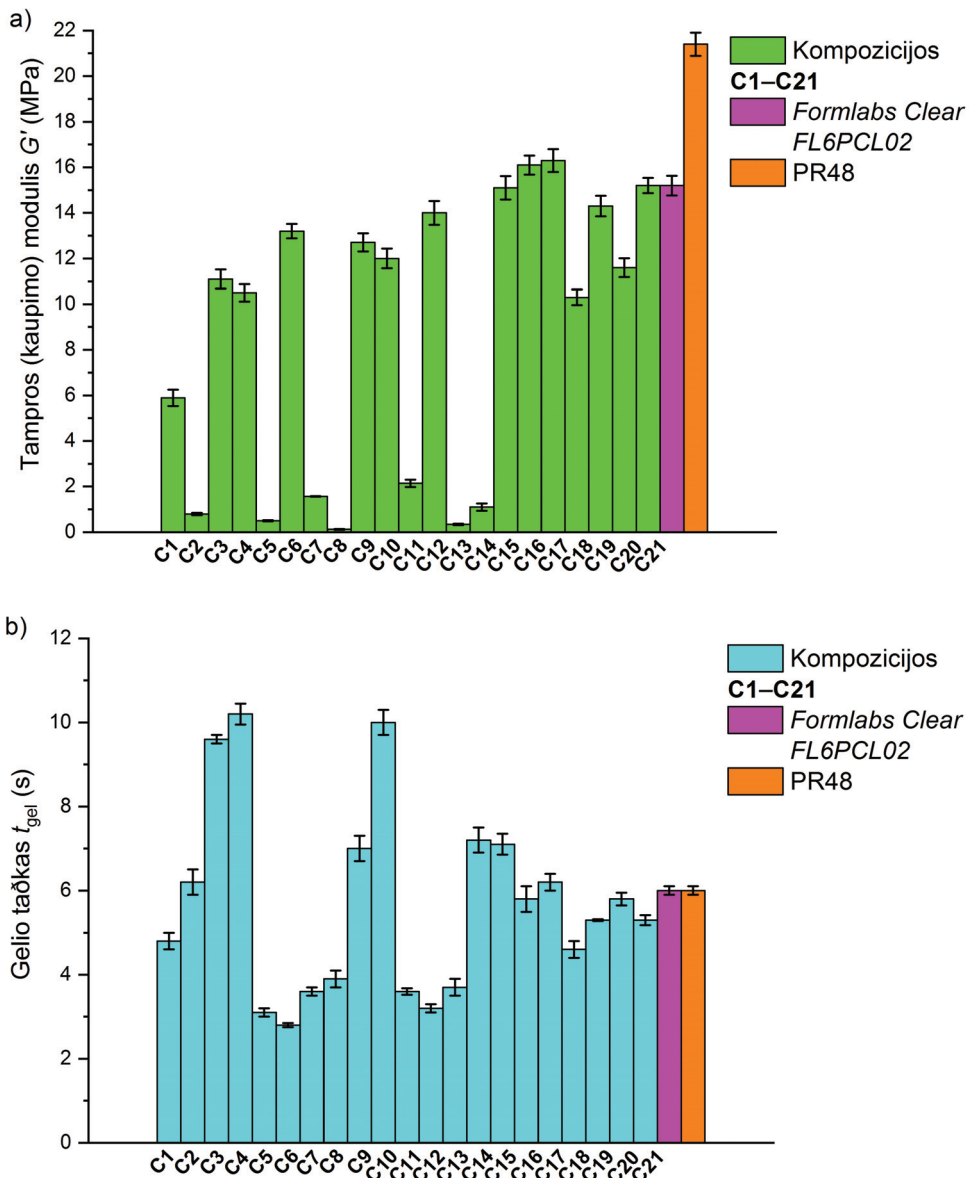
6 pav. Kompozicijų **C1–C21**, PR48 bei *Formlabs Clear FL6PCL02* tampros (kaupimo) modulio (a) ir gelio taško (b) vertės

4.4. Dvigubojo kietinimo fotopolimerų su vanilino akrilatų fragmentais sintezė ir savybių tyrimas

Šis skyrius parašytas remiantis publikuotu straipsniu: *A. Navaruckienė, D. Bridžiuvienė, V. Raudonienė, E. Rainosalo, J. Ostrauskaitė. Vanillin acrylate-*

based thermo-responsive shape memory antimicrobial photopolymers. Express polymer letters. 2022, 16 (3), 279–295 [43]. *JIF: 3.952. Indėlis: 0,200.*

Tiolio kiekio pokytis kompozicijose pakeitė polimerų fotokietinimo kinetiką ir gautų polimerų savybes, kaip buvo aprašyta 4.3 poskyryje. Šio tyrimo tikslas – įvertinti vanilino darinio bei komonomero BDT kiekio įtaką fotokietinimo kinetikai ir gautų polimerų savybėms. Šiam tikslui pasiekti sukurtos šešios kompozicijos. Trys komerciniai vanilino dariniai, vanilino hidroksipropano dimetakrilatas (VHDM), VDM ir VD buvo išbandyti dvigubojo kietinimo sistemose su BDT ir fotoiniciatoriumi TPOL (7 paveikslas).
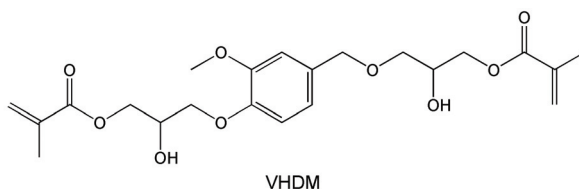
**7 pav.** Vanilino hidroksipropano dimetakrilato (VHDM) struktūrinė formulė

Kompozicijų sudėtis pateikta 4 lentelėje. Šioms kompozicijoms priskirti kodai **D1**–**D6,** kurie atitinka straipsnio kodus **C1**–**C6**. Skirtingas tio- ir akrilgrupių santykis buvo pasirinktas siekiant pakeisti gautų polimerų savybes. Dvigubojo kietinimo proceso metu lygiagrečiai vyksta dvi polimerizacijos reakcijos, tiolio-akrilato fotopolimerizacija ir akrilato homopolimerizacija. Sumažinus tiolio ir akrilgrupių santykį nuo 1:1 iki 1:0,5, akrilatų homopolimerizacija tampa dominuojančia reakcija ir gautų polimerų savybės pasikeičia.

4 lentelė. Dervų **D1**–**D6** sudėtis

Derva	Vanilino darinys	Vanilino darinio kiekis, mol	1,3-benzenditiolio kiekis, mol	Fotoiniciatoriaus TPOL kiekis, mol.%	Tirpiklis
D1	VD	1	1	3	–
D2	VD	1	0,5	3	–
D3	VDM	1	1	3	THF
D4	VDM	1	0,5	3	THF
D5	VHDM	1	1	3	–
D6	VHDM	1	0,5	3	–

G', t_{gel} ir susitraukimo vertės pateiktos 8 paveiksle. Visais atvejais fotokietėjimas vyko greičiau ir gauti standesni polimerai, kai buvo naudojamas mažesnis BDT kiekis ir dominavo akrilatų homopolimerizacija. Sumažinus tiolio kiekį nuo 1 mol iki 0,5 mol, VD dervų fotokietėjimo greitis padidėjo nuo 6,2 s iki 4,8 s, o gautų polimerų standumas – nuo 8,89 MPa iki 11,4 MPa. Tiolio kiekio

sumažinimas taip pat padidino polimerų susitraukimą 4 % dėl gerai žinomo akrilatų polinkio trauktis polimerizacijos metu [44].
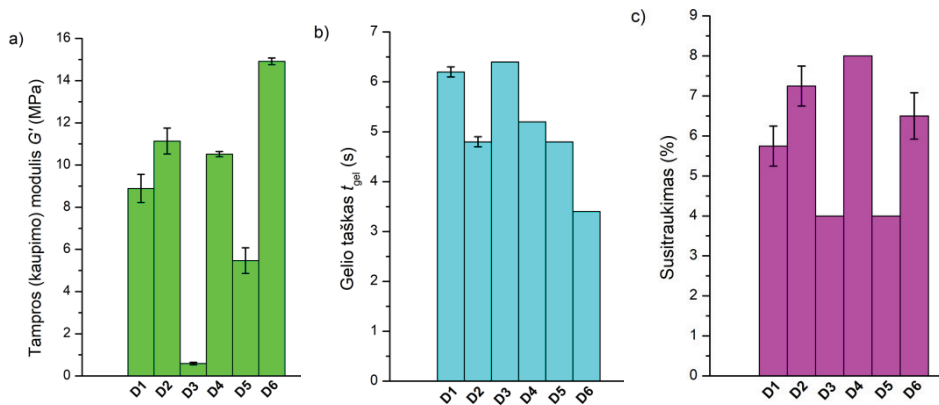
8 pav. Kompozicijų **D1**–**D6** tampros (kaupimo) modulio (a), gelio taško (b) ir susitraukimo (c) vertės

Siekiant ištirti polimerų **D1**–**D6** mechanines savybes buvo atliktas tempimo testas. Mažesnės Jungo modulio ir didesnės ištįsos tempiant vertės buvo gautos polimerų, kurie buvo paruošti naudojant 1 mol BDT (1,4–3,5 MPa ir 19,0–119,7 %) lyginant su polimerais, paruoštais naudojant 0,5 mol BDT (3952,3–11339,4 MPa ir 6,8–12,3 %). Mažiausios Jungo modulio ir ištįsos tempiant vertės buvo gautos polimerų su VDM fragmentais. Tai lėmė tirpiklis, dėl kurio fotopolimerizacijos metu susiformavo linijiniai ar šakoti polimero fragmentai [45]. VHDM polimerai pasižymėjo didžiausiomis Jungo modulio ir ištįsos tempiant vertėmis. Tai lėmė ilgų VHDM grandinių fragmentai, susidarę fotopolimerizacijos metu.

Visi polimerai su vanilino fragmentais pasižymėjo terminio atsako formos atminties savybėmis. Stiklėjimo temperatūra lėmė jų sugebėjimą pakeisti nuolatinę formą į laikinąją ir ją išlaikyti esant tinkamai temperatūrai. Polimero **D6** ($T_g = 40$ °C) formos atminties savybių tyrimo schema pateikta 9 paveiksle. Polimero bandinys buvo pakaitintas iki temperatūros, didesnės nei jo stiklėjimo temperatūra (iki 60 °C) ir deformuotas į norimą formą (šiuo atveju spiralę). Po deformavimo bandinys buvo atvėsintas iki temperatūros, mažesnės už jo T_g (iki 25 °C). Šis procesas vadinamas terminiu programavimu. Tokioje temperatūroje bandinys galėjo išlaikyti nekintančią laikinąją formą neribotą laikotarpį. Dar kartą pakaitinus polimerą iki 60 °C, jis akimirksniu grįžo į savo pradinę, pastoviąją formą, taip parodydamas, kad turi formos atminties savybes. Visi šeši bandiniai su vanilino fragmentais pasižymėjo tokiomis pačiomis savybėmis.
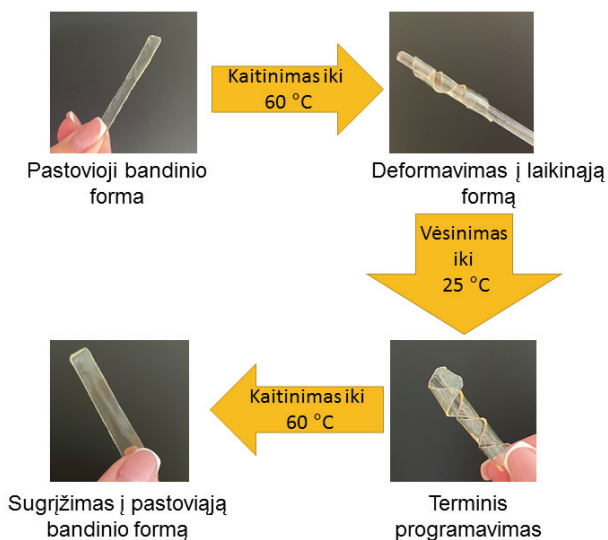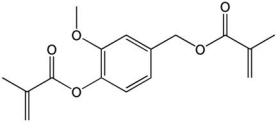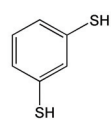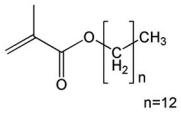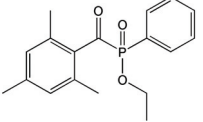
9 pav. Polimero **D6** formos atminties savybių schema

4.5. Vanilino dimetakrilato bei tridecilmetakrilato formos atminties fotopolimerų sintezė ir savybių tyrimas

Šis skyrius parašytas remiantis publikuotu straipsniu: *J. Jaras, A. Navaruckienė, E. Skliutas, J. Jeršovaitė, M. Malinauskas, J. Ostrauskaitė. Thermo-responsive shape memory vanillin-based photopolymers for microtransfer molding. Polymers. 2022, 14 (12), 2460* [46]. *JIF: 4.967. Indėlis: 0,166.*

Pagrindinis monomero VDM trūkumas atliekant polimerų sintezę buvo tirpiklio poreikis, kaip aprašyta 4.4 poskyryje. Siekiant pašalinti šį trūkumą tridecilmetakrilatas (C13-MA) buvo pasirinktas kaip komonomeras, kuris taip pat veikia ir kaip tirpiklis. Siekiant sukurti tinkamą kompoziciją µTM technologijai, VDM buvo sumaišytas su įvairiais kiekiais C13-MA ir BDT, sukurta dvylika kompozicijų, kurių sudėtis pateikta 5 lentelėje. Dervoms buvo suteikti kodai **E1**–**E12**, kurie atitinka straipsnio kodus **C1**–**C12**. VDM kiekis buvo išlaikomas pastovus, C13-MA kiekį didinant nuo 1,5 mol iki 4,5 mol, o BDT kiekį mažinant nuo 1 mol iki 0,25 mol. Kaip buvo aprašoma 4.4 poskyryje, dvigubojo kietinimo metu vyksta dvi reakcijos, tiolio-akrilato polimerizacija ir akrilato homopolimerizacija. Siekiant gauti specifinių savybių polimerus šios reakcijos buvo valdomos, keičiant C13-MA ir BDT kiekius.

5 lentelė. Dervų **E1**–**E12** sudėtis

Derva	VDM kiekis, mol	BDT kiekis, mol	C13-MA kiekis, mol	TPOL kiekis, mol.%
E1	1	1	1,5	3
E2	1	0,75	1,5	3
E3	1	0,5	1,5	3
E4	1	0,25	1,5	3
E5	1	1	3	3
E6	1	0,75	3	3
E7	1	0,5	3	3
E8	1	0,25	3	3
E9	1	1	4,5	3
E10	1	0,75	4,5	3
E11	1	0,5	4,5	3
E12	1	0,25	4,5	3

Tyrimo metu buvo nustatyta, jog C13-MA lėtina fotopolimerizaciją ir didinant jo kiekį gaunami minkštesni polimerai (10 paveikslas). Pavyzdžiui, didinant C13-MA kiekį nuo 1,5 mol iki 4,5 mol, gautų polimerų standumas sumažėja nuo 17,343 MPa (**E4**) iki 2,930 MPa (**E12**). Panašūs rezultatai gauti ir didant BDT kiekį, G' vertė sumažėjo nuo 10,148 MPa (**E8**) iki 0,031 MPa (**E5**) padidinus tiolio kiekį nuo 0,25 mol iki 1 mol. Nors lėtino fotopolimerizacijos procesą ir minkštino polimerus, BDT taip pat mažino polimerų susitraukimą. Padidinus BDT kiekį nuo 0,25 mol iki 1 mol, susitraukimas sumažėjo nuo 10 % (**E12**) iki 1 % (**E9**).
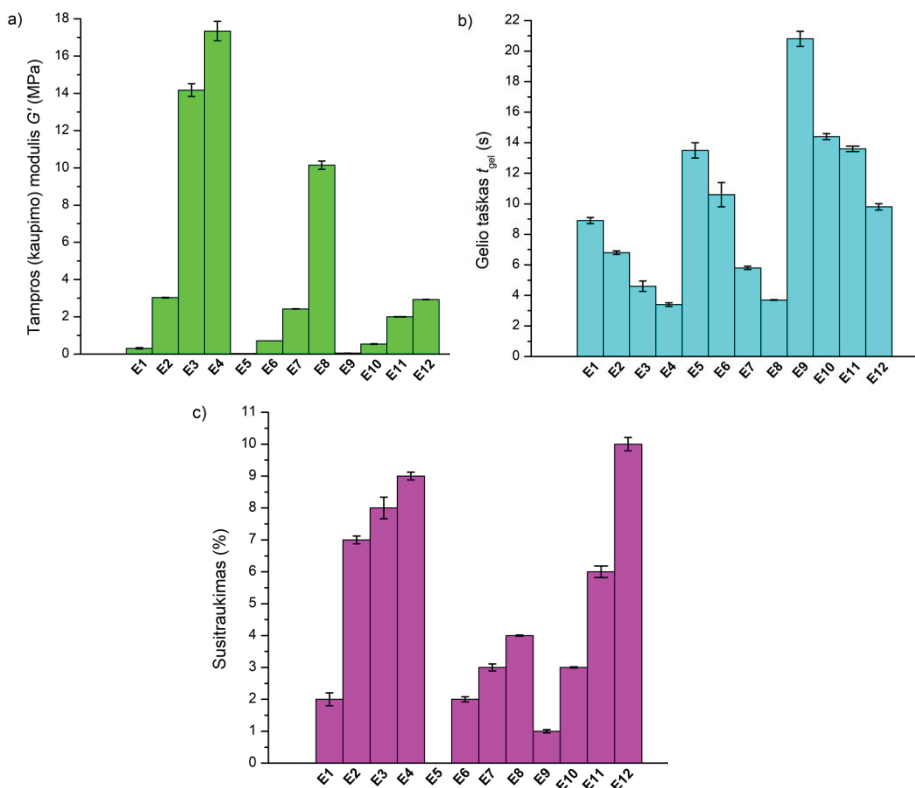
10 pav. Bandinių **E1–E12** tampros (kaupimo) modulio (a), gelio taško (b) ir susitraukimo (c) vertės

Polimerų **E1**, **E2**, **E5** ir **E9** mechaninių savybių ištirti nepavyko, nes jie buvo per minkšti. Didžiausiomis Jungo modulio ir mažiausiomis ištįsos tempiant vertėmis pasižymėjo **E4** polimeras (60,05 MPa ir 5,47 %), kuris buvo paruoštas naudojant mažiausius kiekius C13-MA ir BDT. Nustatyta, jog BDT kiekio padidinimas (polimeras **E3**) padidina pailgėjimo tempiant ir sumažina polimerų Jungo modulio vertes (12,44 MPa ir 17,3 %). Tai įvyko dėl lanksčių tioeterio ryšių, kurie leidžia polimerams tįsti tempimo metu. Panašų efektą suteikė ir C13-MA kiekio didinimas. Nustatyta, jog Jungo modulio vertė sumažėjo nuo 60,05 MPa (polimeras **E4** su 1,5 mol C13-MA) iki 5,53 MPa (polimeras **E12** su 4,5 mol C13-MA), o ištįsa tempiant padidėjo nuo 5,47 % (polimeras **E4**) iki 8,38 % (polimeras **E12**). Tai lėmė ilga C13-MA anglies atomų grandinė.

Visi 12 polimerų pasižymėjo terminio atsako formos atminties savybėmis. Kaip jau buvo paaiškinta 4.4 poskyryje, siekiant pakeisti ir užfiksuoti polimerų bandinių formą jie turi būti pakaitinami virš stiklėjimo temperatūros, deformuojami į laikinąją formą ir vėl atšaldomi iki temperatūros, mažesnės už jų T_g. Vėl pakaitinus polimerų bandinius virš T_g vertės jie akimirksniu grįžta į pastoviąją formą. Polimero **E8** formos atminties savybių schema pateikta 11 paveiksle. Svarstis buvo

naudojamas siekiant parodyti, jog polimeras **E8** yra tvirta medžiaga, jo gebėjimui sugrįžti į pastoviąją formą svarstis įtakos neturi.
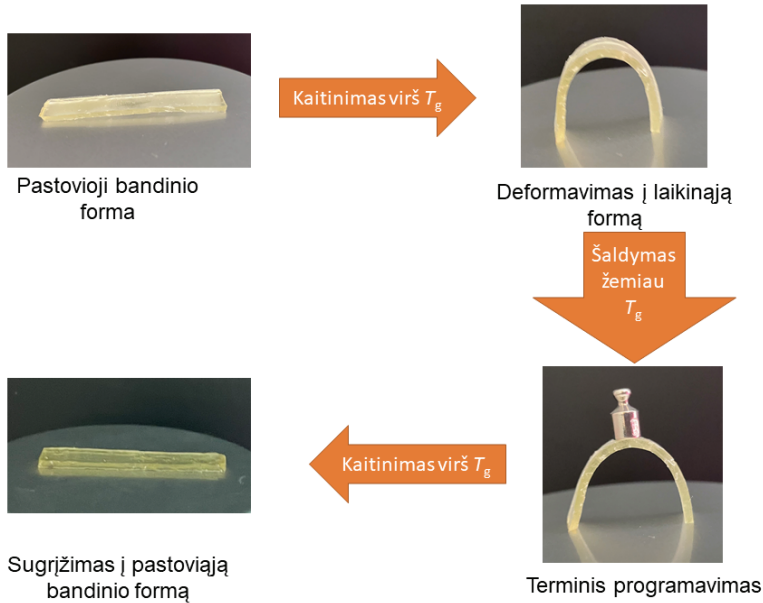
11 pav. Polimero **E8** formos atminties savybių schema

Dvi dervos su vanilino junginiais, **E1** (formuojanti minkštus polimerus) ir **E8** (formuojanti standžius polimerus), buvo atrinktos µTM technologijai. Bandymo rezultatai pateikti 12 paveiksle: (a) dalyje matoma optinio trimačio (3D) spausdinimo būdu suformuota USAF šablono nuotrauka, pagal kurį buvo pagaminta polidimetilsiloksano (PDMS) štampavimo forma (b); (c) ir (d) dalyse matomos iš polimerų **E1** ir **E8** suformuotų replikų nuotraukos. Abi dervos atkartojo unikalias šablono savybes (formas, raides, numerius ir linijas). Abi dervos gali būti naudojamos µTM technologijoje.


12 pav. µTM rezultatai: (a) išspausdinto 1951 USAF šablono nuotrauka; (b) PDMS štampavimo formos nuotrauka; (c) ir (d) **E1** ir **E8** dervų replikų nuotraukos. Brūkšniai nuotraukose atitinka 5 mm

4.6. Vanilino dimetakrilato bei akrilinto epoksidinto sojų aliejaus dvigubojo kietinimo fotopolimerų sintezė ir savybių tyrimas

Šis skyrius parengtas remiantis publikuotu straipsniu: *V. Šereikaitė, A. Navaruckienė, J. Jaras, E. Skliutas, D. Ladika, D. Gray, M. Malinauskas, V. Talačka, J. Ostrauskaitė. Functionalized soybean oil- and vanillin-based dual cure photopolymerizable system for light-based 3D structuring. Polymers. 2022, 14, 5361* [48]. *JIF: 4.967. Indėlis: 0,111.*

Visos penkios polimerų serijos, aprašytos 4.1–4.5 poskyriuose, buvo tinkamos mikroįspaudimo litografijai, tačiau nė viena iš jų netiko optiniam trimačiam (3D) spausdinimui. Atsižvelgus į praėjusių tyrimų rezultatus ir atliktą literatūros analizę buvo sukurta nauja kompozicija **VS**, sudaryta iš 3 mol.% AESO, 1 mol VDM, 0,25 mol pentaeritritoltetrakis(3-merkaptopropionato (PETMP), 2,5 mol % TPO ir 0,08 mol % UVB (13 paveikslas). AESO buvo parinktas kaip komonomeras VDM siekiant padidinti polimero gamtinės anglies kiekį (BRC), sumažinti polimerų kainą ir pritaikyti polimerus optiniam trimačiam (3D) spausdinimui. Apskaičiuotas polimero **VS** BRC buvo 76,45 %.
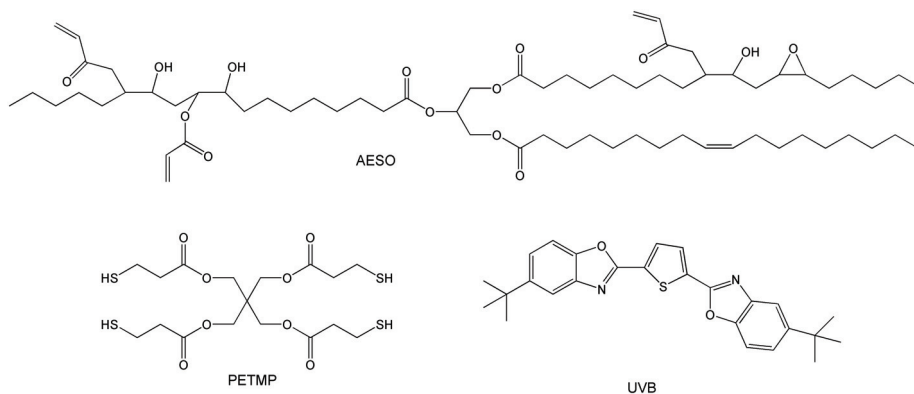
13 pav. Akrilinto epoksidinto sojų aliejaus (AESO), pentaeritritoltetrakis(3-merkaptopropionato) (PETMP) ir 2,5-bis(5-*tret*-butilbenzoksazol-2-il)tiofeno (UVB) struktūrinės formulės

AESO buvo parinktas kaip pagrindinis dervos komponentas dėl tinkamumo optiniam trimačiam (3D) spausdinimui ir gamtinės kilmės. Gryno AESO polimerai yra trapūs, todėl VDM buvo parinktas siekiant pagerinti AESO termines ir mechanines savybes [16]. PETMP buvo parinktas siekiant padidinti gauto polimero lankstumą ir suteikti jam formos atminties savybes [49]. Siekiant gauti mechaniškai stipresnius polimerus buvo nuspręsta akrilatų homopolimerizaciją taikyti kaip dominuojančią reakciją. Dėl šios priežasties buvo pasirinktas nestechiometrinis tio- ir akrilgrupių santykis. Apibendrinta komponentų įtaka polimero charakteristikoms pateikta 14 paveiksle.
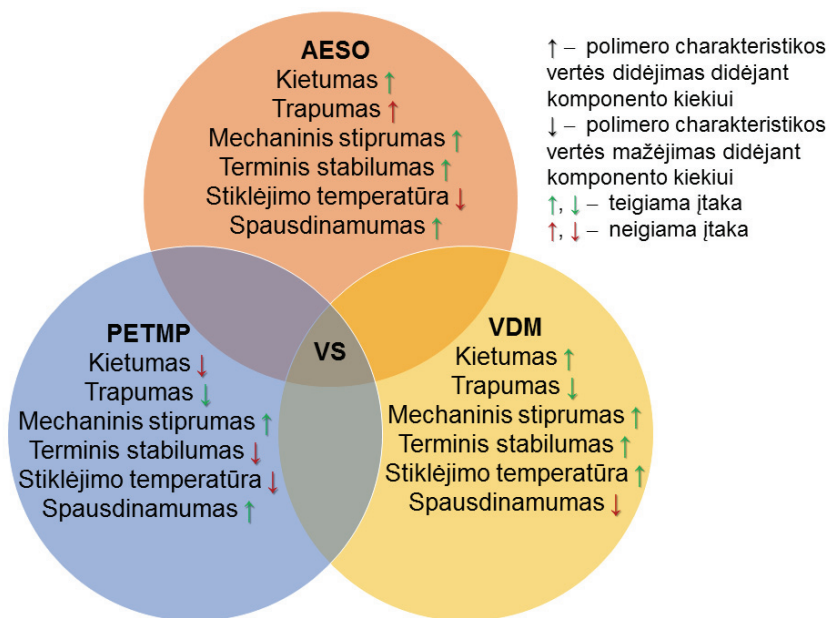
14 pav. Komponento įtakos polimero **VS** charakteristikoms schema

Fotoreometrijos metodu buvo nustatyta, jog polimero **VS** standumas (317,66 MPa) yra net 20 kartų didesnis nei vanilino dimetakrilato ir tiolio polimerų [43]. Ši derva pasiekė gelio tašką vos per 1,5 s be indukcijos periodo. Tokie rezultatai parodo, jog **VS** derva yra tinkama optiniam trimačiam (3D) spausdinimui.

Polimeras **VS** pasižymėjo puikiomis mechaninėmis savybėmis. Polimero Jungo modulio vertė siekė 4753,1 MPa, o ištįsa tempiant buvo 4,72 %. Šios vertės parodo, jog polimeras **VS** yra standi medžiaga.

Derva **VS** buvo išbandyta SLA trimačio (3D) spausdinimo technologijoje. **VS** atkartojo net smulkiausias maketo detales išlaikydama lygų paviršių. 15 paveiksle pateiktos išspausdintos „AmeraLabs Miesto" nuotraukos.
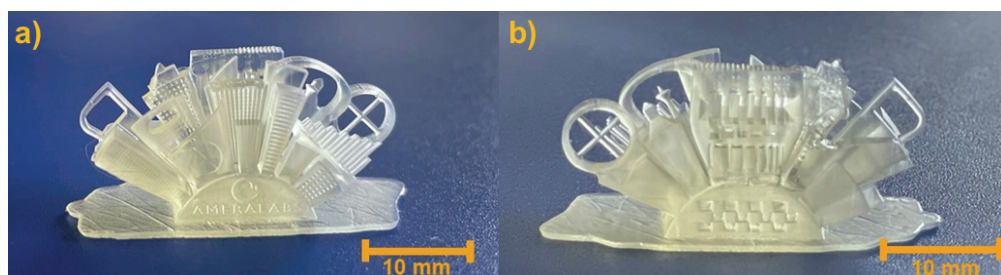
15 pav. Išspausdintos **VS** polimero struktūros priekinės (a) ir galinės (b) pusės nuotraukos

Pagrindiniai spausdinimo proceso trukdžiai naudojant **VS** dervą buvo gana didelė dervos klampa, kurią lėmė AESO naudojimas kompozicijoje ir gana lėtas spausdinimo procesas.

4.7. Pakopinio bei vienalaikio dvigubojo kietinimo sistemų palyginimas ir gautų polimerų savybių tyrimas

Šis skyrius parašytas remiantis publikuotu straipsniu: *G. Motiekaitytė, A. Navaruckienė, V. Raudonienė, D. Bridžiuvienė, J. Jaras, K. Kantminienė, J. Ostrauskaitė. Antimicrobial dual-cured photopolymers of vanillin alcohol diglycidyl ether and glycerol dimethacrylate. Journal of applied polymer science. 2023, 140 (2), e53289* [50]. *JIF: 3.057. Indėlis: 0,142.*

Akrilatai su vanilino fragmentais parodė puikias panaudojimo galimybes atliekant polimerų sintezę ir taikant dvigubojo kietinimo procesą, kaip buvo aprašyta 4.1–4.6 poskyriuose. Vanilino alkoholio diglicidileteris (VDGE) buvo pasirinktas kaip epoksigrupes turintis monomeras siekiant nustatyti jų tinkamumą dvigubojo kietinimo procese ir kaip jie keičia polimerų savybes. Glicerolio dimetakrilatas (GDMK) buvo parinktas kaip komonomeras. Du fotoiniciatoriai, BAPO ir triarilsulfonio heksafluoro fosfatų mišinys (TASHFF) buvo naudoti šiame tyrime (16 paveikslas). Dervoms buvo suteikti kodai **G1**–**G3**, kurie atitinka straipsnyje naudotus kodus **C1**–**C3**. Kompozicijų sudėtis pateikta 6 lentelėje. Žvaigždutė (*) šalia junginio kodo parodo, kad buvo taikomas pakopinis fotokietinimas.
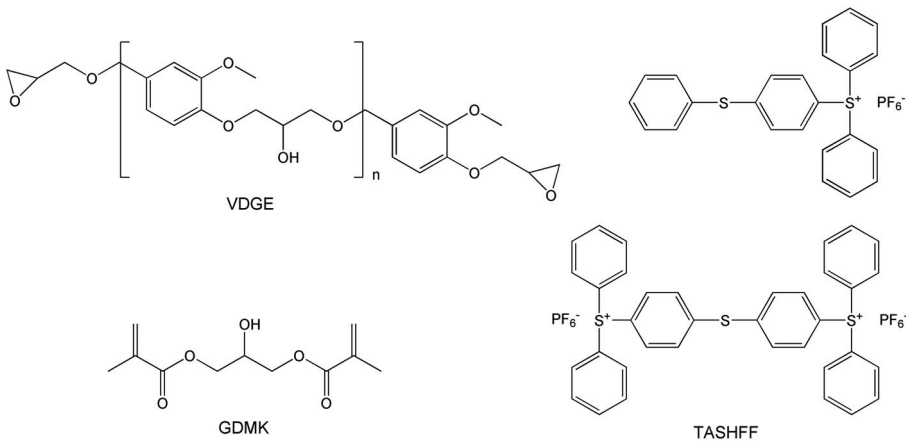
16 pav. Vanilino alkoholio diglicidileterio, $n = 0{,}0$–$0{,}2$ (VDGE), glicerolio dimetakrilato (GDMK) ir triarilsulfonio heksafluoro fosfatų mišinio (TASHFF) struktūrinės formulės

Derva	VDGE kiekis, mol	GDMK kiekis, mol	TASHFF kiekis, mol %	BAPO kiekis, mol %	DCM kiekis, mol
G1	1	0,5	3	3	0,4
G2	1	1	3	3	0,4
G3	0,5	1	3	3	0,2
VDGE	1	0	3	0	0,4
GDMK	0	1	0	3	0

Kietėjimo kinetikai ištirti buvo taikomas fotoreometrijos metodas. Dvigubasis kietinimas buvo išbandytas dviem būdais, kaip vienalaikis ir pakopinis kietinimas. Pakopinio kietinimo metu radikalinės ir katijoninės fotopolimerizacijų atskyrimui buvo naudojamas šviesos filtras. Pirmosios pakopos metu, naudojant šviesos filtrą, buvo inicijuojama radikalinė fotopolimerizacija. Jai įvykus, filtras buvo pašalintas ir inicijuota katijoninė fotopolimerizacija. Gauti rezultatai pateikti 17 paveiksle. Didžiausias skirtumas tarp standumo po pirmosios ir antrosios pakopos buvo pastebėtas **G1*** kompozicijoje. Tai lėmė kompozicijoje esantis didesnis nei kitose dervose VDGE kiekis, kuris polimerizuojamas katijoninės fotopolimerizacijos būdu. Nustatyta, jog didinant GDMK kiekį kompozicijoje gaunami standesni polimerai ir fotopolimerizacija vyksta greičiau.
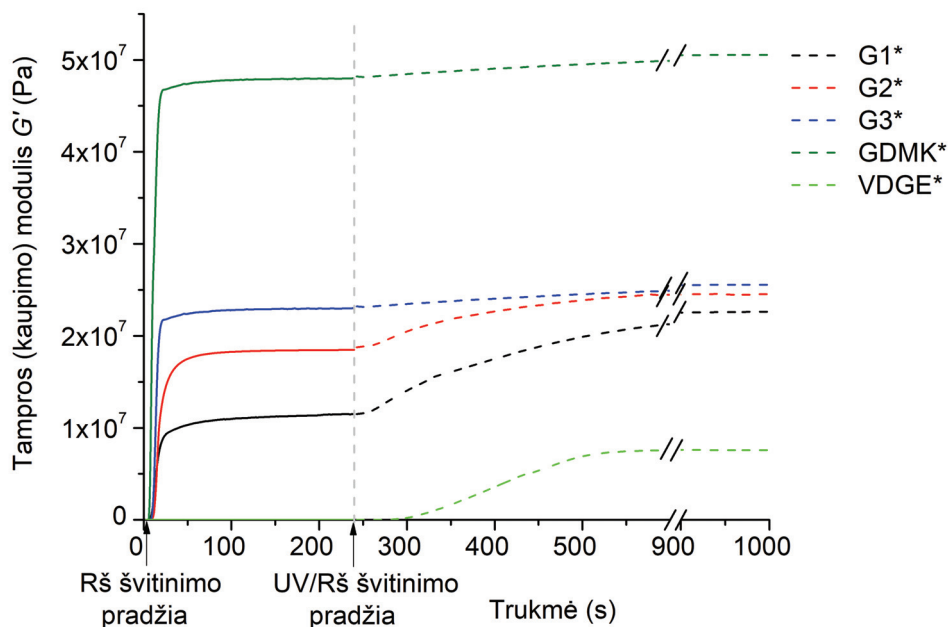
17 pav. Dervų tampros modulio G' priklausomybė nuo švitinimo trukmės (pakopinis kietinimas). Ištisinė linija – bangos ilgis 400–450 nm, punktyrinė linija – bangos ilgis 250–450 nm

Vienalaikio kietinimo metu abi fotopolimerizacijos reakcijos prasidėjo lygiagrečiai. Rezultatai pateikti 18 paveiksle. Šiuo atveju visų dervų fotokietėjimo greitis buvo artimas, jų t_{gel} buvo tarp 12,0–12,5 s. Polimeras **G2** buvo kiečiausias iš visų polimerų su vanilino fragmentais, tačiau jo standumas buvo labai artimas polimero **G3** standumui (28,23 MPa ir 27,51 MPa). Kaip ir pakopinio kietinimo metu, minkščiausias buvo polimeras **G1** (17,97 MPa), kuriame naudotas mažiausias GDMK kiekis. Tolimesniems tyrimams buvo pasirinkti polimerai, gauti vienalaikio kietinimo būdu. Tai lėmė savybes, panašios į pakopinio kietinimo būdu gautų polimerų savybes ir paprastesnis gamybos procesas.
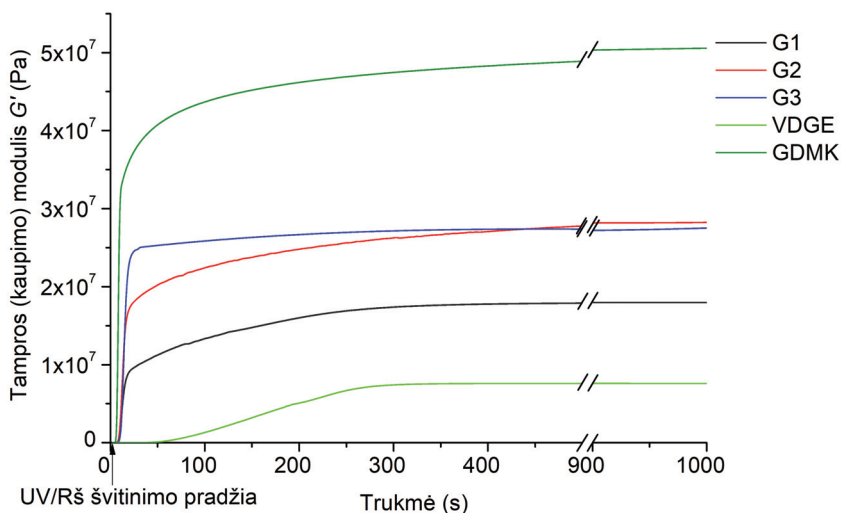
18 pav. Dervų tampros modulio G' priklausomybė nuo švitinimo trukmės (vienalaikis kietinimas)

Nustatyta, jog didėjant VDGE kiekiui dervose, polimerų stiklėjimo temperatūra padidėja nuo 41 °C (**G3**) iki 57 °C (**G1**). Nepaisant to, didinant VDGE kiekį polimerų 10 % masės nuostolių temperatūra sumažėja nuo 274 °C (**G3**) iki 227 °C (**G1**). Šie rezultatai koreliuoja su polimerų reologinėmis charakteristikomis.

Tempimo testas parodė, kad Jungo modulis padidėjo (nuo 76,64 MPa iki 190,71 MPa), o ištįsa tempiant sumažėjo (nuo 4,75 % iki 3,41 %) kai dervose padidėjo GDMK kiekis. Tai lėmė GDMK ir VDGE struktūrų skirtumai. Ilgesnė VDGE molekulė suformuoja ilgesnes polimerines grandines, kurių daugėja didinant VDGE kiekį, ir tai lemia polimerų lankstumą [51].

5. IŠVADOS

1. Sukurtos fotojautrios dervos su vanilino junginiais pasižymi tokiomis ypatybėmis:
   a) standesni polimerai gaunami, kai vanilino diakrilatas naudojamas vietoj vanilino dimetakrilato (tai parodo tampros modulio verčių padidėjimas nuo 0,73 MPa iki 0,81 MPa);
   b) tirpiklio (dichlormetano arba tetrahidrofurano) naudojimas dervose lėtina fotopolimerizaciją ir gaunami polimerai yra mažiau standūs;
   c) 3 mol % yra optimalus fotoiniciatorių fenilbis(2,4,6-trimetilbenzoil)fosfino oksido, difenil(2,4,6-trimetilbenzoil)fosfino oksido ir etil(2,4,6-trimetilbenzoil)fenilfosfinato kiekis, nes gaunamas geriausias kietinimo greičio ir produkto standumo santykis;
   d) dervos su vanilino junginiais yra tinkamos optinio trimačio (3D) spausdinimo technologijai, nes jų fotokietinimo greitis ir gautų polimerų standumas yra panašus į komercinių dervų, skirtų optiniam trimačiam (3D) spausdinimui.

2. Tinkliniai polimerai su vanilino akrilatų fragmentais, gauti fotopolimerizacijos būdu, naudojant ir nenaudojant komonomerų, pasižymi tokiomis savybėmis:
   a) polimerai su vanilino akrilatų fragmentais pasižymi dideliu netirpios frakcijos kiekiu (77–99 %), kuris parodo, jog didžioji dalis produkto yra tinklinės struktūros;
   b) komonomerų (1,3-benzenditiolio ar tridecilmetakrilato) kiekio didinimas dervose sumažina polimerų stiklėjimo temperatūrą ir destrukcijos temperatūrą, esant 10 % masės nuostoliams;
   c) komonomerų 1,3-benzenditiolio, tridecilmetakrilato ar akrilinto epoksidinto sojų aliejaus kiekio didinimas dervose mažina polimerų Jungo modulio vertes ir didina santykinės ištįsos trūkio metu vertes;
   d) polimerai su vanilino ir 1,3-benzenditiolio fragmentais pasižymi terminio atsako formos atminties savybėmis, kurios priklauso nuo jų stiklėjimo temperatūros.

3. Vanilino alkoholio diglicidileterio fotopolimerus galima susintetinti, taikant vienalaikį arba pakopinį dvigubąjį kietinimą:
   a) glicerolio dimetakrilato kiekio padidinimas dervose nuo 0,5 mol iki 1 mol pagreitina fotokietinimą nuo 12,5 s iki 12,0 s, ir polimerų standumas abiejų tipų reakcijose padidėja nuo 17,97 MPa iki 28,23 MPa;
   b) vanilino alkoholio diglicidileterio kiekio padidinimas dervose nuo 0,5 mol iki 1 mol padidina polimerų stiklėjimo temperatūrą nuo 41 °C iki 57 °C ir sumažina destrukcijos temperatūrą, esant 10 % masės nuostoliams, nuo 274 °C iki 227 °C;
   c) fotojautrių sistemų su vanilino junginiais dvigubasis kietinimas yra paprastas būdas gauti didesnio standumo polimerus, nes pakopinio dvigubojo kietinimo metu standumas padidėjo nuo 11,51–23,00 MPa po

pirmo etapo iki 22,63–25,56 MPa po antro etapo, o po vienalaikio dvigubojo kietinimo buvo gauti standesni analogiškos sudėties polimerai (17,97–27,51 MPa).

4. Fotojautrios dervos su vanilino junginiais yra tinkamos naudoti mikroįspaudimo litografijai ir optiniam trimačiam (3D) spausdinimui:

   a) gryno vanilino diakrilato derva ir vanilino dimetakrilato dervos su tridecilmetakrilatu ir 1,3-benzenditioliu yra tinkamos mikroįspaudimo litografijai, nes gali tiksliai atkartoti unikalius šablono požymius (formą, raides, skaičius ir linijas);

   b) fotojautri dvigubojo kietinimo derva, sudaryta iš vanilino dimetakrilato, akrilinto epoksidinto sojų aliejaus ir pentaeritritoltetrakis(3-merkaptopropionato) yra tinkama optinio trimačio (3D) spausdinimo technologijai dėl didelio spausdinimo tikslumo ir gero sluoksnių sukibimo tarpusavyje.

6. REFERENCES

1. ZHANG, C., et al. From plant phenols to novel bio-based polymers. *Progress in Polymer Science*, 2022, vol. 125. pp. 101473.

2. IOANNIDOU, S.F., et. al. Sustainable production of bio-based chemicals and polymers via integrated biomass refining and bioprocessing in a circular bioeconomy context. *Bioresource Technology*, 2020, vol. 307. pp. 123093.

3. THAKUR, S., et. al. Synthesis of Bio-based monomers and polymers using microbes for a sustainable bioeconomy. *Bioresource Technology*, 2022, vol. 344. pp. 126156.

4. YANG, W., et al. Bio-renewable polymers based on lignin-derived phenol monomers: Synthesis, applications, and perspectives. *SusMat*, 2022, vol. 2. pp. 535–568.

5. NOÈ, C., et. al. Cationic photopolymerization of bio-renewable epoxidized monomers. *Progress in Organic Coatings*, 2019. vol. 133. pp. 131–138.

6. HARVEY, B.G., et al. Renewable thermosetting resins and thermoplastics from vanillin. *Green Chemistry*, 2015, vol .17. pp. 1249-1258.

7. KONURAY, O., et.al. State of the Art in Dual-Curing Acrylate Systems. *Polymers*, 2018, vol. 10. pp. 178.

8. LANG, M., et. al. A Review on Modeling Cure Kinetics and Mechanisms of Photopolymerization. *Polymers*, 2022, vol. 14. pp. 2074.

9. SANGERMANO, M., et. al. New Horizons in Cationic Photopolymerization. *Polymers*, 2018, vol. 10. pp. 136.

10. BANERJEE, G., et. al. Vanillin biotechnology: The perspectives and future. *Journal of the Science of Food and Agriculture*, 2019, vol. 99. pp. 499-506.

11. CIRIMINNA, R., et. al. Vanillin: the case for greener production driven by sustainability megatrend. *Chemistry Open*, 2019, vol. 8. pp. 660–667.

12. FACHE, M., et. al. Vanillin, a key-intermediate of biobased polymers. *European Polymer Journal*, 2015, vol. 68. pp. 488–502.

13. HE, B., et. al. Polymerizations of Activated Alkynes. *Progress in Polymer Science*, 2022, vol. 126. pp. 101503.

14. STERNBERG, J., et. al. Green chemistry design in polymers derived from lignin: review and perspective. *Progress in Polymer Science*, 2021, vol. 113. pp. 101344.

15. NEGRELL, C., et. al. From monomer synthesis to polymers with pendant aldehyde groups. *European Polymer Journal*, 2018, vol. 109. pp. 544-563.

16. STANZIONE, J.F., et. al. Vanillin-based resin for use in composite applications. *Green Chemistry*, 2012, vol. 14. pp. 2346-2352.

17. ABDELATY, M., et. al. Poly (N-Isopropyl Acrylamide-Co-Vanillin Acrylate) Dual Responsive Functional Copolymers for Grafting Biomolecules by Schiff's Base Click Reaction. *Open Journal of Organic Polymer Materials*, 2018, vol. 8. pp. 15-32.

18. MEYLEMANS, H., et. al. Synthesis, characterization, and cure chemistry of renewable bis(cyanate) esters derived from 2-methoxy-4-methylphenol. *Biomacromolecules*, 2013, vol. 14. pp. 771-780.

19. FACHE, M., et. al. New vanillin-derived diepoxy monomers for the synthesis of biobase thermosets. *European Polymer Journal*, 2015, vol. 67. pp. 527–538.

20. ZHANG, C., et. al. Renewable polymers prepared from vanillin and its derivatives. *Macromolecular Chemistry and Physics*, 2015, vol. 216. pp. 1816-1822.

21. DAI, M., et. al. Low Dielectric Polymers with High Thermostability Derived from Biobased Vanillin. *ACS Sustainable Chemistry & Engineering,* 2020, vol. 8. pp. 15013-15019.

22. LIGUORI, A. et. al. Photocurable extended vanillin-based resin for mechanically and chemically recyclable, self-healable and digital light processing 3D printable thermosets. *European Polymer Journal*, 2022, vol. 178. pp. 111489.

23. ABDELATY, M.S.A. Environmental functional photo-cross-linked hydrogel bilayer thin films from vanillin (part 2): temperature-responsive layer A, functional, temperature and pH layer B. *Polymer Bulletin*, 2018, vol. 75. pp. 4837–4858.

24. XU, Y., et. al. Photocurable, thermally reprocessable, and chemically recyclable vanillin-based imine thermosets. *ACS Sustainable Chemistry & Engineering,* 2020, vol. 8. pp. 17272-17279.

25. SALMI-MANI, H., et. al. Poly(ethylene terephthalate) films modified by UV-induced surface graft polymerization of vanillin derived monomer for antibacterial activity. *European Polymer Journal*, 2018, vol. 103. pp. 51-58.

26. GONZÁLEZ-CEBALLOS, L., et. al. Metal-free organic polymer for the preparation of a reusable antimicrobial material with real-life application as an absorbent food pad. *Food Packaging and Shelf Life*, 2022, vol. 33. pp. 100910.

27. KUMAR, B., et. al. Recent Research Progress on Lignin-Derived Resins for Natural Fiber Composite Applications. *Polymers*, 2021, vol. 13. pp. 1162.

28. BEI, Y., et. al. Recent progress of biomass based self-healing polymers. *Journal of Applied Polymer Science*, 2022, vol. 139. pp. e51977.

29. JUNG, H., et. al. Review of polymer technologies for improving the recycling and upcycling efficiency of plastic waste. *Chemosphere*, 2023, vol. 320. pp. 138089.

30. RAZA, S., et. al. Recent trends in the development of biomass-based polymers from renewable resources and their environmental applications. *Journal of the Taiwan Institute of Chemical Engineers*, 2020, vol. 115. pp. 293-303.

31. POOJARY, S., et. al. Highly fluorescent materials derived from ortho-vanillin: structural, photophysical electrochemical and theoretical studies. *Journal of Molecular Liquids*, 2019, vol. 275. pp. 792-806.

32. JING, K., et. al. Dynamic optimization of batch free radical polymerization with conditional modeling formulation through the adaptive smoothing strategy. *Computers and chemical engineering*, 2019, vol. 120. pp. 15-29.

33. Sutherland, B.P., et. al. Expanding the Thiol-X Toolbox: Photoinitiation and Materials Application of the Acid-Catalyzed Thiol-ene (ACT) Reaction. *Polymer chemistry*, 2022, vol. 12. pp. 1562-1570.

34. ADAMCHIK, M., et. al. Synthesis of novel glutarimide derivatives *via* the Michael addition of (hetero)aromatic thiols: pronounced effect of sulfur oxidation on

cytotoxicity towards multiple myeloma cell lines. *Mendeleev Communications*, 2023, vol. 33. pp.67-69.

35. MACHADO, T.O., et. al. Thiol-ene polymerisation: A promising technique to obtain novel biomaterials. *European polymer journal*, 2017, vol. 86, pp. 200-215.

36. UCHIYAMA, M., et. al. Cationic RAFT and DT polymerization. *Progress in Polymer Science*, 2022, vol. 124, pp. 101485.

37. MICHAUDEL, Q., et. al. Cationic Polymerization: From Photoinitiator to Photocontrol. *A Journal of the German Chemical Society*, 2017, vol. 56, pp. 9670-9679.

38. GAMARDELLA, F., et. al. Tailor-made thermosets obtained by sequential dual-curing combining isocyanate-thiol and epoxy-thiol click reactions. *Polymer*, 2019, vol. 174, pp. 200-209.

39. NAVARUCKIENĖ, A., et. al. Vanillin-based thiol-ene systems as photoresins for optical 3D printing. *Rapid prototyping journal*, 2020, vol. 26. pp. 402-408.

40. Green, W.A. Industrial Photoinitiators. A Technical Guide, 2010, CRC Press, Taylor and Francis Group, Boca Raton, London, Bew York.

41. NAVARUCKIENĖ, A., et. al. Vanillin acrylate-based resins for optical 3D printing. *Polymers*, 2020, vol. 12. pp. 397.

42. NAVARUCKIENĖ, A., et. al. Influence of vanillin acrylate-based resin composition on resin photocuring kinetics and antimicrobial properties of the resulting polymers. *Materials*, 2021, vol. 14. pp. 653.

43. NAVARUCKIENĖ, A., et. al. Vanillin acrylate-based thermo-responsive shape memory antimicrobial photopolymers. *Express polymer letters*, 2022, vol. 16. pp. 279-295.

44. JIAN, Y., et. al. Volume shrinkage of UV curable coating formulation investigated by real-time laser reflection method. *Journal of Coatings Technology and Research*, 2013, vol. 10. pp. 231–237.

45. VALDEBENITO, A., et. al. Effect of solvent on the free radical polymerization of N,N-dimethylacrylamide. *Polymer International*, 2010, vol. 59. pp. 1246–1251.

46. JARAS, J., et. al. Thermo-responsive shape memory vanillin-based photopolymers for microtransfer molding. *Polymers*, 2022, vol. 14. pp. 2460.

47. ALBESHIR, E.G., et. al. Low-Shrinkage Resin Matrices in Restorative Dentistry-Narrative Review. *Materials*, 2022, vol. 15. pp. 2951.

48. ŠEREIKAITĖ, V., et. al. Functionalized soybean oil- and vanillin-based dual cure photopolymerizable system for light-based 3D structuring. *Polymers*, 2022, vol. 14. pp. 5361.

49. XIE, R., et. al. Glass transition temperature from the chemical structure of conjugated polymers. *Nature Communications*, 2020, vol. 11. pp. 893.

50. MOTIEKAITYTĖ, G., et. al. Antimicrobial dual-cured photopolymers of vanillin alcohol diglycidyl ether and glycerol dimethacrylate. *Journal of applied polymer science*, 2023, vol. 140. pp. e53289.

51. NAIR, D.P., et. al. The Thiol-Michael Addition Click Reaction: A Powerful and Widely Used Tool in Materials Chemistry. *Chemistry of Materials*, 2014, vol. 26. pp. 724.

7. CURRICULUM VITAE

Auksė Navaruckienė

aukse.navaruckiene@ktu.lt

Education:

2010 – 2013	Kaunas "Saulės" gymnasium Secondary school
2013 – 2017	Kaunas University of Technology Chemical engineer, bachelor's degree
2017 – 2019	Kaunas University of Technology Chemical engineer, master's degree
2019 – 2023	Kaunas University of Technology Doctoral studies of Chemical Engineering

Work experience:

2020 03 09 – 2022 12 31	Research Council of Lithuania project no. S-MIP-20-17 junior researcher **Kaunas University of Technology**
2022 05 02 – 2022 05 09	Erasmus+ Traineeship, Junior researcher **University of Upper Alsace, Laboratory of Photochemistry and Macromolecular Engineering (LPIM)**
2021 04 01 – 2021 12 31	INTERREG BSR Program, (ECOLABNET project #R077) junior researcher **Kaunas University of Technology**
2021 01 04 – 2021 03 31	Agency for Science, Innovation and Technology (MITA) project No 01.2.2-MITA-K-702-06-009, junior researscher **Kaunas University of Technology**
2019 04 02 – 2021 03 31	INTERREG BSR Program, (ECOLABNET project #R077) laboratory assistant **Kaunas University of Technology**
2018 10 01 – 2019 04 30	The student research funded by the Lithuanian Science Council project No 09.3.3-LMT-K-712-10-0161 **Kaunas University of Technology**
2018 07 02 – 2018 08 31	The student research funded by the Lithuanian Science Council project No 09.3.3-LMT-K-712 **Kaunas University of Technology**

8. LIST OF PUBLICATIONS

List of publications on the subject of thesis:

1. <u>Navaruckiene, Aukse</u>; Kasetaite, Sigita; Ostrauskaite, Jolita. Vanillin-based thiol-ene systems as photoresins for optical 3D printing // Rapid prototyping journal. Bingley : Emerald. ISSN 1355-2546. eISSN 1758-7670. 2020, vol. 26, iss. 2, p. 402-408. DOI: 10.1108/RPJ-03-2019-0076. IF: 3,095.

2. <u>Navaruckiene, Auksė</u>; Skliutas, Edvinas; Kasetaite, Sigita; Rekštytė, Sima; Raudonienė, Vita; Bridžiuvienė, Danguolė; Malinauskas, Mangirdas; Ostrauskaite, Jolita. Vanillin acrylatebased resins for optical 3D printing // Polymers. Basel : MDPI. ISSN 2073-4360. 2020, vol. 12, iss. 2, art. no. 397, p. 1-14. DOI: 10.3390/polym12020397. IF: 4,329.

3. <u>Navaruckiene, Aukse</u>; Bridziuviene, Danguole; Raudoniene, Vita; Rainosalo, Egidija; Ostrauskaite, Jolita. Influence of vanillin acrylate-based resin composition on resin photocuring kinetics and antimicrobial properties of the resulting polymers // Materials. Basel : MDPI. ISSN 1996-1944. 2021, vol. 14, iss. 3, art. no. 653, p. 1-20. DOI: 10.3390/ma14030653. IF: 3,748.

4. <u>Navaruckiene, Aukse</u>; Bridziuviene, Danguole; Raudoniene, Vita; Rainosalo, Egidija; Ostrauskaite, Jolita. Vanillin acrylate-based thermo-responsive shape memory antimicrobial photopolymers // Express polymer letters. Budapest : Budapest university of technology and economics. ISSN 1788-618X. 2022, vol. 16, iss. 3, p. 279-295. DOI: 10.3144/expresspolymlett.2022.22. IF: 3,952.

5. Jaras, Justinas; <u>Navaruckienė, Auksė</u>; Skliutas, Edvinas; Jeršovaitė, Jurga; Malinauskas, Mangirdas; Ostrauskaitė, Jolita. Thermo-responsive shape memory vanillin-based photopolymers for microtransfer molding // Polymers. Basel : MDPI. ISSN 2073-4360. 2022, vol. 14, iss. 12, art. no. 2460, p. 1-17. DOI: 10.3390/polym14122460. IF: 4,967.

6. Sereikaite, Vilte; <u>Navaruckiene, Aukse</u>; Jaras, Justinas; Skliutas, Edvinas; Ladika, Dimitra; Gray, David; Malinauskas, Mangirdas; Talacka, Vaidas; Ostrauskaite, Jolita. Functionalized soybean oil- and vanillinbased dual cure photopolymerizable system for light-based 3D structuring // Polymers. Basel : MDPI. ISSN 2073-4360. 2022, vol. 14, iss. 24, art. no. 5361, p. 1-14. DOI: 10.3390/polym14245361. IF: 4,967.

7. Motiekaityte, Greta; <u>Navaruckiene, Aukse</u>; Raudoniene, Vita; Bridziuviene, Danguole; Jaras, Justinas; Kantminiene, Kristina; Ostrauskaite, Jolita. Antimicrobial dual-cured photopolymers of vanillin alcohol diglycidyl ether and glycerol dimethacrylate // Journal of applied polymer science. Hoboken, NJ : Wiley. ISSN

List of other publications:

1. Grauzeliene, Sigita; Navaruckiene, Aukse; Skliutas, Edvinas; Malinauskas, Mangirdas; Serra, Angels; Ostrauskaite, Jolita. Vegetable oil-based thiol-ene/thiol-epoxy resins for laser direct writing 3D micro- /nano-lithography // Polymers. Basel : MDPI. ISSN 2073-4360. 2021, vol. 13, iss. 6, art. no. 872, p. 1-15. DOI: 10.3390/polym13060872. IF: 4,967.

2. Jaras, Justinas; Navaruckiene, Aukse; Ostrauskaite, Jolita. Thermoresponsive shape-memory biobased photopolymers of tetrahydrofurfuryl acrylate and tridecyl methacrylate // Materials. Basel : MDPI. ISSN 1996-1944. 2023, vol. 16, iss. 6, art. no. 2156, p. 1-13. DOI: 10.3390/ma16062156. IF: 3,748.

List of conferences:

1. Gineika, Andrius; Baltakys, Kęstutis; Navaruckienė, Auksė; Skliutas, Edvinas; Malinauskas, Mangirdas. Application of synthetic wollastonite for 3D-printed scaffolds // Chemistry and chemical technology: proceedings of international scientific conference, Kaunas, 2022. Kaunas : Kaunas university of technology. ISSN 2538-7359. 2022, p. 82.

2. Navaruckiene, Aukse; Jaras, Justinas; Ostrauskaite, Jolita. Rheological study of vanillin dimethacrylatebased polymers // Chemistry and chemical technology: proceedings of international scientific conference, Kaunas, 2022. Kaunas : Kaunas university of technology. ISSN 2538-7359. 2022, p. 87.

3. Navaruckiene, A.; Jaras, J.; Bridziuviene, D.; Raudoniene, V.; Rainosalo, E.; Ostrauskaite, J. Antimicrobial shape memory vanillin-based polymers // Baltic polymer symposium 2022, Tallinn, Estonia, September 21–23, 2022: programme and abstracts. Tallinn : Tallinn university of technology. 2022, p. 62.

4. Jaras, Justinas; Navaruckiene, Aukse; Skliutas, Edvinas; Jersovaite, Jurga; Malinauskas, Mangirdas; Ostrauskaite, Jolita. Shape memory vanillin-based photocross-linked polymers for microtransfer molding // Baltic polymer symposium 2022, Tallinn, Estonia, September 21–23, 2022: programme and abstracts. Tallinn : Tallinn university of technology. 2022, p. 51.

5. Ostrauskaite, Jolita; Jaras, Justinas; Navaruckiene, Aukse; Grauzeliene, Sigita. Biorenewable polymeric materials for laser 3D meso-scale structuring // MACRO 2022: the 49th world polymer congress, July 17-21 2022, Winnipeg, Canada: book of abstracts. Winnipeg : [s.n.]. 2022, V-ORAL31, p. 310.

6. Ostrauskaite, Jolita; Jaras, Justinas; <u>Navaruckiene, Aukse</u>. Plant-derived polymers for optical 3D printing // 28th PhotoIUPAC, Amsterdam, 17-22 July 2022: book of abstracts. [S.l.] : [s.n.]. 2022, P79, p. 308.

7. Jaras, Justinas; <u>Navaruckienė, Auksė</u>; Skliutas, Edvinas; Jeršovaitė, Jurga; Malinauskas, Mangirdas; Ostrauskaitė, Jolita (temos vadovas). Biorenewable photoresins for nanoimprint lithography // Technorama 2022: Code: innovation: catalogue. Kaunas : KTU. 2022, p. 156-157.

8. <u>Navaruckienė, Auksė</u>; Jaras, Justinas; Bridziuviene, Danguole; Raudoniene, Vita; Rainosalo, Egidija; Ostrauskaitė, Jolita. Vanillin acrylate-based antimicrobial shape memory polymers // Polymers 2022 - New trends in polymer science: health of the planet, health of the people, Turin, Italy, 25 – 27 May 2022: book of abstracts. Basel : MDPI. 2022, A.20, p. 96-97.

9. Ostrauskaite, Jolita; Jaras, Justinas; <u>Navaruckiene, Aukse</u>; Grauzeliene, Sigita. High biorenewable content dual-cured photopolymers // Poly-Char 2022: [Halle | Siegen], May 22-25, 2022: program and abstracts. [S.l.] : [s.n.]. 2022, PEn oral 5, p. 106.

10. Jaras, Justinas; <u>Navaruckiene, Aukse</u>; Ostrauskaite, Jolita. Photorheometrical study of vanillin acrylatebased photoresins // Open readings 2022: 65th international conference for students of physics and natural sciences, March 15-18: abstract book / editors: Š. Mickus, S. Pūkienė, L. Naimovičius. Vilnius : Vilnius university press. 2022, P3-19, p. 229.

11. <u>Navaruckiene, Aukse</u>; Rainosalo, Egidija; Ostrauskaite, Jolita. Vanillin acrylate-based shape memory polymers // Open readings 2022: 65th international conference for students of physics and natural sciences, March 15-18: abstract book / editors: Š. Mickus, S. Pūkienė, L. Naimovičius. Vilnius : Vilnius university press. 2022, P3-4, p. 214.

12. <u>Navaruckiene, Aukse</u>; Motiekaityte, Greta; Pabricaite, Ausrine; Ostrauskaite, Jolita. Vanillin acrylatebased polymers for optical 3D printing // VESPS2021: 6th virtual European symposium of photopolymer science, dedicated to Ewa Andrzejewska: online, June 15 – 17, 2021. Gumpoldskirchen : ChemIT e.U., 2021, PT-40. ISBN 9783950480931. p. 202.

13. <u>Navaruckienė, Auksė</u>; Jaras, Justinas; Bridžiuvienė, Danguolė; Raudonienė, Vita; Ostrauskaitė, Jolita. Vanillin acrylate-based polymers with antibacterial activity // Chemistry and chemical technology: 16th international conference of Lithuanian chemical society, 24 September 2021, Vilnius, Lithuania: book of abstracts. Vilnius : National center for physical sciences and technology. 2021, P111, p. 125.

14. Navaruckiene, Aukse; Bridziuviene, Danguole; Raudoniene, Vita; Rainosalo, Egidija; Ostrauskaite, Jolita. Photorheometric study of vanillin acrylate-based resins and antimicrobial properties of polymers // Proceedings of the green chemistry postgraduate summer school (online/in-person), 4-9 July 2021, Venice, Italy: collection of abstracts / P. Tundo, F. Aricò, A. Visa and M. Hojamberdiev (eds.). Venice : GSSD foundation, 2021. ISBN 9788894553703. p. 183.

15. Navaruckiene, Aukse; Lebedevaite, Migle; Ostrauskaite, Jolita. Real-time photorheometrical study of plant–derived monomer resins // IUPAC-MACRO 2020: the 48th world polymer congress, May 16-20, 2021, Jeju, Korea. [S.l.] : IUPAC. 2021, 4OS8-24, p. 491.

16. Motiekaitytė, Greta; Navaruckienė, Auksė; Ostrauskaitė, Jolita. Vanilino diglicidileterio ir įvairių akrilatų dvigubasis fotokietinimas // Studentų mokslinės konferencijos „Chemija ir cheminė technologija 2021" pranešimų medžiaga: respublikinė studentų mokslinė konferencija, 2021 05 14 / rinkinio sudarytojai: T. Dambrauskas, G. Kručaitė, D. Sinkevičiūtė; Kauno technologijos universitetas. Cheminės technologijos fakultetas. Kaunas : Kauno technologijos universitetas. eISSN 2538-7332. 2021, p. 161.

17. Lebedevaite, Migle; Navaruckiene, Aukse; Ostrauskaite, Jolita. Photocross-linked polymers based on plant-derived monomers for optical 3D printing // Poly-Char Venice international polymer characterization forum, April 12-14, 2021, Zoom platform: book of abstracts. [Venezia] : [IUPAC Polymer division]. 2021, 13-FO01, p. 58.

18. Navaruckiene, Aukse; Bridziuviene, Danguole; Raudoniene, Vita; Rainosalo, Egidija; Ostrauskaite, Jolita. Vanillin acrylate-based photocross-linked polymers: synthesis and investigation of properties // Poly-Char Venice international polymer characterization forum, April 12-14, 2021, Zoom platform: book of abstracts. [Venezia] : [IUPAC Polymer division]. 2021, P-2, p. 122.

19. Motiekaityte, Greta; Navaruckiene, Aukse; Ostrauskaite, Jolita. Real-time photorheometry study of dual photocuring kinetics of bio-based monomers // Open readings 2021: 64th international conference for students of physics and natural sciences, March 16-19, Vilnius, LIthuania: abstract book / editors: Š. Mickus, R. Platakytė, S. Pūkienė. Vilnius : Vilnius university press, 2021, P3-10. ISBN 9786090705902. p. 229.

20. Jaras, Justinas; Navaruckiene, Aukse; Ostrauskaite, Jolita. Synthesis and investigation of tridecyl methacrylate-based photocross-linked polymers // Open readings 2021: 64th

international conference for students of physics and natural sciences, March 16-19, Vilnius, LIthuania: abstract book / editors: Š. Mickus, R. Platakytė, S. Pūkienė. Vilnius : Vilnius university press, 2021, P3-14. ISBN 9786090705902. p. 233.

21. Navaruckiene, Aukse; Bridziuviene, Danguole; Raudoniene, Vita; Ostrauskaite, Jolita. Vanillin acrylate-based polymers: influence of resin composition to photocuring kinetics and properties of the resulting polymers // Open readings 2021: 64th international conference for students of physics and natural sciences, March 16-19, Vilnius, LIthuania: abstract book / editors: Š. Mickus, R. Platakytė, S. Pūkienė. Vilnius : Vilnius university press, 2021, P3-13. ISBN 9786090705902. p. 232.

22. Navaruckiene, A.; Skliutas, E.; Malinauskas, M.; Ostrauskaite, J. Vanillin derivatives as resins for optical 3D printing // NBCM 2020: international conference on nanostructured bioceramic materials, 1-3 December 2020, Vilnius, Vilnius University: conference book. Vilnius : Vilnius Univerity Press, 2020. ISBN 9786090705575. p. 58.

23. Navaruckiene, Aukse; Motiekaityte, Greta; Ostrauskaite, Jolita. Vanillin acrylate-based photocross-linked polymers: synthesis and investigation of properties // CGPM 2020: First international conference on "green" polymer materials, 05-25 November 2020, online. Basel : MDPI. 2020, p. 1-6. DOI: 10.3390/CGPM2020-07205.

24. Navaruckiene, Aukse; Ostrauskaite, Jolita. Vanillin acrylate-based photocross-linked polymers // Green chemistry online postgraduate summer school, 6-10 July 2020, Venice, Italy: book of abstracts. Venice : Green Sciences for Sustainable Development Foundation. 2020, p. 69.

25. Motiekaitytė, Greta; Navaruckienė, Auksė; Ostrauskaitė, Jolita. Photorheometrical study of acrylated vanillin-based resins // Open readings 2020: 63rd international conference for students of physics and natural sciences, March 17-20, Vilnius, Lithuania: abstract book. Vilnius : Vilnius University, 2020, P2-22. ISBN 9786090703779. p. 235.

26. Navaruckienė, A.; Ostrauskaitė, J. Vanillin-based photocross-linked polymers for optical 3D printing // 6th international Baekeland symposium, October 15-18, 2019, Tarragona, Spain: book of abstracts. [Tarragona] : Universitat Rovira i Virgili. 2019, P-31, p. [1-2].

27. Navaruckienė, A.; Ostrauskaitė, J. Real-time photorheometrical study of vanillin-based resins // Baltic polymer symposium 2019, Vilnius, Lithuania, September 18-20, 2019: programme and proceedings. [Vilnius] : [s.n.]. 2019, p. 65.

28. <u>Navaruckienė, A.</u>; Ostrauskaite, J. Vanillin-based photoresins for optical 3D printing // Chemistry and chemical technology: Lithuanian chemists conference, 2019 May 16, Lithuanian Academy of Sciences, Vilnius: conference book. Vilnius : Vilnius University, 2019. eISBN 9786090701676. p. 100.

29. <u>Navaruckiene, A.</u>; Lebedevaite, M.; Ostrauskaite, J. Photosensitive resins composed of plant-derived monomers for optical 3d printing // 4th Green and sustainable chemistry conference, 5-8 May 2019, Dresden, Germany. [S.l.] : [s.n.]. 2019, P1.54, p. [1].

30. <u>Navaruckienė, Auksė</u>; Ostrauskaitė, Jolita. Acrylated vanillin-based photocross-linked polymers // Open readings 2019: 62nd international conference for students of physics and natural sciences, March 19-22, Vilnius, Lithuania: abstract book. Vilnius : Vilnius University, 2019, P3-29. ISBN 9786090701379. p. 305.

9. COPIES OF PUBLICATIONS

Vanillin-based Thiol-ene Systems as Photoresins for Optical 3D Printing

ABSTRACT:

Purpose – This study aims to present a design and investigation of novel vanillin-based thiol-ene photocurable systems as candidate materials for optical 3D printing.
Design/methodology/approach – Two vanillin acrylates, vanillin dimethacrylate and vanillin diacrylate, were tested in thiol-ene photocurable systems with 1,3-benzenedithiol. The kinetics of photocross-linking was investigated by real-time photorheometry using two photoinitiators, diphenyl(2,4,6-trimethylbenzoyl)phosphine oxide or ethyl(2,4,6-trimethylbenzoyl)phenylphosphinate, in different quantities. The dependencies of rheological properties of resins on the used vanillin derivative, photoinitiator, and the presence of solvent, as well as structure, thermal and mechanical properties of the selected polymers were investigated.
Findings – The most rigid polymers were obtained from vanillin diacrylate-based resins without any solvent. The vanillin diacrylate-based polymer possessed higher values of cross-linking density, yield of insoluble fraction, thermal stability and better mechanical properties in comparison to the vanillin dimethacrylate-based polymer.
Originality/value – The kinetics of photocross-linking of vanillin-based thiol-ene systems was investigated by real-time photorheometry for the first time. The designed novel photocurable systems based on vanillin acrylates and 1,3-benzenedithiol are promising renewable photoresins for optical 3D printing on demand.
Keywords: vanillin acrylates; thiol-ene; photocross-linking; real-time photorheometry; optical 3D printing

1. INTRODUCTION

Optical 3D printing, also known as stereolithography, one of additive manufacturing technologies, is a contactless fabrication method offering material processing precision, flexibility and variety of substances to rapid prototyping or low scale manufacturing of mechanical, medical, optical components and devices (Ligon *et al.,* 2017; Barner-Kowollik *et al.,* 2017; Malinauskas *et al.,* 2016; Kotz *et al.,* 2018). It uses photopolymerization process to form 3D polymeric objects from photosensitive low molar mass molecules (Zhang and Xiao, 2018). In such technology, the replacement of petroleum-based materials by materials derived from renewable resources would give the ecological and economic benefits due to the latter low toxicity, improved recovery options at the end of a product's life, less dependency on limited and increasingly expensive fossil resources (Villarrubia-Gomez *et al.,* 2018; Chae and An, 2018; Liu *et al.,* 2019; Bose *et al.,* 2018).

Vanillin is currently one of the only biobased and aromatic compounds that are industrially available (Fache *et al.,* 2015). Mostly it is obtained by extraction from the beans of vanilla orchid (Dong *et al.,* 2014) or by chemical modification of lignin which is the second most prevalent biopolymer (Isola *et al.,* 2018). In the last years vanillin and its derivatives have been used in polymer synthesis as their aromatic resins provide the high rigidity and thermal stability of resulting polymers (Zhang *et al.,* 2015; Stanzione *et al.,* 2012). Vanillin demonstrates high antibacterial activity which allows the use of vanillin containing polymers in food packing or medicine (Salmi-Mani *et al.,* 2018). Various polymers were obtained from vanillin derivatives by free radical polymerization (Zhang *et al.,* 2015) or thermal polymerization (Zhang *et al.,* 2015). The first studies on photopolymerisation of vanillin derivatives appeared recently (Salmi-Mani *et al.,* 2018).

Advantages of photopolymerization are the high reaction rate, low volatile organic compound emission and opportunity to control the reaction by applying irradiation only on the selected areas of the samples (Decker, 2002; Sangermano *et al.,* 2014). Thiol-ene photopolymerization is one of the promising methods for the synthesis of polymers from renewable resourses (Machado *et al.,* 2017). This method is characterized by high reaction speed ("click" reaction), the reaction is not inhibited by oxygen (Yoshimura *et al.,* 2015), and requires only a small amount of photoinitiator or no photoinitiator at all (Cramer *et al.,* 2003). Acrylates, vinyl ethers, allyl ethers and unsaturated hydrocarbons are used for thiol-ene photopolymerization the mostly (Roper *et al.,* 2004). Polymers obtained by thiol-ene photopolymerization show high elastic modulus, low viscosity and high polymer chain growing speed (Zhang *et al.,* 2014). Thiol-ene copolymers are transparent and have good mechanical properties (Cramer *et al.,* 2003). These polymers can be used as restorative dental resins, scaffolds for biomaterial and injectable intraocular lenses (Wang *et al.,* 2013).

1

In this study, after considering the advantages of vanillin and thiol-ene photopolymerization, two commercially available vanillin derivatives, vanillin dimethacrylate (VDM) and vanillin diacrylate (VD), were tested in thiol-ene photocurable systems with 1,3-benzenedithiol (1.3BDT) (Fig.1). Two photoinitiators, ethyl(2,4,6-trimethylbenzoyl)phenylphosphinate (TPOL) and diphenyl(2,4,6-trimethylbenzoyl)phosphine oxide (TPO) (Fig.1), were examined in UV/Vis curing process. TPOL was selected since it is in liquid form at room temperature and can be easily incorporated into a formulation (Green, 2010). TPO was selected because of its tendency not to add yellowish color to polymers and high reaction speed (Albuquerque *et al.,* 2013). TPOL and TPO are commonly used in 3D printing because of photobleaching effect, which provides transparent coatings and allows to cure coating in its lower layers (Green, 2010). The influence of selected vanillin derivative, photoinitiator, and the presence of solvent to photocross-linking rate and rigidity of the resulting polymers was evaluated by real-time photorheometry.
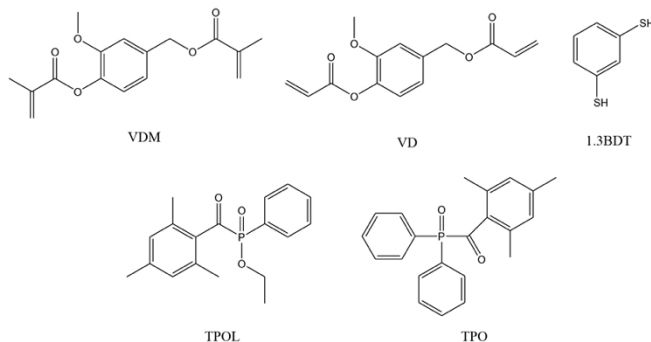
Fig. 1. Structures of vanillin dimethacrylate (VDM), vanillin diacrylate (VD), 1,3-benzenedithiol (1.3BDT), ethyl(2,4,6-trimethylbenzoyl)phenylphosphinate (TPOL), and diphenyl(2,4,6-trimethylbenzoyl)phosphine oxide (TPO)

1. MATERIALS AND METHODS

1.1. Materials

Vanillin dimethacrylate (VDM) and vanillin diacrylate (VD) were purchased from Specific Polymers. 1,3-Benzenedithiol (1.3BDT) and diphenyl(2,4,6-trimethylbenzoyl)phosphine oxide (TPO) were recieved from Sigma-Aldrich. Ethyl(2,4,6-trimethylbenzoyl)phenylphosphinate (TPOL) was purchased from Fluorochem. Dichloromethane (DCM) was purchased from Reachem Slovakia. All these materials were used as received.

1.2. Real-time photorheometry

UV/Vis real time photorheometry curing tests were performed with resins containing 1 mol of vanillin derivative (VDM or VD), 1 mol of thiol (1.3BDT), and 1, 3 or 5 mol.% of photoinitiator (TPO or TPOL) (Table I) on a MCR302 rheometer from Anton Paar equipped with the plate/plate measuring system. A minimal amount of DCM was used in some resins to dissolve solid components or for comparative investigations. The Peltier-controlled temperature chamber with the glass plate (diameter 38 mm) and the top plate PP08 (diameter 8 mm) was used. The samples were irradiated by UV/Vis light in a wavelength range of 250-450 nm through the glass plate of the temperature chamber using UV/Vis spot curing system OmniCure S2000, Lumen Dynamics Group Inc. Measuring gap was set to 0.1 mm. Shear mode with the frequency of 10 Hz and shear strain of 0.9 % were used in all cases. Storage modulus G', loss modulus G", loss factor tanδ (tanδ = G"/G'), and complex viscosity η^* were recorded as a function of irradiation time. G', G", and η^* values were taken after 350 s of UV/Vis irradiation (Table II). The gel point t_{gel} was defined as a crossover point of G' and G" modulus.

2

Table 1. Composition of the resins **C1-C10**

Resin	Vanillin derivative	Thiol	Photoinitiator	Amount of photoinitiator, mol.%	Solvent
C1	VDM		TPOL	1	DCM
C2	VDM		TPO	1	DCM
C3	VD		TPOL	1	-
C4	VD		TPO	1	-
C5	VDM	1.3BDT	TPOL	3	DCM
C6	VD		TPOL	3	-
C7	VD		TPOL	3	DCM
C8	VDM		TPO	3	DCM
C9	VD		TPO	3	-
C10	VD		TPO	3	DCM
C11	VDM		TPOL	5	DCM
C12	VDM		TPO	5	DCM
C13	VD		TPOL	5	-
C14	VD		TPO	5	-

1.3.   Preparation of cross-linked polymer specimens

The mixtures containing 1 mol of vanillin derivative (VDM or VD), 1 mol of 1.3BDT, 1, 3 or 5 mol.% of TPOL and, if needed, a minimal amount of DCM were stirred with a magnetic stirrer until homogenous phase was reached, then poured on a plastic sheet or into the Teflon mold and cured for 1-3 min under the Helios Italquartz UV lamp (model GR.E 500 W) with UV/Vis light at intensity of 310 mW/cm^2.

1.4.   Characterization techniques

FT-IR spectra were recorded using Perkin Elmer Spectrum BX II FT-IR spectrometer. The reflection was measured during the test. The range of wavenumber was (650-4000) cm^{-1}.

The yield of insoluble fraction was determined after polymer sample (0.5 g) extraction with acetone for 24 h using a Soxhlet extractor. After the extraction, the insoluble fractions were dried under vacuum until no changes of the weight were observed. The yield of insoluble fraction was determined as a difference of the weight of the sample taken for the extraction and the weight of the insoluble fraction obtained after extraction and drying.

Differential scanning calorimetry (DSC) measurements were performed on a Perkin Elmer DSC 8500 apparatus at a heating rate of 20 ˚C/min under nitrogen atmosphere (50 mL/min). The aluminum hermetic pans were used. The temperature was ranged from -90 ˚C to 100 ˚C. The heating-cooling-heating cycle was used. The data were taken from the second heating curve.

Thermogravimetrical analysis (TGA) was performed on a Perkin Elmer TGA 4000 apparatus. The temperature was ranged from 10 ˚C to 800 ˚C with the heating rate of 20 ˚C/min under nitrogen atmosphere (100 mL/min). The aluminum oxide pans were used.

The stress-strain curves of the films were obtained with a material testing machine BDO-FBO.5TH (Zwick/Roell). The strain rate for tensile test of all samples was 50 mm/min. Mechanical testing was performed on dog bone shaped specimens with the length of 45 mm and the thickness of 0.1 (±0.02) mm. At least 3 tests were made to obtain the accurate results.

The top pressure test was performed on a material testing machine BDO-FBO.5TH (Zwick/Roell). The compression force was 5 N in all cases. The thickness of specimens was 3.2 (±0.2) mm, the width of specimens was 30.0 (±0.00) mm. The specimens were placed in a Teflon mold of the same size to avoid the expansion of specimens to the sides during the test. At least 10 tests for each specimen were made to obtain the accurate results. The compression modulus was calculated by the following equation:

3

78

$$E_c = \frac{F \cdot l_0}{S \cdot \Delta l}$$

where E_c is a compression modulus (MPa); F is a force (N); S is a surface area of specimen (mm^2); l_0 is an initial thickness of specimen (mm); and Δl is the difference of an initial thickness of specimen and thickness of a loaded specimen (mm).

The bending test was performed on TA Instruments RSA-G2 Solids Analyzer. Three point bending test was used. The thickness of specimens was 1.7 (±0.1) mm, the width was 5.00 (±0.00) mm, and the length was 40.00 (±0.00) mm.

Cross-linking density was calculated according to the theory of rubber elasticity using the following equation:

$$G' = \nu RT$$

where ν is a cross-linking density (mol/m^3); G' is the steady-state value of storage modulus taken from the real-time photoreometry measurement curve after 350 seconds (Pa); R is the universal gas constant (8.314 J/mol·K); T is the temperature (K) (Flory, 1953).

2. RESULTS AND DISCUSSION

2.1. *Monitoring of photocross-linking kinetics by real-time photorheometry*

Real-time photorheometry was used to monitor the evolution of thiol-ene photocross-linking process. As an example, the dependencies of storage modulus G', loss modulus G", loss factor tanδ, and complex viscosity η* of the VDM-based resin **C5** on irradiation time are presented in Fig. 2. When irradiation of the resin **C5** started, the values of storage modulus G', loss modulus G", and complex viscosity η* started to increase indicating the beginning of cross-linking process. The onset of gelation process is described as the gel point (t$_{gel}$), i.e. the point at which G' and G" modulus curves intersect (Mezger, 2011). As the irradiation of the resin **C5** proceeded with time, the values of G', G" modulus and η* continued to increase due to the gel aging and settled down into steady-state indicating the end of the cross-linking process. All vanillin-based resins investigated in this study showed the similar behaviours. Real-time photorheometry data of all resins are summarized in Table II.
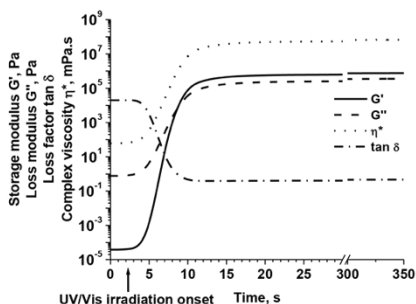

Fig. 2. Dependencies of storage modulus G', loss modulus G", loss factor tan δ, and complex viscosity η* of the resin **C5** on irradiation time

Table 2. Rheological characteristics of the resins **C1-C14**

Resin	Storage modulus G', MPa	Loss modulus G", MPa	Complex viscosity η*, MPa s	Gel point* t_{gel}, s
C1	0.48 ± 0.04	0.10 ± 0.04	0.0078 ± 0.0002	12 ± 0.20
C2	0.48 ± 0.02	0.07 ± 0.03	0.0077 ± 0.0003	11 ± 0.30
C3	17.80 ± 0.34	4.69 ± 0.40	0.2900 ± 0.0240	15 ± 0.40
C4	20.2 ± 0.52	9.31 ± 0.22	0.3540 ± 0.0320	11 ± 0.35
C5	0.73 ± 0.03	0.23 ± 0.03	0.0120 ± 0.0023	8 ± 0.25
C6	9.92 ± 0.32	5.54 ± 0.20	0.1800 ± 0.0152	7 ± 0.20
C7	0.81 ± 0.04	0.16 ± 0.05	0.0130 ± 0.0024	12 ± 0.45
C8	0.58 ± 0.22	0.31 ± 0.04	0.0100 ± 0.0022	10 ± 0.20
C9	9.34 ± 0.46	3.62 ± 0.15	0.1600 ± 0.0134	8 ± 0.20
C10	0.45 ± 0.02	0.15 ± 0.02	0.0076 ± 0.0005	10 ± 0.25
C11	1.33 ± 0.42	0.13 ± 0.01	0.0212 ± 0.0016	10 ± 0.30
C12	0.18 ± 0.03	0.10 ± 0.03	0.0033 ± 0.0006	10 ± 0.40
C13	1.96 ± 0.20	3.00 ± 0.24	0.0570 ± 0.0032	12 ± 0.20
C14	3.34 ± 0.40	4.28 ± 0.32	0.0860 ± 0.0042	8 ± 0.20

*- calculated from the UV/Vis irradiation onset.

It was determined that rheological characteristics of the resins **C1-C14** depend on their composition. As the storage modulus G' characterizes the rigidity of the formed thermosetting polymers (Candan *et al.,* 2016), the more rigid polymers were obtained from VD-based resins without any solvent **C3**, **C4**, **C6**, **C9**, **C13**, **C14** (Table II and Fig. 3, as an example). It could be explained by the higher reactivity of acrylic group in comparison to methacrylic group (Anseth *et al.,* 1994) leading to the formation of more cross-linked structure of the polymers (section 3.2) and by the influence of solvent leading to the reduction of the cross-linking rate (Fig. 4) and the density of cross-links (section 3.2). The more rigid polymers **C4**, **C9**, **C14** were obtained from VD-based resins when TPO was used as photoinitiator in comparison to the plymers **C3**, **C6**, **C13** (Table II and Fig. 3, as an example). This could be explained by the higher reactivity of TPO comparing to TPOL (Green, 2010). The tendency of the reduction of G' values and therewith the rigidity of the formed VD-based polymers (series of **C3**, **C6**, **C13** and series of **C4**, **C9**, **C14**) with the increase of photoinitiator concentration was observed (Table 2). The addition of solvent into the resins redused the rigidity of VDM- and VD-based polymers **C5**, **C7**, **C11** synthesized using photoinitiator TPO in comparison to those with TPOL (**C8**, **C10**, **C12**, respectively).

The polymers **C5** and **C6** were selected for further investigations according to the photocross-linking rate and polymer rigidity.
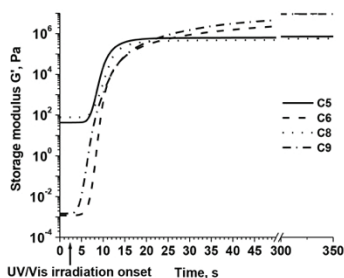
Fig. 3. Dependencies of storage modulus G' of VDM-based resins (**C5**, **C8**) and VD-based resins (**C6**, **C9**) on irradiation time. Resins containing TPO (**C8**, **C9**), resins containing TPOL (**C5**, **C6**)
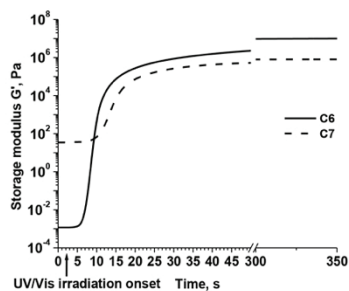
5

Fig. 4. Dependencies of storage modulus G' of the resin without DCM (**C6**) and containing DCM (**C7**) on irradiation time

2.2.   Characterization of photocross-linked polymer structure

The formation of polymers was confirmed by FT-IR spectroscopy and Soxhlet extraction experiment. FT-IR spectral analysis confirmed that the photocross-linked polymers were constructed from the fragments of both monomers, vanillin derivative and 1.3BDT. The signal of C=C group which was present at 1607 cm^{-1} in the FT-IR spectra of VDM and VD was reduced in polymer spectra. The signal of S-H group which was present at 2561 cm^{-1} in the spectrum of 1.3-BDT disappeared and the characteristic C-S group stretch at 1153-1119 cm^{-1} appeared in the FT-IR spectra of the cross-linked polymers. As an example, the FT-IR spectra of VDM, 1.3BDT and the cross-linked polymer **C5** are presented in Fig. 5.
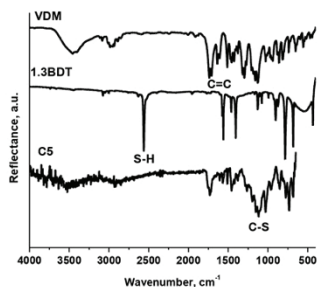

Fig. 5. FT-IR spectra of VDM, 1.3BDT and the cross-linked polymer **C5**

The Soxhlet extraction was performed and cross-linking density was calculated to confirm the cross-linked structure of vanillin-based polymers. The high yields of insoluble fraction showed that both monomers, vanillin derivative and thiol, participated in the formation of the cross-linked structure. The dependence of the used vanillin monomer on the yield of insoluble fraction and cross-linking density was observed. The higher values of the yield of insoluble fraction (92 %) and cross-linking density (3952 mol/m^3) were obtained for VD-based polymer **C6** in comparison to those of the VDM-based polymer **C5** (87 % and 291 mol/m^3, respectively). The lower values of the yield of insoluble fraction and cross-linking density of polymers mainly could be due to DCM behaviour not only as a solvent but also as a chain transfer agent. It was confirmed by investigation of the VD-based polymers prepared with and without DCM. For example, the yield of insoluble fraction (78 %) and cross-linking density (322 mol/m^3) of the VD-based polymer **C7** prepared using DCM were much lower than those of the VD-based polymer **C6** which was prepared without DCM.

2.3. *Thermal properties of photocross-linked polymers*

The temperature range in which polymers can be used is very important for their application. Therefore, thermal characteristics of the cross-linked polymers **C5** and **C6** were determined by DSC and TGA. The synthesized cross-linked polymers are amorphous materials as only the glass transitions were observed in DSC curves. Glass transition temperatures (T_g) of both polymers **C5** and **C6** are very similar (-4 ˚C and -5 ˚C, respectively) and do not depend on cross-linking density and the yield of insoluble fraction. These T_g values are comparable with those of the cross-linked polymers synthesized from acrylated epoxidized soybean oil and 1.3BDT (T_g: -8-1 ˚C) (Miezinyte *et al.*, 2019), as well as T_g of the cross-linked polymers synthesized from acrylated epoxidized soybean oil and VDM (T_g from -2.6 ˚C to -1.6 ˚C) (Lebedevaite *et al.*, 2019), which were considered as potential materials for optical 3D printing.

Thermal decomposition of the synthesized polymers **C5** and **C6** occured in two-three steps (Fig. 6). Additional step in the thermogravimetric curve of the VDM-based polymer **C5** could be explained by the presence of the short linear or branched macromolecules. The temperature of 10 % weight loss of the VD-based polymer **C6** (270 ˚C) was higher than that of the VDM-based polymer **C5** (250 ˚C) and correlated with the higher yield of insoluble fraction and cross-linking density of the VD-based polymer **C6**.
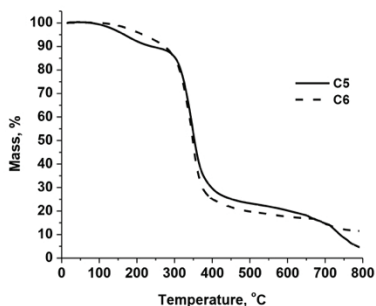
Fig. 6 The thermogravimetric curves of the cross-linked polymers **C5** and **C6**

2.4. *Mechanical properties of photocross-linked polymers*

The mechanical characterization of polymers is important in designing their future applications. Thus, mechanical characteristics of the cross-linked polymers **C5** and **C6** are summarized in Table III. The images of the films and tablet shape specimens are presented in Fig. 7. The higher values of tensile strength, elastic modulus and lower value of elongation to failure were obtained for the polymer **C5** compared to those of the polymer **C6** due to the lower cross-linking

7

density and the yield of insoluble fraction of the polymer **C5**. The specimens of both polymers did not break during the bending test. The determined force of 30 % specimen bent for the polymer **C5** was lower than that of the polymer **C6**. Consequently, the cross-linked polymer **C6** is more rigid than the polymer **C5**. The same dependence of mechanical properties on polymer cross-linking density was obtained after the top pressure test. The polymer **C6** demonstrated higher compression modulus and lower deformation during compression test than those of the polymer **C5**. Hence, the polymer **C6** was more pressure resistant due to the higher cross-linking density. Both polymers **C5** and **C6** possessed slightly lower compression modulus that that of the polymers synthesized from acrylated epoxidized soybean oil and 1.3BDT (1.5-2.5 MPa) (Miezinyte *et al.*, 2019).
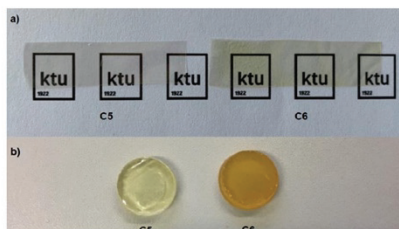

Fig. 7 The images of the films (a) and tablet shape specimens (b) of the cross-linked polymers
C5 and **C6**

Table 3. Mechanical characteristics of the cross-linked vanillin-based polymers

Polymer	Tensile strength, MPa	Elongation to failure, %	Elastic modulus, MPa	Force of specimen bend of 30 %, N	Deformation during compression, %	Compression modulus, MPa
C5	25 ± 1.5	0.5 ± 0.02	2953 ± 9.5	0.02 ± 0.02	14.29 ± 0.02	0.70 ± 0.02
C6	5 ± 0.9	31 ± 3.60	16 ± 4.6	0.18 ± 0.40	10.55 ± 0.02	0.94 ± 0.02

3. CONCLUSIONS

Cross-linked polymers were obtained by thiol-ene photopolymerization of vanillin dimethacrylate or vanillin diacrylate and 1,3-benzenedithiol using ethyl(2,4,6-trimethylbenzoyl)phenylphosphinate or diphenyl(2,4,6-trimethylbenzoyl)phosphine oxide as photoinitiator. The kinetics of photocross-linking of vanillin-based thiol-ene systems was investigated by real-time photorheometry for the first time. This method was found to provide fast and valuable information about the influence of photosensitive resin formulations on the reaction rate and rheological properties of resins, as well as rigidity of the resulting polymers that can be used to evaluate and select resins for manufacturing of polymeric products with desired mechanical properties by light-based technologies. The most rigid polymers were obtained from vanillin diacrylate-based resins without any solvent. The vanillin diacrylate-based polymer possessed higher values of cross-linking density, yield of insoluble fraction, thermal stability, and better mechanical properties in comparison to the vanillin dimethacrylate-based polymer. The real-time photorheometry measurements confirmed the quick formation of cross-linked structure polymers which mechanical and thermal properties could be sufficient for various practical application. The designed novel photocurable systems based on vanillin acrylates and 1,3-benzenedithiol are promising renewable photoresins for optical 3D printing on demand.

ACKNOWLEDGEMENTS

8

REFERENCES

Albuquerque, P.P.A.C., Moreira, A.D.L., Moraes, R.R., Cavalcante, L.M. and Schneider, L.F.J. (2013), "Color stability, conversion, water sorption and solubility of dental composites formulated with different photoinitiator systems", *Journal of Dentistry*, Vol. 41, pp. e67-e72, doi: 10.1016/j.jdent.2012.11.020.

Anseth, K.S., Wang, C.M. and Bowman, C.N. (1994), "Reaction Behaviour and Kinetic Constants for Photopolymerizations of Multi (Meth) Acrylate Monomers", *Polymer*, Vol. 35, pp. 3243-3250, doi: 10.1016/0032-3861(94)90129-5.

Barner-Kowollik, C., Bastemeyer, M., Blasco, E., Delaittre, G., Müller, P., Richter, B. and Wegener, M. (2017), "3D Laser micro- and nano-printing: challenges for chemistry", *Angewandte Chemie International Edition*, Vol. 56, pp. 15828–15845, doi:10.1002/anie.201704695.

Bose, S., Ke, D, Sahasrabudhe, H. and Bandyopadhyay, A. (2018), "Additive manufacturing of biomaterials", *Progress in Materials Science*, Vol. 93, pp. 45-111, doi: 10.1016/j.pmatsci.2017.08.003.

Candan, Z., Gardner, D.J. and Shaler, S.M. (2016), "Dynamic mechanical thermal analysis (DMTA) of cellulose nanofibril/nanoclay/pMDI nanocomposites", *Composites Part B*, Vol. 90, pp. 126-132, doi: 10.1016/j.compositesb.2015.12.016.

Chae, Y. and An, Y.J. (2018), "Current research trends on plastic pollution and ecological impacts on the soil ecosystem: A review", *Enviromental Pollution*, Vol. 240, pp. 387-395, doi: 10.1016/j.envpol.2018.05.008.

Cramer, N.B., Davies, T., O'Brien, A.K. and Bowman, C.N. (2003), "Mechanism and Modeling of a Thiol-Ene Photopolymerization", *Macromolecules*, Vol. 36, pp. 4631-4636, doi: 10.1021/ma034072x.

Decker, C. (2002), "Light-induced crosslinking polymerization", *Polymer International*, Vol. 5, pp. 1141-1150, doi: 10.1002/pi.821.

Dong, Z., Gu, F., Xu, f. and Wang, Q. (2014), "Comparison of four kinds of extraction techniques and kinetics of microwave-assisted extraction of vanillin from Vanilla planifolia Andrews", *Food Chemistry*, Vol. 149, pp. 54-61.

Fache, M., Boutevin, B. and Caillol, S. (2015), "Vanillin, a key-intermediate of biobased polymers", *European Polymer Journal*, Vol. 68, pp. 481-487, doi: 10.1016/j.eurpolymj.2015.03.050.

Flory, P. J. (1953), *Principles of Polymer Chemistry*, Cornell University Press, Ithaca.

Green, W.A. (2010), *Industrial Photoinitiators. A Technical Guide*, CRC Press, Taylor and Francis Group, Boca Raton, London, Bew York.

Isola, C., Sieverding, H.L., Nunam-Al-Mobin, A.M., Rajappagowda, R., Boakye, E.A., Raynie, D.E., Smirnova, A.L. and Stone, J.J. (2018), "Vanillin derived from lignin liquefaction: a sustainability evaluation", *International Journal of Life Cycle Assessment*, Vol. 23, pp. 1761-1772, doi: 10.1007/s11367-017-1401-0.

Kotz, F., Risch, P., Helmer, D. and Rapp, B.E. (2018), "Highly Fluorinated Methacrylates for Optical 3D Printing of Microfluidic Devices", *Micromachines*, Vol. 9, pp. 1-11, doi:10.3390/mi9030115.

Lebedevaite, M., Ostrauskaite, J., Skliutas, E. and Malinauskas, M. (2019), "Photoinitiator free Resins Composed of Plant-Derived Monomers for the Optical µ-3D Printing of Thermosets", *Polymers*, Vol.11, pp. 116 , doi: 10.3390/polym11010116.

Ligon, S.C., Liska, R., Stampfl, J., Gurr, M. and Mülhaupt, R. (2017), "Polymers for 3D Printing and Customized Additive Manufacturing", *Chemical Reviews*, Vol. 117, pp. 10212−10290, doi: 10.1021/acs.chemrev.7b00074.

Liu, J., Sun, L., Xu, W., Wang, Q., Yu, S. and Sun, J. (2019), "Current advances and future perspectives of 3D printing natural-derived biopolymers", *Carbohydrate Polymers*, Vol. 207, pp. 297-316, doi: 10.1016/j.carbpol.2018.11.077.

Machado, T.O., Sayer, C. and Araujo, P.H.H. (2017), "Thiol-ene polymerization: A promising technique to obtain novel biomaterials", *European Polymer Journal*, Vol. 86, pp. 200-215, doi: 10.1016/j.eurpolymj.2016.02.025.

Malinauskas, M., Žukauskas, A., Hasegawa, S., Hayasaki, Y., Mizeikis, V., Buividas R. and Juodkazis, S. (2016), "Ultrafast laser processing of materials: from science to industry", *Light: Science & Applications*, Vol. 5, pp. 1-14, doi:10.1038/lsa.2016.133.

Mezger, T.G. (2011), *The Rheology Handbook, 3rd ed.*, Vincentz Network, Hanover.

Miezinyte, G., Ostrauskaite, J., Rainosalo, E., Skliutas and E., Malinauskas, M. (2019) "Photoresins based on acrylated epoxidized soybean oil and benzenedithiols for optical 3D printing", *Rapid Prototyping Journal*, Vol. 25, pp.378-387, doi: 10.1108/RPJ-04-2018-0101.

Roper, T.M., Kwee, T., Lee, T.Y., Guymon, C.A. and Hoyle, C.E. (2004), "Photopolymerization of pigmented thiol-ene systems", *Polymer*, Vol. 45, pp. 2921-2929, doi: 10.1016/j.polymer.2004.02.038.

Salmi-Mani, H., Terreros, G., Barroca-Aubry, N., Aymes-Chodur, C., Regeard, C. and Roger, P. (2018), "Poly(ethylene terephthalate) films modified by UV-induced surface graft polymerization of vanillin derived monomer for antibacterial activity", *European Polymer Journal*, Vol. 103, pp. 51-58, doi: 10.1016/j.eurpolymj.2018.03.038.

Sangermano, M., Razza, N. and Crivello, J.V. (2014), "Cationic UV-Curing: Technology and Applications", *Macromolecular Materials and Engineering*, Vol. 299, pp. 775–793, doi: 10.1 002/mame.201300349.

Stanzione, J.F., Sadler, J.P., La Scala, J.J., Reno, K.H. and Wool, R.P. (2012), "Vanillin-based resin for use in composite applications", *Green Chemistry*, Vol. 14, pp. 2346-2352, doi: 10.1039/C2GC35672D.

Villarrubia-Gomez, P., Cornell, S.E. and Fabres, J. (2018), "Marine plastic pollution as a planetary boundary threat – The drifting piece in the sustainability puzzle", *Marine Policy*, Vol. 96, pp. 213-220, doi:10.1016/j.marpol.2017.11.035

Wang, K., Lu, J., Yin, R., Chen, L., Du, S., Jiang, Y. and Yu, Q. (2013), "Preparation and properties of cyclic acetal based biodegradable gel by thiol-ene photopolymerization", *Materials Science and Engineering*, Vol. 33, pp. 1261-1266, doi: 10.1016/j.msec.2012.12.024.

Yoshimura, T., Shimasaki, T., Teramoto, N. and Shibata, M. (2015), "Bio-based polymer networks by thiol-ene photopolymerization of allyl-etherified eugenol derivatives", *European Polymer Journal*, Vol. 67, pp. 397-408, doi: 10.1016/j.eurpolymj.2014.11.013.

Zhang, M., Deng, Q., Shi, L., Li, Z., Pang, H., Zhang, Y., Yu, J. and Hu, S. (2014), "Fabrication of Resonant Subwavelength Grating Based on Thiol-ene", in *Proceedings of 7th International Symposium on Advanced Optical Manufacturing and Testing Technologies, China*, 2014, SPIE, Vol. 9283, pp. 1-6, doi: 10.1117/12.2068526.

Zhang, C., Madbouly, S.A. and Kessler, M.R. (2015), "Renewable Polymers Prepared from Vanillin and its Derivatives", *Macromolecular Chemistry and Physics*, Vol. 216, pp. 1816-1822, doi: 10.1002/macp.201500194.

Zhang, J. and Xiao, P. (2018), "3D printing of photopolymers", *Polymer Chemistry*, Vol. 9, pp. 1530-1540, doi: 10.1039/c8py00157j.

Zhang, C., Yan, M., Cochran, E.W. and Kessler, M.R. (2015), "Biorenewable polymers based on acrylated epoxidized soybean oil and methacrylated vanillin", *Materials Today Communications*, Vol. 5, pp. 18-22, doi: 10.1016/j.mtcomm.2015.09.003.

9

84

![polymers logo] *polymers*

Article

Vanillin Acrylate-Based Resins for Optical 3D Printing

Aukse Navaruckiene [1], Edvinas Skliutas [2], Sigita Kasetaite [1], Sima Rekštytė [2], Vita Raudoniene [3], Danguole Bridziuviene [3], Mangirdas Malinauskas [2] and Jolita Ostrauskaite [1,*]

[1] Department of Polymer Chemistry and Technology, Kaunas University of Technology, Radvilenu Rd. 19, LT-50254 Kaunas, Lithuania; aukse.navaruckiene@ktu.lt (A.N.); sigita.kasetaite@ktu.lt (S.K.)

[2] Laser Research Center, Faculty of Physics, Vilnius University, Sauletekis Ave. 10, LT-10223 Vilnius, Lithuania; edvinas.skliutas@ff.vu.lt (E.S.); sima.rekstyte@ff.vu.lt (S.R.); mangirdas.malinauskas@ff.vu.lt (M.M.)

[3] Biodeterioration Research Laboratory, Nature Research Center, Akademijos Str. 2, LT-08412 Vilnius, Lithuania; vita.raudoniene@gamtc.lt (V.R.); danguole.bridziuviene@gamtc.lt (D.B.)

* Correspondence: jolita.ostrauskaite@ktu.lt; Tel.: +370-37-300192

Abstract: The investigation of biobased systems as photocurable resins for optical 3D printing has attracted great attention in recent years; therefore, novel vanillin acrylate-based resins were designed and investigated. Cross-linked polymers were prepared by radical photopolymerization of vanillin derivatives (vanillin dimethacrylate and vanillin diacrylate) using ethyl(2,4,6-trimethylbenzoyl)phenylphosphinate as photoinitiator. The changes of rheological properties were examined during the curing with ultraviolet/visible irradiation to detect the influences of solvent, photoinitiator, and vanillin derivative on cross-linking rate and network formation. Vanillin diacrylate-based polymers had higher values of yield of insoluble fraction, thermal stability, and better mechanical properties in comparison to vanillin dimethacrylate-based polymers. Moreover, the vanillin diacrylate polymer film showed a significant antimicrobial effect, only a bit weaker than that of chitosan film. Thermal and mechanical properties of vanillin acrylate-based polymers were comparable with those of commercial petroleum-derived materials used in optical 3D printing. Also, vanillin diacrylate proved to be well-suited for optical printing as was demonstrated by employing direct laser writing 3D lithography and microtransfer molding techniques.

Keywords: vanillin dimethacrylate; vanillin diacrylate; photopolymerization; optical 3D printing; direct laser writing; replica molding

1. Introduction

3D printing, also known as additive manufacturing, is a growing technology that has drawn increasing attention globally and has made a revolutionary impact on product fabrication in areas like medicine, the food industry, textiles, architecture, and construction [1]. Polymers are widely used in our everyday life due to their lightness, firmness, and relatively low cost; however, they are hard to form into intricate geometries. Additive manufacturing is the solution of creating complex geometries from plastics [2]. Several 3D printing technologies exist, allowing to create structures out of photo-curable resins. In stereolithography, resins are formed into 2D patterned layers [3], which become solid after exposing to UV light. By repeating this procedure, a 3D structure can be created layer by layer [4]. On the other hand, direct laser writing (DLW) 3D lithography can employ ultrashort pulses of focused VIS or near IR radiation instead of linearly absorbed UV light. This way

a nonlinear light–matter interaction is achieved that confines the absorption and, subsequently, the cross-linking reaction in a small volume inside the resin, thus enabling full 3D (nonlayered) fabrication of structures with subwavelength feature sizes [5]. For 2D or quasi-3D structures, microtransfer molding (nanoimprint lithography) can be used. It employs the solidification of a resin (usually by UV light or thermally) inside the soft mold, thus replicating the master structure that was used to create the mold [6]. This technique is especially suitable in cases when many identical objects are required, as the same master structure can be used to make several molds, each suitable to create hundreds of replicas.

Advantages of photopolymerization are energy efficiency, high reaction rates, freedom from solvents [7], and the ability to photocure only the desired area of the resin [8]. Photopolymerization does not require any specific temperatures and can be performed at ambient conditions [9]. These features allow photopolymerization to be used in many engineering and manufacturing fields such as dental restoration, coatings, and 3D printing [10]. Radical photopolymerization is one of the most widely used photopolymerization processes. In this process, photoinitiator is used to generate radicals through cleavage and hydrogen abstraction reactions [11]. Acrylates and methacrylates are mostly used in free radical photopolymerization [12].

Vanillin is mostly obtained by extraction from the beans of vanilla orchids or by chemical modification of lignin, which is the second most prevalent biopolymer. Due to its aromatic structure, vanillin could replace widely used petro-based aromatic monomers [13]. Vanillin polymers exhibit re-processability and biodegradability under acid solution [14], as well as biodegradability in soil [15]. Recently, vanillin has been used to synthesize high-performance flame-retardant epoxy resins containing phosphorus [16]. Vanillin is one of the known natural compounds with antimicrobial properties [17]. It was determined that the polymeric films of vanillin derivatives also showed antimicrobial activity, which allow the use of vanillin-based polymers in food packing and medicine [18].

In this study, two commercially available vanillin derivatives, vanillin dimethacrylate (VDM) and vanillin diacrylate (VD), were tested in photocurable systems using ethyl(2,4,6-trimethylbenzoyl)phenylphosphinate (TPOL) as photoinitiator (Figure 1). TPOL was selected due to its high reaction rate and liquid form at room temperature [12]. TPOL is commonly used in optical 3D printing due to the photobleaching effect, which provides transparent coatings and allows coatings to cure in its lower layers [12]. The influence of the selected vanillin derivative, amount of photoinitiator, and the solvent's to photocross-linking rate and rigidity of resulting polymers were evaluated by real-time photorheometry. The yield of insoluble fraction, cross-linking density, and swelling value of selected polymers were calculated to confirm the cross-linked structure. Antimicrobial activity of the selected polymer film was determined and compared with that of chitosan and oxyethyl starch films. Thermal and mechanical properties were investigated and compared with those of other acrylate polymers based on natural phenolics, acrylated epoxidized soybean oil-based polymers, and commercial petroleum-derived materials used in optical 3D printing.
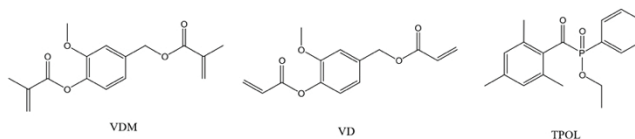
Figure 1. Chemical structures of vanillin dimethacrylate (VDM), vanillin diacrylate (VD), and ethyl(2,4,6-trimethylbenzoyl)phenylphosphinate (TPOL).

86

2. Materials and Methods

2.1. Materials

Vanillin dimethacrylate (VDM) and vanillin diacrylate (VD) (both from Specific Polymers), ethyl(2,4,6-trimethylbenzoyl)phenylphosphinate (TPOL, Fluorochem), dichloromethane (DCM, Reachem Slovakia), and chitosan and hydroxyethyl starch (both from Sigma-Aldrich) were used as received. The Autodesk Standard Clear Prototyping Resin (PR48) was received from Autodesk. FormLabs Clear FL6PCL02 resin was received from FormLabs.

2.2. Real-Time Photorheometry

UV/Vis curing tests were performed with resins containing 1 mol of vanillin derivative (VDM or VD) and 1, 3, or 5 mol.% of photoinitiator (TPOL) (Table 1) on a MCR302 rheometer (Anton Paar, Graz, Austria) equipped with the plate/plate measuring system. A minimal amount of DCM was used in some resins to dissolve solid components or for comparative investigations. The Peltier-controlled temperature chamber with the glass plate (diameter 38 mm) and the top plate PP08 (diameter 8 mm) was used. The measuring gap was set to 0.1 mm. The samples were irradiated by UV/Vis light in a wavelength range of 250–450 nm through the glass plate of the temperature chamber using UV/Vis spot curing system OmniCure S2000 (Lumen Dynamics Group Inc., Mississauga, ON, Canada). The temperature was 24 °C. Shear mode with the frequency of 10 Hz and shear strain of 0.9% were used in all cases. Storage modulus G', loss modulus G'', loss factor tanδ (tan$\delta = G''/G'$), and complex viscosity η^* were recorded as a function of irradiation time. G', G'', and η^* values were taken after 350 s of UV/Vis irradiation (Table 2). The gel point t_{gel} was defined as a crossover point of G' and G'' modulus.

Table 1. Composition of the resins **C1–C9**.

Resin	Vanillin Derivative	Solvent	Amount of Photoinitiator TPOL, mol.%
C1	VD	-	1
C2	VD	DCM	1
C3	VDM	DCM	1
C4	VD	-	3
C5	VD	DCM	3
C6	VDM	DCM	3
C7	VD	-	5
C8	VD	DCM	5
C9	VDM	DCM	5

Table 2. Rheological characteristics of the resins **C1–C9**.

Resin	Storage Modulus G', MPa	Loss Modulus G'', MPa	Complex Viscosity η^*, MPa·s	Gel Point [a] t_{gel}, s
C1	7.35	6.34	0.15	14
C2	13.40	2.35	0.22	20
C3	13.00	1.65	0.21	6
C4	18.10	2.70	0.29	6
C5	11.30	1.64	0.18	12
C6	18.20	2.94	0.29	5
C7	13.30	5.78	0.23	10
C8	14.50	2.02	0.23	14
C9	19.80	3.36	0.32	6
FormLabs Clear FL6PCL02	15.20	3.35	0.25	6
PR48	21.40	4.19	0.35	6

[a] calculated from the UV/Vis irradiation onset.

2.3. Preparation of Cross-Linked Polymer Specimens

The mixtures containing 1 mol of vanillin derivative (VDM or VD), 1, 3, or 5 mol.% of TPOL, and, if needed, a minimal amount of DCM (0.25 mL of DCM was used for 1 g of acrylate) were stirred at room temperature (25 °C) with a magnetic stirrer until homogenous phase was reached, then poured into a Teflon mold and cured for 1–4 min under a UV lamp (Helios Italquartz, model GR.E 500 W, Milan, Italy) with UV/Vis light at intensity of 310 mW/cm².

2.4. Characterization Techniques

Fourier transform infrared spectroscopy (FT-IR) spectra were recorded using a Spectrum BX II FT-IR spectrometer (Perkin Elmer, Llantrisant, UK). The reflection was measured during the test. The range of wavenumbers was (650–4000) cm^{-1}.

Cross-linked polymers **C3–C6** FT-IR (cm^{-1}): 1714–1758, 1710–1732, 1730–1754 (ν, C=O), 1603, 1603–1649, 1603–1647 (ν, C=C), 737, 801–802 (ν, CH$_2$).

The yield of insoluble fraction was determined by Soxhlet extraction. Polymer samples of 0.5 g were extracted with acetone for 24 h. After the extraction, the insoluble fractions were dried under vacuum until no changes of the weight were observed. The yield of insoluble fraction was calculated as a difference of the weight before extraction and after extraction and drying.

Differential scanning calorimetry (DSC) measurements were performed on a DSC 8500 apparatus (Perkin Elmer, Llantrisant, UK). The heating rate of 20 °C/min under nitrogen atmosphere (50 mL/min) was used. The temperature ranged from −30 to 140 °C. A heating–cooling–heating cycle was used. Aluminum hermetic pans were used. The data were taken from the second heating curve.

Thermogravimetrical analysis (TGA) was performed on a TGA 4000 apparatus (Perkin Elmer, Llantrisant, UK). A heating rate of 20 °C/min under nitrogen atmosphere (100 mL/min) was chosen, and the temperature ranged from 10 to 800 °C. Aluminum oxide pans were used.

The top pressure test was performed on a BDO-FBO.5TH material testing machine (Zwick/Roell, Kennesaw, GA, USA). In all cases, the compression force was 5 N. The speed of compression was 50 mm/min. All tests were performed at 20 °C. The specimen was pressed with a cylindrical steel rod with a flat end of 8 mm diameter. The width of specimens was 30.0 (±0.00) mm and the thickness of specimens was 2.2 (±0.2) mm. In order to avoid the expansion of specimens to the sides during the test, the specimens were placed in a Teflon mold of the same size. To obtain accurate results, 10 tests for each specimen were made. The compression modulus was calculated by the following equation:

$$E_c = \frac{F \cdot l_0}{S \cdot \Delta l} \tag{1}$$

where E_c is a compression modulus (MPa); S is a surface area of specimen (mm²); F is a force (N); Δl is the difference of an initial thickness of specimen and thickness of a loaded specimen (mm); and l_0 is an initial thickness of specimen (mm).

The bending test was performed on RSA-G2 Solids Analyzer (TA Instruments, New Castle, Delaware, USA). The thickness of specimens was 1.7 (±0.1) mm, the width was 5.00 (±0.00) mm, and the length was 40.00 (±0.00) mm. Tests were carried out at 20 °C. The speed of bending was 0.1 mm/s. Three-point contact bending geometry with a 25 mm gap between end contacts was used.

Bending modulus was calculated using the following equation:

$$\delta = \frac{3 \cdot F \cdot L}{2 \cdot w \cdot d^2} \tag{2}$$

where δ is the bending modulus (Pa); F is the maximum force applied to the specimen (N); L is the length of the specimen (m); w is the width of the specimen (m); and d is the thickness of the specimen (m) [19].

The swelling value of the cross-linked polymer specimens was obtained by measuring the volume of specimens swollen in chloroform and toluene at 25 °C. The polymer film specimens of 15 (±0.1) mm length, 5 (±0.00) mm width, and 0.5 (±0.05) mm thickness were used. A glassy container

88

comprised two spherical parts of 50 mL joined by a tube graduated with the accuracy of 0.02 mL was used. One spherical part was separated from the graduated tube by a liquid-permeable partition. This spherical part was fitted with the neck closed by a stopper. The swelling agent was poured, and the sample was placed in through this neck. The initial volume of the polymer film was measured before placing into the measuring container. The measuring container was kept in such position that a sample was immersed in the swelling agent during the test and turned in such position that the liquid leaked to another side of the container at every 5 min. The change of the volume of the swelling agent was measured. The swelling value was calculated by the following equation:

$$\alpha = \frac{V - V_0}{V_0} \cdot 100 \tag{3}$$

where α is a swelling value (%); V is a volume of swollen specimen (mL); and V_0 is an initial volume of specimen (mL).

The antimicrobial activity of the polymers was estimated quantitatively by inoculating specimens with microbial suspension. The test microorganisms were Gram-negative bacterium *Escherichia coli* ATCC 25,922 (*E. coli*) and Gram-positive bacterium *Staphylococcus aureus* ATCC 29,213 (*S. aureus*). The concentration of inoculum suspension was assessed with a spectrophotometer (Evolution 60S, Thermo Fisher Scientific, Waltham, MA, USA) and then corrected by seeding the suspension on Mueller Hinton agar (MHA). The final inoculum concentration of *E. coli* was 7×10^5 and 8×10^5 CFU/mL of *S. aureus*. The films of chitosan and hydroxyethyl starch prepared by casting from aqueous solutions were used for comparison. The testing specimens of **C4**, chitosan, and hydroxyethyl starch in dimensions of 10×10 mm were placed into sterile Petri dishes of 50 mm diameter, inoculated with 10 µL of prepared bacterial suspension, and incubated in humid chambers at (35 ± 2) °C. After 2, 6, and 24 h the specimens were washed with 2 mL of sterile 0.85% saline, and serial dilutions of culture suspensions were sown on MHA in Petri dishes. The dishes with bacteria were incubated for 48 h at (35 ± 2) °C. After incubation, colony numbers were counted, and percent reduction was calculated by the following equation: $(a - b)/a \times 100\%$, where a is a concentration of colony forming units (CFU/mL) in inoculum; and b is a mean of recovered bacteria (CFU/mL) on specimens from triplicate after incubation.

2.5. Optical Micro-Fabrication Techniques

Two types of optical printing techniques were used to produce 3D objects out of custom made photocross-linkable resins. At first, direct laser writing (DLW) 3D lithography experiments were conducted employing a Pharos laser (515 nm, 300 fs, 200 kHz, Light Conversion Ltd., Vilnius, Lithuania), $20 \times$ NA = 0.8 and $63 \times$ NA = 1.4 objectives, and combined movement of the linear stages and galvano-scanners. The setup is shown in Figure 2a, and its detailed description can be found in a previous publication [20]. The goal was to figure out if the resins were suitable for ultrafast laser pulse initiated 3D polymerization. Woodpile structures were chosen as test objects. Their 3D model consisted of two layers of 2D gratings, connected by vertical columns 20 µm high. The gratings comprised orthogonal sets of logs 15 µm wide and 75 µm long with a 15 µm gap between them, resulting in a 30 µm period of the structure. Each log was fabricated by performing multiple parallel scans, and the number depended on the distance d_{xy} between them. d_{xy} was set to 0.25 and 0.5 µm. Optimal exposure parameters were determined by varying the laser power (P), which corresponded to the light intensity (I) at the sample and scanning velocity (v). During the fabrication, the resin was placed on a glass substrate through which it was irradiated by the laser beam. After the exposure, the samples were developed in dichloromethane for 30 min, removing the uncured resin and leaving only the produced structures on the substrate.

89
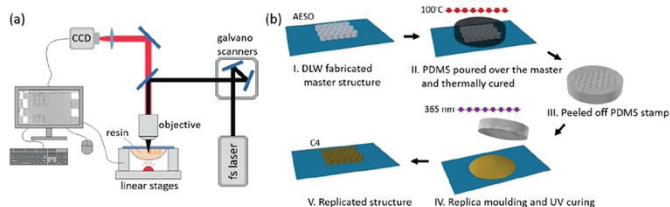
Figure 2. (**a**) Optical setup for direct laser writing (DLW) 3D lithography. (**b**) Steps of making the replica by the microtransfer molding (μTM) technique.

Secondly, a microtransfer molding (μTM) technique, also known as nanoimprint lithography, was employed [21]. Steps involved in making the replica are depicted in Figure 2b. First, a master structure was fabricated out of acrylated epoxidized soybean oil (AESO) by DLW. Polydimethylsiloxane (PDMS) was poured over this structure and thermally cured at 100 °C for 1 h, thus creating a soft mold (stamp). It was then used to make a replica out of **C4** resin. The chosen structure was a 3D sculpture of Marvin—a SLT model, used as a benchmark sample for the material testing in the 3D printing community. A UV diode emitting 365 nm wavelength light (CS2010, Thorlabs, Newton, NJ, USA) was used to cure the **C4** resin and obtain the replica.

The fabricated structures were characterized using scanning electron microscopes (SEM, Hitachi TM-1000, Tokyo, Japan and Prisma E, Eindhoven, The Netherlands).

3. Results

3.1. Monitoring of Photocross-Linking Kinetics by Real-Time Photorheometry

The photopolymerization of vanillin acrylate-based (VD and VDM) resins with various concentrations of TPOL as photoinitiator was studied by real-time photorheometry. As an example, Figure 3 shows the evolution of storage modulus G', loss modulus G'', loss factor tanδ, and complex viscosity η^* of the VDM-based resin **C9** during UV/Vis irradiation. The cross-linking process began when the values of G', G'', and η^* started to increase. The gel point (t_{gel}) (defined as $G'=G''$) [22] of resin **C9** was reached after 6 s from UV/Vis irradiation onset. As irradation of the resin proceeded with time, the values of G', G'' modulus, and η^* continued to increase due to gel aging and settling down into a steady-state, indicating the end of the cross-linking process. All vanillin acrylate-based resins showed similar behaviours. Real-time photorheometry data of all resins are summarized in Table 2.
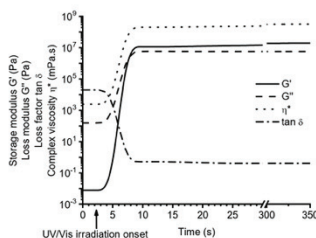
Figure 3. Dependencies of storage modulus G', loss modulus G'', loss factor tanδ, and complex viscosity η^* of resin **C9** on irradiation time, at 24 °C.

As the storage modulus G' characterizes the rigidity of the formed thermosetting polymers [23], the dependencies of G' on irradiation time of the resins with 1, 3, and 5 mol.% of TPOL are shown in Figure 4a. Comparing the shape of the G' curves of the resins with different concentrations of photoinitiator, the fastest photocross-linking and the highest final rigidity were demonstrated by resin **C4** with 3 mol.% of TPOL in the VD-based resins without solvent series (**C1**, **C4**, and **C7**). The presence of solvent had a higher influence on the photocross-linking rate than the concentration of photoinitiator. In VD-based resins with solvent series (**C2**, **C5**, and **C8**), the photocross-linking rates of two resins with 3 mol.% and 5 mol.% of TPOL (**C5** and **C8** respectively) were very similar and faster than that of resin **C2**, although a more rigid polymer was obtained from resin **C8**. In VDM-based resins with solvent series (**C3**, **C6**, and **C9**), the photocross-linking rate did not depend on the concentration of TPOL, although a more rigid polymer was obtained from resin **C9** with 5 mol.% of TPOL. Comparing the gel points (t_{gel}) of the resins (Table 2), the t_{gel} was reached the fastest when 3 mol.% of the TPOL was used in the case of all resin series. When a higher amount of photoinitiator was used, the effectiveness of photocross-linking was reduced due to the rapid photocross-linking of the surface layer, which reduced light penetration into the deeper layers of the material [24]. The addition of the solvent into the resin slowed down the photocross-linking process, and less-rigid polymers were obtained. For example, the resin **C4** without solvent reached the gel point after 6 s and a rigidity of 18.10 MPa was obtained, while resin **C5** reached the gel point only after 12 s and obtained a rigidity of 11.30 MPa (Table 2). This could be due to the solvent action as a chain transfer agent which slows down the photocross-linking process [25]. The photocross-linking of all VDM-based resins (**C3**, **C6**, and **C9**) was faster compared to all VD-based resins (**C1**, **C2**, **C4**, **C5**, **C7**, and **C8**), although the acrylate group was earlier described as more active than the methacrylate group [26]. This could be due to the darker color of VD-based resins compared with VDM-based resins that could cause a slower polymerization process by making it harder for the light to reach and cure the deeper layers of the resins [27].
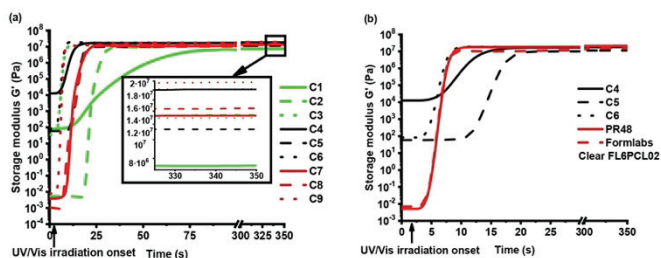

Figure 4. (**a**) Dependencies of storage modulus G' of the resins **C1**–**C9** on irradiation time. Concentration of TPOL in the resins: green curves—1 mol.%, black curves—3 mol.%, red curves—5 mol.%. (**b**) Dependencies of storage modulus G' of the resins **C4**–**C6**, FormLabs Clear FL6PCL02 and PR48 on irradiation time, at 24 °C.

The series of resins with 3 mol.% of TPOL (**C4**, **C5**, and **C6**) were selected for further investigations according to the photocross-linking rate and polymer rigidity. These resins were compared with commercial acrylate resins for optical 3D printing, FormLabs Clear FL6PCL02 and PR48 (Figure 4b). Both commercial resins demonstrated similar photocross-linking rates (both $t_{gel} = 6$ s) as resin **C4** ($t_{gel} = 6$ s) (Table 2). However, resin **C6** demonstrated a slightly higher photocross-linking rate ($t_{gel} = 5$ s) than commercial resins. Moreover, the rigidity of resins **C4** ($G' = 18.10$ MPa) and **C6** ($G' = 18.20$ MPa) was slightly higher than that of FormLabs Clear FL6PCL02 ($G' =$

15.20 MPa), but less than that of PR48 (G' = 21.40 MPa). Resin **C5** demonstrated poor behavior compared with commercial resins. The photocross-linking was slower (t_{gel} = 12 s) and the rigidity was the lowest (G' = 18.10 MPa) from all the selected resins **C4**, **C6**, and commercial resins (Table 2).

3.2. Characterization of Photocross-Linked Polymer Structure

The chemical structure of the vanillin-based polymers was identified by FT-IR spectroscopy. The signals of C=C group, which were present at 1607 cm^{-1}, and C=O group, which were present at 1730 cm^{-1}, in the FT-IR spectra of VDM and VD were reduced in the polymer spectra. The large increase of C-C group signal was detected at 1128–1131 cm^{-1}, which shows the formation of polymer. As an example, the FT-IR spectra of VD and the cross-linked polymers **C4** and **C5** are presented in Figure 5.
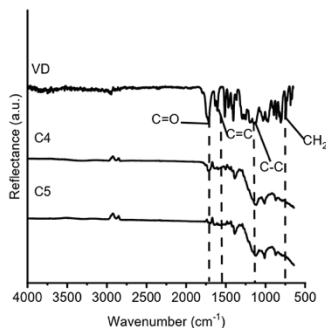

Figure 5. FT-IR spectra of VD and the cross-linked polymers **C4** and **C5**.

To confirm the formed cross-linked structure of polymers, Soxhlet extraction was performed. The highest value of the yield of insoluble fraction was obtained for polymer **C4**, for which synthesis of VD was used without addition of DCM in comparison to polymer **C5** (96% in comparison to 77%) (Table 3). Swelling tests are of great importance to characterize the network structure. The higher swelling values showed that longer chains between the cross-linking points were formed in the polymer. Both C4 and C5 are vanillin diacrylate-based polymers; the only difference is that a small amount of DCM was used in the reaction mixture of C5, which resulted in the formation of the lower yield of insoluble fraction (Table 3) and the lower crosslinking density confirmed by the higher swelling values of polymer C5 (Figure 6, Table 3). C6 is vanillin dimethacrylate-based polymer in which preparation of a small amount of DCM was used; thus, higher swelling values were obtained in chloroform. Some other factors such as the polymer–solvent interaction can affect swelling properties as well. Vanillin dimethacrylate is soluble in chloroform and insoluble in toluene. The poor interaction of vanillin dimethacrylate-based polymer chains with toluene was the reason why the swelling of polymer C6 in toluene was worse than that in chloroform (Figure 6).
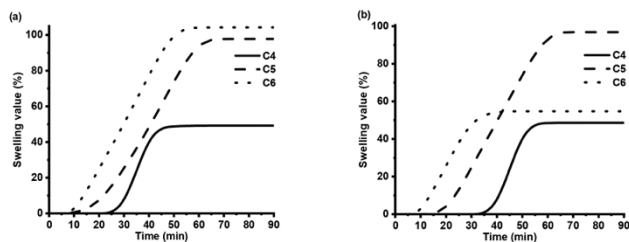
92

Figure 6. The swelling values of polymers **C4**–**C6** in chloroform (**a**) and toluene solvent (**b**)

Table 3. Characteristics of the cross-linked vanillin-based polymers.

Polymer	Yield of Insoluble Fraction, %	Swelling Value in Chloroform, %	Swelling Value in Toluene, %
C4	96	49.22 ± 0.06	48.62 ± 0.06
C5	77	97.83 ± 0.06	96.85 ± 0.06
C6	89	104.21 ± 0.06	54.72 ± 0.06

3.3. Thermal Properties of Photocross-Linked Polymers

DSC and TGA were used to study the thermal characteristics of the photocross-linked polymers **C4**-**C6**. Synthesized polymers are amorphous materials; therefore, only a glass transition was obtained in DSC curves (Figure 7a). The glass transition temperatures (T_g) of polymers **C4** and **C6** were very similar (87 and 86 ˚C, respectively) and depended on the cross-linking density and the yield of insoluble fraction. A lower glass transition temperature was observed for polymer **C5** (63 ˚C), with the lowest cross-linking density determined from the swelling test results. The glass transition temperatures of obtained polymers were similar to the acrylate resins based on natural phenolics, presented as candidate materials for stereolithography (79 ˚C) [28].
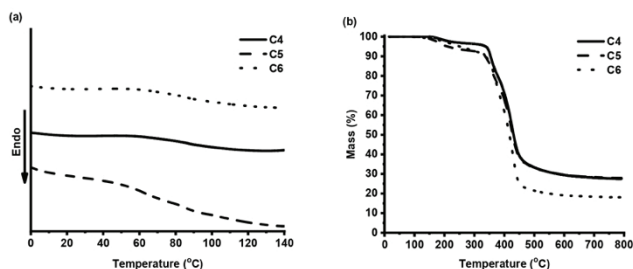
Figure 7. DSC thermograms (**a**) and thermogravimetric curves (**b**) of cross-linked polymers **C4**–**C6**.

Thermal decomposition of the synthesized polymers occurred in two steps (Figure 7b). The first step in the TGA curves can be explained by the presence of the branched or linear macromolecules. The temperature of 10% weight loss ($T_{dec.-10\%}$) of the VD-based polymer **C4** (350 ˚C) was higher than that of the VD-based polymer **C5** prepared using DCM (330 ˚C) and the VDM-based polymer **C6** (340 ˚C). Higher $T_{dec.-10\%}$ correlated with the higher yield of insoluble fraction and cross-linking density. The temperature of 10% weight loss of obtained polymers was similar or even slightly higher than that of some acrylated epoxidized soybean oil-based polymers (297–356 ˚C) tested in 3D printing [20].

3.4. Mechanical Properties of Photocross-Linked Polymers

Only resin **C4** was suitable for the preparation of the specimens for bending and top pressure tests because the specimens of resins **C5** and **C6** cracked during the photocross-linking process, and it was impossible to make uniform specimens for these tests. To improve the mechanical properties of these polymers, addition of reactive diluents will be carried out in further studies. Commercial photoresins PR48 and FormLabs Clear FL6PCL02 were tested in the same conditions to compare their mechanical characteristics with those of polymer **C4**. The mechanical testing results are summarized in Table 4. All polymers demonstrated low deformation during compression tests. Polymer **C4** demonstrated a lower compression modulus than that of the polymers prepared from the commercial resins PR48 and FormLabs Clear FL6PCL02, but a much higher compression modulus than the acrylated epoxidized soybean oil based polymers (0.19–0.66 Pa) tested in 3D printing [20]. The specimens of all polymers did not break during the bending test. Very similar 30% specimen bending forces and bending modulus were obtained for polymers **C4** and PR48. The specimen prepared from FormLabs Clear FL6PCL02 demonstrated a lower 30% specimen bending force and bending modulus.

Table 4. Mechanical characteristics of the cross-linked vanillin-based polymers.

Polymer	Deformation during Compression, %	Compression Modulus, MPa	Force of Specimen Bend of 30 %, N	Bending Modulus, MPa
C4	4.95 ± 0.02	2.01 ± 0.02	3.65 ± 0.04	9.47 ± 0.04
PR48	1.79 ± 0.02	5.56 ± 0.02	3.39 ± 0.07	8.80 ± 0.07
FormLabs Clear FL6PCL02	1.39 ± 0.02	7.17 ± 0.02	0.42 ± 0.02	1.09 ± 0.02

According to the results, resin **C4** was selected for further testing by optical micro-fabrication techniques, and the testing of antimicrobial activity was carried out.

3.5. Antimicrobial Activity

The testing of antimicrobial activity was performed for polymer **C4** and two reference polymer films of chitosan and hydroxyethyl starch. The results of antibacterial activity testing demonstrated that polymer **C4** killed 99% of both Gram-negative *E. coli* and Gram-positive *S. aureus* after 6 h of contact time, and after 24 h, all bacteria on this film were lifeless (Figure 8). Bacteria on the hydroxyethyl starch film, having no antibacterial activity, even began to propagate after 2 contact hours. In comparison with chitosan, which is known to have a very strong antibacterial activity [29], polymer **C4** showed only a bit weaker activity. In our experiment, bacteria on the chitosan film were killed completely after 2 contact hours. These results are in agreement with other studies indicating significant antimicrobial effects of vanillin and vanillin incorporation into complex compounds [18,30,31].
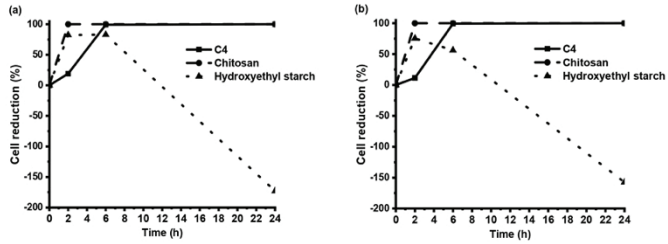
94

Figure 8. The reduction of *E. coli* (**a**) and *S. aureus* (**b**) cells during 24 h of contact time with specimens of polymer **C4**, chitosan, and hydroxyethyl starch.

3.6. Characterization of Optically Printed Structures

A test to assess the optimal fabrication parameters was performed, and the capability to produce 3D microporous woodpile structures out of the resin **C4** via DLW was demonstrated. An array of 75 × 75 μm² woodpiles is shown in Figure 9a,b. Manufacturing parameters and focusing conditions are provided in the caption of Figure 9.
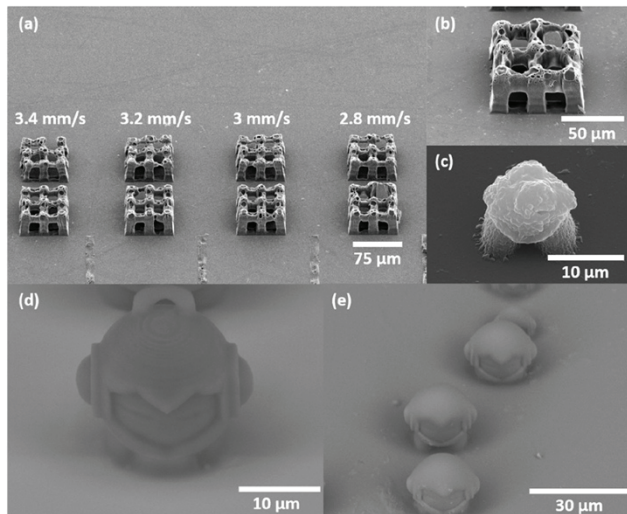
Figure 9. (**a**) Array of the 75 × 75 µm² size woodpile structures out of **C4** resin: v varies from 2.8 to 3.4 mm/s, P = 0.4 mW (I = 1.2 TW/cm²) and d_{xy} = 0.25 µm (lower row), P = 0.5 mW (I = 1.5 TW/cm²) and d_{xy} = 0.5 µm (upper row). (**b**) Close-up of the 75 × 75 µm² woodpile structure: v = 1 mm/s, P = 0.3 mW (I = 0.9 TW/cm²), d_{xy} = 0.25 µm. (**c**) Sculpture of Marvin out of **C4** resin: v = 1.8 mm/s, P = 0.1 mW (I = 0.3 TW/cm²), d_{xy} = 0.25 µm. (**d**) Sculpture of Marvin out of AESO: v = 1.2 mm/s, P = 0.18 mW (I = 0.6 TW/cm²), d_{xy} = 0.25 µm. (**e**) Sculptures of Marvin out of **C4** resin molded from the master structure (section (**d**)) via microtransfer molding; 365 nm wavelength light source was used for curing. Objects in sections (**a**) and (**b**) were manufactured with 20 × 0.8 NA objective, (**c**) and (**d**) 63 × 1.4 NA. All SEM images were obtained at 45° angle.

Produced objects corresponded to the used 3D model, however with deviations including tilted columns and not fully formed logs. These could happen due to the too low degree of cross-linking, which causes shrinkage, when d_{xy} 0.5 µm was applied. Also, the voids on the woodpile's surfaces were observed. The voids were caused by bubbles, which have appeared due to the inhomogeneity of the resin, resulting in the deviation of the optical damage threshold through the whole material. Thus, in exposing resin **C4** with tightly focused laser irradiation, some parts were over-exposed and induced bubble formation. Using a higher numerical aperture objective, a sculpture of Marvin was produced (Figure 9c). The basic shape of the given STL model was polymerized, but detailed parts of the face, ears, and the loop were missing. To obtain a well-defined Marvin out of **C4** resin, a µTM technique was employed. A master structure of Marvin was produced out of AESO (Figure 9d). The replicated structures of Marvin were manufactured by curing the **C4** resin inside a PDMS mold with UV diode. The obtained objects are demonstrated in Figure 9e. In this case, the produced Marvin had a smooth surface and detailed parts, except loops, which were not replicated due to the limited capability of the µTM technique to replicate closed loops. Differences in material surface appearance emerged because of the different illumination conditions. Using DLW, objects were made of stitched scanning point-by-point manner and thresholded light-matter interaction, sensitive to the material's inhomogeneity. On the other hand, with µTM a uniform UV irradiation distribution resulted in homogeneous curing.

4. Conclusions

Novel vanillin acrylate-based resins were designed and investigated as candidate materials for optical 3D printing. The kinetics of photocross-linking of vanillin dimethacrylate or vanillin diacrylate using ethyl(2,4,6-trimethylbenzoyl)phenylphosphinate as photoinitiator were investigated by real-time photorheometry. The photocross-linking of the vanillin dimethacrylate-based resins was faster compared with the vanillin diacrylate-based resins. The gel point was reached the fastest when 3 mol.% of photoinitiator was used. The addition of solvent into the resin slowed down the photocross-linking process, and less-rigid polymers were obtained. The vanillin diacrylate-based polymer prepared without solvent possessed higher values of yield of insoluble fraction, thermal stability, and lower swelling values in comparison to the vanillin dimethacrylate-based polymer. Only the vanillin diacrylate-based polymer prepared without solvent was appropriate for testing of mechanical properties. It demonstrated similar properties to those of the commercially available photocurable resins. Subsequently, the possibility to optically structure this resin was successfully demonstrated. Although acquisition of a smooth surface of the structures proved to be challenging when employing DLW 3D lithography due to material inhomogeneity, the microtransfer molding technique allowed to overcome this limitation. For the improvement of the mechanical properties of other polymers, the addition of reactive diluents will be carried out in further studies. Vanillin diacrylate polymer film showed a significant antimicrobial effect only a bit weaker than that of chitosan film.

experiments and characterized the antimicrobial activity; all authors contributed to writing the manuscript. All authors have read and agreed to the published version of the manuscript.

References

1. Liu, J.; Sun, L.; Xu, W.; Wang, Q.; Yu, S.; Sun, J. Current advances and future perspectives of 3D printing natural-derived biopolymers. *Carbohydr. Polym.* **2019**, *207*, 297–316, doi:10.1016/j.carbpol.2018.11.077.
2. Li, N.; Huang, S.; Zhang, G.; Qin, R.; Liu, W.; Xiong, H.; Shi, G.; Blackburn, J. Progress in additive manufacturing on new materials: A review. *J. Mater. Sci. Technol.* **2019**, *35*, 242–269, doi:10.1016/j.jmst.2018.09.002.
3. Li, Y.; Zhong, J.; Wu, L.; Weng, Z.; Zheng, L.; Peng, S.; Zhang, X. High performance POSS filled nanocomposites prepared via UV-curing based on 3D stereolithography printing. *Compos. Part A* **2019**, *117*, 276–286, doi:10.1016/j.compositesa.2018.11.024.
4. Dizon, J.RC.; Espera Jr., A.H.; Chen, Q.; Advincula, R.C. Mechanical characterization of 3D-printed polymers. *Addit. Manuf.* **2018**, *20*, 44–67, doi:10.1016/j.addma.2017.12.002.
5. Barner-Kowollik, Ch.; Bastmeyer, M.; Blasco, E.; Delaittre, G.; Muller, P.; Richter, B.; Wegener, M. 3D Laser micro- and nanoprinting: Challenges for chemistry. *Angew. Chem. Int. Ed.* **2017**, *56*, 15828–15845, doi:10.1002/anie.201704695.
6. Schift, H. Nanoimprint lithography: 2D or not 2D? A review. *Appl. Phys. Part A* **2015**, *121*, 415–435, doi:10.1007/s00339-015-9106-3.
7. Andrzejewska, E. Photopolymerization kinetics of multifunctional monomers. *Prog. Polym. Sci.* **2001**, *26*, 605–665, doi:10.1016/S0079-6700(01)00004-1.
8. Sangermano, M.; Razza, N.; Crivello, J.V. Cationic UV-Curing: Technology and Applications. *Macromol. Mater. Eng.* **2014**, *299*, 775–793, doi:10.1 002/mame.201300349.
9. Yagci, Y.; Jockusch, S.; Turro, N.J. Photoinitiated Polymerization: Advances, Challenges, and Opportunities. *Macromolecules* **2010**, *43*, 6245–6260, doi:10.1021/ma1007545.
10. Wu. J.; Zhao, Z.; Hamel, C.M.; Mu, X.; Kuang, X.; Guo, Z.; Qi, H.J. Evolution of material properties during free radical photopolymerization. *J. Mech. Phys. Solids.* **2018**, *112*, 25–49, doi:10.1016/j.jmps.2017.11.018.
11. Kaur, M.; Srivastava, A.K. Photopolymerization: A Review. *J. Macromol. Sci. Polymer. Rev.* **2002**, C42, 481–512, doi:10.1081/MC-120015988.
12. Green, W.A. *Industrial Photoiniciators. A Technical Guide*, 1st ed.; CRC Press: Boca Raton, FL, USA; Taylor and Francis Group: London, UK, 2001; ISBN 978-14-3982-745-1.
13. Fache, M.; Boutevin, B.; Caillol, S. Vanillin Production from Lignin and Its Use as a Renewable Chemical. *Sustain. Chem. Eng.* **2016**, *4*, 35–46, doi:10.1021/acssuschemeng.5b01344.
14. Yu, Q.; Peng, X.; Wang, Y.; Geng, H.; Xu, A.; Zhang, X.; Xu, W.; Ye, D. Vanillin-based degradable epoxy vitrimers: Reprocessability and mechanical properties study. *Eur. Polym. J.* **2019**, *117*, 55–63, doi:10.1016/j.eurpolymj.2019.04.053.
15. Steinmetz, Z.; Kurtz, M.P.; Zubrod, J.P.; Meyer, A.H.; Elsner, M.; Schaumann, G.E. Biodegradation and photooxidation of phenolic compounds in soil-A compound-specific stable isotope approach. *Chemosphere* **2019**, *230*, 210–218, doi:10.1016/j.chemosphere.2019.05.030.
16. Wang, S.; Ma, S.; Xu, C.; Liu, Y.; Dai, J.; Wang, Z.; Liu, X.; Chen, J.; Shen, X.; Wei, J.; et al. Vanillin-Derived High-Performance Flame Retardant Epoxy Resins: Facile Synthesis and Properties. *Macromolecules* **2017**, *50*, 1892–1901, doi:10.1021/acs.macromol.7b00097.
17. Fitzgerald, D.J.; Stratford, M.; Gasson, M.J.; Ueckert, J.; Bos, A.; Narbad, A. Mode of antimicrobial of vanillin against Escherichia coli, *Lactobacillus plantarum* and *Listeria innocua. J. Appl. Microbiol.* **2004**, *97*, 104–113, doi:10.1111/j.1365-2672.2004.02275x.

18. Salmi-Mani, H.; Terreros, G.; Barroca-Aubry, N.; Aymes-Chodur, C.; Regeard, C.; Roger, P. Poly(ethylene terephthalate) films modified by UV-induced surface graft polymerization of vanillin derived monomer for antibacterial activity. *Eur. Polym. J.* **2018**, *103*, 51–58, doi:10.1016/j.eurpolymj.2018.03.038.

19. Licari, J.J.; Swanson, D.W. *Adhesives Technology for Electronic Applications*, 2nd ed.; Elsevier Science: Amsterdam, The Netherlands, 2011; ISBN 978-08-1551-600-2.

20. Lebedevaite, M.; Ostrauskaite, J.; Skliutas, E.; Malinauskas, M. Photoinitiator free Resins Composed of Plant-Derived Monomers for the Optical μ-3D Printing of Thermosets. *Polymers* **2019**, *11*, 116, doi:10.3390/polym11010116.

21. Danilevičius, P.; Rekšytė, S.; Balčiūnas, E.; Kraniauskas, A.; Širmenis, R.; Baltriukienė, D.; Bukelskienė, V.; Gadonas, R.; Sirvydis, V.; Piskarskas, A.; et al. Laser 3D micro/nanofabrication of polymers for tissue engineering applications. *Opt. Laser Technol.* **2013**, *45*, 518–524, doi.org/10.1016/j.optlastec.2012.05.038.

22. Mezger, T.G. *The Rheology Handbook*, 3rd ed.; Vincentz Network: Hanover, Germany, 2011; ISBN 978-38-6630-864-0.

23. Candan, Z.; Gardner, D.J.; Shaler, S.M. Dynamic mechanical thermal analysis (DMTA) of cellulose nanofibril/nanoclay/pMDI nanocomposites. *Compos. Part B* **2016**, *90*, 126–132, doi:10.1016/j.compositesb.2015.12.016.

24. Macarie, L.; Ilia, G. The influence of temperature and photoinitiator concentration on photoinitiated polymerization of diacrylate monomer. *Cent. Eur. J. Chem.* **2005** 3, 721-730, doi:10.2478/BF02475199.

25. Valdebenito, A.; Encinas, M.V. Effect of solvent on the free radical polymerization of N,N-dimethylacrylamide. *Polym. Int.* **2010**, *59*, 1246–1251, doi:10.1002/pi.2856.

26. Miyazaki, K.; Horibe, T. Polymerization of multifunctional methacrylates and acrylates. *J. Biomed. Mater. Res.* **1988**, *22*, 1011–1022, doi:10.1002/jbm.820221105.

27. Shortall, A.C. How light source and product shade influence cure depth for a contemporary composite. *J. Oral. Rehabil.* **2005**, *32*, 906–911, doi:10.1111/j.1365-2842.2005.01523.x.

28. Ding, R.; Du, Y.; Goncalves, R.B.; Francis, L.F.; Reineke, T.M. Sustainable near UV-curable acrylates based on natural phenolics for stereolithography 3D printing. *Polym. Chem.* **2019**, *10*, 1067–1077, doi:10.1016/j.eurpolymj.2019.04.053.

29. Benhabiles, M.S.; Salah, R.; Lounici, H.; Drouiche, N.; Goosen, M.F.A.; Mameri, N. Antibacterial activity of chitin, chitosan and its oligomers prepared from shrimp shell waste. *Food Hydrocoll.* **2012**, *29*, 48–56, doi:10.1016/j.foodhyd.2012.02.013.

30. Ngarmsak, M.; Delaquis, P.; Toivonen, P.; Ngarmsak, T.; Ooraikul, B.; Mazza, G. Antimicrobial activity of vanillin against spoilage microorganisms in stored fresh-cut mangoes. *J. Food Prot.* **2006**, *69*, 1724–1727, doi:10.4315/0362-028x-69.7.1724.

31. Ünver, H.; Cantürk, Z.; Özarda, M.G. Evaluation of antimicrobial effect against some microorganisms and apoptotic activity against Candida species of new vanillin derivatives. *CBU J. Sci.* **2019**, 15 87-94, doi:10.18466/cbayarfbe.475456.

Article

Influence of Vanillin Acrylate-Based Resin Composition on Resin Photocuring Kinetics and Antimicrobial Properties of the Resulting Polymers

Aukse Navaruckiene [1], Danguole Bridziuviene [2], Vita Raudoniene [2], Egidija Rainosalo [3] and Jolita Ostrauskaite [1,*]

[1] Department of Polymer Chemistry and Technology, Kaunas University of Technology, Radvilenu Rd. 19, LT-50254 Kaunas, Lithuania; aukse.navaruckiene@ktu.lt

[2] Biodeterioration Research Laboratory, Nature Research Center, Akademijos Str. 2, LT-08412 Vilnius, Lithuania; danguole.bridziuviene@gamtc.lt (D.B.); vita.raudoniene@gamtc.lt (V.R.)

[3] Chemistry and Bioeconomy Team, Centria University of Applied Sciences, Talonpojankatu 2, FI-67100 Kokkola, Finland; egidija.rainosalo@centria.fi

[*] Correspondence: jolita.ostrauskaite@ktu.lt; Tel.: +370-37-300192

Abstract: The investigation of the influence of vanillin acrylate-based resin composition on photocuring kinetics and antimicrobial properties of the resulting polymers was performed in order to find efficient photocurable systems for optical 3D printing of bio-based polymers with tunable rigidity, as well as with antibacterial and antifungal activity. Two vanillin derivatives, vanillin diacrylate and vanillin dimethacrylate, were tested in photocurable systems using phenyl bis(2,4,6-trimethylbenzoyl)phosphine oxide as a photoinitiator. The influence of vanillin acrylate monomer, amount of photoinitiator, presence and amount of dithiol, and presence of solvent on photocuring kinetics was investigated by real-time photoreometry. Polymers of different rigidity were obtained by changing the photocurable resin composition. The photocuring kinetics of the selected vanillin acrylate-based resins was comparable with that of commercial petroleum-based acrylate resins for optical 3D printing. Polymers based on both vanillin acrylates showed a significant antibacterial activity against *Escherichia coli* and *Staphylococcus aureus*. Vanillin diacrylate-based polymer films also demonstrated an antifungal activity in direct contact with *Aspergillus niger* and *Aspergillus terreus*. Vanillin diacrylate-based dual curing systems were selected as the most promising for optical 3D printing of bio-based polymers with antibacterial and antifungal activity.

Keywords: thermosets; bio-based polymers; photocuring; photoreometry; antimicrobial polymers; optical 3D printing

1. Introduction

Recently, the search for bio-based photocurable resins for optical 3D printing has received considerable academic and industry attention due to the possibility of efficient development and production of sustainable products on-demand. Optical 3D printing is getting popular in the manufacturing companies since it is a cheap and fast way to produce new products in complex shapes [1]. It provides such benefits as lower material loss, reduced product weight, and the possibility to print spare parts without using fixtures or molds [2,3]. Optical 3D printing is used in various areas, such as dentistry [4], medicine [5], construction industry [6], etc. [7]. Increasing the popularity of optical 3D printing leads to the environmental problems, such as lack of bio-based materials with the same properties as petroleum-based materials [8] and recycling problems of the used products [9]. Additionally, nowadays, the antimicrobial activity of polymers is more important than ever. Food packaging for perishable products, such as meat and meat products [10], antimicrobial coatings for medical instruments, and implantable biomedical devices [11] are only a few examples of the possible application of such polymers.

One of the possible starting materials for the synthesis of bio-based polymers with an antimicrobial activity is vanillin [12]. Natural vanillin can be extracted from two different species of vanilla orchids: *Vanilla tahitensis* and *Vanilla planifolia* [13]. A cheaper way to obtain vanillin is the chemical modification of lignin [14]. Vanillin produced from lignin is considered as a natural vanillin [15] and is 250 times cheaper than synthetic vanillin [16]. Pure vanillin demonstrates impressive antibacterial activity against *Escherichia coli* and *Zygosaccharomyces rouxii* bacteria [13]. Some of the vanillin derivatives were also investigated for antibacterial and antifungal activity and were moderately active against them [17–21].

Photopolymerization is a valuable tool for the production of vanillin-based polymers. It can be used in a wide range of such areas as automotive, optical, and electronic equipment coatings [22], nanotechnology [23], stereolithography [24], medicine [25], etc. Photopolymerization is a fast polymerization process, which allows curing only the selected area of the product [22,26]. Vanillin acrylate, methacrylate, or acrylamide are the most common compounds for chain-growth polymerization [27]. Their polymerization is easily induced by UV light when the appropriate photoinitiator is used [28]. Vanillin-based photopolymers were successfully synthesized using acrylated epoxidized soybean oil as a comonomer [29].

Several photocuring techniques, free-radical photopolymerization, thiol-Michael photopolymerization, and dual curing combining both of them, were used in this study. Free-radical photopolymerization is relatively insensitive to impurities [30] and does not require the exclusion of moisture [31]. Heating is not required for this reaction, it can be run at room temperature or below [32] in solvent-free systems [33] with a spatial and temporal control of initiation [34] and it is a rapid process that occurs within a matter of minutes [35]. The main disadvantage of free-radical photopolymerization is the poor control of molecular weight and its distribution [36], as well as oxygen inhibition [37]. Thiol-Michael photopolymerization is a light activated reaction [38] which proceeds rapidly with no side products [39]. Its main advantages over free-radical photopolymerization are no inhibition by moisture and oxygen [40] and generation of homogenous materials [41]. Other advantages are high reaction rate [42], spatial and temporal control [43], and selective reactivity [44]. Dual curing is an effective tool to control the polymer network formation to obtain thermosets with desirable properties [45].

This work is a continuation of the previous studies [46,47] and focuses on the comparison of the influence of the resin composition on photocuring kinetics of free-radical, thiol-Michael, and dual curing systems with phenyl bis(2,4,6-trimethylbenzoyl) phosphine oxide (BAPO), as well as on antibacterial and antifungal properties of the resulting polymers. BAPO was selected for this study due to its advantage to release four radicals from a single monomer. Therefore, increasing the initiation performance [48] compared to ethyl (2,4,6-thimethylbenzoyl) phenyl phosphinate (TPOL) and diphenyl (2,4,6-trimethyl benzoyl) phosphine oxide (TPO) [46,47], which delivers two radicals [49]. Moreover, BAPO shows a more intensive absorbance, which indicates its higher photosensitivity and thus efficiency in comparison to TPOL and TPO [46,47]. BAPO is a type I photoinitiator which can participate in both thiol-Michael and radical photopolymerization reactions [50]. It does not require the addition of a co-initiator and generates radicals by a photocleavage process [51]. BAPO absorbs light at a relatively short wavelength, and as a result, polymers produced using BAPO have a very pale yellow color or no color at all [52]. These polymers demonstrate a high color stability and do not get yellow over time [53,54].

This work was performed in order to find efficient photocurable systems for optical 3D printing of bio-based polymers with tunable rigidity, as well as with antibacterial and antifungal activity.

2. Materials and Methods

Vanillin dimethacrylate (VDM) and vanillin diacrylate (VD) were purchased from Specific Polymers (Castries, France). 1,3-Benzenedithiol (BDT), phenyl bis(2,4,6-trimethylbenzo

yl)phosphine oxide (BAPO), chitosan, and hydroxyethyl starch were purchased from Sigma-Aldrich (Darmstadt, Germany). Dichloromethane (DCM) was purchased from Reachem Slovakia (Bratislava, Slovakia). All the materials were used as received. The FormLabs Clear FL6PCL02 resin was received from FormLabs (Somerville, MA, USA). The Autodesk Standard Clear Prototyping Resin (PR48) was received from Autodesk (Mill Valley, CA, USA).

UV/Vis real-time photorheometry curing tests were performed with the resins containing 1 mol of vanillin derivative (VDM or VD), 0.5 or 1 mol of thiol (BDT) or without it, solvent DCM or without it, and 1, 3, or 5 mol% of photoinitiator (BAPO) (Figure 1) on a MCR302 rheometer (Anton Paar, Graz, Austria) equipped with the plate/plate measuring system. The Peltier-controlled temperature chamber with the glass plate (diameter 38 mm) and the top plate PP08 (diameter 8 mm) was used. The measuring gap was set to 0.1 mm. The samples were irradiated by UV/Vis light in a wavelength range of 250–450 nm through the glass plate of the temperature chamber using the UV/Vis spot curing system OmniCure S2000 (Lumen Dynamics Group Inc., Mississauga, ON, Canada). The shear mode with the frequency of 10 Hz and shear strain of 0.9% were used in all cases. The values of the storage modulus (G') after 350 s of irradiation and the values of the gel point (t_{gel}), defined as a crossover point of the storage modulus G' and loss modulus G'', were selected for the analysis during this study. The arithmetic average of each parameter of three measurements of each resin was calculated. The variation of the experimental results did not exceed 5% within the group.
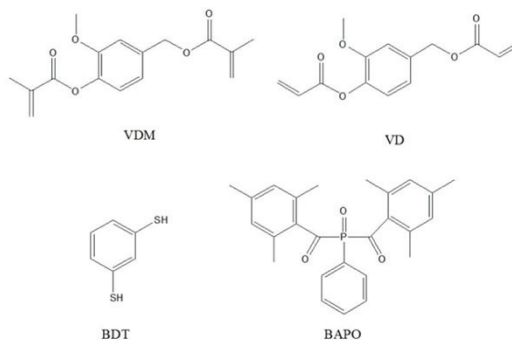
Figure 1. Structures of vanillin dimethacrylate (VDM), vanillin diacrylate (VD), 1,3-benzenedithiol (BDT), and phenylbis(2,4,6-trimethylbenzoyl)phosphine oxide (BAPO).

Resin codes indicating the resin content were created as follows:

- 1 VDM or 1 VD shows that 1 mol of vanillin derivative, vanillin dimethacrylate (VDM), or vanillin diacrylate (VD) was used;
- 1 BDT or 0.5 BDT shows the presence and amount (1 mol or 0.5 mol) of 1,3-benzenedithiol;
- the number before BAPO indicates the concentration of the photoinitiator (1 BAPO means that 1 mol% of BAPO, 3BAPO—3 mol% of BAPO, and 5 BAPO—5 mol% of BAPO were used);
- DCM indicates the presence of dichloromethane in the resin composition.

For example, **1VDM/1BDT/1BAPO/DCM** is a resin composed of 1 mol of vanillin dimethacrylate, 1 mol of 1,3-benzenedithiol, 1 mol% of bis(2,4,6-trimethylbenzoyl)phosphine oxide, and a minimal amount of dichloromethane is needed to dissolve the solid components (0.25 g of DCM for 1 g of vanillin acrylate).

101

The vanillin-based polymer films were prepared by mixing all the materials with a magnetic stirrer at room temperature (25 °C) until the homogenous phase was reached and then poured into a Teflon mold and cured for 1–2 min under an UV lamp (Helios Italquartz, model GR.E 500 W, Milan, Italy) with UV/Vis light at an intensity of 310 mW/cm^2. Photocross-linked polymer films were not washed after the UV curing. The films of chitosan and hydroxyethyl starch were prepared by casting from aqueous solutions (2% of chitosan and 9% of hydroxyethyl starch) of the commercial solid powders and drying at room temperature (25 °C).

The yield of insoluble fraction was determined by Soxhlet extraction. Polymer samples of 0.5 g were extracted with acetone for 24 h. After the extraction, the insoluble fractions were dried under a vacuum until no changes of the weight were observed. The yield of the insoluble fraction was calculated as a difference of the weight before extraction and after extraction and drying. The arithmetic average of the yield of insoluble fraction of the three film samples of each polymer was calculated. The variation of the experimental results did not exceed 5% within the group.

The swelling value of the cross-linked polymer specimens was obtained by measuring the volume of specimens swollen in acetone and toluene at 25 °C. The polymer film specimens of 10 ($\pm$0.1) mm length, 3 ($\pm$0.00) mm width, and 1.5 ($\pm$0.1) mm thickness were used. The initial volume of the polymer specimen was measured before placing it into the measuring container. After the solvent was poured into the measuring container, the change of the volume of the swelling agent was measured every 5 min until no change was obtained.

$$\alpha = \frac{V - V_0}{V_0} \cdot 100 \tag{1}$$

where α is a swelling value (%); V is a volume of the swollen specimen (mL); and V_0 is an initial volume of the specimen (mL). The arithmetic average of the swelling value of the three film samples of each polymer was calculated. The variation of the experimental results did not exceed 5% within the group. No change of the volume was observed after 90 min for all the polymer samples. This value was taken for the comparison of swelling values of different polymers.

The study of the antimicrobial (antibacterial and antifungal) activity of polymers was performed in two ways: By the contact of polymer film specimens with a microbial growing culture on a solid medium and by the direct contact with microbial spores. The test microorganisms were Gram-negative bacterium *Escherichia coli* ATCC 25,922 (*E. coli*) and Gram-positive bacterium *Staphylococcus aureus* ATCC 29,213 (*S. aureus*), which were procured from the American Type Culture Collection (Manassas, VA, USA)., as well as fungal strains: *Aspergillus niger* 1089-13 (*A. niger*) and *Aspergillus terreus* 1084-10 (*A. terreus*) which were taken from the collection of Biodeterioration Research Laboratory, Nature Research Center (Vilnius, Lithuania).

In the first way performed according to ISO 846:1998 [55], Petri dishes with a Mueller Hinton Agar (MHA, Liofilmchem, Roseto degli Abruzzi, Italy) medium were inoculated with test bacterium *E. coli* or *S. aureus* and dishes with a Malt Extract Agar (MEA, Liofilmchem, Italy) medium were inoculated with *A. niger* or *A. terreus*. The test specimens of vanillin-based polymers and chitosan in dimensions of 10 mm × 10 mm × 0.4 mm and hydroxyethyl starch in dimensions of 20 mm × 20 mm × 0.4 mm were placed on the medium in the center of the dishes. Chitosan and hydroxyethyl starch were used as reference polymers. The films of chitosan and hydroxyethyl starch were prepared by casting from aqueous solutions. The dishes with bacteria were incubated for 48 h at 35 $\pm$ 2 °C and the dishes with fungi were incubated for 5 days at 26 $\pm$ 2 °C. After incubation, the antimicrobial activity was evaluated by the growth inhibition zones (mm) of microorganisms that have shown up around the specimens. Each specimen was tested in triplicate experiments. The mean value of the zones and mean standard deviation was calculated.

The second way of the polymer antimicrobial activity estimation was performed by a direct polymer film specimen inoculation with the suspension of microbial spores. The

concentration of the inoculum of bacterium suspension was assessed with a spectrophotometer (Evolution 60S, Thermo Fisher Scientific, Waltham, MA, USA) at 600 nm and fungal suspension at 530 nm, then corrected by seeding the bacterium suspension on a Mueller Hinton Agar (MHA, Liofilmchem, Italy) and the fungal suspension on a Malt Extract Agar (MEA, Liofilmchem, Italy). The final inoculum concentrations were 6×10^5 for *E. coli*, 7×10^5 for *S. aureus*, 2.2×10^6 for *A. niger*, and 2×10^6 colony forming units/mL (CFU/mL) for *A. terreus*. The testing specimens of vanillin-based polymers and chitosan in dimensions of 10 mm × 10 mm × 0.4 mm, and the testing specimens of hydroxyethyl starch in dimensions of 20 mm × 20 mm × 0.4 mm were placed into 50 mm diameter sterile Petri dishes, inoculated with 10 µl of prepared bacterial or fungal suspension and incubated in humid chambers with bacteria at 35 ± 2 °C and with fungi at 26 ± 2 °C. Each specimen was tested in triplicate experiments. After 24 h, the specimens were washed with 2 mL of saline (0.9%) and serial dilutions of culture suspensions were sown on MHA for bacteria and on MEA for fungi in Petri dishes. The dishes with bacteria were incubated for 48 h at 35 ± 2 °C and the dishes with fungi were incubated for 5 days at 26 ± 2 °C. After incubation, colony numbers were counted and the percent reduction was calculated according to the formula: $(a − b)/a \times 100\%$, where a is the concentration of the colony forming units (CFU/mL) in inoculum suspension; b is a mean of the recovered spores (CFU/mL) on specimens from triplicate experiments after incubation. The log reduction of viable spores was calculated according to the formula: $\log(a) − \log(b)$, where a is the concentration of the colony forming units (CFU/mL) in the inoculum suspension; b is a mean of the recovered spores (CFU/mL) on specimens from triplicate experiments after incubation.

Statistical Analysis. The collected data were statistically analyzed using ANOVA for the Microsoft Excel programme. All the experiments were performed three times and the results were assumed as the average values ± standard deviation. The estimated p-value was below 0.05 within the groups.

3. Results and Discussion

3.1. Influence of Resin Composition on Photocuring Kinetics

The photocuring kinetics of vanillin acrylate-based photocurable resins of different compositions was investigated by real-time photoreometry and compared. The values of the storage modulus (G') and the gel point (t_{gel}) were analyzed during this study. The trends of loss modules are the same as those of the storage modules during irradiation of all vanillin-based resins, thus, only storage modules will be analyzed in this work.

The gel point is a point at which a high-viscosity Newtonian fluid turns into a solid elastic material [52]. It characterizes the formation of the polymer network. The storage modulus is a measure of the deformation energy stored by the sample during the shear process and representing the elastic behavior of the material [56]. It characterizes the rigidity of the resulting polymers.

3.1.1. Influence of Photoinitiator Concentration

VDM-based resins prepared with or without BDT showed a clear dependence of an increase in the t_{gel} value with the increasing BAPO concentration (Figure 2a). BAPO is a highly reactive photoinitiator and its very low concentration is sufficient to initiate polymerization effectively. In VDM-based resins, the lowest value of t_{gel} was determined when 1 mol% of BAPO was used. However, at higher photoinitiator concentrations, the t_{gel} values increased. It could be due to the generation of the higher concentration of free radicals at the surface, which block the sufficient energy from penetrating, leading to the reduced rate of polymerization [57]. The t_{gel} values of the VDM-based resins with or without BDT and 1–3 mol% of BAPO are very similar. However, a significant reduction of the G' values was obtained when BDT was used, showing the formation of linear polymer chains with flexible thioether linkages [52] in these cases (**1VDM/1BDT/1BAPO/DCM**, **1VDM/1BDT/3BAPO/DCM**) (Figure 2b). The higher the G' value and rigidity of the re-

103

sulted VDM-based polymer with BDT (**VDM/1BDT/5BAPO/DCM**) was obtained probably due to the increase of termination reactions of macroradicals with free radicals which usually occur at the high photoinitiator concentration [48,58], and thus the shorter polymer chains leading to the less rigid polymer were formed in this case. The G' values of pure VDM resins increased with an increase in the BAPO concentration (**VDM/1BAPO/DCM, VDM/3BAPO/DCM**). However, the G' value of the resin with 5 mol% of BAPO (**VDM/5BA PO/DCM**) was lower due to the effect of termination reactions.
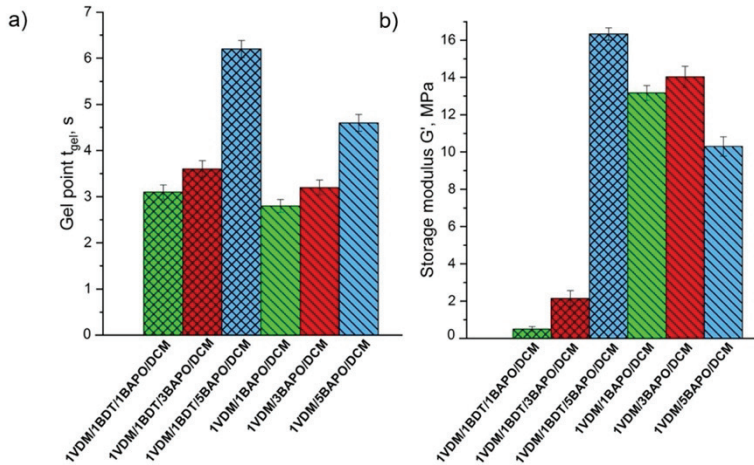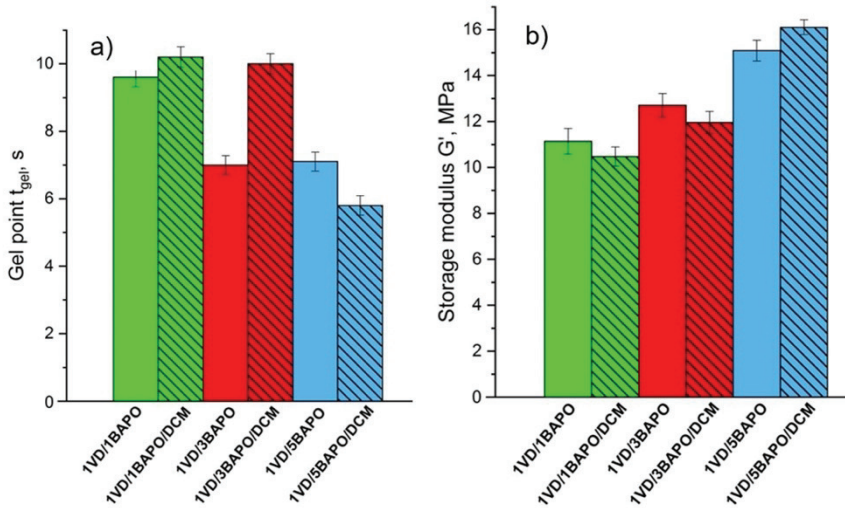

Figure 2. Gel point t_{gel} (**a**) and storage modulus G' (**b**) of the VDM-based resins. Green columns—1 mol% of BAPO; red columns—3 mol% of BAPO; blue columns—5 mol% of BAPO; leaning lines from bottom to top—presence of 1,3-benzenedithiol (BDT); leaning lines from top to bottom—presence of dichloromethane (DCM).

Acrylates are more reactive than methacrylates, as secondary acrylate radicals are very unstable in comparison to highly stable tertiary methacrylate radicals [59]. Due to this reason, the lower t_{gel} values and thus the higher polymerization rate of VD-based resins were obtained with an increase in the BAPO concentration. The comparison of the t_{gel} and G' values of VD-based resins prepared with 1 and 3 mol% of BAPO is presented in Figure 3. The lower t_{gel} values and the higher photocuring rate were demonstrated by VD-based resins when 3 mol% rather than 1 mol% of BAPO were used. The t_{gel} values of the resins prepared with thiol and the pure VD-based resin without solvent, **1VD/1BDT/3BAPO**, **1VD/1BDT/3BAPO/DCM**, and **1VD/3BAPO** were 3.6, 3.9, and 7.0 s, respectively (Figure 3a). VD-based resins prepared with BDT and with or without DCM resulted in more rigid polymers when 1 mol% of BAPO was used (**1VD/1BDT/1BAPO, 1VD/1BDT/1BAPO/DCM**), while the pure VD-based resin resulted in a more rigid polymer when 3 mol% of BAPO were used (**1VD/3BAPO**) (Figure 3b). It was due to the different mechanisms of photopolymerization. The higher amount of photoinitiator in the thiol-Michael photopolymerization (when BDT was used in the resins) resulted in a higher concentration of thiolate anions and the formation of a higher amount of linear polymer chains with flexible thioether linkages [60,61] and thus, the lower rigidity of polymers (Figure 3b).

104
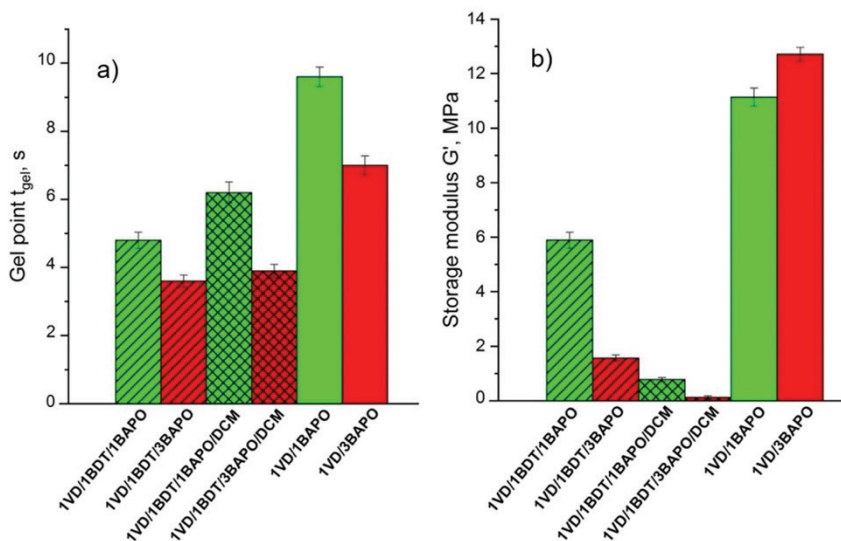
Figure 3. Gel point t_{gel} (**a**) and storage modulus G' (**b**) of the VD-based resins. Green columns—1 mol% of BAPO; red columns—3 mol% of BAPO; leaning lines from bottom to top—presence of BDT; leaning lines from top to bottom—presence of DCM.

Photocuring of resin **1VD/5BAPO/DCM** with 5 mol% of BAPO was the fastest (gel point 5.8 s) compared with resin **1VD/1BAPO/DCM** containing 1 mol% of BAPO (gel point 10.2 s) and resin **1VD/3BAPO/DCM** containing 3 mol% of BAPO (gel point 10.0 s) (Figure 4a). The solvent created a more homogenous phase for resin **1VD/5BAPO/DCM** and that led to a better dissolution of BAPO, faster photocuring, and the formation of a more rigid polymer. In pure VD-based systems with and without DCM, the rigidity increased gradually with the increase of the photoinitiator concentration since a high amount of molecules was available for the generation of free radicals. The highest rigidity was shown by polymers with 5 mol% of BAPO, while the lowest was shown with 1 mol% of BAPO (Figure 4b), as the higher concentration of reactive species resulted in a higher rigidity of polymers [62].
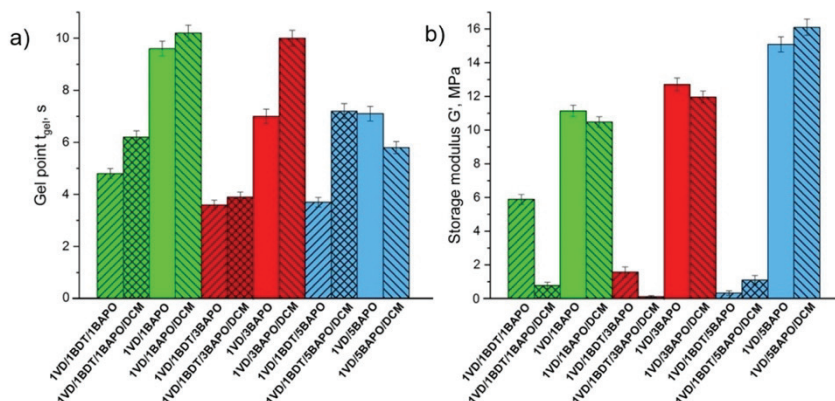
Figure 4. Gel point t_{gel} (**a**) and storage modulus G' (**b**) of the VD-based resins. Green columns—1 mol% of BAPO; red columns—3 mol% of BAPO; blue columns—5 mol% of BAPO; leaning lines from top to bottom—presence of DCM.

For a further investigation, 3 mol% of BAPO was chosen as it resulted in faster or only a slightly slower photocuring than that with 1 mol% of BAPO. However, 5 mol% of BAPO could not be used in further studies due to the left undissolved particles of BAPO in polymers **1VD/1BDT/5BAPO** and **1VD/5BAPO,** which were prepared without DCM.

3.1.2. Influence of Dichloromethane

VD-based resins were selected to characterize the influence of DCM to the photocuring rate and rigidity of the obtained polymers since only VD-based resins could be prepared without a solvent, as VD is in a liquid state at room temperature while VDM is a solid material.

In most cases, DCM slowed down the photocuring process and less rigid polymers were obtained (Figure 5). These results were characteristic for all resins with 1 and 3 mol% of BAPO. This can be explained by the DCM action as a chain transfer agent slowing the photocuring process [58]. For example, the resin without solvent **1VD/3BAPO** reached t_{gel} after 7 s and G' of 12.7 MPa after 350 s, while the same resin with solvent **1VD/3BAPO/DCM** reached t_{gel} only after 10 s and G' of 12.0 MPa after 350 s.
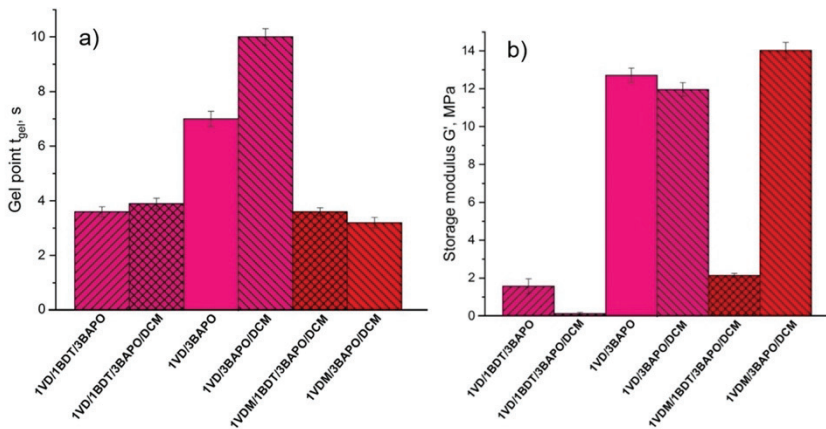
Figure 5. Gel point t_{gel} (**a**) and storage modulus G' (**b**) of the VD-based resins. Green columns—1 mol% of BAPO; red columns—3 mol% of BAPO; blue columns—5 mol% of BAPO; leaning lines from bottom to top—presence of BDT; leaning lines from top to bottom—presence of DCM.

The same results were obtained for the VD-based resins with 5 mol% of BAPO, resin **1VD/1BDT/5BAPO** photocured faster than **1VD/1BDT/5BAPO/DCM**. The addition of DCM lowered the concentration of monomers in the resin and led to more chain transfer reactions [50], which resulted in a high t_{gel} value and lower G′ of **1VD/1BDT/5BAPO/DCM**. Different results were obtained for the pure VD-based resins with 5 mol% of BAPO, **1VD/5BAPO** and **1VD/5BAPO/DCM,** which undergo a free radical photopolymerization mechanism. The concentration of BAPO was too high in resin **1VD/5BAPO** and small undissolved particles of BAPO were still visible in the polymer after photocuring. In this case, a more rigid polymer was obtained when DCM was used, as a solvent homogenized resin by dissolving the high amount of photoinitiator particles. Therefore, resin **1VD/5BAPO/DCM** resulted in a higher rigidity of the obtained polymer and faster curing (t_{gel} = 5.8 s, G' = 16.1 MPa) than that of **1VD/5BAPO** (t_{gel} = 7.1 s, G' = 15.1 MPa).

3.1.3. Influence of Vanillin Derivative

A series of resins with different vanillin derivatives (VDM or VD), DCM, and 3 mol% of BAPO were selected to determine the influence of vanillin acrylate monomer to photocuring kinetics (Figure 6). In all these cases, more rigid polymers were formed from VDM-based resins compared to VD-based resins due to the higher stability of methacrylate radicals, which slow down the photopolymerization process and form a more uniform polymeric network [59]. The VDM-based resin without thiol **1VDM/3BAPO/DCM** reached G′ of 14.00 MPa after 350 s, while G′ of the VD-based resin without thiol **1VD/3BAPO/DCM** was 12.00 MPa after 350 s. As for the reaction rate, the VDM-based resin **1VDM/3BAPO/DCM** reached the gel point faster than the VD-based resin **1VD/3BAPO/DCM** (3.2 and 10.0 s, respectively). VD-based resins are supposed to polymerize faster than VDM-based ones, but in this case, the reaction was slowed down by the color of the VD. VDM is a white color powder which results in a colorless resin when dissolved in DCM. VD is a dark yellow liquid which results in a yellow resin. The darker color makes it harder for the light to reach deeper layers of the resin and polymerize it [63]. This was confirmed by the swelling values and the yield of insoluble fraction. VDM-based polymers demonstrated a higher yield of insoluble fraction and lower swelling values in both tested solvents. The yield of insolu-

ble fraction of the VDM-based polymer without thiol **1VDM/3BAPO/DCM** was 84.14% when the VD-based polymer without thiol **1VD/3BAPO/DCM** was 80.71% (Figure 7). The swelling values observed after 90 min in acetone and toluene correlates to the yield of insoluble fraction. The VDM-based polymer without thiol **1VDM/3BAPO/DCM** reached the swelling value of 12% in acetone and 8% in toluene, while the VD-based polymer without thiol **1VD/3BAPO/DCM** reached the swelling value of 20% in acetone and 10% in toluene (Figure 8). Resins, prepared with thiol demonstrated similar results. The VDM-based resin with thiol **1VDM/1BDT/3BAPO/DCM** reached G' of 2.14 MPa after 350 s, while G' of the VD-based resin without thiol **1VD/1BDT/3BAPO/DCM** was 0.12 MPa after 350 s. Both resins reached t_{gel} at a similar time, but the VDM-based resin reached it slightly faster (3.6 s) than the VD-based resin (3.9 s), as a result of the darker color of the VD-based resin [63]. VDM-based polymers with thiols also demonstrated a higher yield of insoluble fraction and lower swelling values in both tested solvents. The yield of insoluble fraction of the VDM-based polymer with thiol **1VDM/1BDT/3BAPO/DCM** was 88.54% when the VD-based polymer with thiol **1VD/1BDT/3BAPO/DCM** was 85.22% (Figure 7). The swelling values observed after 90 min in acetone and toluene correlates to the yield of insoluble fraction. The VDM-based polymer with thiol **1VDM/1BDT/3BAPO/DCM** reached the swelling value of 25% in acetone and 15% in toluene, while the VD-based polymer with thiol **1VD/1BDT/3BAPO/DCM** reached the swelling value of 90% in acetone and 24% in toluene (Figure 8). Higher swelling values were obtained in acetone as vanillin acrylates are soluble in acetone and insoluble in toluene. The poor interaction of vanillin acrylate-based polymer chains with toluene was the reason for the worse swelling than in acetone. The higher swelling values and lower yields of insoluble fractions showed that longer chains between cross-linking points were formed.

Figure 6. Gel point t_{gel} (**a**) and storage modulus G' (**b**) of the VD and VDM-based resins with 3 mol% of BAPO. Pink columns—VD-based resin; red columns—VDM-based resin; leaning lines from bottom to top—presence of 1.3 BDT; leaning lines from top to bottom—presence of DCM.

108
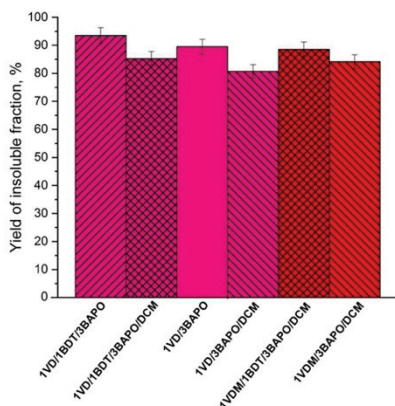
Figure 7. The yield of insoluble fraction of the VD and VDM-based polymers with 3 mol% of BAPO after 24 h extraction in acetone. Pink columns—VD-based polymer; red columns—VDM-based polymer; leaning lines from bottom to top—presence of 1.3 BDT; leaning lines from top to bottom—presence of DCM.
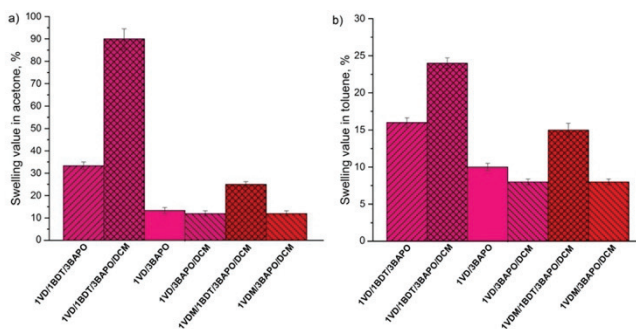
Figure 8. The swelling values of polymers in acetone (**a**) and in toluene (**b**) after 90 min of the VD and VDM-based polymers with 3 mol% of BAPO. Pink columns—VD-based polymer; red columns—VDM-based polymer; leaning lines from bottom to top—presence of 1.3 BDT; leaning lines from top to bottom—presence of DCM.

3.1.4. Influence of Thiol Addition and Its Amount

The reaction mechanism had a significant influence on the photocuring kinetics of VDM-based and VD-based resins. BAPO is a universal photoinitiator, which can initiate both free-radical and thiol-Michael photopolymerizations. The free-radical photopolymerization occurred when only vanillin acrylate was used as a monomer. The thiol-Michael photopolymerization occurred in vanillin acrylate-based resins containing BDT, when the ratio of the acrylate and thiol groups was 1:1 and 1:0.5. Dual curing, combining free-radical and thiol-Michael mechanisms, occurred when a lower amount than the stoichiomet-

ric of thiol was used (acrylate: thiol, 1:0.5). The polymers with the higher amount of thioether bonds are formed from the resins with the stoichiometric ratio of acrylate and thiol monomers (acrylate: thiol, 1:1), while the polymers with the higher amount of carbon-carbon bonds are formed from the resins with the lower than stoichiometric amount of thiol (acrylate: thiol, 1:0.5). The incorporation of thiol fragments into polymer chains leads to the significant changes of polymer mechanical properties [52]. How this has affected the rigidity of vanillin-based polymers will be described below. Nevertheless, both hard and rigid as well as soft and flexible polymers are desirable for optical 3D printing of thermoset products for particular applications.

The resins with 3 mol% of BAPO were selected to investigate the influence of thiol addition and its amount on vanillin acrylate-based resin photocuring kinetics. In vanillin acrylate-based resins, different results of the reaction rate (gel point) were observed using free radical and thiol-Michael mechanisms, as it could be expected. For example, the G' curves of VD-based resins prepared with thiol and with or without the solvent, **1VD/1BDT/3BAPO** and **1VD/1BDT/3BAPO/DCM**, and VD-based resins prepared without thiol and with or without the solvent, **1VD/3BAPO** and **1VD/3BAPO/DCM**, are presented in Figure 9. In all these cases, the reaction was faster when resins were prepared with the stoichiometric amount of thiol (acrylate: thiol,1:1), due to the high reactivity of the thiol radicals formed in the initiation stage of polymerization [52]. Moreover, BDT had a significant influence on the rigidity of the polymers. In all cases, polymers were less rigid when the stoichiometric amount of BDT (acrylate: thiol,1:1) was used in the resins. It was due to the formation of many different polymer chains of different lengths with flexible thioether linkages [48]. For example, the VD-based resin with thiol **1VD/1BDT/3BAPO** reached the gel point after 3.6 s and its G' was only 1.7 MPa after 350 s, while the VD-based resin without thiol **1VD/3BAPO** reached the gel point only after 7.0 s, but the obtained G' was 12.7 MPa after 350 s. As for the resins based on VDM, the reaction was slightly slower, when thiols were used. VDM has a lower reactivity than the VD due to the higher stability of methylacrylate radicals. This stability slows down the thiol-Michael photopolymerization [64]. The VDM-based resin with thiol and solvent **1VDM/1BDT/3BAPO/DCM** reached the gel point after 3.6 s and the VDM-based resin with the solvent and without thiol **1VDM/3BAPO/DCM** reached the gel point after 3.2 s.
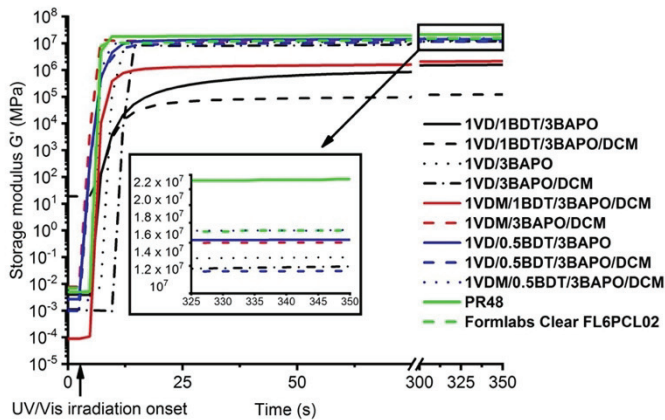

Figure 9. Dependencies of storage modulus G' of the VD and VDM-based resins, containing 3 mol% of BAPO and commercial resins PR48 and Formlabs Clear FL6PCL02 on the irradiation time.

The analogous series of the resins with the lower than the stoichiometric amount of thiol (acrylate: thiol, 1:0.5) and 3 mol% of BAPO were prepared by combining the free-radical and thiol-Michael photopolymerization in order to get the dual curing systems. Resins **1VD/0.5BDT/3BAPO**, **1VD/0.5BDT/3BAPO/DCM**, and **1VDM/0.5BDT/3BAPO/DCM** resulted in a 2 s slower photocuring (t_{gel} = 5.3, 5.8, and 5.3 s, respectively) than the resins polymerized only by the thiol-Michael reaction mechanism (acrylate: thiol, 1:1). However, all the polymers prepared with a 0.5 mole of BDT demonstrated a higher rigidity than the polymers prepared with 1 mole of BDT. The VD-based resin with a 0.5 mole of thiol and 3 mol% BAPO (**1VD/0.5BDT/3BAPO**) reached G' of 14.3 MPa after 350 s, which was higher than that of the pure VD-based polymer synthesized with 3 mol% of BAPO (**1VD/3BAPO**, G' = 12,7 MPa, after 350 s). The analogous polymer prepared with solvent (**1VD/0.5BDT/3BAPO/DCM**) was slightly less rigid and reached G' of 11.6 MPa after 350 s. The addition of solvent into the resin also slightly slowed down the photocuring process and the rigidity of polymers due to the chain transfer reactions [61]. Similar results were observed for the VDM-based resin with the lower than stoichiometric amount of thiol (acrylate: thiol, 1:0.5), 3 mol% of BAPO, and DCM (**1VDM/0.5BDT/3BAPO/DCM**). The resulted polymer reached G' of 15.2 MPa after 350 s, which was higher than that of the VDM homopolymer synthesized with 3 mol% of BAPO and DCM (**1VDM/3BAPO/DCM**, G' = 14.0 MPa, after 350 s). The higher rigidity of polymers, prepared with a 0.5 mole of thiol is the result of the dual curing process. During this process, the macromolecular chains of acrylate homopolymer and copolymer interpenetrate. That results in a higher density and thus the higher rigidity of polymers [45]. On the other hand, the free-radical photopolymerization is slower than the thiol-Michael photopolymerization and this combination of the two reaction mechanisms (when acrylate: thiol, 1:0.5) results in a slower photocuring process than the thiol-Michael photopolymerization (when acrylate: thiol, 1:1) [61].

The viscosity of the resins depended on their composition. The higher amount of BDT was added to the resin, the lower viscosity of the resin was determined. The most viscous resin was **1VD/3BAPO** without BDT. Its viscosity was 75,024 ± 137 mPa·s. The viscosity of the resin with 0.5 mol of BDT (**1VD/0.5BDT/3BAPO**) was 3007 ± 42 mPa·s, and that with 1 mol of BDT (**1VD/1BDT/3BAPO**) was 468 ± 15 mPa·s. No change in the resin viscosity was observed and no difference was observed between the UV curing kinetics curves of freshly prepared vanillin-based resins containing BDT or without it and those kept in the dark for several days.

A series of the resins with 3 mol% of BAPO were compared with commercial petroleum-derived acrylate resins, Formlabs Clear FL6PCL02 and PR48 (Figure 9). Both commercial resins demonstrated a similar photocuring rate (both t_{gel} = 6 s). Most of the VD-based and VDM-based resins demonstrated an even higher photocuring rate than commercial resins, for example, **1VD/1BDT/3BAPO** (t_{gel} = 3.6 s), **1VD/1BDT/3BAPO/DCM** (t_{gel} = 3.9 s), **1VDM/1BDT/3BAPO/DCM** (t_{gel} = 3.6 s), **1VDM/3BAPO/DCM** (t_{gel} = 3.2 s), **1VD/0.5BDT/3BAPO** (t_{gel} = 5.3 s), **1VD/0.5BDT/3BAPO/DCM** (t_{gel} = 5.8 s), and **1VDM/0.5BDT/3BAPO/DCM** (t_{gel} = 5.3 s). Only pure VD-based resins with and without the solvent, **1VD/3BAPO** (t_{gel} = 7.0 s) and **1VD/3BAPO/DCM** (t_{gel} = 10.0 s), demonstrated the lower photocuring rate than that of commercial resins due to the lower rate of free radical photopolymerization. As for rigidity, VD-based and VDM-based resins prepared with or without the solvent and without thiol, **1VD/3BAPO** (G' = 12.70 MPa), **1VD/3BAPO/DCM** (G' = 12.00 MPa), and the pure VDM-based resin with the solvent **1VDM/3BAPO/DCM** (G' = 14.00 MPa) showed a similar rigidity as Formlabs Clear FL6PCL02 (G' = 15.20 MPa), but a lower rigidity than PR48 (G' = 21.40 MPa). Dual-cured polymers demonstrated a similar rigidity, **1VD/0.5BDT/3BAPO** (G' = 14.23 MPa), **1VD/0.5BDT/3BAPO/DCM** (G' = 11.60 MPa), and **1VDM/0.5BDT/3BAPO/DCM** (G' = 15.20 MPa), and the VDM-based resin **1VDM/0.5BDT/3BAPO/DCM** demonstrated even the same rigidity as Formlabs Clear FL6PCL02 (G' = 15.20 MPa), but a lower rigidity than PR48 (G' = 21.40 MPa). However, the VDM homopolymer **1VDM/3BAPO/DCM** was very brittle, so vanillin diacrylate-

based double-curing systems **1VD/0.5BDT/3BAPO** and **1VD/0.5BDT/3BAPO/DCM** were selected as the most promising for optical 3D printing.

3.2. Influence of Resin Composition on the Resulting Polymer Antibacterial and Antifungal Activity

The antibacterial and antifungal activity of the selected vanillin acrylate-based polymer films was exhibited on a cultural medium by measuring growth inhibition zones and during the direct contact with the specimens by calculating the log reduction and percent reduction of viable microbial spores. Two reference polymer films of chitosan, a well-known antibacterial polymer and hydroxyethyl starch having no such activity were used. The dependency of the antibacterial and antifungal activity on the vanillin derivative and the presence of thiol was observed.

During the development of bacteria on the culture medium, only a slight inhibition of **1VD/3BAPO** and chitosan films by *E. coli* was observed (Table 1, Figures 10 and 11.). The growth inhibition of Gram-positive bacterium *S. aureus* was slightly more pronounced. In this case, almost all the films tested were active except **1VDM/1BDT/3BAPO/DCM** and the hydroxyethyl starch film. It was determined that only the films prepared by radical photopolymerization were active against *E. coli* and only VD-based films were active against *S. aureus*. VDM-based films were less active against microorganisms probably due to the lower concentration of carbonyl groups, the presence of which has a positive effect on the antimicrobial activity of compounds [65].

The vanillin acrylate-based polymers showed a more pronounced antibacterial activity by the direct spore contact with the films (Table 1). Almost all the films tested and chitosan completely abolished the bacterial viability after 24 h of contact with spores, with the exception of **1VDM/1BDT/3BAPO/DCM** and hydroxyethyl starch films. The polymer film of **1VDM/1BDT/3BAPO/DCM** reduced the number of viable *E. coli* spores to log 1.98, and the loss of viability spores was 98.96%. Meanwhile, the hydroxyethyl starch film reduced the number of *E. coli* and *S. aureus* spores to log 1.25 and 2.85, respectively, and the loss of viability spores was 94.42 and 99.86%, respectively. It was determined that VD-based films had a better antibacterial activity than VDM-based films against *E. coli*, but all the tested polymers showed the same antibacterial activity against *S. aureus*.

Table 1. Antibacterial activity characteristics of polymer film specimens.

Polymer Film	*Escherichia coli*			*Staphylococcus aureus*		
	Growth Inhibition Zone, mm	Log Reduction after 24 h	Percent Reduction after 24 h	Growth Inhibition Zone, mm	Log Reduction after 24 h	Percent Reduction after 24 h
1VD/1BDT/3BAPO	0	0	100	2.1 ± 0.8	0	100
1VD/1BDT/3BAPO/ DCM	0	0	100	2.0 ± 0.0	0	100
1VD/3BAPO	1.0 ± 0.7	0	100	2.1 ± 0.8	0	100
1VDM/1BDT/3BAPO/ DCM	0	1.98	98.96	0	0	100
Chitosan	2.0 ± 0.7	0	100	2.5 ± 0.5	0	100
Hydroxyethyl starch	0	1.25	94.42	0	2.85	99.86
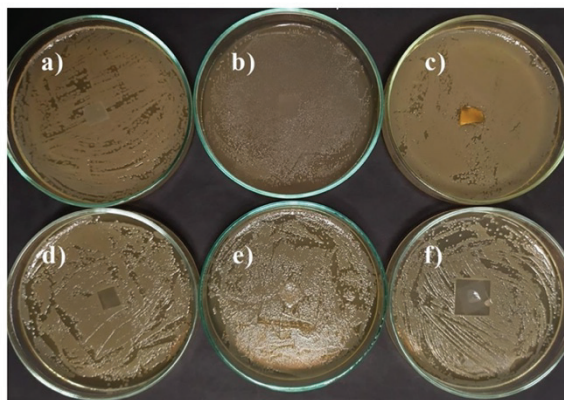
Figure 10. Toxicity testing of polymer film specimens for fungus *Escherichia coli* on a Mueller Hinton Agar (MHA) medium: (**a**) **1VD/1BDT/3BAPO**, (**b**) **1VD/1BDT/3BAPO/DCM**, (**c**) **1VD/3BAPO**, (**d**) **1VDM/1BDT/3BAPO/DCM**, (**e**) chitosan, (**f**) hydroxyethyl starch.
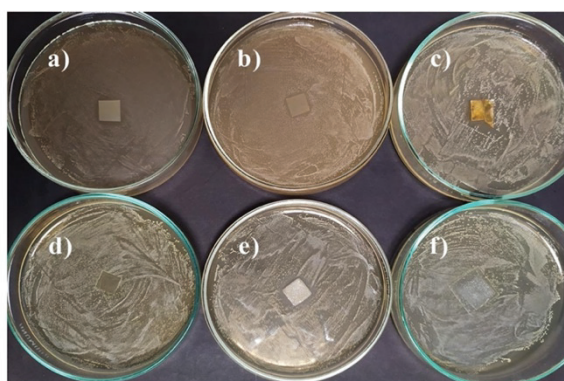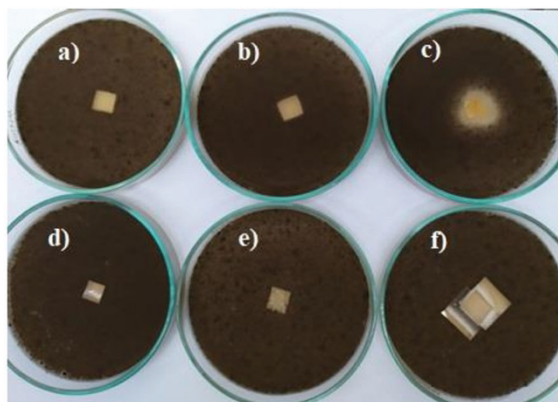

Figure 11. Toxicity testing of polymer film specimens for fungus *Staphylococcus aureus* on a MHA medium: (**a**) **1VD/1BDT/3BAPO**, (**b**) **1VD/1BDT/3BAPO/DCM**, (**c**) **1VD/3BAPO**, (**d**) **1VDM/1BDT/3BAPO/DCM**, (**e**) chitosan, (**f**) hydroxyethyl starch.

The antifungal activity of vanillin-based polymers depended on the fungal species. The growth of *A. niger* on the culture medium was slightly inhibited only by **1VD/3BAPO**, while *A. terreus*—was inhibited by **1VD/1BDT/3BAPO** and **1VD/1BDT/3BAPO/DCM** films (Table 2, Figures 12 and 13). The antifungal activity against *A. niger* was visible only for the VD-based film prepared without thiol. The addition of thiol resulted in the antifungal activity against *A. terreus*. Moreover, *A.niger* was affected by a higher concentration of carbonyl groups, which are less active against fungi than against bacteria [66], while *A. terreus* was only affected by a higher concentration of carbonyl groups in the VD-based film

113

prepared without thiol and the presence of sulphur with the great antifungal activity [67] in VD-based films prepared with thiol. The main reason for these results is the higher concentration and the great antifungal activity of sulphur, which is present in VD-based films prepared with thiol [68].

Table 2. Antifungal activity characteristics of polymer film specimens.

Polymer Film	*Aspergillus niger*			*Aspergillus terreus*		
	Growth Inhibition Zone, mm	Log Reduction after 24 h	Percent Reduction after 24 h	Growth Inhibition Zone, mm	Log Reduction after 24 h	Percent Reduction after 24 h
1VD/1BDT/3BAPO	0	0	100	2.2 ± 0.4	3.15	99.93
1VD/1BDT/3BAPO/ DCM	0	0	100	2.2 ± 0.4	3.70	99.98
1VD/3BAPO	3.2 ± 0.8	2.33	99.54	0	3.40	99.96
1VDM/1BDT/3BAPO/ DCM	0	2.89	99.87	0	2.92	99.88
Chitosan	0	0	100	0	2.11	99.23
Hydroxyethyl starch	0	3.07	99.92	0	2.35	99.56

Figure 12. Toxicity testing of polymer film specimens for fungus *Aspergillus niger* on a Malt Extract Agar (MEA) medium: (**a**) **1VD/1BDT/3BAPO**, (**b**) **1VD/1BDT/3BAPO/DCM**, (**c**) **1VD/3BAPO**, (**d**) **1VDM/1BDT/3BAPO/DCM**, (**e**) chitosan, (**f**) hydroxyethyl starch.

114
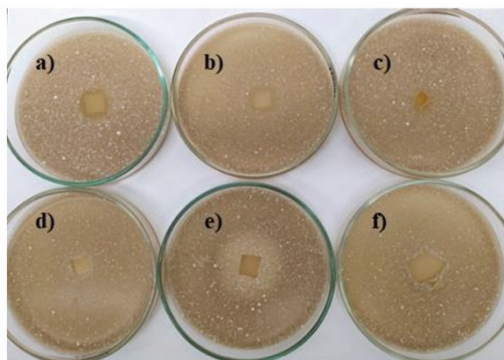
Figure 13. Toxicity testing of polymer film specimens for fungus *Aspergillus terreus* on a MEA medium: (**a**) **1VD/1BDT/3BAPO**, (**b**) **1VD/1BDT/3BAPO/DCM**, (**c**) **1VD/3BAPO**, (**d**) **1VDM/1BDT/3BAPO/DCM**, (**e**) chitosan, (**f**) hydroxyethyl starch.

The antifungal activity of vanillin acrylate-based polymer films was more pronounced when a direct contact of the fungal spores with the films was used, but it depended on the fungal species, as well. The polymer films of **1VD/1BDT/3BAPO**, **1VD/1BDT/3BAPO/ DCM**, and chitosan completely abolished the viability of *A. niger* within 24 h due to the higher concentration of carbonyl groups and sulphur, as mentioned earlier. The viability of *A. terreus* was reduced the most by the film of **1VD/1BDT/3BAPO/DCM** with 99.98% of spores losing viability. Other VD-based polymer films pronounced a similar antifungal activity for *A. terreus*. Only the antifungal activity of **1VDM/1BDT/3BAPO/DCM** was less pronounced for this fungus as the concentration of antifungal agents was lower in the VDM-based film. The results of studies performed by different methods differ since film biocides are not released into the environment and act more efficiently in contact with the microorganism [69].

4. Conclusions

All components of the resins have a significant influence on photocuring kinetics and properties of the resulting polymers. The addition of solvent into the resin slowed down the photocuring process and less rigid polymers were obtained. The addition of thiol increased the photocuring rate but reduced the rigidity of the resulting polymers. Dual curing, combining free-radical and thiol-Michael mechanisms, resulted in a slightly slower photocuring process than the thiol-Michael photopolymerization, but more rigid polymers were formed. The reaction rate of the selected vanillin acrylate-based resins was similar or even faster than that of commercial petroleum-based acrylate resins for optical 3D printing. However, the resulting polymers were slightly less rigid. Vanillin acrylate- and vanillin methacrylate-based polymers showed a significant antibacterial activity against *Escherichia coli* and *Staphylococcus aureus* in direct contact and on the medium. Toxicity to the microscopic fungus *Aspergillus niger* and *Aspergillus terreus* was less pronounced, the viability of *Aspergillus niger* spores in direct contact was reduced by all the investigated vanillin acrylate-based resins. The viability of *Aspergillus terreus* was also reduced by the vanillin diacrylate-based resins, although the reduction of viability by the vanillin dimethacrylate-based polymer was lower. Vanillin diacrylate-based dual curing systems were selected as the most promising for optical 3D printing of bio-based polymers with an antibacterial and antifungal activity.

115

References

1. Niaki, M.K.; Torabi, S.A.; Nonino, F. Why manufacturers adopt additive manufacturing technologies: The role of sustainability. *J. Clean. Prod.* **2019**, *222*, 381–392. [CrossRef]
2. Böckin, D.; Tillman, A.M. Environmental assessment of additive manufacturing in the automotive industry. *J. Clean. Prod.* **2019**, *226*, 977–987. [CrossRef]
3. Chergui, A.; Hadj-Hamou, K.; Vignat, F. Production scheduling and nesting in additive manufacturing. *Comput. Ind. Eng.* **2018**, *126*, 292–301. [CrossRef]
4. Javaid, M.; Haleem, A. Current status and applications of additive manufacturing in dentistry: A literature-based review. *J. Oral Biol. Craniofac. Res.* **2019**, *9*, 179–185. [CrossRef] [PubMed]
5. Alabort, E.; Barba, D.; Reed, R.C. Design of metallic bone by additive manufacturing. *Scr. Mater.* **2019**, *164*, 110–114. [CrossRef]
6. Craveiro, F.; Duarte, J.P.; Bartolo, H.; Bartolo, P.J. Additive manufacturing as an enabling technology for digital construction: A perspective on Construction 4.0. *Autom. Constr.* **2019**, *103*, 251–267. [CrossRef]
7. Qin, Y.; Qi, Q.; Scott, P.J.; Jiang, X. Status, comparison, and future of the representations of additive manufacturing data. *Comput. Aided Des.* **2019**, *111*, 44–64. [CrossRef]
8. Quan, H.; Zhang, T.; Xu, H.; Luo, S.; Nie, J.; Zhu, X. Photo-curing 3D printing technique and its challenges. *Bioact. Mater.* **2020**, *5*, 110–115. [CrossRef]
9. Zhong, Y.; Godwin, P.; Jin, Y.; Xiao, H. Biodegradable polymers and green-based antimicrobial packaging materials: A mini-review. *Adv. Ind. Eng. Polym. Res.* **2020**, *3*, 27–35. [CrossRef]
10. Wang, C.; Chang, T.; Dong, S.; Zhang, D.; Ma, C.; Chen, S.; Li, H. Biopolymer films based on chitosan/potato protein/linseed oil/ZnO NPs to maintain the storage quality of raw meat. *Food Chem.* **2020**, *332*, 127375. [CrossRef]
11. Li, Z.; Wang, S.; Yang, X.; Liu, H.; Shan, Y.; Xu, X.; Shang, S.; Songa, Z. Antimicrobial and antifouling coating constructed using rosin acid-based quaternary ammonium salt and N-vinylpyrrolidone via RAFT polymerization. *Appl. Surf. Sci.* **2020**, *530*, 147193. [CrossRef]
12. Ribes, S.; Ruiz-Rico, M.; Pérez-Esteve, E.; Fuentes, A.; Barat, J.M. Enhancing the antimicrobial activity of eugenol, carvacrol and vanillin immobilised on silica supports against Escherichia coli or Zygosaccharomyces rouxii in fruit juices by their binary combinations. *LWT* **2019**, *113*, 108326. [CrossRef]
13. Gallageand, N.J.; Møller, B.L. Vanillin–Bioconversion and Bioengineering of the Most Popular Plant Flavor and Its De Novo Biosynthesis in the Vanilla Orchid. *Mol. Plant.* **2015**, *8*, 40–57. [CrossRef]
14. Wang, Y.; Sun, S.; Li, F.; Cao, X.; Sun, R. Production of vanillin from lignin: The relationship between β-O-4 linkages and vanillin yield. *Ind. Crops Prod.* **2018**, *116*, 116–121. [CrossRef]
15. Fache, M.; Boutevin, B.; Caillol, S. Vanillin, a key-intermediate of biobased polymers. *Eur. Polym. J.* **2015**, *68*, 488–502. [CrossRef]
16. Harshvardhan, K.; Suri, M.; Goswami, A.; Goswami, T. Biological approach for the production of vanillin from lignocellulosicbiomass (Bambusa tulda). *J. Clean. Prod.* **2017**, *149*, 485–490. [CrossRef]
17. Kumar, L.V.; Nath, G.R. Synthesis, characterization and biological studies of cobalt(II), nickel(II), copper(II) and zinc(II) complexes of vanillin-4-methyl-4- phenyl-3-thiosemicarbazone. *J. Chem. Sci.* **2019**, *131*. [CrossRef]
18. Mourtzinos, I.; Konteles, S.; Kalogeropoulos, N.; Karathanos, V.T. Thermal oxidation of vanillin affects its antioxidant and antimicrobial properties. *Food Chem.* **2009**, *114*, 791–797. [CrossRef]
19. Sun, J.; Yin, Y.; Sheng, G.H.; Yang, Z.B.; Zhu, H.L. Synthesis, molecular modeling and structural characterization of vanillin derivatives as antimicrobial agents. *J. Mol. Struct.* **2013**, *1039*, 214–218. [CrossRef]
20. Polo, L.; Greñu, B.D.; Bella, E.D.; Pagani, S.; Torricelli, P.; Vivancos, J.L.; Ruiz-Rico, M.; Barat, J.M.; Aznar, E.; Martínez-Máñez, R.; et al. Antimicrobial activity of commercial calcium phosphate based materials functionalized with vanillin. *Acta Biomater.* **2018**, *81*, 293–303. [CrossRef]
21. Martelli, G.; Giacomini, D. Antibacterial and antioxidant activities for natural and synthetic dual-active compounds. *Eur. J. Med. Chem.* **2018**, *158*, 91–105. [CrossRef] [PubMed]

22. Khudyakov, I.V. Fast photopolymerization of acrylate coatings: Achievements and problems. *Prog. Org. Coat.* **2018**, *121*, 151–159. [CrossRef]
23. Lari, H.N.; Chaouki, J.; Tavares, J.R. Continuous aerosol photopolymerization to coat de-agglomerated nanoparticles. *Chem. Eng. J.* **2020**, *390*, 124526. [CrossRef]
24. Zakeri, S.; Vippola, M.; Levänen, E. A comprehensive review of the photopolymerization of ceramic resins used in stereolithography. *Addit. Manuf.* **2020**, *35*, 101177. [CrossRef]
25. Li, S.; Zhou, D.; Pei, M.; Zhou, Y.; Xu, W.; Xiao, P. Fast gelling and non-swellable photopolymerized poly (vinyl alcohol) hydrogels with high strength. *Eur. Polym. J.* **2020**, *134*, 109854. [CrossRef]
26. Andrzejewska, A. Three-Dimensional Microfabrication Using Two-photon Polymerization. In *Three-Dimensional Microfabrication Using Two-Photon Polymerization*, 1st ed.; Baldaccini, T., Ed.; Elsevier Inc.: Amsterdam, The Netherlands, 2016; Volume 1, pp. 62–81.
27. Zhang, C.; Yan, M.; Cochran, E.W.; Kessler, M.R. Biorenewable polymers based on acrylated epoxidized soybean oil and methacrylated vanillin. *Mater. Today Commun.* **2015**, *5*, 18–22. [CrossRef]
28. Salmi-Mani, H.; Terreros, G.; Barroca-Aubry, N.; Aymes-Chodur, C.; Regeard, C.; Roger, P. Poly(ethylene terephthalate) films modified by UV-induced surface graft polymerization of vanillin derived monomer for antibacterial activity. *Eur. Polym. J.* **2018**, *103*, 51–58. [CrossRef]
29. Lebedevaite, M.; Ostrauskaite, J.; Skliutas, E.; Malinauskas, M. Photoinitiator free Resins Composed of Plant-Derived Monomers for the Optical μ-3D Printing of Thermosets. *Polymers* **2019**, *11*, 116. [CrossRef]
30. Mota-Morales, J.D.; Sánchez-Leija, R.J.; Carranza, A.; Pojman, J.A.; del Monte, F.; Luna-Bárcenas, G. Free-radical polymerizations of and in deep eutectic solvents: Green synthesis of functional materials. *Prog. Polym. Sci.* **2018**, *78*, 139–153. [CrossRef]
31. Xu, G.; Blum, F.D. Surfactant-enhanced free radical polymerization of styrene in emulsion gels. *Polymer* **2008**, *49*, 3233–3238. [CrossRef]
32. Yong, X.; Kuksenok, O.; Balazs, A.C. Modeling free radical polymerization using dissipative particle dynamics. *Polymer* **2015**, *72*, 217–225. [CrossRef]
33. Kong, J.; Chen, X. Dynamic optimization of batch free radical polymerization with conditional modeling formulation through the adaptive smoothing strategy. *Comput. Chem. Eng.* **2019**, *120*, 15–29. [CrossRef]
34. Sari, E.; Mitterbauer, M.; Liska, R.; Yagci, Y. Visible light induced free radical promoted cationic polymerization using acylsilanes. *Prog. Org. Coat.* **2019**, *132*, 139–143. [CrossRef]
35. Jung, J.; Park, C.; Yun, G.J. Free radical polymerization simulation and molecular entanglement effect on large deformation behavior. *Eur. Polym. J.* **2019**, *114*, 223–233. [CrossRef]
36. Bisht, H.S.; Chatterjee, A.K. Living Free-Radical Polymerization: A Review. *J. Macromol. Sci. Polym. Rev.* **2007**, *41*, 139–173. [CrossRef]
37. Corrigan, N.; Yeow, J.; Judzewitsch, P.; Xu, J.; Boyer, C. Seeing the Light: Advancing Materials Chemistry through Photopolymerization. *Angew. Chem. Int. Ed.* **2019**, *58*, 5170–5189. [CrossRef] [PubMed]
38. Ortiz, R.A.; Valdez, A.E.G.; Aguilar, M.G.M.; Duarte, M.L.B. An effective method to prepare sucrose polymers by Thiol-Ene photopolymerization. *Carbohydr. Polym.* **2009**, *78*, 282–286. [CrossRef]
39. Murphy, K.A.; Zebertavage, A.S.; Kiliman, B.E.; Shipp, D.A. Thiol-Ene Polymerizations Using Imide-Based Monomers. *J. Polym. Sci. Part A Polym. Chem.* **2013**, *51*, 4637–4642. [CrossRef]
40. Yoshimura, T.; Shimasaki, T.; Teramoto, N.; Shibata, M. Bio-based polymer networks by thiol-ene photopolymerization of allyl-etherified eugenol derivatives. *Eur. Polym. J.* **2015**, *67*, 397–408. [CrossRef]
41. Hoyle, C.E.; Lowe, A.B.; Bowman, C.N. Thiol-click chemistry: A multifaceted toolbox for small molecule and polymer synthesis. *Chem. Soc. Rev.* **2010**, *39*, 1355–1387. [CrossRef]
42. Northrop, B.H.; Coffey, R.N. Thiol–Ene Click Chemistry: Computational and Kinetic Analysis of the Influence of Alkene Functionality. *J. Am. Chem. Soc.* **2012**, *134*, 13804–13817. [CrossRef] [PubMed]
43. Aoyagi, S.; Shimasaki, T.; Teramoto, N.; Shibata, M. Bio-based polymer networks by thiol-ene photopolymerization of allylated l-glutamic acids and l-tyrosines. *Eur. Polym. J.* **2018**, *101*, 151–158. [CrossRef]
44. Nair, D.P.; Cramer, N.B.; Scott, T.F.; Bowman, C.N.; Shandas, R. Photopolymerized thiol-ene systems as shape memory polymers. *Polymer* **2010**, *51*, 4383–4389. [CrossRef] [PubMed]
45. Konuray, O.; Fernández-Francos, X.; Ramis, X.; Serra, À. State of the Art in Dual-Curing Acrylate Systems. *Polymers* **2018**, *10*, 178. [CrossRef] [PubMed]
46. Navaruckiene, A.; Skliutas, E.; Kasetaite, S.; Rekstyte, S.; Raudoniene, V.; Bridziuviene, D.; Malinauskas, M.; Ostrauskaite, J. Vanillin Acrylate-Based Resins for Optical 3D Printing. *Polymer* **2020**, *12*, 397. [CrossRef]
47. Navaruckiene, A.; Kasetaite, S.; Ostrauskaite, J. Vanillin-based thiol-ene systems as photoresins for optical 3D printing. *Rapid Prototyp. J.* **2020**, *26*, 402–408. [CrossRef]
48. Meereis, C.; Leal, F.; Lima, G.; Carvalho, R.; Piva, E.; Ogliari, F. BAPO as an alternative photoinitiator for the radical polymerization of dental resins. *Dent. Mater.* **2014**, *30*, 945–953. [CrossRef]
49. Decker, C.; Zahouily, K.; Decker, D.; Nguyen, T.; Viet, T. Performance analysis of acylphosphine oxides in photoinitiated polymerization. *Polymer* **2001**, *18*, 7551–7560. [CrossRef]

117

50. Green, W.A. *Industrial Photoiniciators. A Technical Guide*, 1st ed.; CRC Press: Boca Raton, FL, USA; Taylor and Francis Group: London, UK, 2001; ISBN 978-14-3982-745-1.

51. Oliveira, D.C.; Rocha, M.G.; Gatti, A.; Correr, A.B.; Ferracane, J.L.; Sinhoret, M.A.C. Effect of different photoinitiators and reducing agents on cure efficiency and color stability of resin-based composites using different LED wavelengths. *J. Dent.* **2015**, *43*, 1565–1572. [CrossRef]

52. Salgado, V.E.; Albuquerque, P.P.; Cavalcante, L.M.; Pfeifer, C.S.; Moraes, R.R.; Schneider, L.F.J. Influence of photoinitiator system and nanofiller size on the optical properties and cure efficiency of model composites. *Dent. Mater.* **2014**, *30*, 264–271. [CrossRef]

53. Albuquerque, P.P.; Moreira, A.D.L.; Moraes, R.R.; Cavalcante, L.M.; Schneider, L.F.J. Color stability, conversion, water sorption and solubility of dental composites formulated with different photoinitiator systems. *J. Dent.* **2013**, *41*, e67–e72. [CrossRef] [PubMed]

54. Monteiro, A.A.; Salgadob, V.E.; Vitti, R.P.; Bertolo, M.V.L.; Cavalcante, L.M.; Schneider, L.F.J. Effect of adhesive-monomers and photoinitiator on C=C conversion and color stability of model self-adhesive flowable composites. *Int. J. Adhes. Adhes.* **2018**, *87*, 119–123. [CrossRef]

55. ISO. *846:1998 Plastics-Evaluation of the Action of Microorganisms*; ISO: Geneva, Switzerland, 1998.

56. Mezger, T.G. *The Rheology Handbook*, 3rd ed.; Vincentz Network: Hanover, Germany, 2011; ISBN 978-38-6630-864-0.

57. Doğruyol, Z.; Arsu, N.; Doğruyol, S.K.; Pekcan, Ö. Producing critical exponents from gelation for various photoinitiator concentrations; a photo differential scanning calorimetric study. *Prog. Org. Coat.* **2012**, *74*, 181–185. [CrossRef]

58. Valdebenito, A.; Encinas, M.V. Effect of solvent on the free radical polymerization of N,N- dimethylacrylamide. *Polym. Int.* **2010**, *59*, 1246–1251. [CrossRef]

59. Wen, M.; Ng, L.V.; Payne, J.; Francis, L.; Scriven, L.; McCormick, A. *Kinetic Study of Free-Radical Polymerization of Multifunctional Acrylates and Methacrylates, Proceedings of the IS & T's 50th Annual Conference, Hyatt Regency Hotel, Cambridge, MA, USA, 18–23 May 1997*; Society for Imaging Science and Technology: Springfield, VA, USA, 1997.

60. Jiang, L.; Xiong, W.; Zhou, Y.; Liu, Y.; Huang, X.; Li, D.; Baldacchini, T.; Jiang, L.; Lu, Y. Performance comparison of acrylic and thiol-acrylic resins in two-photon polymerization. *Opt. Express* **2016**, *24*, 13687–13701. [CrossRef] [PubMed]

61. Nair, D.P.; Podgórski, M.; Chatani, S.; Gong, T.; Xi, W.; Fenoli, C.R.; Bowman, C.N. The Thiol-Michael Addition Click Reaction: A Powerful and Widely Used Tool in Materials Chemistry. *Chem. Mater.* **2014**, *26*, 724–744. [CrossRef]

62. Bail, R.; Patel, A.; Yang, H.; Rogers, C.M.; Rose, F.R.; Segal, J.I.; Ratchev, S.M. The Effect of a Type I Photoinitiator on Cure Kinetics and Cell Toxicity in Projection-Microstereolithography. *Procedia CIRP* **2013**, *5*, 222–225. [CrossRef]

63. Shortall, A.C. How light source and product shade influence cure depth for a contemporary composite. *J. Oral Rehabil.* **2005**, *32*, 906–911. [CrossRef]

64. Xi, W.; Peng, H.; Aguirre-Soto, A.; Kloxin, C.J.; Stansbury, J.W.; Bowman, C.N. Spatial and temporal control of thiol-michael addition via photocaged superbase in photopatteening and two-stage polymer networks formulation. *Macromolecules* **2014**, *47*, 6159–6165. [CrossRef]

65. Sanchez-Calvo, J.M.; Barbero, G.R.; Guerrero-Vasquez, G.; Duran, A.G.; Macias, M.; Rodriguez-Iglesias, M.A.; Molinillo, J.M.G.; Macias, F.A. Synthesis, antibacterial and antifungal activities of naphthoquinone derivatives: A structure-activity relationship study. *Med. Chem. Res.* **2016**, *25*, 1274–1285. [CrossRef]

66. Shakhatreh, M.A.; Al-Smadi, M.L.; Khabour, O.F.; Shuaibu, F.A.; Hussein, E.I.; Alzoubi, K.H. Study of the antibacterial and antifungal activities of synthetic benzyl bromides, ketones, and corresponding chalcone derivatives. *Drug Des. Dev. Ther.* **2016**, *10*, 3653–3660. [CrossRef] [PubMed]

67. Cooper, R.M.; Williams, J.S. Elemental sulphur as an induced antifungal substance in plant defence. *J. Exp. Bot.* **2004**, *55*, 1947–1953. [CrossRef] [PubMed]

68. Tweedy, B.G. Inorganic sulfur as a fungicide. In *Residue Reviews*, 1st ed.; Gunther, F.A., Gunther, J.D., Eds.; Springer: New York, NY, USA, 1981; Volume 78, pp. 43–64.

69. Santos, M.; Fonseca, A.; Mendonça, P.; Branco, R.; Serra, A.; Morais, P.; Coelho, J. Recent Developments in Antimicrobial Polymers: A Review. *Materials* **2016**, *9*, 599. [CrossRef] [PubMed]

Research article

Vanillin acrylate-based thermo-responsive shape memory antimicrobial photopolymers

Aukse Navaruckiene[1] , *Danguole Bridziuviene[2]* , *Vita Raudoniene[2]* , *Egidija Rainosalo[3]* ,
*Jolita Ostrauskaite[1]**

[1]Department of Polymer Chemistry and Technology, Kaunas University of Technology, Radvilenu Rd. 19, LT-50254 Kaunas, Lithuania
[2]Biodeterioration Research Laboratory, Nature Research Center, Akademijos Str. 2, LT-08412 Vilnius, Lithuania
[3]Centria University of Applied Sciences, Talonpojankatu 2, FI-67100 Kokkola, Finland

Abstract. Vanillin acrylate-based thermo-responsive shape memory photopolymers with high thermal stability, tunable mechanical properties, and antimicrobial activity have been developed. Photocurable resins containing one of the three commercial vanillin derivatives, vanillin diacrylate, vanillin dimethacrylate, and vanillin hydroxypropane dimethacrylate, and 1,3-benzenedithiol were tested. The results of dual curing systems with different ratios of thiol and acrylate (1:1 and 0.5:1) were compared. The reduction of thiol content increased the rate of photocuring, improved the mechanical performance of polymers (Young's modulus was increased from 1.4–3.5 to 3952.3–11339.4 MPa), and their heat resistance (the 10% weight loss increased from 277–327 to 294–341 °C). All polymers were able to return to their primary shape after deformation and maintain their temporary shape at a temperature lower than their glass transition temperature (–3–46 °C). Furthermore, all-polymer films exhibited significant antibacterial activity against *Escherichia coli* and *Staphylococcus aureus* (cell reduction reached 99.8–100% after 24 h) and antifungal activity against *Aspergillus flavus* and *Aspergillus niger* (cell reduction reached 72.3–100% after 24 h).

Keywords: thermosetting resins, photopolymerization, dual-curing, shape memory, antimicrobial activity

1. Introduction

Recently, shape memory polymers have received much attention due to their unique ability to obtain temporary shapes and return to their permanent shape in response to stimulus [1]. These polymers have a wide application area, such as intelligent medical devices, heat-shrinkable tubes for electronics [2], aerospace applications, and self-healing materials [3]. Nowadays, technologies are an integral part of everyday life, and the need for smart materials is growing rapidly [4], leading to the increasing interest in new bio-based shape memory polymers suitable for future applications in the fast-growing field of smart materials [5].

Bio-based materials attract the interest of the scientific community as an ecological and economical alternative to petrochemical-based materials [6]. Bio-based high-performance materials are becoming a major trend in the research and development of shape memory polymers [7]. The typical characteristics of high-performance polymers are high mechanical strength and high heat resistance [8]. In recent years, new bio-based shape-memory polymers have been synthesized from plant-derived materials by thermal polymerization. Only a few bio-based shape memory polymers have been prepared by UV photopolymerization [9]. However, most bio-based shape memory polymers have low glass

transition temperatures, which limits their applications [7].

Antimicrobial shape-memory materials are attracting a lot of attention in biomedical applications [10], *e.g.*, bone scaffolding [11]. For example, a self-healable conductive polyurethane with shape memory and antimicrobial properties has been synthesized and shown to be suitable for use as a bone scaffold [12]. Antimicrobial shape memory composites have been developed by combining synthetic polymers possessing shape memory properties and natural polymers [13]. However, most antimicrobial materials that possess shape memory properties are not bio-based. To fill this gap, this study focused on developing novel bio-based antimicrobial shape memory polymers using vanillin derivatives.

Approximately 20% of vanillin is produced from natural sources. It can be extracted directly from plants, such as vanilla orchid beans or produced by the chemical modification of lignin. Lignin is the main source of plant-derived vanillin [14]. In the last years, vanillin and its derivatives have been used in polymer synthesis because their aromatic structure provides polymers with high rigidity and thermal stability [15]. Hydroxyl and aldehyde groups present in vanillin can be modified, and new derivatives might be used as monomers for polymerization [16]. Vanillin demonstrates high antibacterial activity that leads to its extensive use in food packaging or medicine [17]. Both thermal polymerization [18, 19] and photopolymerization [20] have been used for polymer synthesis from vanillin derivatives. Vanillin methacrylate was successfully copolymerized with acrylate epoxidized soybean oil. The mechanical properties of these polymers were improved by increasing the amount of vanillin methacrylate fragments in the polymer [19]. Vanillin methacrylate and vanillin dimethacrylate were also used in radical polymerization. The polymers obtained demonstrated high thermal stability and had a huge potential in the production of polymer composites [18]. Vanillin acrylate has also been used in radical polymerization. Vanillin acrylate-based polymers were stiff materials with a high glass transition temperature (up to 168 °C) and could be used as organic coatings [19]. Recently, the use of vanillin for the synthesis of renewable polymers has attracted a lot of interest as it is one of the commercially available bio-based aromatic compounds [21]. However, none of these studies focused on the use of vanillin derivatives in dual curing systems or

in the production of shape memory polymers. In this study, for the first time, the photocuring kinetics of vanillin acrylate-based dual curing systems and mechanical, thermal, and antimicrobial properties of the resulting polymers have been investigated.

Dual curing is one of the possible ways to obtain shape-memory materials. The combination of two simultaneous or sequential curing reactions [22] results in the formation of interpenetrating or semi-interpenetrating polymer networks [23]. This allows the development of materials with unique thermal and mechanical properties that could not be obtained using other polymerization reactions [24, 25]. Dual-cured thermosets were successfully prepared using off-stoichiometric formulations of thiol-acrylate systems [26]. The resulting materials display a wide range of properties [27] and are easily adaptable to a wide variety of applications, such as shape-memory polymers, optical materials, protective coatings, photolithography, holographic materials, *etc.* [28].

In this work, commercial vanillin acrylates were selected with the aim of finding efficient photocurable systems suitable for industrial application in environmentally friendly light-based additive manufacturing technologies. Three vanillin derivatives, vanillin diacrylate (VD), vanillin dimethacrylate (VDM), and vanillin hydroxypropane dimethacrylate (VHDM), were tested in photopolymerization with 1,3-benzenedithiol (BDT). By varying the ratio of acrylate to thiol (from 1:1 to 1:0.5), the rate of thiol-acrylate photopolymerization and free-radical photopolymerization was tuned, and polymers possessing different mechanical and thermal properties were obtained. Ethyl(2,4,6-trimethylbenzoyl)phenylphosphinate (TPOL) was selected as the photoinitiator, as it is preferred due to the photobleaching effect that provides transparent coatings and allows the lower layers of the coating to cure [29]. Real-time photorheometry was used to monitor the photocuring kinetics, rheological parameters, and shrinkage, as these parameters have a significant impact on the application of polymer resins. The yield of insoluble fraction and swelling value of the polymers were calculated to confirm their crosslinked structure. The thermal and mechanical properties were investigated and compared with those of other acrylate-based photopolymers [30]. Also, the antibacterial and antifungal properties of the polymer films were investigated as well. All of the properties mentioned above enable the wide use of vanillin-based antimicrobial shape

memory polymers in a huge variety of applications, including smart materials.

2. Experimental
2.1. Materials
Vanillin diacrylate (VD), vanillin dimethacrylate (VDM), and vanillin hydroxypropane dimethacrylate (VHDM) (all from Specific Polymers), 1,3-benzenedithiol (BDT), ethyl(2,4,6-trimethylbenzoyl) phenylphosphinate (TPOL, Fluorochem) (Figure 1), tetrahydrofurane (THF, Eurochemicals), chitosan and hydroxyethyl starch (both from Sigma-Aldrich) were used as received.

2.2. Preparation of crosslinked polymer specimens
The mixtures containing 1 mol of vanillin derivative (VD, VDM or VHDM), 3 mol% of TPOL, 1 or 0.5 mol of BDT were stirred with a magnetic stirrer at room temperature (25 °C) for 1 min. VDM was dissolved in small volume of THF before mixing with other resin components (0.2 ml of THF for 1 g of

Figure 1. Chemical structure of vanillin hydroxypropane dimethacrylate (VHDM), vanillin dimethacrylate (VDM), vanillin diacrylate (VD), 1,3-benzenedithiol (BDT) and ethyl(2,4,6-trimethylbenzoyl) phenylphosphinate (TPOL).

VDM). When homogenous mixtures were obtained, the resins were poured into a Teflon mold and cured for 2–5 min under a UV/Vis lamp (Helios Italquartz, model GR.E 500 W, Milan, Italy) with an intensity of 310 mW/cm². The composition of the resins is presented in Table 1.

2.3. Characterization techniques
Fourier transformation infrared spectroscopy (FT-IR) spectra were recorded using a Spectrum BX II FT-IR spectrometer (Perkin Elmer, Llantrisant, UK) in the range of 650–4000 cm⁻¹. Reflection was measured during the test.

The Soxhlet extraction was used to determine the yield of the insoluble fraction. Polymer samples of 0.3 g were extracted with acetone for 24 h. After 24 h, the insoluble fractions were dried under vacuum until no change in mass was observed. The yield of the insoluble fraction was calculated as the difference in mass before and after the extraction and drying.

The swelling values of the crosslinked polymer specimens were obtained by measuring the mass of specimens swollen in acetone at 25 °C. Polymer film specimens of 20±0.1 mm length, 9±0.05 mm width, and 1±0.05 mm thickness were used. The change of mass was measured every 10 min and the percentage change in mass was calculated.

Differential scanning calorimetry (DSC) measurements were performed on a DSC 8500 apparatus (Perkin Elmer, Llantrisant, UK). The heating rate of 20 °C/min under nitrogen atmosphere (50 ml/min) and the temperature range of –40–110 °C of the heating–cooling–heating cycle were used. Hermetic aluminum pans were used. The glass transition temperature was calculated as a midpoint of the glass transition step of the second heating curve using the TA Universal Analysis software.

Thermogravimetric analysis (TGA) was performed on a TGA 4000 apparatus (Perkin Elmer, Llantrisant, UK). A heating rate of 20 °C/min under a nitrogen
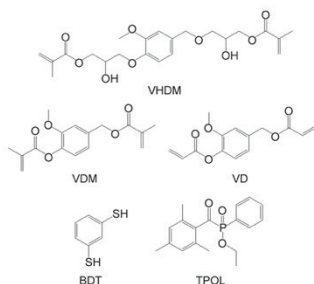
Table 1. Composition of resins **C1–C6**.

Resin	Vanillin derivative	Amount of vanillin derivative [mol]	Amount of 1,3-benzenedithiol [mol]	Amount of the photoinitiator TPOL [mol%]	Solvent
C1	VD	1	1.0	3	–
C2	VD	1	0.5	3	–
C3	VDM	1	1.0	3	THF
C4	VDM	1	0.5	3	THF
C5	VHDM	1	1.0	3	–
C6	VHDM	1	0.5	3	–

121

atmosphere (100 ml/min) was chosen. The temperature range of 10–800 °C was used. Aluminum oxide pans were used.

Measurement of the temperature at which the material starts to soften under compression load was carried out on an MCR302 rheometer (Anton Paar, Graz, Austria) in the temperature range from –40 to 60 °C with a heating rate of 2 °C/min. The thickness of specimens was 1.0±0.15 mm. 8 mm diameter flat end road was used to apply the load. The maximum load was 5 N applied with a frequency of 1 Hz.

The mechanical properties of the synthesized polymers were determined by the tensile test, which was performed on a Testometric M500-50CT testing machine (Testometric Co Ltd, Rochdale, UK) with flat-face grips at room temperature (25 °C). The dimensions of the test specimens were $50\pm0.00\times10\pm0.00\times1\pm0.15$ mm. The gap between the grips was set to 20 mm, and a test was performed at the speed of 5 mm/min until the specimen broke. Young's modulus, tensile strength, and elongation at break were determined.

Statistical analysis. The collected data were statistically analyzed using ANOVA for the Microsoft Excel program. All experiments were carried out in triplicate, except for the tensile test in which five replicates were used, and the results are presented as the average values ± standard deviation. The estimated p-value was below 0.05 within the groups.

2.4. Real-time photorheometry

UV/Vis curing tests were performed with vanillin acrylate-based resins containing 1 mol of acrylate (VD, VDM, or VHDM), 1 or 0.5 mol of BDT, 3 mol% of TPOL, and a small amount of THF (only in VDM-based resins) on an MCR302 rheometer (Anton Paar, Graz, Austria) equipped with the plate/plate measuring system. The Peltier-controlled temperature chamber with the glass plate (diameter was 38 mm) and the top plate PP15 (diameter was 15 mm) was used. The measurement gap was set to 0.1 mm, and the samples were irradiated with UV/Vis light in a wavelength range of 250–450 nm through the glass plate using the UV/Vis spot curing system OmniCure S2000 (Lumen Dynamics Group Inc., Mississauga, ON, Canada). The temperature was 25 °C. In all cases, a shear mode with a frequency of 10 Hz and a shear strain of 1% was used. The storage modulus (G'), the loss modulus (G''), the loss factor (tan δ), and the complex viscosity (η^*) were recorded as a function of the irradiation time. Values for each parameter were collected every 1 second, of 125 points per 125 seconds of photocuring. The gel point (t_{gel}) indicated the formation of the polymeric network and was calculated as the intersection point of G' and G''. The shrinkage was calculated from the reduction of the height of sample during the polymerization process. The normal force was set to 0 N during the measurement of sample shrinkage. The mean value and standard deviation were obtained from five measurements of each resin.

2.5. Antimicrobial test

The study of the antimicrobial (antibacterial and antifungal) activity of polymers was performed using two strains of bacteria, Gram-negative bacteria *Escherichia coli* ATCC 25922 (*E. coli*) and Gram-positive bacteria *Staphylococcus aureus* ATCC 29213 (*S. aureus*), and two fungal strains, *Aspergillus niger* 0999-14 (*A. niger*) and *Aspergillus flavus* 1087-03 (*A. flavus*). Microorganism suspensions were prepared from fully mature cultures. The concentration of suspensions was determined by measuring the optical density with a spectrophotometer (Evolution 60S, Thermo Fisher Scientific, Waltham, MA, USA) and then was corrected by plating on nutrient media. The final inoculum concentrations were $7.6\cdot10^6$ for *E. coli*, $4.7\cdot10^6$ for *S. aureus*, $2.6\cdot10^6$ for *A. niger*, and $1.66\cdot10^6$ colony-forming units/ml [CFU/ml] for *A. flavus*. The test films (10×10 mm) were placed in empty Petri dishes. Then 10 µl of the bacterial or fungal suspension was applied to their surface. For comparison, chitosan and hydroxyethyl starch films were infected in the same manner. Plates with infected films were incubated for 24 h in a humid chamber (90% relative humidity) at 37 °C in the case of infection with bacteria and at 26 °C in the case of infection with the fungi. After 2, 6, and 24 h of incubation, 2 ml of saline was applied to each film to remove the spores. The resulting suspensions were seeded on nutrient media (bacteria on Mueller Hinton Agar (MHA, Liofilmchem, Italy) and microscopic fungi on Malt Extract Agar (MEA, Liofilmchem, Italy)) and incubated at 37 °C with bacteria and 26 °C with fungi. After 1–2 days of incubation, the grown bacterial colonies were counted, whereas the fungal colonies were counted after 5–6 days. The percentage reduction was calculated according to the formula: $(a-b)/a\cdot100\%$, and the lg reduction of viable spores was calculated according to the formula:

122

$\lg a - \lg b$, where a is the concentration of the colony-forming units [CFU/ml] in inoculum suspension; b is a mean of viable spores [CFU/ml] on specimens from triplicate experiments after incubation.

3. Results and discussions
3.1. Monitoring of photocuring kinetics by real-time photorheometry

The photocuring of vanillin acrylate-based resins was studied by real-time photorheometry. The reaction speed (described by t_{gel}, induction period and slope of the curve) is the limiting factor in applications requiring fast polymerization and crosslinking. For example, in optical 3D printing, a lower value of t_{gel} can increase the speed of the printing process from hours to minutes as the models are composed of different layers. All of these layers require their individual time to polymerize, which results in a long process when resins with high t_{gel} values are used [31]. Shrinkage is the second important parameter for optical 3D printing and other applications of polymers. High shrinkage values can limit the preparation of final products from resins as they make it hard to obtain the desired size [32]. The rigidity of polymers is important in their final application; however, both soft and flexible polymers and hard and rigid polymers are used in different areas of application. In this study, real-time photorheometry was used to monitor the storage modulus G' which characterizes the rigidity of the formed polymers and shrinkage, which characterizes the volume loss [%] during the photocuring process [33]. The real-time photorheometry data for all resins are summarized in Table 2. The dependencies of the storage modulus G', the loss modulus G'', loss factor $\tan\delta$, and complex viscosity η^* of the resin C9 on irradiation time are presented in Figure 2.

The dependence of the storage modulus G' on irradiation time of all vanillin-based resins is presented in Figure 3. As seen from the comparison of the
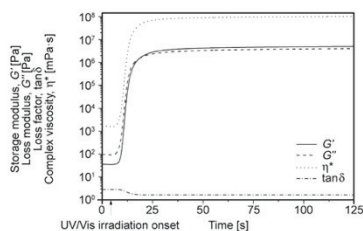

Figure 2. Dependencies of storage modulus G', loss modulus G'', loss factor $\tan\delta$, and complex viscosity η^* of resin C9 on irradiation time.

shape of the G' curves of all resins and the data from Table 1, the highest final rigidity was demonstrated by dual-cured polymers with 1 mol of vanillin derivative (VD, VDM, or VHDM) and 0.5 mol of thiol (BDT) compared to polymers with 1 mol of thiol (BDT). The radical homopolymerization of acrylates became dominant in the dual-curing system, combining free-radical and thiol-acrylate photopolymerization in a higher ratio of acrylate to thiol [34]. Another advantage of the dominant radical homopolymerization of acrylates was the increase in the rate of photocuring. In all cases (C2, C4, C6), the t_{gel} was reached faster when 0.5 mol of thiol was used. For example, C5 reached the gel point at 4.8 s and the rigidity of 5.47 MPa, while C6 reached the gel point at 3.4 s and the rigidity of 14.92 MPa.

The induction period, measured as the onset of the G' increase, of polymers prepared with 0.5 mol of thiol was also shorter than that of polymers prepared with 1 mol of thiol. After the onset of UV irradiation, G' of polymers with 0.5 mol of thiol increased rapidly with as little as a 1 second induction period, and the curve reached the plateau faster than that of polymers with 1 mol of thiol. The induction period of VD and VHDM-based polymers with 0.5 mol thiol was the same; only VDM-based polymer C4 had a slightly

Table 2. Rheological characteristics of vanillin acrylate-based resins.

Resin	Storage modulus, G' [MPa]	Loss modulus, G'' [MPa]	Loss factor, $\tan\delta$	Complex viscosity, η^* [MPa·s]	Gel point, t_{gel} [s]	Shrinkage [%]
C1	8.89±0.67	2.37±0.71	0.35±0.02	0.149±0.001	6.2±0.10	5.75±0.50
C2	11.14±0.61	2.96±0.05	0.21±0.01	0.181±0.027	4.8±0.10	7.25±0.50
C3	0.59±0.06	0.30±0.01	0.51±0.04	0.011±0.001	6.4±0.00	4.00±0.00
C4	10.52±0.12	1.56±0.16	0.15±0.01	0.169±0.001	5.2±0.00	8.00±0.00
C5	5.47±0.61	4.15±0.05	0.76±0.05	0.109±0.001	4.8±0.00	4.00±0.00
C6	14.92±0.16	5.01±0.72	0.34±0.02	0.250±0.031	3.4±0.10	6.50±0.58

123

longer induction period due to the action of THF as a chain transfer agent that slows the photocuring process [35]. Polymers prepared with 1 mol of thiol had an induction period similar for all acrylates and a slightly longer induction period than polymers prepared with 0.5 mol of thiol. The G' curves were not so steep for these polymers and reached the plateau slower than for polymers with 0.5 mol thiol. These parameters have indicated that photopolymerization of resins with 1 mol thiol is a slower process [36].

Resins for various applications are required to have low shrinkage values or no shrinkage at all during the polymerization process, as it is one of the key parameters for high-quality final product [37]. It was determined that all polymers, prepared with 0.5 mol of thiol, shrunk more than those prepared with 1 mole of thiol. The higher shrinkage is the result of the free-radical photopolymerization of acrylates, one of two reactions that take place during the dual curing process [34]. Acrylates have a tendency to shrink during the polymerization process because long-distance connections through weak van der Waals forces are replaced by short, strong covalent bonds between carbon atoms in monomer units [37]. In this case, the use of the higher amount of thiol has the advantage of reducing the shrinkage during the photocuring process by lowering the amount of acrylate in the resin and the resulting polymer. For example, the double amount of thiol in VDM-based resin lowered the shrinkage twice, from 8% (**C4**) when 0.5 mol of thiol were used to 4% (**C3**) when 1 mol of thiol was used. The structure of the vanillin derivative also had an influence on photocuring kinetics and the value of shrinkage of the resulted polymers. For resins prepared with 0.5 mol of thiol, the lowest rigidity and the highest gel point value were shown by VDM-based resin with THF (**C3**), and the resulted polymer shrunk most of all polymers. The photocuring induction period of the VDM-based resin was also higher than that of the VD- and VHDM-based resins. This can be explained by the action of THF as a chain transfer agent that slows the photocuring process [35]. The VD-based resin with 0.5 mol of thiol demonstrated similar results to the VDM-based resin; although **C2** resin was slightly more rigid, it reached the gel point faster and shrunk less lightly than the VDM-based one. The explanation for these results is the different reactivity of the acrylate and methacrylate groups. Methacrylates are less reactive than acrylates as tertiary methacrylate radicals are highly stable

compared to unstable secondary acrylate radicals [38]. Despite that, the VD-based polymer with 0.5 mol of thiol reached the plateau slightly slower than other resins with 0.5 mol of thiol. That indicated that the photopolymerization slowed down at the end. This can be explained by the darker color of vanillin diacrylate, which makes it harder to cure the deeper layers of the resin and slows the photopolymerization [39]. The best results among all resins, prepared with 0.5 mol of thiol, were demonstrated by the VHDM-based resin **C6**, which was the most rigid, had the lowest value of t_{gel}, and shrunk the least. The chemical structure of VHDM is the reason for these results. VHDM is a longer molecule in comparison with VD and VDM, and the reaction rate increases linearly by increasing the distance between polymerizable groups in the polymerization process [40].

Similar results were obtained by comparing resins obtained from different vanillin derivatives and 1 mol of thiol. The only difference was the rigidity of VD- and VHDM-based polymers. The VD-based polymer **C1** was more rigid than the VHDM-based polymer **C5**. This difference could be due to the high amount of thiol radicals formed in the initiation stage of polymerization when 1 mol of thiol was used. That led to the formation of many different polymer chains of different lengths with flexible thioether linkages, resulting in a lower rigidity of the obtained polymers [41]. The VHDM-based polymer formed a large number of polymeric chains with longer distances between the linkages in the presence of 1 mol of thiol compared to the VD-based polymer, which resulted
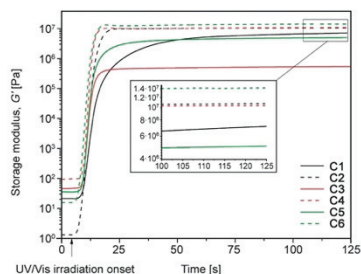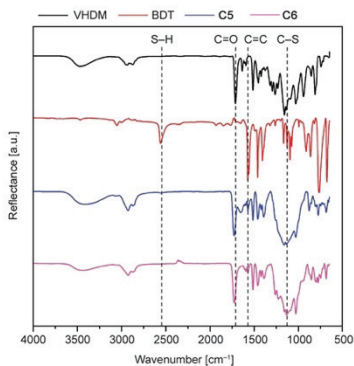
Figure 3. Dependency of storage modulus G' of the resins on irradiation time. — VD-based resins, — VDM-based resins, — VHDM-based resins, solid line – presence of 1 mol of BDT, split line – presence of 0.5 mol of BDT.

in lower rigidity of polymer **C5**. These results were confirmed by the higher swelling values of this polymer.

3.2. Characterization of photocross-linked polymer structure

The chemical structure of the vanillin-based polymers was identified by FT-IR spectroscopy. The intensity of the signals attributed to the C=C group, which were present at 1607 cm^{-1}, and the signals of the C=O group, which were present at 1730 cm^{-1}, in the FT-IR spectra of VD, VDM, and VHDM, were reduced in their polymer spectra. The signal of the S–H group, which was present at 2,561 cm^{-1} in the spectrum of BDT, was weaker in the spectra of the polymers with 1 mol of thiol, and the signal of the C–S group was observed at 1153–1119 cm^{-1} indicated the formation of polymers. The S–H group signal is absent in the spectra of the polymers with 0.5 mol of thiol, indicating that all S–H groups reacted to form a polymer network. A weak signal of C=C groups is present in the FT-IR spectra of all polymers, indicating that a small amount of unreacted acryl groups is left in the polymers. As an example, the FT-IR spectra of VHDM, BDT, and the crosslinked polymers **C5** and **C6** are presented in Figure 4.

The Soxhlet extraction was performed to confirm the crosslinked structure of the polymers. The high yield of the insoluble fraction showed that all monomers participated in the formation of the crosslinked structure. The results are summarized in Table 3. The lower

values of the insoluble fraction (82–87%) were obtained when 1 mol of BDT was used compared to polymers with 0.5 mol of BDT (95–100%). Higher values of the insoluble fraction correlate with the swelling values of the resulting polymers (Figure 5). Lower values of the polymer swelling indicate that shorter chains were formed between the crosslinking points in the polymers. A small signal of unreacted thiol groups was observed in FT-IR spectra of polymers prepared with 1 mol of thiol (**C1, C3,** and **C5**). The presence of unreacted functional groups shows that fewer crosslinks were formed in the polymers, and thus the high swelling value of polymer samples and the reduced yield of insoluble fraction were obtained [42]. During extraction in acetone, soluble components (unreacted monomers, linear oligomers, or branched oligomers) were washed out, resulting in lower values of the gel fraction. The swelling values of polymers with 0.5 mol of thiol were much lower (4–9%) than those of polymers prepared with 1 mol of thiol (35–22%) as the result of the denser interpenetrating networks formed.

The highest swelling value in acetone of all vanillin acrylate-based polymers synthesized with 1 mol of thiol was determined for the VHDM-based polymer **C5**. This is the result of a more flexible polymer network due to the longer chains between the crosslinking points [43]. VD- and VDM-based polymers with

Figure 4. FT-IR spectra of VHDM, BDT and the cross-linked polymers **C5** and **C6**.
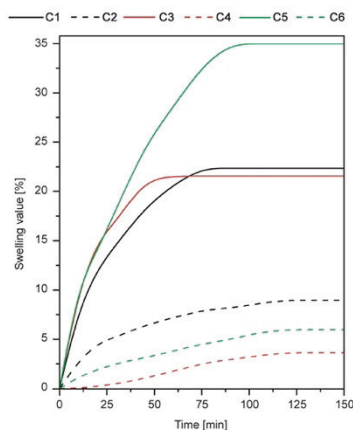
**Figure 5.** The swelling values of vanillin-basedpolymers in acetone.

125

Table 3. Characteristics of the crosslinked vanillin-based polymers.

Polymer	Yield of insoluble fraction [%]	Swelling value in acetone [%]
C1	85±0.5	22±2.0
C2	99.6±0.5	9±1.0
C3	82±0.5	22±2.0
C4	95±1.0	4±0.5
C5	87±0.5	35±2.5
C6	99.9±0.0	6±0.5

1 mol of BDT resulted in similar swelling values in acetone. This might be due to the similar polymer structure as similar length chains between the cross-linking points, which influence the swelling value of polymers, were formed in the polymers [44].

For polymers synthesized with 0.5 mol of thiol, the swelling value in acetone was quite similar (9–4%). The swelling value for VD-based polymer **C2** was the highest due to the longer chains between the crosslinking points in the polymer structure in comparison with VDM- and VHDM-based polymers synthesized with 0.5 mol of thiol [43]. The swelling test confirmed that longer chains between the crosslinking points were formed in the polymer during photopolymerization of VD with 0.5 mol of BDT. The shortest chains between the crosslinking points were formed in the VDM-based polymer **C4**, as its swelling value in acetone was the lowest. However, the differences in swelling values in acetone between different vanillin acrylate-based polymers are relatively insignificant and deviate in less than 10%.

3.3. Thermal properties

DSC and TGA were used to study the thermal properties of the vanillin acrylate-based photo-cross-linked polymers. The results are summarized in Table 4. The synthesized polymers are amorphous materials and underwent the glass transition (T_g) only, as seen from the DSC curves (Figure 6). The T_g of the polymers synthesized with 1 mol of BDT (−3–17 °C) was significantly lower than that of the polymers synthesized with 0.5 mol of BDT (40–46 °C). It was due to the unreacted BDT and the formation of the less dense inner structure, which decreased their T_g [45]. The lowest T_g (−3 °C) was recorded for VDM-based polymer **C3** synthesized with 1 mol of thiol and solvent. The low value of T_g was the result of the formation of a large amount of the thioether linkages, the low crosslinking density, and the yield of the insoluble fraction [46]. The T_g
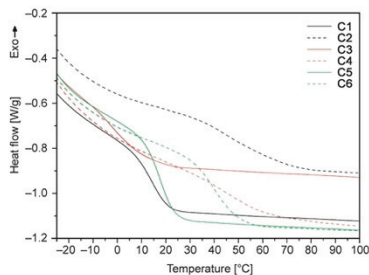
Figure 6. DSC thermograms of cross-linked polymers. — VD-based resins, — VDM-based resins, — VHDM-based resins, solid line – presence of 1 mol of BDT, split line – presence of 0.5 mol of BDT.

of VD- and VHDM-based polymers synthesized with 1 mol of thiol was similar; only the VDM-based polymer synthesized with 1 mol of thiol had a lower T_g. These results correlated with the results of the swelling test. The highest T_g was shown by VD- and VDM-based polymers synthesized with 0.5 BDT and THF (only for VDM-based polymer); the T_g of both polymers, **C2** and **C4**, was 46 °C. Rigidity is one of the factors that affect the T_g of polymers [47]. The same value of a T_g is the result of similar rigidity of the polymers obtained from the photorheological study. Slightly lower T_g (40 °C) was observed for VHDM-based polymer synthesized with 0.5 thiols, **C6**. The rigidity of this VHDM-based polymer was higher than that of the VD- and VDM-based ones, and this led to the higher T_g value of this polymer. A slightly lower glass transition temperature was obtained due to the flexible backbone structure of the VHDM-based polymer, as the T_g of flexible materials is lower than that of hard and rigid polymers [48].

Table 4. Thermal characteristics of vanillin-based polymers.
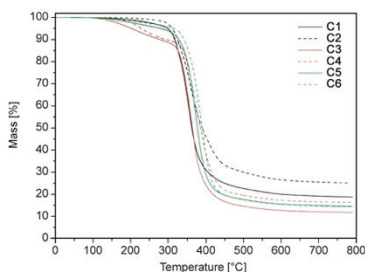
Polymer	$T_{dec.-10\%}$ [°C]*	T_g** [°C]	10 μm deformation temperature*** [°C]
C1	317	14	9
C2	324	46	16
C3	277	−3	−12
C4	294	46	5
C5	327	17	8
C6	341	40	14

*from TGA curves,
**from DSC curves,
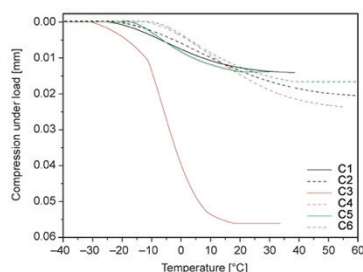***from compression under load curves.

126

Thermal decomposition of the synthesized polymers occurred in two steps for VDM-based polymers with THF and in one step for VD and VHDM-based polymers without any solvent. (Figure 7). The first step can be explained by the formation of linear or branched macromolecules in the presence of the solvent, which acts as a chain transfer agent [49]. The first step in the TGA curve of polymer **C3** can also be explained by the evaporation or cleavage of the fragments with unreacted BDT, as unreacted thiol group signals were observed in the FT-IR spectrum of polymer **C3** [42]. The temperature of 10% weight loss ($T_{dec.-10\%}$) of all synthesized polymers was in the range of 277–341 °C. Similarly to the glass transition temperature, the values of $T_{dec.-10\%}$ for polymers synthesized from the resins with 0.5 mol of BDT were higher. These results correlated with the yield of the insoluble fraction of polymers as higher decomposition temperatures were obtained for polymers with a higher yield of insoluble fraction and denser internal network structure. The value of $T_{dec.-10\%}$ for VHDM-based polymer synthesized with 0.5 mol of thiol **C6** ($T_{dec.-10\%} = 341$ °C) was the highest and the lowest $T_{dec.-10\%}$ was recorded for VDM-based polymer synthesized with 1 mol of thiol and solvent **C3** ($T_{dec.-10\%} = 277$ °C). $T_{dec.-10\%}$ of the synthesized polymers were in a similar range as for some acrylated epoxidized soybean oil-based polymers (297–356 °C) tested in optical 3D printing [50]. This similarity indicates that vanillin-based polymers obtained in this study can be potentially used in optical 3D printing. Their thermal characteristics are comparable with those of soybean oil-based polymers used in optical 3D printing technology.

The curves of the specimen deformation under load are presented in Figure 7. The 10 μm deformation temperature was chosen for comparison because, at this value of deformation, all six polymers can be compared. It would be impossible to compare them using different deformation values because deformation values of polymers prepared with 0.5 mol of thiol are very low, while the ones for polymers prepared with 1 mol of thiol are higher. The values of the temperature at which the 10 μm deformation of the sample is reached are summarized in Table 4. The 10 μm deformation temperature is the temperature at which polymers deform under a load of 5 N. Even at a temperature lower than T_g; these polymers can slightly deform. This deformation increases as the temperature increases. The highest temperature of the deformation beginning was exhibited by the **C6** specimen (Figure 8). In all cases, the deformation of the polymers prepared with 1 mol of thiol started at a lower temperature than that of the polymers synthesized with 0.5 mol of thiol. Furthermore, the 10 μm deformation temperature of polymers synthesized with 1 mol thiol was lower than that of the same vanillin acrylate-based polymers synthesized with 0.5 mol of thiol. For example, the 10 μm deformation temperature of vanillin diacrylate-based polymer synthesized with 1 mol of thiol **C1** was 9 °C, while that of vanillin diacrylate-based polymer synthesized with 0.5 mol of thiol **C2** was 16 °C. All of these results correlated with the T_g determined by DSC.

Figure 7. Thermogravimetric curves of cross-linked polymers. — VD-based resins, — VDM-based resins, — VHDM-based resins, solid line – presence of 1 mol of BDT, split line – presence of 0.5 mol of BDT.

Figure 8. Compression under load as a function of temperature of cross-linked polymers. — VD-based resins, — VDM-based resins, — VHDM-based resins, solid line – presence of 1 mol of BDT, split line – presence of 0.5 mol of BDT.

The lowest 10 µm deformation temperature was obtained for VDM-based polymers **C3** and **C4**. It can be explained by the formation of a large number of the thioether linkages, the low cross-linking density, and the yield of the insoluble fraction. The VD- and VHDM-based polymers synthesized with 1 and 0.5 mol of thiol showed very similar 10 µm deformation temperatures, although those of the VHDM-based polymers were slightly lower, which can be explained by the flexible backbone structure of the VHDM-based polymer.

3.4. Shape memory properties of vanillin-based polymers

The shape memory of polymers significantly expands their field of application. In order to test shape memory properties of vanillin-based polymers, the polymer samples were heated above their glass transition temperature and then deformed to the desired temporary shape, in this case – a coil. The glass stick was used to form polymer samples. When the temporary shape was obtained, it was fixed by cooling the polymer sample below its T_g. The temporary shape did not change with time, while samples were kept at a temperature below their T_g. The ability of the samples to return to their permanent shape was verified by heating them above their T_g. All polymer samples returned to their permanent shape within a short period of time. The recovery to the original shape conditions of these polymers is determined by their glass transition temperature [1]. The scheme of the heating-cooling-heating cycles is presented in Figure 9.

The ability to obtain a new shape while heated above T_g and maintain it after cooling of the polymer specimen below T_g was demonstrated by all synthesized vanillin-based polymers. All of them were able to return to their primary shape after heating above T_g. The polymers, prepared with 1 mol of thiol, were transformed to a temporary shape at room temperature (25 °C) and then placed in the fridge (–20 °C) to maintain their temporary shape. These polymers were able to maintain their temporary shape in the fridge but did not maintain it at room temperature, as their T_g is below 25 °C, and that limits their application. The VDM-based polymer **C3** sample returned to its permanent shape at room temperature, the fastest of all polymers synthesized with 1 mol of thiol, within less than 90 seconds. VD and VHDM-based polymer **C1** and **C5** samples returned to their permanent shape slower; it took about 180 s to fully recover at room temperature. The transformation of the **C1** sample is presented in Figure 9b.

Polymers, prepared with 0.5 mol of thiol, were transformed to a temporary shape at 60 °C and then cooled to room temperature (25 °C). The samples of
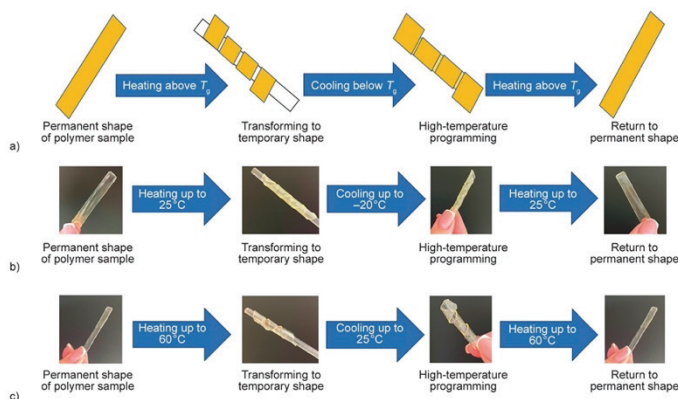
Figure 9. The scheme of shape memory behaviour of polymer samples, a) principal scheme of experiment, b) sample of VD-based polymer synthesized with 1 mol of thiol, **C1**, c) sample of VHDM-based polymer synthesized with 0.5 mol of thiol, **C6**.
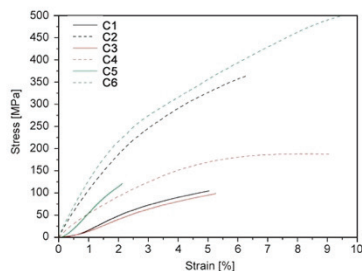
128

these polymers were able to maintain their temporary shape at room temperature. No change in shape was noticed after 48 hours at 25 °C. To return to a permanent shape, polymer samples were heated to 60 °C. At this temperature, all samples immediately returned to their permanent shape in less than a second. Samples of acrylate-based polymers demonstrated the same results, as their T_g s are very similar, and no differences were observed between VD-, VDM- and VHDM-based polymers synthesized with 0.5 mol of thiol. The transformation of **C6** is presented in Figure 9c.

3.5. Mechanical characteristics

The tensile test was performed to investigate the mechanical properties of vanillin-based polymers. The results are presented in Table 5 and Figure 10. Polymers synthesized with 1 mol of vanillin derivative and 1 mol of thiol are soft and flexible materials; all of them demonstrated low values of Young's modulus (1.4–3.5 MPa) and tensile strength (0.02–4.1 MPa) compared to polymers prepared with 0.5 mol of thiol. Significantly high values of elongation at break were shown by VD- and VHDM-based polymers synthesized with 1 mol of thiol, **C1** (102.8%), and **C5** (119.7%). The high elongation at break values and shape memory abilities of these polymers allow using them as thermo-responsive smart materials in various areas such as aerospace, medicine, civil engineering and *etc.* [51]. The lower values of Young's modulus and tensile strength of polymers synthesized with 1 mol of thiol compared to those of polymers synthesized with 0.5 mol of thiol are due to the polymer structure. The crosslinking density of the polymers synthesized with 0.5 mol of thiol is higher as the short chains between the crosslinking points were formed. Polymers synthesized with 1 mol of thiol demonstrated lower values of mechanical characteristics as they have longer chains between

Figure 10. Tensile stress-strain curves of cross-linked polymers. — VD-based resins, — VDM-based resins, — VHDM-based resins, solid line – presence of 1 mol of BDT, split line – presence of 0.5 mol of BDT.

the crosslinking points. These results were confirmed by the swelling test. Vanillin-based polymers synthesized with 1 mol of thiol have longer chains between the crosslinking points, which resulted in lower mechanical strength and higher elongation at break values [52]. Different results were shown by vanillin-based polymers synthesized with 0.5 mol of thiol. The high values of Young's modulus, tensile strength, and low values of elongation at break show that these polymers are mechanically strong and rigid materials. Polymers synthesized from vanillin derivatives and 0.5 mol of thiol demonstrated similarly and, in most cases, even higher mechanical strength compared to acrylated epoxidized soybean oil-based polymers used in digital light processing 3D printing [53].

As confirmed by elongation at break values, VHDM-based polymers synthesized with 0.5 and 1 mol of thiol have a more flexible structure than VD- and VDM-based polymers. Flexible polymers can stretch more before breaking [48], and this ability is caused by their structure. The swelling test has confirmed that longer chains between the crosslinking points were formed during the photopolymerization of VHDM, resulting in higher values of elongation at break. VDM-based polymers demonstrated the lowest values of Young's modulus, tensile strength, and elongation at break compared to VD- and VHDM-based polymers. The lower values of the mechanical characteristics were caused by linear or branched macromolecules formed in the presence of a solvent, which could act as a chain transfer agent [49].

Table 5. Mechanical characteristics of the polymers obtained by tensile test.

Polymer	Young's modulus [MPa]	Tensile strength [MPa]	Elongation at break [%]
C1	3.5±0.2	4.1±0.7	102.8±3.6
C2	9610.8±372.4	349.9±19.0	6.8±1.1
C3	1.4±0.2	0.02±0.0	19.0±3.2
C4	3952.3±52.3	177.9±11.6	9.7±0.3
C5	1.4±0.1	1.2±0.1	119.7±12.1
C6	11339.4±934.0	439.0±8.2	12.3±1.2

129

3.6. Antimicrobial activity of polymers

The antibacterial and antifungal activity of the vanillin acrylate-based polymer films was evaluated during the direct contact with the specimens by calculating the log reduction and percent reduction of viable microbial spores. Two reference polymer films of chitosan, a well-known antibacterial polymer, and hydroxyethyl starch possessing no such activity were used as a control. The (W) in the polymer code indicates that the polymer film was washed before antimicrobial testing in acetone for 24 h. The results are presented in Table 6 and Table 7.

The antibacterial activity of the polymer films differed in the initial stage (after 2 and 6 h) (Figure 11). After 2 h of exposure, the **C2** film inhibited the viability of *E. coli* the most (91.8%), and *S. aureus* was inhibited the most by the **C1** film (82.0%). Additionally, Gram-negative *E. coli* was inhibited more than

S. aureus. After 6 hours of exposure, *E. coli* was already inhibited by more than 90% on 6 films (**C2, C3, C3(W), C4, C4(W)** and **C6**), and growth of *S. aureus* was inhibited on 4 films (**C1, C3, C3(W)** and **C5**). However, after 24 hours of exposure, bacterial viability was completely inhibited on all films tested, except the one of *S aureus* on **C2**. The structure of polymers is important for their antimicrobial activity. One of the functional groups responsible for antimicrobial properties is the aromatic ring. Compounds with different amounts of this functional group were tested against *Bacillus subtilis* and *S. aureus* as Gram-positive bacteria and *Salmonella typhimurium* and *Proteus Vulgaris* as Gram-negative bacteria and showed antibacterial effect [54]. All vanillin-based photopolymers have aromatic rings in their structure and show high antibacterial activity against *S. aureus*. Hydroxyl [55], sulfur [56], and

**Table 6.** Characteristics of antibacterial activity of polymer film samples.

Polymer film	*Escherichia coli*		*Staphylococcus aureus*	
	Lg reduction after 24 h	Percent reduction after 24 h [%]	Lg reduction after 24 h	Percent reduction after 24 h [%]
C1	6.88±0.00	100±0.00	6.67±0.00	100±0.00
C2	6.88±0.00	100±0.00	2.67±0.02	99.8±0.02
C3	6.88±0.00	100±0.00	6.67±0.00	100±0.00
C3(W)*	6.88±0.00	100±0.00	6.67±0.00	100±0.00
C4	6.88±0.00	100±0.00	6.67±0.00	100±0.00
C4(W)*	6.88±0.00	100±0.00	6.67±0.00	100±0.00
C5	6.88±0.00	100±0.00	6.67±0.00	100±0.00
C6	6.88±0.00	100±0.00	6.67±0.00	100±0.00
Chitosan	6.88±0.00	100±0.00	6.67±0.00	100±0.00
Hydroxyethyl starch	3.58±0.02	99.9±0.02	1.08±0.02	91.6±0.02

*W – washed for 24 h in acetone

Table 7. Characteristics of antifungal activity characteristics of polymer film samples.

| Polymer film	*Aspergillus flavus*		*Aspergillus niger*	
	Lg reduction after 24 h	Percent reduction after 24 h [%]	Lg reduction after 24 h	Percent reduction after 24 h [%]
C1	6.22±0.00	100±0.00	0.80±0.09	84.4±0.09
C2	1.20±0.04	93.7±0.04	0.76±0.10	82.9±0.10
C3	1.49±0.05	96.7±0.05	0.65±0.12	77.9±0.12
C3(W)*	1.45±0.05	96.4±0.05	0.55±0.12	72.3±0.12
C4	1.16±0.04	93.1±0.04	0.86±0.09	86.3±0.09
C4(W)*	1.25±0.04	94.3±0.04	1.02±0.06	90.6±0.06
C5	3.22±0.01	99.9±0.01	1.12±0.05	92.5±0.05
C6	1.22±0.04	94.0±0.04	0.66±0.12	78.5±0.12
Chitosan	1.76±0.06	97.9±0.06	2.93±0.01	99.9±0.01
Hydroxyethyl starch	1.53±0.05	97.0±0.05	0.43±0.14	63.5±0.14

*W – washed for 24 h in acetone

130
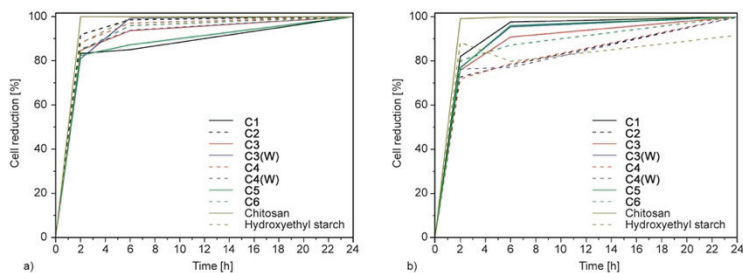
Figure 11. The reduction of *E. coli* (a) and *S. aureus* b) cells during 24 h of contact time with specimens of vanillin-based polymers, chitosan, and hydroxyethyl starch.

carbonyl [57] groups also contribute to the antimicrobial effect. It has been scientifically shown that decreasing the value of these groups leads to a lower antibacterial effect. The presence of these groups also increases the antibacterial properties of vanillin-based photopolymers. As seen from the comparison of these results with the ones for chitosan films, some of the bacteria may remain viable on the tested films for some time, but the final result is the same after 24 h. The viability of the bacteria tested on the hydroxyethyl starch film also decreased, but they still remained viable after 24 h.

The antifungal activity of the films varied depending on the type of fungus (Table 6). Higher antifungal activity was observed for *A. flavus* than for *A. niger*, and it gradually intensified with increasing exposure time. The viability of *A. flavus* was also inhibited on the reference samples; however, the percent reduction was higher on the **C1** and **C5** films than on the chitosan and hydroxyethyl starch films (100 and 99.9%,

respectively). Other polymer films showed a similar percentage reduction in the range of 93.1–94.3 %.

After inoculation of the test films with the suspension of *A. niger* spore, the percent reduction was slightly reduced after 6 h of exposure compared to 2 h of exposure, which could be explained by the onset of sporulation (Figure 12). However, after 24 h, the viability of *A. niger* decreased due to unfavorable development conditions for the fungus and, therefore, the percent reduction increased. The results showed that the viability of *A. niger* on the hydroxyethyl starch film also decreased. The highest percent reduction was found on **C4(W)** film, but it was lower than the one on chitosan film. The lower values of percent reduction against *A. flavus* and *A. niger* after 24 h were demonstrated by VD-, VDM- and VHDM-based films prepared with 0.5 mol of thiol compared to VD, VDM, and VHDM-based films prepared with 1 mol of thiol. The main reason for this difference could be the higher concentration of sulfur resulting
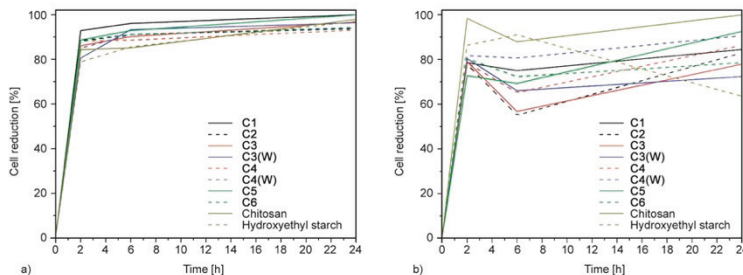
Figure 12. The reduction of *A. flavus* (a) and *A. niger* (b) cells during 24 h of contact time with specimens of vanillin-based polymers, chitosan, and hydroxyethyl starch.

from the higher amount of thiol, which has marked antifungal activity [56]. The only exception was the VDM-based film, in which the percent reduction against *A. niger* was lower when 1 mol of thiol was used for the synthesis of the polymer in comparison to that of the polymer synthesized with 0.5 mol of thiol. In this case, *A. niger* was affected by a higher concentration of carbonyl groups in the VDM-based film prepared with 0.5 mol of thiol [57].

The lowest value of cell reduction against *A. niger* after 24 h was shown by **C3** and **C3(W)** films. Polymer **C3** showed a 77.9% of percentage reduction, while the same polymer **C3(W)** reached only 72.3% after 24 h washing procedure in acetone. It can be assumed that lower values of cell reduction were obtained due to a lower amount of carbonyl groups and sulfur in the washed sample, and the lower value after the washing procedure was due to the low value of the yield of the insoluble fraction of **C3** polymer, as all unreacted parts of monomers and oligomers were washed out from the film and lowered the concentration of carbonyl groups and sulfur. Different results were shown by **C4** polymer film before and after washing. Polymer **C4** film without washing reached a reduction of 86.3%. The reduction was increased to 90.6% in polymer **C4(W)**, which was washed before the test. Polymer **C4** with a high yield of insoluble fraction resulted in the purer polymer after washing in acetone for 24 h. Because of that, only a small amount of unreacted monomers was washed out, and a higher concentration of carbonyl groups was left in the polymer resulting in better antifungal activity against *A. niger*.

4. Conclusions

Novel antimicrobial vanillin acrylate-based shape memory photopolymers with high antibacterial and antifungal activity have been developed and investigated for the first time. A dual-curing process, combining free-radical photopolymerization and thiol-acrylate photopolymerization, was applied for the synthesis of these polymers. The reduction of the thiol content increased the rate of photocuring, improved mechanical performance of the polymers (Young's modulus was increased from 1.4–3.5 to 3952.3–11339.4 MPa), and their heat resistance (the 10% weight loss increased from 277–327 to 294–341 °C). Radical homopolymerization of acrylates resulted in a higher ratio of acrylate to thiol in the obtained polymers. The specimens of all synthesized vanillin-based

polymers were able to obtain a new shape while heated above their glass transition temperature (–3–46 °C), maintain it after cooling below their glass transition temperature, and return to their primary shape after heating above their glass transition temperature. These properties have determined them as shape memory polymers and possible candidates for application as smart materials. All vanillin acrylate-based polymer films showed a significant antibacterial activity against *Escherichia coli* and *Staphylococcus aureus* (cell reduction reached 100% after 24 h by most polymers), which was similar to that of the chitosan film. Vanillin-based polymer films also showed antifungal activity against *Aspergillus flavus* (cell reduction reached 93.1–100% after 24 h) and *Aspergillus niger* (cell reduction reached 72.3–92.5% after 24 h).

References
[1] Yang K., Du J., Zhang Z., Ren T.: A facile strategy to fabricate robust triple-shape memory polymer. Materials Letters, **257**, 126753 (2019).
https://doi.org/10.1016/j.matlet.2019.126753
[2] Behl M., Lendlein A.: Shape-memory polymers. Materials Today, **10**, 20–28 (2007).
https://doi.org/10.1016/S1369-7021(07)70047-0
[3] Hager M. D., Bode S., Weber C., Schubert U. S.: Shape memory polymers: Past, present and future developments. Progress in Polymer Science, **50**, 3–33 (2015).
https://doi.org/10.1016/j.progpolymsci.2015.04.002
[4] Hassani F. A., Shi Q., Wen F., He T., Haroun A., Yang Y., Feng Y., Lee C.: Smart materials for smart healthcare–moving from sensors and actuators to self-sustained nanoenergy nanosystems. Smart Materials in Medicine, **1**, 92–124 (2020).
https://doi.org/10.1016/j.smaim.2020.07.005
[5] Nasseri R., Deutschman C. P., Han L., Pope M. A., Tam K. C.: Cellulose nanocrystals in smart and stimuli-responsive materials: A review. Materials Today Advances, **5**, 100055 (2020).
https://doi.org/10.1016/j.mtadv.2020.100055
[6] Grauzeliene S., Valaityte D., Motiekaityte G., Ostrauskaite J: Bio-based crosslinked polymers synthesized from functionalized soybean oil and squalene by thiol–ene UV curing. Materials, **14**, 2675 (2021).
https://doi.org/10.3390/ma14102675

132

[7] Sha X-L., Yuan L., Liang G., Gu A.: Preparation of high performance bio-based benzoxazine resin through a green solvent-free strategy for shape memory application. Polymer, **202**, 122673 (2020).
https://doi.org/10.1016/j.polymer.2020.122673

[8] Lu C., Liu Y., Liu X., Wang C., Wang J., Chu F.: Sustainable multiple- and multistimulus-shape-memory and self-healing elastomers with semi-interpenetrating network derived from biomass *via* bulk radical polymerization. ACS Sustainable Chemistry & Engineering, **6**, 6527–6535 (2018).
https://doi.org/10.1021/acssuschemeng.8b00329

[9] Khasraghi S. S., Shojaei A., Sundararaj U.: Bio-based UV curable polyurethane acrylate: Morphology and shape memory behaviors. European Polymer Journal, **118**, 514–527 (2019).
https://doi.org/10.1016/j.eurpolymj.2019.06.019

[10] Chu H-Y., Fu H., Liu A., Wang P., Cao Y-L., Du A-F., Wang C-C.: Two silver-based coordination polymers constructed from organic carboxylate acids and 4, 4′-bipyridine-like bidentate ligands: Synthesis, structure, and antimicrobial performances. Polyhedron, **188**, 114684 (2020).
https://doi.org/10.1016/j.poly.2020.114684

[11] Pandey A., Singh G., Singh S., Jha K., Prakash C.: 3D printed biodegradable functional temperature-stimuli shape memory polymer for customized scaffoldings. Journal of the Mechanical Behavior of Biomedical Materials, **108**, 103781 (2020).
https://doi.org/10.1016/j.jmbbm.2020.103781

[12] Shaabani A., Sedghi R., Motasadizadeh H., Dinarvand R.: Self-healable conductive polyurethane with the body temperature-responsive shape memory for bone tissue engineering. Chemical Engineering Journal, **411**, 128449 (2021).
https://doi.org/10.1016/j.cej.2021.128449

[13] Bil M.: The effect of chitosan form on the shape memory properties of polyurethane based composites. Materials Letters, **284**, 129007 (2020).
https://doi.org/10.1016/j.matlet.2020.129007

[14] Ciriminna R., Fidalgo A., Meneguzzo F., Parrino F., Ilharco L. M., Pagliaro M.: Vanillin: The case for greener production driven by sustainability megatrend. ChemistryOpen, **8**, 660–667 (2019).
https://doi.org/10.1002/open.201900083

[15] Stanzione J. F., Sadler J. P., la Scala J. J., Reno K. H., Wool R. P.: Vanillin-based resin for use in composite applications. Green Chemistry, **14**, 2346–2352 (2012).
https://doi.org/10.1039/C2GC35672D

[16] Meylemans H. A., Harvey B. G., Reams J. T., Guenthner A. J., Cambrea L. R., Groshens T. J., Baldwin L. C., Garrison M. D., Mabry J. M.: Synthesis, characterization, and cure chemistry of renewable bis(cyanate) esters derived from 2-methoxy-4-methylphenol. Biomacromolecules, **14**, 771–780 (2013).
https://doi.org/10.1021/bm3018438

[17] Salmi-Mani H., Terreros G., Barroca-Aubry N., Aymes-Chodur C., Regeard C., Roger P.: Poly(ethylene terephthalate) films modified by UV-induced surface graft polymerization of vanillin derived monomer for antibacterial activity. European Polymer Journal, **103**, 51–58 (2018).
https://doi.org/10.1016/j.eurpolymj.2018.03.038

[18] Zhang C., Madbouly S. A., Kessler M. R.: Renewable polymers prepared from vanillin and its derivatives. Macromolecular Chemistry and Physics, **216**, 1816–1822 (2015).
https://doi.org/10.1002/macp.201500194

[19] Zhang C., Yan M., Cochran E. W., Kessler M. R.: Biorenewable polymers based on acrylated epoxidized soybean oil and methacrylated vanillin. Materials Today Communications, **5**, 18–22 (2015).
https://doi.org/10.1016/j.mtcomm.2015.09.003

[20] Aymes-Chodur C., Salmi-Mani H., Dragoe D., Aubry-Barroca N., Buchotte M., Roger P.: Optimization of microwave plasma treatment conditions on polydimethylsiloxane films for further surface functionalization. European Polymer Journal, **150**, 110416 (2021).
https://doi.org/10.1016/j.eurpolymj.2021.110416

[21] Fache M., Boutevin B., Caillol S.: Vanillin, a key-intermediate of biobased polymers. European Polymer Journal, **68**, 488–502 (2015).
https://doi.org/10.1016/j.eurpolymj.2015.03.050

[22] Roig A., Ramis X., de la Flor S., Serra À.: Dual-cured thermosets from glycydil methacrylate obtained by epoxy-amine reaction and methacrylate homopolymerization. Reactive and Functional Polymers, **159**, 104822 (2021).
https://doi.org/10.1016/j.reactfunctpolym.2021.104822

[23] Ye Y-S., Rick J., Hwang B-J.: Water soluble polymers as proton exchange membranes for fuel cells. Polymers, **4**, 913–963 (2012).
https://doi.org/10.3390/polym4020913

[24] Fouassier J. P., Lalevée J.: Photochemical production of interpenetrating polymer networks; Simultaneous initiation of radical and cationic polymerization reactions. Polymers, **6**, 2588–2610 (2014).
https://doi.org/10.3390/polym6102588

[25] Roland C. M.: Interpenetrating polymer networks (IPN): Structure and mechanical behavior. in 'Encyclopedia of polymeric nanomaterials' (eds.: Kobayashi, S., Müllen K.) Springer, Berlin, 1–9 (2013).
https://doi.org/10.1007/978-3-642-36199-9_91-1

[26] Xi W., Peng H., Aguirre-Soto A., Kloxin C. J., Stansbury J. W., Bowman C. N.: Spatial and temporal control of thiol-Michael addition *via* photocaged superbase in photopatterning and two-stage polymer networks formation. Macromolecules, **47**, 6159–6165 (2014).
https://doi.org/10.1021/ma501366f

133

[27] Konuray A. O., Ruiz A., Morancho J. M., Salla J. M., Fernández-Francos X., Serra À., Ramis X.: Sequential dual curing by selective Michael addition and free radical polymerization of acetoacetate-acrylate-methacrylate mixtures. European Polymer Journal, **98**, 39–46 (2018).
https://doi.org/10.1016/j.eurpolymj.2017.11.003

[28] Gamardella F., Sabatini V., Ramis X., Serra À.: Tailor-made thermosets obtained by sequential dual-curing combining isocyanate-thiol and epoxy-thiol *click* reactions. Polymer, **174**, 200–209 (2019).
https://doi.org/10.1016/j.polymer.2019.04.041

[29] Green W. A.: Industrial photoiniciators. A technical guide. CRC Press, Florida (2010).

[30] Navaruckiene A., Skliutas E., Kasetaite S., Rekštytė S., Raudoniene V., Bridziuviene D., Malinauskas M., Ostrauskaite J.: Vanillin acrylate-based resins for optical 3D printing. Polymers, **12**, 397 (2020).
https://doi.org/10.3390/polym12020397

[31] Bagheri A., Jin J.: Photopolymerization in 3D printing. ACS Applied Polymer Materials, **1**, 593–611 (2019).
https://doi.org/10.1021/acsapm.8b00165

[32] Gurr M., Mülhaupt R.: Rapid prototyping. in 'Polymer science: A comprehensive reference' (eds.: Matyjaszewski K., Möller M.) Elsevier, Edinburgh, 77–99 (2012).

[33] Mezger T. G.: The rheology handbook. Vincentz Network, Hanover (2011).

[34] Konuray O., Fernández-Francos X., Ramis X., Serra À.: State of the art in dual-curing acrylate systems. Polymers, **10**, 178 (2018).
https://doi.org/10.3390/polym10020178

[35] Nair D. P., Podgórski M., Chatani S., Gong T., Xi W., Fenoli C. R., Bowman C. N.: The thiol-Michael addition click reaction: A powerful and widely used tool in materials chemistry. Chemistry of Materials, **26**, 724–744 (2014).
https://doi.org/10.1021/cm402180t

[36] Candan Z., Gardner D. J., Shaler S. M.: Dynamic mechanical thermal analysis (DMTA) of cellulose nanofibril/nanoclay/pMDI nanocomposites. Composites Part B: Engineering, **90**, 126–132 (2016).
https://doi.org/10.1016/j.compositesb.2015.12.016

[37] Jian Y., He Y., Jiang T., Li C., Yang W., Nie J.: Volume shrinkage of UV-curable coating formulation investigated by real-time laser reflection method. Journal of Coatings Technology and Research, **10**, 231–237 (2013).
https://doi.org/10.1007/s11998-012-9446-2

[38] Simula A., Ballard N., Aguirre M., Leiza J. R., van Es S., Asua J. M.: Nitroxide mediated copolymerization of acrylates, methacrylates and styrene: The importance of side reactions in the polymerization of acrylates. European Polymer Journal, **110**, 319–329 (2019).
https://doi.org/10.1016/j.eurpolymj.2018.11.041

[39] Shortall A. C.: How light source and product shade influence cure depth for a contemporary composite. Journal of Oral Rehabilitation, **32**, 906–911 (2005).
https://doi.org/10.1111/j.1365-2842.2005.01523.x

[40] Buruiana T., Melinte V., Stroea L., Buruiana E.: Urethane dimethacrylates with carboxylic groups as potential dental monomers. Synthesis and properties. Polymer Journal, **41**, 978–987 (2009).
https://doi.org/10.1295/polymj.PJ2009131

[41] Meereis C. T. W., Leal F. B., Lima G. S., de Carvalho R. V., Piva E., Ogliari F. A.: BAPO as an alternative photoinitiator for the radical polymerization of dental resins. Dental Materials, **30**, 945–953 (2014).
https://doi.org/10.1016/j.dental.2014.05.020

[42] Popescu I., Turtoi M., Suflet D. M., Dinu M. V., Darie-Nita R. N., Anghelache M., Calin M., Constantin M.: Alginate/poloxamer hydrogel obtained by thiol-acrylate photopolymerization for the alleviation of the inflammatory response of human keratinocytes. International Journal of Biological Macromolecules, **180**, 418–431 (2021).
https://doi.org/10.1016/j.ijbiomac.2021.03.082

[43] Saalwächter K., Chassé W., Sommer J-U.: Structure and swelling of polymer networks: Insights from NMR. Soft Matter, **29**, 6587–6593 (2013).
https://doi.org/10.1039/C3SM50194A

[44] Subraman R., Izquierdo-Alvarez A., Bhattacharya P., Meerts M., Moldenaers P., Ramon H., van Oosterwyck H.: The influence of swelling on elastic properties of polyacrylamide hydrogels. Frontiers in Materials, **7**, 212 (2020).
https://doi.org/10.3389/fmats.2020.00212

[45] Campo E. A.: Thermal properties of polymeric materials. in 'Selection of polymeric materials' (ed.: Campo E. A.) William Andrew, New York, 103–140 (2008).
https://doi.org/10.1016/B978-081551551-7.50005-X

[46] Xie R., Weisen A. R., Lee Y., Aplan M. A., Fenton A. M., Masucci A. E., Kempe F., Sommer M., Pester C. W., Colby R. H., Gomez E. D.: Glass transition temperature from the chemical structure of conjugated polymers. Nature Communications, **11**, 893 (2020).
https://doi.org/10.1038/s41467-020-14656-8

[47] Ebnesajjad S.: Introduction to plastics. in 'Chemical resistance of commodity thermoplastics' (eds.: Baur E., Ruhrberg K., Woishnis W.) William Andrew, New York, XIII–XXV (2016).
https://doi.org/10.1016/B978-0-323-47358-3.00017-X

[48] Shrivastava A.: Introduction to plastics engineering. in 'Introduction to plastics engineering' (ed.: Shrivastava A.) William Andrew, New York, 1–16 (2018).
https://doi.org/10.1016/B978-0-323-39500-7.00001-0

[49] Valdebenito A., Encinas M. V.: Effect of solvent on the free radical polymerization of *N,N*-dimethylacrylamide. Polymer International, **59**, 1246–1251 (2010).
https://doi.org/10.1002/pi.2856

[50] Lebedevaite M., Ostrauskaite J., Skliutas E., Malinauskas M.: Photoinitiator free resins composed of plant-derived monomers for the optical μ-3D printing of thermosets. Polymers, **11**, 116 (2019).
https://doi.org/10.3390/polym11010116

134

[51] Mukherjee A., Deepmala, Srivastava P., Sandhu J. K.: Application of smart materials in civil engineering: A review. Materials Today, in press (2021).
https://doi.org/10.1016/j.matpr.2021.03.304

[52] Aguilar-Vega M.: Structure and mechanical properties of polymers. in 'Handbook of polymer synthesis, characterization, and processing' (eds.: Saldívar-Guerra E., Vivaldo-Lima E.) Wiley, New Jersey, 425–434 (2013).
https://doi.org/10.1002/9781118480793.ch21

[53] Lebedevaite M., Talacka V., Ostrauskaite J.: High biorenewable content acrylate photocurable resins for DLP 3D printing. Journal of Applied Polymer Science, **138**, 50233 (2020).
https://doi.org/10.1002/app.50233

[54] Patel C., Bassin J. P., Scott M., Flye J., Hunter A. P., Martin L., Goyal M.: Synthesis and antimicrobial activity of 1,2-benzothiazine derivatives. Molecules, **21**, 861 (2016).
https://doi.org/10.3390/molecules21070861

[55] Sanchez-Maldonado A. F., Schieber A., Gänzle M. G.: Structure–function relationships of the antibacterial activity of phenolic acids and their metabolism by lactic acid bacteria. Journal of Applied Microbiology, **111**, 1176–1184 (2011).
https://doi.org/10.1111/j.1365-2672.2011.05141.x

[56] Tweedy B. G.: Inorganic sulfur as a fungicide. in 'Residue reviews' (eds.: Gunther F. A., Gunther J. D.) Springer, New York, Vol. 78, 43–64 (1981).
https://doi.org/10.1007/978-1-4612-5910-7_3

[57] Shakhatreh M. A., Al-Smadi M. L., Khabour O. F., Shuaibu F. A., Hussein E. I., Alzoubi K. H.: Study of the antibacterial and antifungal activities of synthetic benzyl bromides, ketones, and corresponding chalcone derivatives. Drug Design, Development and Therapy, **10**, 3653–3660 (2016).
https://doi.org/10.2147/DDDT.S116312

135

Article

Thermo-Responsive Shape Memory Vanillin-Based Photopolymers for Microtransfer Molding

Justinas Jaras [1], Aukse Navaruckiene [1], Edvinas Skliutas [2], Jurga Jersovaite [2], Mangirdas Malinauskas [2] and Jolita Ostrauskaite [1,*]

[1] Department of Polymer Chemistry and Technology, Kaunas University of Technology, Radvilenu Rd. 19, LT-50254 Kaunas, Lithuania; justinas.jaras@ktu.edu (J.J.); aukse.navaruckiene@ktu.lt (A.N.)

[2] Laser Research Center, Faculty of Physics, Vilnius University, Sauletekis Ave. 10, LT-10223 Vilnius, Lithuania; edvinas.skliutas@ff.stud.vu.lt (E.S.); jurga.jersovaite@ff.stud.vu.lt (J.J.); mangirdas.malinauskas@ff.vu.lt (M.M.)

* Correspondence: jolita.ostrauskaite@ktu.lt; Tel.: +370-37-300192

Abstract: Novel thermo-responsive shape-memory vanillin-based photopolymers have been developed for microtransfer molding. Different mixtures of vanillin dimethacrylate with tridecyl methacrylate and 1,3-benzenedithiol have been tested as photocurable resins. The combination of the different reaction mechanisms, thiol-acrylate photopolymerization, and acrylate homopolymerization, that were tuned by changing the ratio of monomers, resulted in a wide range of the thermal and mechanical properties of the photopolymers obtained. All polymers demonstrated great shape-memory properties and were able to return to their primary shape after the temperature programming and maintain their temporary shape. The selected compositions weretested by the microtransfer molding technique and showed promising results. The developed thermo-responsive shape-memory bio-based photopolymers have great potential for forming microtransfered structures and devices applicable on non-flat surfaces.

Keywords: bio-based polymers; dual curing; shape-memory; photocuring; microtransfer molding

1. Introduction

Increased oil prices and environmental awareness have prompted the scientific community to seek alternative feedstocks for polymers, which nowadays are mainly derived from fossil fuels [1,2]. The main source of sustainable and environmentally friendly polymers are renewable raw materials, such as plants [3]. Currently, vanillin is one of a few bio-based and aromatic compounds that are industrially available [4]. Its derivatives have been successfully used in various polymerization techniques. For example, vanillin acrylate-based polymers, synthesized by thermal polymerization, possess high glass transition temperature and high mechanical strength [5]. Recently, vanillin-based polymers, synthesized by photopolymerization, demonstrated significant antimicrobial activity and were applied in optical 3D printing [6]. However, there are only a few examples of the usage of vanillin derivatives in dual curing systems [7].

Dual curing is a process that combines two curing reactions that occur simultaneously or sequentially [8]. In this process, the properties of the resulting materials can be easily changed by manipulating the composition of the resins by changing the ratio of the selected monomers [9]. Polymers with unique mechanical and thermal properties can be obtained during the dual curing process as the result of interpenetrating, or semi-interpenetrating, polymer networks [10]. Due to these extraordinary features, dual curing attracts huge attention among scientists as one of the possible ways to create smart materials, such as shape-memory polymers [11].

Shape-memory polymers are a part of intelligent polymeric systems, also known as smart materials [12]. Their unique property of changing their shape in response to

a stimulus has significantly broadened their areas of application [13]. Bio-based shape-memory polymers attract huge interest in the scientific community, however, only a few examples of UV photocured shape-memory polymers are available [14]. Recently, novel shape-memory bio-based polymers have been successfully synthesized from castor oil with the introduction of dynamic pyrazole–urea bonds [15]. Bovine serum albumin-based shape-memory bioplastics have been produced and adapted for stereolithography [16]. Cholesterol was successfully used in the synthesis of thermo-responsive shape-memory polymers [17]. The novel poly(cholesteryl methacrylate) coatings were characterized as potential substrates for tissue engineering, showing the importance of shape-memory polymers [18]. In this work, we focused our attention on the development of novel bio-based shape-memory photopolymers suitable for the manufacturing of various structures and devices by nanoimprint lithography.

Photocuring requires a smaller amount of resources to produce the required part compared to other techniques [19]. It is a simple way to create unique products of complex shapes while also reducing manufacturing costs and carbon dioxide emission [20]. The final product can be successfully manufactured during the molding process and does not need further modification before usage [21]. Moreover, even the most complex parts can be duplicated easily if the original part was damaged during the operation process [22]. Microtransfer molding, or nanoimprint lithography, is a great way to reduce waste as it uses a minimal amount of material needed for the final product [23], and it is a versatile technique for nanofabrication of a wide range of micro and nanostructures and devices [24]. It offers the ability to fabricate nanostructures that exhibit vertically aligned nanoarrays and nanopatterns, and the ability to have precise control over the size and geometry of the nanostructures, and to form nanostructures attached to a bulk support. The main advantage of this technique is its fast, easy, and inexpensive, but accurate, reproduction of various 2D or 3D objects from the nanoscale to the macroscale [25,26].

In this work, different mixtures of bio-based monomer vanillin dimethacrylate with tridecyl methacrylate and 1,3-benzenedithiol, have been tested to find an efficient photocurable system for microtransfer molding. Ethyl (2,4,6-trimethylbenzoyl) phenylphosphinate was selected as the photoinitiator, due to its ability to cure the deep layers of the resin and its photobleaching effect [27]. This work is a continuation of our previous studies [7,28]. In the present work, the addition of tridecyl methacrylate to the resin composition has led to a reduction in the use of expensive vanillin monomer and, thus, to a reduction in the cost of the polymers, without sacrificing their properties. The polymers obtained demonstrated a wide range of thermal and mechanical properties as a result of the combination of the different reaction mechanisms, thiol-acrylate photopolymerization and acrylate homopolymerization, which were tuned by changing the ratio of monomers. The increase in tridecyl methacrylate content resulted in less rigid polymers, lower photocuring rate, and lower Young's modulus values. The reduction of thiol content increased the shrinkage of polymers, the photocuring rate, and the thermal and mechanical characteristics of the resulting polymers. All polymers demonstrated shape-memory properties. The most promising compositions have been tested by the microtransfer molding technique and showed promising results as photoresins for nanoimprint lithography. Microtransfered structures and devices formed from the developed thermo-responsive shape-memory bio-based photopolymers can be applied on non-flat surfaces, convex or concave, such as cylinders, tubes, etc.

2. Materials and Methods

2.1. Materials

Vanillin dimethacrylate (VDM, Specific Polymers, Castries, France), 1,3-benzenedithiol (BDT, Fluorochem, Glossop, United Kingdom), tridecyl methacrylate (C13-MA, VISIOMER® Terra C13-MA, Evonik, Essen, Deutschland), ethyl(2,4,6 trimethylbenzoyl)phenylphosphinate (TPOL, Fluorochem, Glossop, United Kingdom), (Figure 1) were used as received.
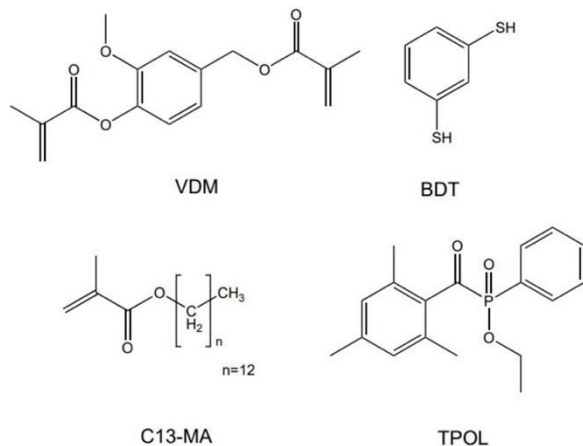
Figure 1. Chemical structures of vanillin dimethacrylate (VDM), 1,3-benzenedithiol (BDT), tridecyl methacrylate (C13-MA), and ethyl(2,4,6-trimethylbenzoyl)phenylphosphinate (TPOL).

2.2. Preparation of Cross-Linked Polymer Specimens

The mixtures containing 1 mol of VDM, 3 mol.% of TPOL, 1, 0.75, 0.5, or 0.25 mol of BDT and 1.5, 3, or 4.5 mol of C13-MA were stirred with a magnetic stirrer at room temperature (25 °C) for 1 min. When homogeneous mixtures were obtained, the resins were poured into a Teflon mold and cured for 5–7 min in the UV irradiation chamber BS-02 (Opsytec Dr. Grobel, Ettlinger, Germany) with an intensity of 30 mW/cm^2 and a wavelength range of 280–400 nm. The composition of the resins is presented in Table 1.

Table 1. Composition of resins **C1–C12**.

Resin	Amount of VDM, Mol	Amount of BDT, Mol	Amount of C13-MA, Mol	Amount of TPOL, Mol.%
C1	1	1	1.5	3
C2	1	0.75	1.5	3
C3	1	0.5	1.5	3
C4	1	0.25	1.5	3
C5	1	1	3	3
C6	1	0.75	3	3
C7	1	0.5	3	3
C8	1	0.25	3	3
C9	1	1	4.5	3
C10	1	0.75	4.5	3
C11	1	0.5	4.5	3
C12	1	0.25	4.5	3

2.3. Characterization Techniques

Fourier transformation infrared (FT-IR) spectroscopy spectra were recorded using a Spectrum BX II FT-IR spectrometer (Perkin Elmer, Llantrisant, UK). Reflection was measured during the test. The range of wavenumbers was (650–4000) cm^{-1}.

The Soxhlet extraction was used to determine the yield of the insoluble fraction. 0.2 g polymer samples were extracted with acetone for 24 h. After 24 h, the insoluble fractions

were dried under vacuum until no weight changes were observed. The yield of insoluble fraction was calculated as the weight difference before and after extraction and drying.

Thermogravimetrical analysis (TGA) was performed on a TGA 4000 apparatus (Perkin Elmer, Llantrisant, UK). A heating rate of 20 °C/min was chosen in a nitrogen atmosphere (100 mL/min). The temperature range of (10−800) °C was used. Aluminium oxide pans were used.

Dynamical mechanical thermal analysis (DMTA) was performed on an MCR302 rheometer (Anton Paar, Graz, Austria) equipped with the SRF10-SN30777 measuring system. The Peltier-controlled temperature chamber was used. The temperature was increased from −80 °C to 100 °C, with a heating rate of 2.99 °C/min. The normal force was set at −0.1 N during the measurement. In all cases, the torsion mode was used with a frequency of 1 Hz and a torsion strain of 0.1%. The storage modulus (G'), the loss modulus (G''), and the loss factor (tanδ) were recorded as functions of temperature.

The mechanical properties of the synthesized polymers were determined by the tensile test. The tensile test was performed on a Testometric M500-50CT testing machine (Testometric Co. Ltd., Rochdale, UK) with flat-faced grips at room temperature (21.5 °C). The dimensions of the test specimens were 70 ($\pm$0.01) $\times$ 10 ($\pm$0.01) $\times$ 2 ($\pm$0.15) mm. The gap between the grips was set to 20 mm and the test was performed at a speed of 5 mm/min until the specimen broke. Young's modulus, tensile strength, and elongation at break were determined.

2.4. Real-Time Photorheometry

UV/Vis curing tests were performed with resins containing 1 mol of vanillin dimethacrylate, 3 mol.% of TPOL, 1, 0.75, 0.5, or 0.25 mol of BDT and 1.5, 3.0, or 4.5 mol of C13-MA on a MCR302 rheometer (Anton Paar, Graz, Austria) equipped with the plate/plate measuring system. The measuring gap was set to 0.1 mm and the samples were irradiated by UV/Vis light in a wavelength range of 250–450 nm through the glass plate using the OmniCure S2000 UV/Vis spot curing system (Lumen Dynamics Group Inc., Mississauga, ON, Canada). The temperature was 25 °C. The shear mode with a frequency of 10 Hz and a shear strain of 1% was used in all cases. The storage modulus (G'), the loss modulus (G'') and the complex viscosity (η^*) were recorded as a function of the irradiation time and the values of each parameter taken after 300 s of photocuring are presented in Table 2. The gel point (t_{gel}) was calculated as the intersection point of the G' and G'' curves. The shrinkage was calculated from the reduction of the height of the sample during the polymerization process. The normal force was set at 0 N during the measurement of the sample shrinkage. Five measurements of each resin were used to obtain the mean value and standard deviation.

Table 2. Rheological Characteristics of Resins.

Resin	Storage Modulus, G', MPa	Loss Modulus, G'', MPa	Loss Factor, tanδ	Complex Viscosity η^*, MPa·s	Gel Point t_{gel}, s	Induction Period, s	Shrinkage, %
C1	0.312	0.128	0.409	0.054	8.9	4.9	2
C2	3.030	2.061	0.680	0.635	6.8	2.6	7
C3	14.173	5.872	0.414	2.440	4.6	0.7	8
C4	17.343	5.661	0.327	2.900	3.4	0.3	9
C5	0.031	0.020	0.646	0.005	13.5	9.2	0
C6	0.721	0.333	0.461	0.013	10.6	7.3	2
C7	2.420	1.290	0.534	0.437	5.8	5.1	3
C8	10.148	4.470	0.442	1.760	3.7	0.9	4
C9	0.055	0.018	0.328	0.009	20.8	12.3	1
C10	0.542	0.230	0.425	0.094	14.4	11.9	3
C11	2.002	1.010	0.502	0.357	13.6	11.6	6
C12	2.930	1.450	0.497	0.520	9.8	8.8	10

2.5. Microtransfer Molding Technique

A microtransfer molding (µTM) technique, or nanoimprint lithography, was used to test **C1** and **C8** resins to make replicas [29]. First, a master structure was manufactured out of PlasGray material with the Asiga Pico2 39 UV table-top 3D printer (Asiga, Alexandria, Australia). Next, polydimethylsiloxane (PDMS) was poured over this structure and thermally cured at 100 C for 1 h, thus creating a soft mold (stamp). It was then used to make a replica of both resins. The printed structure was a 1951 USAF resolution target (25% of the downloaded vector file size), used as a sample in optical engineering for testing imaging systems. A UV diode emitting 365 nm wavelength light (CS2010, Thorlabs, Newton, NJ, USA) was used to cure the **C1** and **C8** resins and obtain the replicas. The curing time was set to 5 min for each sample. The soft mold and the replicas made were characterized using the Olympus IX73 optical microscope (Olympus Corporation, Tokyo, Japan).

3. Results

3.1. Monitoring of Photocuring Kinetics by Real-Time Photorheometry

The photocuring of the three-component resins was studied by real-time photorheometry. In this study, the most important parameters, the photocuring rate (characterized by t_{gel}, induction period and slope of the curves), rigidity (characterized by storage modulus G'), and shrinkage (described by volume loss during photopolymerization) have been monitored and examined [30]. The real-time photorheometry data of all resins are summarized in Table 2.

The dependence of the storage modulus G' on the irradiation time of all resins is presented in Figure 2. The storage modulus represents the stiffness and rigidity of the polymers that are the important parameters for the applications of the polymers. It was determined that the resin composition had a huge influence on the photocuring kinetics and on the properties of the resulting polymers. The most rigid polymer was **C4** prepared with the lowest amount of C13-MA and BDT. The highest amount of VDM in **C4** compared to other polymers caused the high rate of acrylate homopolymerization. After comparing polymer **C4** with **C8** and **C12**, it was determined that the rigidity of the polymers decreased with increasing volume of tridecyl methacrylate in the resins. The rigidity of the polymers was reduced from 17.343 (**C4**) to 2.930 (**C12**) MPa by increasing the content of C13-MA from 1.5 to 4.5 mol. The long carbon chain of tridecyl methacrylate was the reason for the formation of the soft and flexible polymer [31]. By increasing the amount of C13-MA, the amount of polymer to plasticize long flexible alkyl chains was increased, and, thus, the rigidity of the polymer was reduced, while the increase in the amount of VDM, having a relatively short and partially aromatic structure in comparison to C13-MA, resulted in higher rigidity of the polymers.

The amount of thiol also had a great impact on the polymer structure and, therefore, its characteristics. It was determined that the polymer rigidity was increased by reducing the amount of thiol in the composition. The high amount of thiol resulted in a higher rate of thiol-ene photopolymerization, which is a slower reaction in comparison to free radical polymerization. A high number of short polymer chains was formed as a result of competing free radical and thiol-ene photopolymerizations, and even increased with increasing amounts of thiol. However, according to the literature, thiols not only reduce the rigidity of polymers but also increase their flexibility due to the formation of flexible thioether linkages [7]. For example, the rigidity of polymers **C5**–**C8**, prepared with 3 mol of C13-MA, was increased from 0.031 (**C5**) to 10.148 (**C8**) MPa by decreasing the amount of thiol from 1 to 0.25 mol. This tendency was also visible in polymers **C1**–**C4** prepared with 1.5 mol of C13-MA, and polymers **C9**–**C12** prepared with 4.5 mol of C13-MA. It is important to note that different areas of application require different materials, and both, rigid and soft, materials are needed.
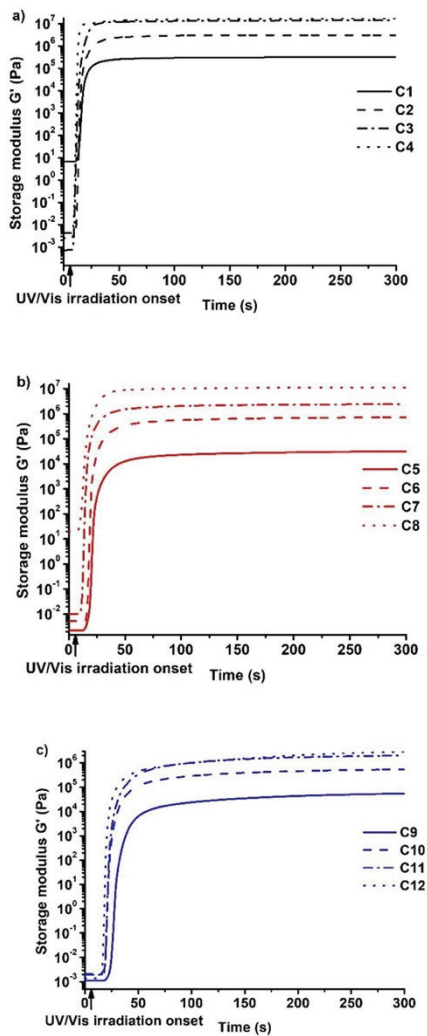
Figure 2. Dependency of storage modulus G′ of the resins **C1**–**C4** (**a**), **C5**–**C8** (**b**), and **C9**–**C12** (**c**) on the irradiation time.

The photocuring rate (described by the t_{gel}, induction period, and slope of the curve) is the other important parameter for the optimal curing process. The gel point is extremely important in microtransfer molding technology. The lowest values of t_{gel} and the shortest induction period were demonstrated by polymers prepared with the lowest amount of thiol. The curve of storage modulus of these polymers also reached the plateau faster than that of other vanillin-based polymers. As was stated earlier, free radical photopolymerization is a faster process in comparison to thiol-ene photopolymerization. However, not only the reaction mechanism, but also the structure of the monomer affects the gel point. C13-MA has a much longer structure compared to vanillin dimethacrylate and, as a result of that, the increase in C13-MA in compositions slowed the photopolymerization process, while the increase in VDM made it faster [28]. Subsequently, the lowest t_{gel} value was acquired by resin **C4** (t_{gel} = 3.4 s) prepared with 0.25 mol of thiol and 1.5 mol of tridecyl methacrylate. Resin **C12**, which was prepared with the same amount of thiol and a higher amount of C13-MA, had a much higher gel point (t_{gel} = 9.8 s) compared to resin **C4**, which was the result of an increased amount of flexible tridecyl methacrylate chains.

The shrinkage is also very important for the application of polymers. Low values of shrinkage are needed to form precise and unique structures, as high shrinkage could result in failed molding attempts. Values as low as 0–5% are mandatory in order to obtain high-quality products [32]. The lowest shrinkage values were demonstrated by polymers prepared with the highest amount of thiol. The shrinkage values of the polymers with 1 mol of thiol and different amounts of tridecyl methacrylate, **C1**, **C5**, and **C9**, were as low as 0–2%. However, resins with a lower amount of thiol and a higher amount of acrylate shrunk more. For example, the shrinkage increased from 1 to 10% as a result of the reduction of the amount of thiol from 1 to 0.25 mol in the resins **C9–C12**. This can be explained by the dominant reaction mechanism, as it is well known that acrylates have a high shrinkage rate during free radical polymerization [33], while thiol-ene photopolymerization results in a lower shrinkage volume [34]. That is because long-distance connections via weak Van der Waals force are replaced by short, strong covalent bonds between carbon atoms in monomer units during free radical acrylate polymerization, which results in shrinkage of the polymers [33].

After analyzing all of these results, the **C8** resin was selected as the most promising composition for the microtransfer molding technique. This composition demonstrated one of the lowest gel point values and relatively low shrinkage, which makes the process faster and allows the creation of complex and accurate shapes. Furthermore, the induction period of this resin was less than 1 s and the resultant polymer was a stiff material with a high value of G′. All these properties made the **C8** resin a suitable candidate for the microtransfer molding technique. For comparison, the resin **C1** that forms soft but non-brittle polymer was also selected for microtransfer molding.

3.2. Characterization of Photocross-Linked Polymer Structure

The chemical structure of the photocross-linked polymers was confirmed by FT-IR spectroscopy. Signals of C=O, which were present at 1714–1735 cm^{-1}, and those of the C=C group, which were present at 1606–1639 cm^{-1} in VDM and C13-MA spectra, were also reduced in polymer spectra. The signals of the S-H group, which were present at 2560 cm^{-1} in the BDT spectra, were not visible in the polymer spectra and the new signal of the C-S group was detected at 1120–1122 cm^{-1} in the polymer sample spectra. These changes in the polymer spectra indicated the formation of cross-linked structures in the polymers. As an example, the FT-IR spectra of VDM, C13-MA, BDT, and polymers **C5–C8** are presented in Figure 3.

The Soxhlet extraction was also performed in order to confirm the cross-linked structure of the polymers. The yield of the insoluble fraction of these polymers was in the range of 61–90% (Table 3). The high yield of the insoluble fraction indicated that the dense polymer network was formed during photopolymerization. However, polymers **C1**, **C5**, and **C9**, which were prepared with 1 mol of thiol, demonstrated a relatively low value of

the yield of the insoluble fraction (61–70%). This was probably due to the large amount of soluble linear or branched polymer fragments, which were formed as the result of spatial hindrances as the polymer chains were unable to pass through each other during the photo polymerization process [35]. Acrylate free radical homopolymerization is faster than thiol-ene photopolymerization, and, as a result of that, the spatial hindrances were increased by increasing the amount of thiol.
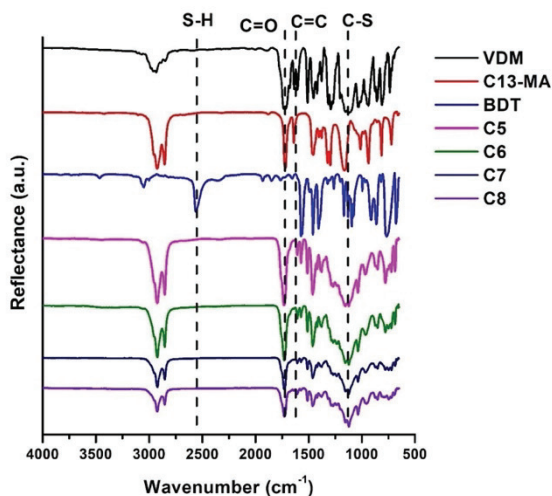

Figure 3. FT-IR spectra of VDM, C-13MA, BDT, and cross-linked polymers **C5–C8**.

Table 3. Yield of insoluble fraction, thermal, and thermomechanical characteristics of the polymers.

Resin	Yield of Insoluble Fraction, %	$T_{dec.-10\%}$, °C *	T_g, °C **	Storage Modulus G′ at −80 °C, MPa ***	Storage Modulus G′ at 100 °C, MPa ****
C1	69	308	−10	761.99	3.36
C2	84	328	10	1539.61	1.17
C3	87	329	28	1649.52	3.90
C4	90	332	54	2350.37	21.67
C5	61	328	−9	386.44	0.19
C6	82	338	0	499.35	0.88
C7	88	346	18	778.79	2.22
C8	85	344	28	902.59	4.84
C9	70	322	−7	19.08	0.58
C10	81	323	−1	911.49	3.15
C11	88	324	7	890.68	2.27
C12	79	331	17	661.37	2.69

* from TGA curves. ** from DMTA curves. *** before glass transition temperature. **** after glass transition temperature.

3.3. Thermal Properties of Cross-Linked Polymers

Dynamical mechanical thermal analysis (DMTA) and thermogravimetrical analysis (TGA) were used to study the thermal properties of the polymers. The results are summarized in Table 3. DMTA was used to determine the glass transition temperature (T_g) of the

polymer samples. The DMTA curves are presented in Figure 4. The glass transition of the polymers was in the range of −10–54 °C. It was determined that the higher values of T_g were obtained when the lower volume of thiol was used. For example, T_g increased from −10 °C for polymer **C1** to 54 °C for polymer **C4** by reducing the amount of BDT from 1 to 0.25 mol. The low glass transition temperature was the result of softer polymer with a less dense structure and low yield of the insoluble fraction [36]. The amount of C13-MA also had a great influence on T_g. For example, the increase in the amount of C13-MA from 1.5 mol in the polymer **C2** to 4.5 mol in the polymer **C10** reduced the T_g from 10 to −1 °C. This was the result of a long carbon chain of C13-MA. Long chains made the polymer softer and flexible, and decreased the glass transition temperature of the polymers [37].

The thermal decomposition of the polymers occurred in one step (Figure 5). The temperature of 10% weight loss ($T_{dec.−10\%}$) was in the range of 308–346 °C. Consequently, to the glass transition temperature, the temperature of 10% weight loss was reduced by increasing the amount of BDT in the polymer. For example, $T_{dec.−10\%}$ increased from 308 °C to 332 °C by decreasing the amount of thiol from 1 to 0.25 mol. The results were correlated with the yield of the insoluble fraction of the polymers, as higher decomposition temperatures were shown by the polymers with the higher yield of the insoluble fraction and the denser inner polymer network. Different results were observed when the amount of C13-MA was increased. There was no consistent increase or decrease in $T_{dec.−10\%}$ when the amount of tridecyl methacrylate increased. Very similar values of the temperature of 10% weight loss were observed when 1.5 and 4.5 mol of C13-MA were used. However, polymers prepared with 3 mol of C13-MA demonstrated higher values of 10% weight loss. For example, polymers **C4** and **C12**, which were prepared with 1.5 and 4.5 mol of C13-MA, reached the temperature of 332 °C and 331 °C, respectively, while polymer **C8**, prepared with 3 mol of C13-MA, reached the temperature of 344 °C.

3.4. Thermomechanical Properties of Cross-Linked Polymers

Dynamical mechanical thermal analysis (DMTA) was performed to characterize the mechanical properties of the developed polymers. The dependence of the storage modulus G′ on temperature was measured (Figure 6) and the values of G′ before and after the glass transition temperature were compared (Table 3). For the compatible results, the storage modulus values were taken from the plateau of the curve as the plateau indicates that polymer is in the steady state and that no changes in its structure are happening. The chosen temperatures were −80 °C (before T_g) and 100 °C (after T_g). After the results were compared, it was determined that the storage modulus of these polymers decreases greatly as the temperature increases to values higher than those of their T_g. Because of this, the developed polymers are rigid materials below their glass transition temperature and become soft and flexible when the temperature increases above their T_g. For example, the storage modulus of polymer **C1** was reduced from 761.99 MPa to 3.36 MPa when the temperature increased from −80 °C to 100 °C. These results correlate to the rheological and thermal characteristics, as the same tendencies occur when these polymers are compared. For example, polymers **C4**, **C8**, and **C12**, prepared with different amounts of C13-MA, show that the storage modulus reduces from 2350.37 MPa to 661.37 MPa (at −80 °C) when the amount of C13-MA increases from 1.5 mol to 4.5 mol, which was the result of an increased amount of flexible tridecyl methacrylate chains, as mentioned above. Increased amounts of BDT in the polymer also reduced the rigidity of the polymers. For example, rigidity was reduced from 902.59 MPa (polymer **C8** at −80 °C) to 386.44 MPa (polymer **C5** at −80 °C) by increasing the amount of thiol from 0.25 mol to 1 mol, due to the formation of flexible thioether linkages, as also mentioned earlier.
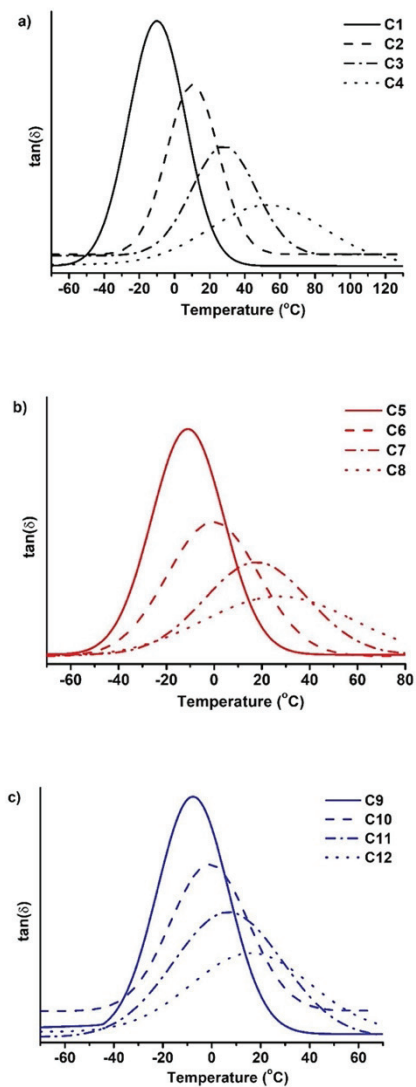
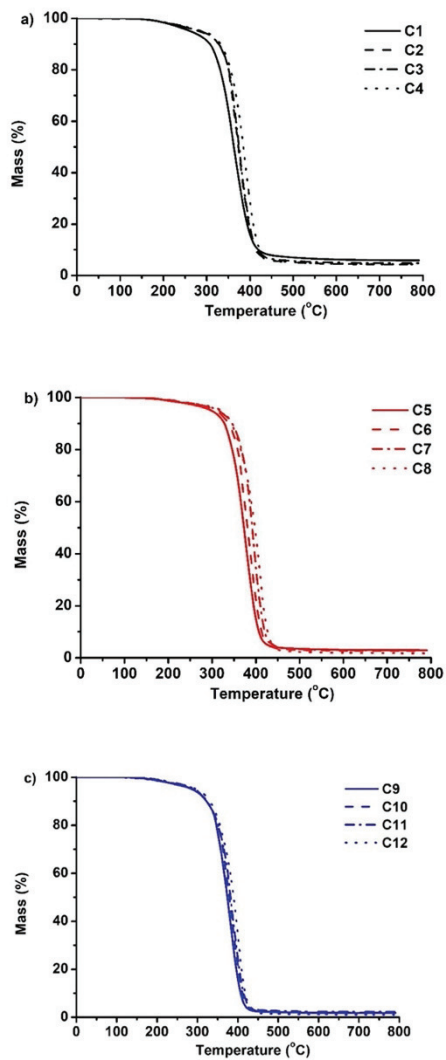**Figure 4.** DMTA thermograms of cross-linked polymers **C1–C4** (**a**), **C5–C8** (**b**), and **C9–C12** (**c**).

145

Figure 5. Thermogravimetric curves of cross-linked polymers **C1–C4** (**a**), **C5–C8** (**b**), and **C9–C12** (**c**).
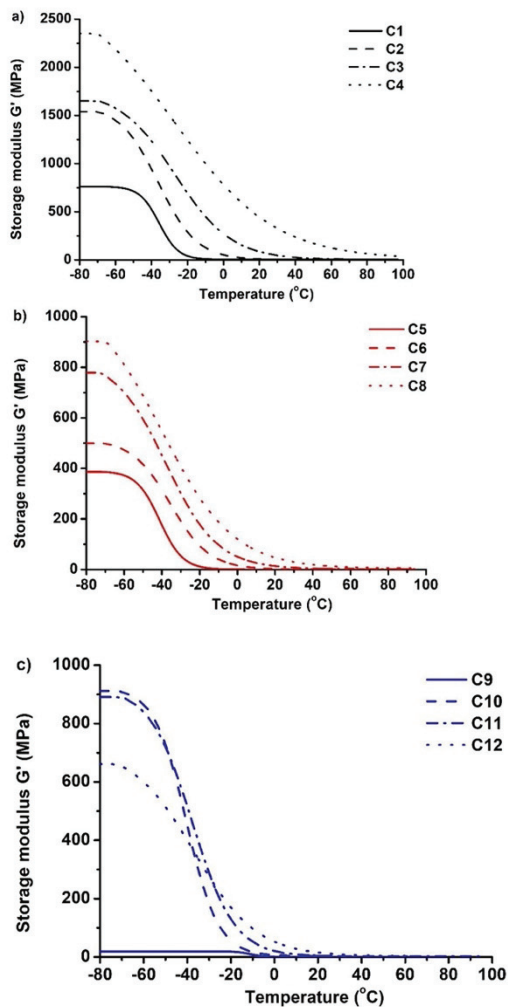
Figure 6. Dependency of the storage modulus G′ of polymers **C1–C4 (a)**, **C5–C8 (b)**, and **C9–C12 (c)** on temperature.

3.5. Shape-Memory Properties of Cross-Linked Polymers

Thermo-responsive shape-memory polymers attract huge interest in the scientific community because of their unique ability to remember their shape. To show shape-

147

memory properties, polymer samples were heated above their glass transition temperature, reformed to the temporary shape, and cooled down to the temperature lower than their T_g. All polymers were rigid materials and were able to maintain their temporary shape when the temperature was below their T_g. To return to a permanent shape, polymer samples were heated above their glass transition temperature, and all polymers were able to return to a permanent shape within seconds. The recovery to original shape conditions of these polymers is determined by their glass transition temperature [14].

Polymers were transformed to their temporary shape at 60 °C temperature and then placed in the refrigerator (-20 °C) to maintain their temporary shape. All developed polymers were able to maintain their permanent shape at a temperature below 0 °C, however, only a few of them were able to maintain it at room temperature (25 °C). Because of this, the application of these polymers is limited. The most promising results were demonstrated by the polymers **C3**, **C4**, and **C8**, because these polymers have relatively high glass transition temperature (from 28 to 54 °C) and can maintain their temporary shape at room temperature and above. The transformation of the **C8** sample is presented in Figure 7.
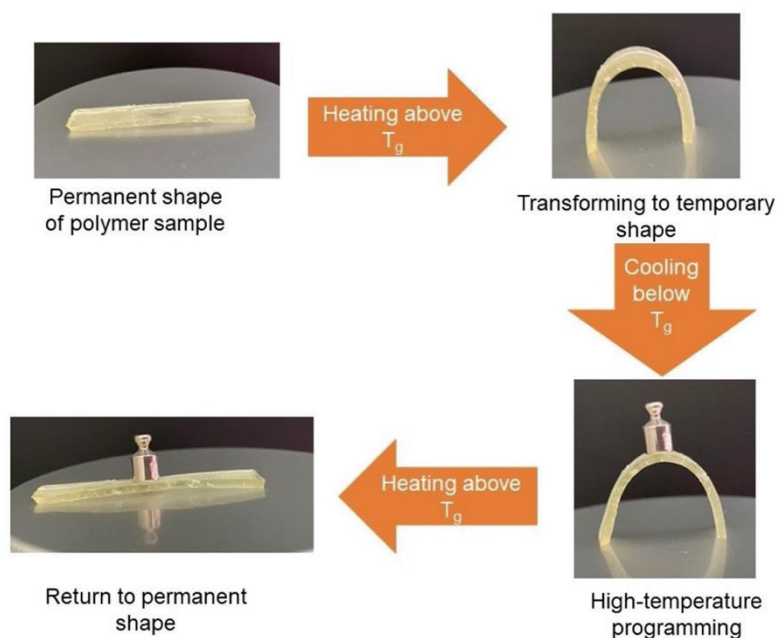
Figure 7. Scheme of shape-memory behaviour of polymer samples.

3.6. Mechanical Characteristics of Cross-Linked Polymers

The tensile test was performed to investigate the mechanical properties of the obtained polymers. The results are presented in Table 4. Polymers **C1**, **C2**, **C5**, and **C9** were too soft and/or brittle for testing machine, and it was impossible to detect the break during the measurement. The highest values of Young's modulus and the lowest values of elongation

and break were demonstrated by polymer **C4**, which was prepared with the lowest amount of C13-MA and BDT (60.05 MPa and 5.47%). Polymer **C3**, which was prepared with the same amount of VDM and C13MA as polymer **C4**, but with a higher amount of thiol, demonstrated a lower Young's modulus value and greater elongation at break value (12.44 MPa and 17.3%). This behaviour was caused by the highly flexible thioether linkages. These linkages also explain why polymers with higher amounts of thiol stretched more during the tensile test and their elongation at break value was higher. Tridecyl methacrylate had a similar effect as thiol on the mechanical properties of the polymers. The increased amount of C13-MA in the composition led to the lower values of Young's modulus. For example, by increasing the amount of C13-MA from 1.5 to 3 and then to 4.5 mol the Young's modulus decreased as follows, from 60.05 MPa (polymer **C4**) to 23.033 MPa (polymer **C8**) and, finally, to 5.53 MPa (polymer **C12**). The elongation at break increased with increasing C13-MA in the resin from 5.47% (polymer **C4**) to 6.49% (polymer **C8**) and, finally, to 8.38% (polymer **C12**). This behaviour can be explained by the long carbon chain of tridecyl methacrylate. As a result, the polymer can stretch more, and is softer and more flexible [34].

Table 4. Mechanical characteristics of the polymers obtained by the tensile test.

Resin	Young's Modulus, MPa	Tensile Strength, MPa	Elongation at Break, %
C1	- *	-	-
C2	-	-	-
C3	12.436	1.256	17.30
C4	60.050	1.976	5.47
C5	-	-	-
C6	1.865	0.140	12.19
C7	3.991	0.309	11.10
C8	23.033	0.960	6.49
C9	-	-	-
C10	2.317	0.040	22.36
C11	3.054	0.129	10.71
C12	5.531	0.227	8.38

*—not determined due to excessively soft and/or brittle polymer.

3.7. Characterization of Microtransfered Structures

Two photocurable resins forming nonbrittle polymers, one rigid (**C8**) and the other soft (**C1**), have been tested in microtransfer molding (μTM). The results are depicted in Figure 8. Image (a) demonstrates the 3D printed USAF target. The thickest 3D printed lines were approximately 220–230 μm width, meanwhile the thinnest lines were about 68–69 μm width. Image (b) shows the PDMS stamp, which coincided well with the 3D printed target. The following images (c) and (d) depict replicas made of **C1** and **C8** resins. In both cases, the replicas corresponded to the PDMS mold, keeping its shape and all features (lines, letters, and numbers). Only minor drawbacks were observed on the replicas, which were voids (usually appearing due to air bubbles while dropcasting the resin) and loss of sharp edges due to peeling of the stamp. Despite this, both **C1** and **C8** resins showed great potential to be used for the μTM technique.
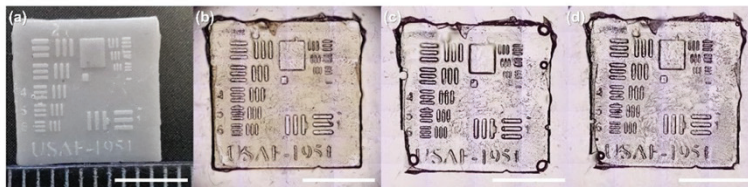
Figure 8. Results of μTM. (**a**) 3D printed 1951 USAF target (25% of the downloaded vector file size). (**b**) Soft PDMS mold. (**c**) and (**d**) are replicas made from **C1** and **C8** resins, respectively. Scale bars are the same in all the images and represent 5 mm.

4. Conclusions

Novel thermo-responsive shape-memory vanillin-based photopolymers have been developed and applied in microtransfer molding. Different mixtures of the two biobased monomers vanillin dimethacrylate and tridecylmethacrylate, to which 1,3-benzenedithiol has been added, have been tested as photocurable resins. The reduction of the thiol content was determined to increase the shrinkage of the polymers, the photocuring rate, and the values of the thermal and mechanical characteristics of the resulting polymers. The increase in tridecyl methacrylate content resulted in less rigid polymers, lower photocuring rate, and lower glass transition temperature. All polymers demonstrated great shape-memory properties and were able to return to their primary shape after the temperature programing. Furthermore, they were able to maintain their temporary shape when the temperature was lower than their glass transition temperature. Two photocurable resins forming nonbrittle polymers, one rigid and the other soft, have been tested in microtransfer molding and both resins demonstrated perfect replication, proving the novel bio-based photoresins to be suitable for microtransfer molding technique.

The developed thermo-responsive shape-memory bio-based photopolymers have great potential for forming microtransfered structures and devices that can be used on nonflat surfaces. This work offers a sustainable route for exploiting biorenewable materials to replace established commercial photoresins applied in stamping technologies that are already being scaled up for cost-effective everyday use.

References

1. Poulopoulou, N.; Kasmi, N.; Bikiaris, D.N.; Papageorgiou, D.G.; Floudas, G.; Papageorgiou, G.Z. Sustainable Polymers from Renewable Resources: Polymer Blends of Furan-Based Polyesters. *Macromol. Mater. Eng.* **2018**, *303*, 1800153. [CrossRef]
2. Schneiderman, D.K.; Hillmyer, M.A. 50th anniversary perspective: There is a great future in sustainable polymers. *Macromolecules* **2017**, *50*, 3733–3749. [CrossRef]
3. Zhu, Y.; Romain, C.; Williams, C.K. Sustainable polymers from renewable resources. *Nature* **2016**, *540*, 354–362. [CrossRef] [PubMed]
4. Fache, M.; Boutevin, B.; Caillol, S. Vanillin, a key-intermediate of biobased polymers. *Eur. Polym. J.* **2015**, *68*, 481–487. [CrossRef]
5. Zhang, C.; Yan, M.; Cochran, E.W.; Kessler, M.R. Biorenewable polymers based on acrylated epoxidized soybean oil and methacrylated vanillin. *Mater. Today Commun.* **2015**, *5*, 18–22. [CrossRef]
6. Navaruckiene, A.; Skliutas, E.; Kasetaite, S.; Rekštytė, S.; Raudoniene, V.; Bridziuviene, D.; Malinauskas, M.; Ostrauskaite, J. Vanillin Acrylate-Based Resins for Optical 3D Printing. *Polymers* **2020**, *12*, 397. [CrossRef]
7. Navaruckiene, A.; Bridziuviene, D.; Raudoniene, V.; Rainosalo, E.; Ostrauskaite, J. Vanillin acrylate-based thermo-responsive shape memory antimicrobial photopolymers. *Express Polym. Lett.* **2022**, *16*, 279–295. [CrossRef]
8. Roig, A.; Ramis, X.; de la Flor, S.; Serra, À. Dual-cured thermosets from glycydil methacrylate obtained by epoxy-amine reaction and methacrylate homopolymerization. *React. Funct. Polym.* **2021**, *159*, 1381–5148. [CrossRef]
9. Ramis, X.; Fernández-Francos, X.; de la Flor, S.; Ferrando, F.; Serra, À. Click-based dual-curing thermosets and their applications. In *Thermosets Structure, Properties, and Applications*, 2nd ed.; Guo, Q., Ed.; Elsevier: Amsterdam, The Netherlands, 2017; Chapter 16.
10. Konuray, O.; Fernández-Francos, X.; Ramis, X.; Serra, À. State of the Art in Dual-Curing Acrylate Systems. *Polymers* **2018**, *10*, 178. [CrossRef]
11. Gamardella, F.; Sabatini, V.; Ramis, X.; Serra, À. Tailor-made thermosets obtained by sequential dual-curing combining isocyanate-thiol and epoxy-thiol click reactions. *Polymer* **2019**, *174*, 200–209. [CrossRef]
12. Zhao, Q.; Qi, H.J.; Xie, T. Recent progress in shape memory polymer: New behavior, enabling materials, and mechanistic understanding. *Prog. Polym. Sci.* **2015**, *50*, 79–120. [CrossRef]
13. Zare, M.; Prabhakaran, M.P.; Parvin, N.; Ramakrishna, S. Thermally-induced two-way shape memory polymers: Mechanisms, structures, and applications. *Chem. Eng. J.* **2019**, *374*, 706–720. [CrossRef]
14. Hager, M.D.; Bode, S.; Weber, C.; Schubert, U.C. Shape memory polymers: Past, present and future developments. *Prog. Polym. Sci.* **2015**, *50*, 3–33. [CrossRef]
15. Zhang, J.; Zhang, C.; Shang, Q.; Hu, Y.; Song, F.; Jia, P.; Zhu, G.; Huang, J.; Liu, C.; Hu, L.; et al. Mechanically robust, healable, shape memory, and reprocessable biobased polymers based on dynamic pyrazole-urea bonds. *Eur. Polym. J.* **2022**, *169*, 111133. [CrossRef]
16. Sanchez-Rexach, E.; Smith, P.T.; Gomez-Lopez, A.; Fernandez, M.; Cortajarena, A.L.; Sardon, H.; Nelson, A. 3D-printed bioplastics with shape-memory behavior based on native bovine serum albumin. *ACS Appl. Mater. Interfaces* **2021**, *13*, 19193–19199. [CrossRef]
17. Stetsyshyn, Y.; Raczkowska, J.; Budkowski, A.; Awsiuk, K.; Kostruba, A.; Nastyshyn, S.; Harhay, K.; Lychkovskyy, E.; Ohar, H.; Nastishin, Y. Cholesterol-Based Grafted Polymer Brushes as Alignment Coating with Temperature-Tuned Anchoring for Nematic Liquid Crystals. *ACS Langmuir* **2016**, *32*, 11029–11038. [CrossRef]
18. Raczkowska, J.; Stetsyshyn, Y.; Awsiuk, K.; Lekka, M.; Marzec, M.; Harhay, K.; Ohar, H.; Ostapiv, D.; Sharan, M.; Yaremchuk, I.; et al. Temperature-responsive grafted polymer brushes obtained from renewable sources with potential application as substrates for tissue engineering. *Appl. Surf. Sci.* **2017**, *407*, 546–554. [CrossRef]
19. Javaid, M.; Haleem, A.; Singh, R.P.; Suman, R.; Rab, S. Role of additive manufacturing applications towards environmental sustainability. *Adv. Ind. Eng. Polym. Res.* **2021**, *4*, 312–322. [CrossRef]
20. Haleem, A.; Javaid, M. Additive manufacturing applications in industry 4.0: A review 04. *J. Ind. Integr. Manag.* **2019**, *4*, 1930001. [CrossRef]
21. Gu, W.; Styger, E.; Warner, D.H. Assessment of additive manufacturing for increasing sustainability and productivity of smallholder agriculture. *3D Print. Addit. Manuf.* **2020**, *7*, 300–310. [CrossRef]
22. Rejeski, D.; Zhao, F.; Huang, Y. Research needs and recommendations on environmental implications of additive manufacturing. *Addit. Manuf.* **2018**, *19*, 21–28. [CrossRef]
23. Colorado, H.A.; Velásquez, E.I.; Monteiro, S.N. Sustainability of additive manufacturing: The circular economy of materials and environmental perspectives. *J. Mater. Res. Technol.* **2020**, *9*, 8221–8234. [CrossRef]
24. Zhang, X.; Cox, L.; Wen, Z.; Xi, W.; Ding, Y.; Bowman, C.N. Implementation of two distinct wavelengths to induce multistage polymerization in shape memory materials and nanoimprint lithography. *Polymer* **2018**, *156*, 162–168. [CrossRef] [PubMed]
25. Xu, Z.Y.; Li, L.; Du, L.; Wang, L.; Shi, L.Y.; Yang, K.K.; Wang, Y.Z. Multiscale shape-memory effects in a dynamic polymer network for synchronous changes in color and shape. *Appl. Mater. Today* **2022**, *26*, 101276. [CrossRef]
26. Lan, X.; Huang, W.; Leng, J. Shape Memory Effect in Micro-Sized Shape Memory Polymer Composite Chains. *Appl. Sci.* **2019**, *9*, 2919. [CrossRef]
27. Green, W.A. *Industrial Photoiniciators, A Technical Guide*, 2nd ed.; CRC Press: Boca Raton, FL, USA, 2010.

151

28. Navaruckiene, A.; Bridziuviene, D.; Raudoniene, V.; Rainosalo, E.; Ostrauskaite, J. Influence of Vanillin Acrylate-Based Resin Composition on Resin Photocuring Kinetics and Antimicrobial Properties of the Resulting Polymers. *Materials* **2021**, *14*, 653. [CrossRef]

29. Danilevičius, P.; Rekšytė, S.; Balčiūnas, E.; Kraniauskas, A.; Širmenis, R.; Baltriukienė, D.; Bukelskienė, V.; Gadonas, R.; Sirvydis, V.; Piskarskas, A.; et al. Laser 3D micro/nanofabrication of polymers for tissue engineering applications. *Opt. Laser Technol.* **2013**, *45*, 518–524. [CrossRef]

30. Mezger, T.G. *The Rheology Handbook*, 3rd ed.; Vincentz Network: Hanover, Germany, 2011.

31. Buruiana, T.; Melinte, V.; Stroea, L.; Buruiana, E. Urethane Dimethacrylates with Carboxylic Groups as Potential Dental Monomers. Synthesis and Properties. *Polym. J.* **2009**, *41*, 978–987. [CrossRef]

32. Gurr, M.; Mülhaupt, R. Rapid prototyping. In *Polymer Science: A Comprehensive Reference*, 1st ed.; Matyjaszewski, K., Möller, M., Eds.; Elsevier: Edinburgh, UK, 2012; Volume 1, pp. 77–99.

33. Jian, Y.; He, Y.; Jiang, T.; Li, C.; Yang, W.; Nie, J. Volume shrinkage of UV-curable coating formulation investigated by real-time laser reflection method. *J. Coat. Technol. Res.* **2013**, *10*, 231–237. [CrossRef]

34. Albeshir, E.G.; Alsahafi, R.; Albluwi, R.; Balhaddad, A.A.; Mitwalli, H.; Oates, T.W.; Hack, G.D.; Sun, J.; Weir, M.D.; Xu, H.H.K. Low-Shrinkage Resin Matrices in Restorative Dentistry-Narrative Review. *Materials* **2022**, *15*, 2951. [CrossRef]

35. Imakaev, M.V.; Tchourine, K.M.; Nechaev, S.K.; Mirny, L.A. Effect of topological constraints on globular polymers. *Soft Matter* **2015**, *11*, 665–671. [CrossRef] [PubMed]

36. Xie, R.; Weisen, A.R.; Lee, Y.; Aplan, M.A.; Fenton, A.M.; Masucci, A.E.; Kempe, F.; Sommer, M.; Pester, C.W.; Colby, R.H.; et al. Glass transition temperature from the chemical structure of conjugated polymers. *Nat. Commun.* **2020**, *11*, 893. [CrossRef] [PubMed]

37. Shrivastava, A. Introduction to plastics engineering. In *Plastics Design Library, Introduction to Plastics Engineering*, 1st ed.; Shrivastava, A., Ed.; William Andrew Publishing: New York, NY, USA, 2018; Volume 1, pp. 1–16.

Article

Functionalized Soybean Oil- and Vanillin-Based Dual Cure Photopolymerizable System for Light-Based 3D Structuring

Vilte Sereikaite [1], Aukse Navaruckiene [1], Justinas Jaras [1], Edvinas Skliutas [2], Dimitra Ladika [3], David Gray [3], Mangirdas Malinauskas [2], Vaidas Talacka [4] and Jolita Ostrauskaite [1,*]

[1] Department of Polymer Chemistry and Technology, Kaunas University of Technology, Radvilenu Rd. 19, LT-50254 Kaunas, Lithuania
[2] Laser Research Center, Faculty of Physics, Vilnius University, Sauletekis Ave. 10, LT-10223 Vilnius, Lithuania
[3] Institute of Electronic Structure and Laser, Foundation for Research and Technology-Hellas, 70013 Heraklion, Greece
[4] AmeraLabs, Kęstučio Str. 6A, LT-44320 Kaunas, Lithuania
* Correspondence: jolita.ostrauskaite@ktu.lt; Tel.: +370-37-300192

Abstract: A novel dual cure photopolymerizable system was developed by combining two plant-derived acrylic monomers, acrylated epoxidized soybean oil and vanillin dimethacrylate, as well as the thiol monomer pentaerythritol tetrakis (3-mercaptopropionate). Carefully selected resin composition allowed the researchers to overcome earlier stability/premature polymerization problems and to obtain stable (up to six months at 4 °C) and selectively-polymerizable resin. The resin demonstrated rapid photocuring without an induction period and reached a rigidity of 317.66 MPa, which was more than 20 times higher than that of the other vanillin-based polymers. Improved mechanical properties and thermal stability of the resulting cross-linked photopolymer were obtained compared to similar homo- and copolymers: Young's modulus reached 4753 MPa, the compression modulus reached 1634 MPa, and the temperature of 10% weight loss was 373 °C. The developed photocurable system was successfully applied in stereolithography and characterized with femtosecond pulsed two-beam initiation threshold measurement for the first time. The polymerization threshold of the investigated polymer was determined to be controlled by the sample temperature, making the footprint of the workstations cheaper, faster, and more reliable.

Keywords: vanillin dimethacrylate; acrylated epoxidized soybean oil; photocross-linking; dual-curing; stereolithography; two-beam initiation threshold; multiphoton polymerization

1. Introduction

Considering recent challenges related to climate change and the state of the environment, it is particularly important to develop new materials that combine specific technical and optional smart properties with sustainability and applicability for high-tech manufacturing. Light-based 3D structuring is a unique contactless fabrication method that offers material processing precision, flexibility, and the rapid manufacturing of mechanical, medical, and optical components and devices [1]. Real-time synchronization of fast beam deflection and precise sample positioning can be implemented for state-of-the-art mesoscale ultrafast laser 3D structuring, namely, the production of submicrometer precision functional prototypes of practically-applicable millimeter scale dimensions [2]. This breakthrough technological advancement makes laser 3D printing suitable and appealing for both scientific research and industrial scale additive manufacturing. For such a technology, the replacement of petroleum-based materials by plant-derived materials would provide immediate ecological and long-term economic benefits.

Although the use of biorenewable polymers is increasing in various applications, the main challenge remains, to develop biobased polymer analogues with the same or better technical properties (reactivity, stability, durability, etc.) as petroleum-based polymers [3].

153

Plant oils and plant phenolics are great biorenewable sources of starting materials for polymer synthesis [4,5]. Acrylated epoxidized soybean oil (AESO) with a high number of functional groups is produced industrially and is widely used in foams, adhesives, coatings, and even in light-based 3D printing [6,7], including multiple scales and exposure sources [8]. However, the use of pure AESO leads to poor mechanical and thermal properties of the resulting products [9]. This issue can be solved by adding various comonomers with rigid structure to the resin composition [10]. In this study, vanillin dimethacrylate was chosen as a biobased comonomer because of its aromatic structure and high reactivity. Vanillin is one of the few biobased aromatic compounds that are industrially available [11]. Furthermore, vanillin-based polymers demonstrate good mechanical and thermal properties, as well as extraordinary antimicrobial activity similar to that of chitosan-based polymers [12,13]. In this study, the best features of both biobased monomers, AESO and vanillin dimethacrylate, were combined in the dual-curing photopolymerizable system. Although dual cure is a very promising technique for controlling the structure and properties of 3D-printed polymeric objects, there are only a few examples of the usage of AESO [14] or vanillin derivatives [15] in dual cure systems.

Dual cure is a technique that combines two simultaneous or sequential curing reactions of the same or a different energy source [16]. As a result, interpenetrating or semi-interpenetrating polymer networks with unique properties are formed [17]. Acrylic monomers are widely used in dual-curing systems [18] and the resulting polymers with numerous industrial applications, such as adhesives, coatings, and biomaterials, can be synthesized by carefully selecting the acrylate monomer [19]. The most common comonomers for acrylates are thiols. They react with acrylates in two different ways, the thiol-acrylate Michael addition and the radical-mediated thiol-acrylate reaction. Both mechanisms are appropriate for the formation of dual-curing systems [18].

In this study, radical-mediated thiol-acrylate photopolymerization and acrylate homopolymerization were used to compose a novel dual-curing system. Two different biobased monomers, acrylated epoxidized soybean oil and vanillin dimethacrylate, were used with pentaerythritol tetrakis(3-mercaptopropionate) for the first time. Diphenyl(2,4,6-trimethylbenzoyl) phosphine oxide was selected as the photoinitiator due to its photobleaching effect and its ability to cure deep layers of resin [20]. The developed photopolymerizable system was stable and well-suited for the light-based 3D structuring of complex shape objects with excellent mechanical properties and thermal stability. Furthermore, the order of effective nonlinear absorption (n_{eff}) in photoresists is a key element in the development of materials with improved sensitivity for additive manufacturing based on multiphoton absorption polymerization [21]. Z-can, intensity-scan, or a pump and probe technique can be used to determine the n_{eff}. However, it characterizes material properties rather than the order of undergoing the polymerization reaction process. Other indirect methods such as non-linear fluorescence excitation or thermal lensing can be implemented for this task; however, they do not measure the n_{eff} directly. Line-width [22] and exposure-time duration (ETM) [23] techniques allow for the determination of the n_{eff} from the polymerized structures; however, both suffer from the required additional steps such as sample posttreatment and scanning electron microscopy, which are time consuming for systematic measurements. The pros and cons of the aforementioned approaches are well-discussed in a review paper by N. Liaros and J. T. Fourkas [24]. A quick, reliable, and, most importantly, in situ method is highlighted as a two-beam initiation threshold (2-BIT) [25]. Also, the method includes normalization of the power of each beam to the polymerization threshold power to correct the differences in beam size, pulse length, or focal volume. While other scientific groups are looking for ways to simplify two-photon polymerization techniques via laser systems [26,27], light projection conditions [28], or photoinitiation agents [29,30], in this work, a method of using impact of dual cure is presented. The 2-BIT experiment was performed for the *in situ* measurement of nonlinear material excitation mechanisms and, in principle, validated its suitability for laser 3D nanolithography, while revealing important peculiarities of nontrivial material behaviour depending on sample handling conditions.

2. Materials and Methods

2.1. Materials

Acrylated epoxidized soybean oil (AESO, Fluorochem, Glossop, UK), vanillin dimethacrylate (VDM, Specific Polymers, Castries, France), pentaerythritol tetrakis(3-mercaptopropionate) (PETMP, Fluorochem, Glossop, UK), diphenyl(2,4,6-trimethylbenzoyl) phosphine oxide (TPO, Fluorochem, Glossop, UK), and 2,5-bis(5-tert-butyl-2-benzoxazolyl)thiophene (UVB, MPI Chemie, Houten, The Netherlands) (Figure 1) were used as received.
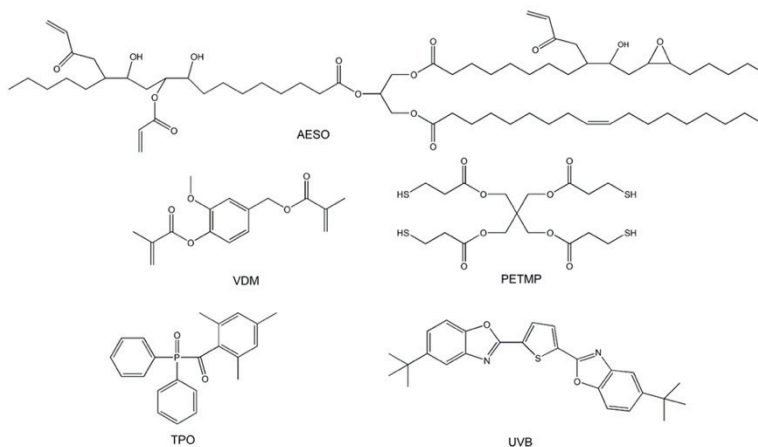
Figure 1. Chemical structures of acrylated epoxidized soybean oil (AESO), vanillin dimethacrylate (VDM), pentaerythritol tetrakis(3-mercaptopropionate) (PETMP), and diphenyl(2,4,6-trimethylbenzoyl) phosphine oxide (TPO).

2.2. Preparation of Cross-Linked Polymer Specimens

The mixture containing 3 mol of AESO, 1 mol of VDM, 0.25 mol of PETMP, 2.5 wt.% of TPO, and 0.08 wt.% of UVB was stirred with magnetic stirrer at room temperature (25 °C) for 5 min. When the homogeneous mixture was obtained, the resin was poured into a round Teflon mold and cured for 3–5 min in the UV irradiation chamber BS-02 (Opsytec Dr. Grobel, Ettlinger, Germany) with an intensity of 30 mW/cm^2 and a wavelength range of 280–400 nm. The VS code was assigned to this resin and polymer.

2.3. Characterization Techniques

Fourier transformation infrared (FT-IR) spectroscopy spectra were recorded using a Spectrum BX II FT-IR spectrometer (Perkin Elmer, Llantrisant, UK). Reflection was measured during the test. The wavenumber range was 650–4000 cm^{-1}.

The Soxhlet extraction was used to determine the yield of the insoluble fraction. A 0.2 g polymer sample was extracted with acetone for 24 h. The insoluble fraction was then dried under vacuum until no changes in weight were observed. The yield of the insoluble fraction was calculated as the weight difference before and after extraction and drying. Three samples of polymer were used to obtain the mean value and standard deviation.

The swelling value of the cross-linked polymer samples was obtained by measuring the mass of the samples swollen in acetone and toluene at room temperature (25 °C). The initial mass of the polymer sample was measured before placing it into the solvent. The

change in the mass of the sample was measured every 5 min until no change was obtained. The swelling value was calculated according to the following equation:

$$\alpha = \frac{M - M_0}{M_0} \cdot 100 \tag{1}$$

where α is the swelling value (%); M is the mass of the swollen sample (g); M_0 is the initial mass of the sample (g). Three samples of polymer were used to obtain the mean value and standard deviation.

Thermogravimetrical analysis (TGA) was performed on a TGA 4000 apparatus (Perkin Elmer, Llantrisant, UK). A heating rate of 20 °C/min under nitrogen atmosphere (100 mL/min) was chosen. The temperature range of 20–800 °C was used. Aluminium oxide pans were used.

Dynamical mechanical thermal analysis (DMTA) was performed on an MCR302 rheometer (Anton Paar, Graz, Austria). The Peltier-controlled temperature chamber was used. The temperature was increased from −20 °C to 100 °C with a heating rate of 2.0 °C/min. The normal force was set at 5 N during the measurement. In all cases, the shear mode was used with a frequency of 1 Hz and a shear strain of 0.1%. The storage modulus (G'), the loss modulus (G''), and the loss factor (tan δ) were recorded as a function of temperature. Three polymer samples were used to obtain the mean value and standard deviation.

The mechanical characteristics of the synthesized polymer were determined by the tensile and compression tests. Tensile test was performed on a Testometric M500-50CT testing machine (Testometric Co Ltd., Rochdale, UK) with flat-faced grips at room temperature (20 °C). Bone-shaped polymer specimens with a total length of 70 (±0.0) mm, a shoulder at each end (length of 15 (±0.0) mm, a width of 10 (±0.0) mm), and a gauge section width of 5 (±0.0) mm in between were used. Polymer specimens were printed using the stereolithography technique (SLA) (Section 2.6). The gap between the grips was set to 40 mm and the test was performed at a speed of 5 mm/min until the specimen broke. Young's modulus, tensile strength, and elongation at break were determined. Five polymer samples were used to obtain the mean value and standard deviation.

The compression test was performed on a Testometric M500-50CT testing machine (Testometric Co Ltd., Rochdale, UK) with HDGG100 grips at room temperature (25 °C). The dimensions of the round tablets used for the test were 15 (±0.10) × 3 (±0.30). The tablets were produced using a Teflon mold. The test was carried out at a speed of 5 mm/min until the sample broke. The compression modulus was determined. Five samples of polymer were used to obtain the mean value and standard deviation.

The biorenewable carbon (BRC) content was calculated according to the following equation:

$$BRC, \% = \frac{Bio\ Sourced\ Carbon}{Bio\ Sourced\ Carbon + Fossil\ Carbon} \cdot 100 \tag{2}$$

2.4. Real-Time Photorheometry

The UV/Vis cure tests of the resin were performed on an MCR302 rheometer (Anton Paar, Graz, Austria) equipped with the plate/plate measuring system. The Peltier-controlled temperature chamber with a glass plate (diameter 38 mm) and a PP15 top plate (diameter 15 mm) was used. The measurement gap was set to 0.1 mm and the samples were irradiated with UV/Vis light in a wavelength range of 250–450 nm through the glass plate using the OmniCure S2000 UV/Vis spot curing system (Lumen Dynamics Group Inc., Mississauga, ON, Canada). The shear mode was used with a frequency of 10 Hz and a shear strain of 1%. The storage modulus (G'), the loss modulus (G''), and the complex viscosity (η*) were recorded as a function of the irradiation time. The gel point (t_gel) was calculated as an intersection point of the G' and G'' curves. The induction period was measured as the beginning of the increase in G'. The shrinkage was calculated from the reduction in the height of the sample during the photocuring process. The normal force

was set to 0 N during the measurement of the sample shrinkage. Five measurements of each resin were used to obtain the mean value and standard deviation.

The crosslinking density was calculated according to the theory of rubber elasticity using the following equation:

$$G' = \nu RT \tag{3}$$

where ν is the cross-linking density (mol/m^3); G' is the steady-state value of the storage modulus taken from the real-time photorheometry curve after 600 s (Pa); R is the universal gas constant (8.314 J/mol K); T is the temperature (K) [31]. The experiment was carried out three times to obtain the mean value and standard deviation.

2.5. Two-Beam Initiation Threshold Experiment

The 2-BIT experiment allows in situ measurement of non-linear material excitation mechanisms during laser direct writing (LDW) [25]. The 2-BIT experiment was implemented using a Femto second Fiber Laser (FemtoFiber pro NIR, Toptica Photonics AG emitting at 780 nm with pulse duration 150 fs, average output power 500 mW, and repetition rate 80 MHz) (TOPTICA Photonics AG, Munich, Germany). An exact experimental setup of 2-BIT was presented previously [32]. The synthesized polymer was placed between two microscope coverslips (REF VBS638, Biosigma, Cona VE, Italy) separated with a double layer of polyimide film tape. The sample was fixed on piezoelectricstages Nanocube P-611.3S (Physik Instrumente, Karlsruhe, Germany). The 3DPoli software, version 6.22, (Femtika, Vilnius, Lithuania) was used to manage sample positioning. The stages were programmed to make back-forward movements of 75 µm length at a constant velocity of 20 µm/s. The combined laser beams were focused to the sample using the Zeiss Plan-Apochromat oil-immersion, 100×/N.A. = 1.4 objective lens (Carl Zeiss AG, Oberkochen, Germany). At first, the average power P (mW) of each beam individually was recorded when the presence of the polymerized features was observed via live imaging and determined as the polymerization threshold for a single beam (P_{single}). Then, two beams were combined and, while manually controlling the attenuation of both beams with half-waveplates, new polymerization thresholds were recorded (P_{2beam}). A graph of normalized polymerization thresholds (P_{2beam}/P_{single}) was obtained.

2.6. SLA 3D Printing

The SLA 3D printer Phrozen Sonic Mini 4K with a 405 nm LED source was used for polymer sample printing. The printing volume was 134 × 75 × 130 mm, the XY resolution was 35 µm, the layer thickness was 50 µm, and the exposure time was 12 s. After printing, the polymer samples were washed with isopropyl alcohol for 20 min and post-cured under an LED lamp (395 nm, 80 W).

3. Results and Discussion

3.1. Selection of Resin Composition

A complex composition of the photocurable resin was made in order to obtain a stable and highly biorenewable carbon content resin suitable for SLA 3D printing of mechanically strong and stiff, but not brittle, polymer objects. The selection of resin components was based on the known features of the compounds and the results of our previous research on this topic. AESO was selected as the main component of the resin due to its biobased origin, the high number of functional groups, the photocuring rate suitable for light-based 3D printing, and the formation of stiff polymer [33]. However, the pure AESO polymer is known to be brittle [9]. VDM was chosen as a biobased aromatic comonomer that improves the mechanical characteristics of the pure AESO polymer [34]. Although pure VDM is not well-suited for SLA 3D printing due to its too-rapid curing and poor stability of the resin during storage [35], in the present study, the aforementioned disadvantages of VDM were not expressed, probably due to its low content in the resin. PETMP, which has four functional groups capable of forming flexible thioether linkages, was added to the mixture of AESO and VDM because it can not only provide flexibility to the rigid polymer network,

but also define the shape memory properties of the resulting polymers [36]. The lower-than-stoichiometric amount of thiol groups and acrylic groups allowed for the domination of radical homopolymerization of acrylates and thus obtaining more rigid and mechanically stronger polymers [15]. The flexible aliphatic chains of AESO and PETMP lowered the glass transition temperature of the polymer, while the benzene rings present in VDM and the high amount of AESO functional groups, responsible for the high crosslinking density, led to the high thermal stability of the polymer. Also, the mechanical strength of the polymer is determined by high cross-linking density and aromatic structural fragments. The influence of the amount of each component on some values of the polymer parameters is summarized in Figure 2. Therefore, taking into account all known features of the components, the photocurable resin VS was composed of 3 mol of AESO, 1 mol of VDM, and 0.25 mol of PETMP (acrylic:thiol groups ratio: 2:1), including 2.5 wt.% of the photoinitiator TPO. The resin of such a composition was stable and did not cure during storage for at least six months at a temperature of 4 °C. The calculated biorenewable carbon content of the polymer VS was 76.45%.
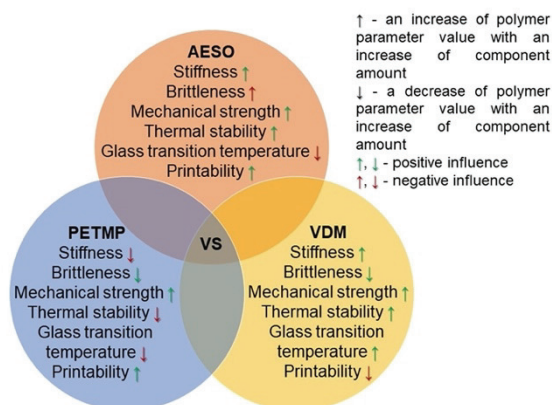
Figure 2. Scheme of the influence of component amounts on some parameters of the polymer VS.

3.2. Monitoring of Photocuring Kinetics by Real-Time Photorheometry

The photocuring kinetics of the resin VS was studied by real-time photorheometry. This method was chosen to determine the photocuring rate, the rigidity of the resulting polymer, and also the shrinkage of the sample during photocuring, which are the main factors for the successf of the optical 3D printing process. Figure 3 shows the evolution of the storage modulus G′, loss modulus G″, loss factor tan δ, and complex viscosity η* of the resin VS during UV/Vis irradiation. The cross-linking process began when the values of G′, G″, and η* started to increase. The gel point (t_{gel}) (defined as G′ = G″) [37] of the resin was reached after 1.5 s from the onset of UV/Vis irradiation. No induction period was obtained, as the values of G′ and G″ started to increase at the same time as UV irradiation started. As the resin irradiation continued, the values of G′, G″, and η* were increasing due to gel aging and then settled into steady state, indicating the end of the cross-linking process. The irradiation was maintained for 600 s. The storage modulus value, which indicates the rigidity of the resulted polymer, reached 317.66 MPa and was more than 20 times higher than those of the other vanillin dimethacrylate- and thiol-based polymers [15]. The shrinkage during photocuring was relatively low and reached 5.5%, which is very important in optical 3D printing technology to produce right-sized objects [38]. Overall,

the rheological characteristics make the resin VS a very promising candidate for light-based 3D structuring due to low shrinkage, very high rigidity, and almost instantaneous curing after the start of UV irradiation.
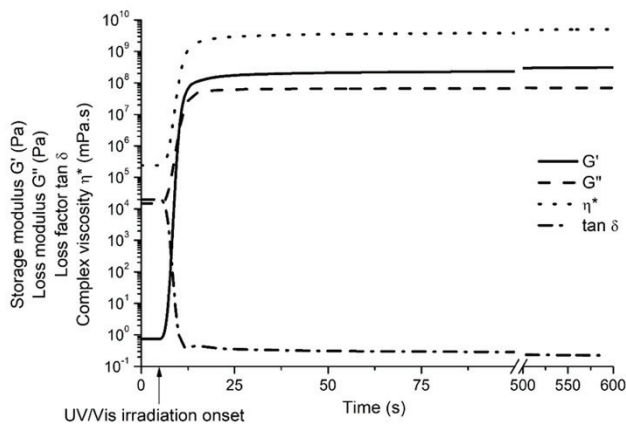
Figure 3. Dependencies of the rheological characteristics of the resin VS on the irradiation time.

3.3. Characterization of the Photocross-Linked Polymer Structure

The chemical structure of the polymer VS was identified by FT-IR spectroscopy. The signals of the C = C group which were present at 1605 cm^{-1} in the FT-IR spectra of AESO and VDM were reduced in their polymer spectra. The signal of the S-H group that was present at 2569 cm^{-1} in the PEMPT spectrum completely disappeared in the polymer VS spectrum, indicating that all S-H groups were consumed in the formation of a polymer network. The FT-IR spectra of AESO, PETMP, VDM, and the cross-linked polymer VS are presented in Figure S1.

The Soxhlet extraction was performed, and the crosslinking density was calculated to confirm the crosslinked structure of the polymer. The polymer VS showed a high yield of insoluble fraction (95%) and a high crosslinking density (127,825 $\pm$ 206 mol/m^3), which confirmed that all monomers participated in the formation of the cross-linked structure. The high crosslinking density resulted in low swelling values of the polymer, which were in the range of 8–10% in two solvents of different polarity (Figure 4). The swelling value in toluene was slightly higher than that in acetone. The reason for this is the polymer-solvent interaction, as toluene is a nonpolar solvent and its structure is more similar to the polymer VS in comparison to the polar solvent acetone.

159
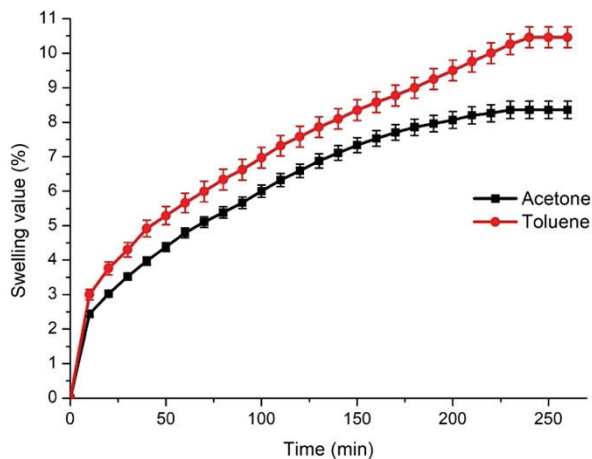
Figure 4. Swelling values of the polymer VS in acetone and toluene.

3.4. Thermal Properties of Cross-Linked Polymer

DMTA and TGA were used to study the thermal characteristics of the photocross-linked polymer VS, and the results are presented in Figure S2. These tests were chosen to determine the glass transition and thermal stability of the polymer, which exerted a huge influence on the selection of the application areas of the polymers. The thermal decomposition of the polymer VS occurred in one step. The temperature of 10% weight loss ($T_{dec\,-10\%}$) was 373 °C. The high thermal stability of the polymer was the result of a high yield of the insoluble fraction and a high cross-linking density. The thermal stability of the polymer VS was higher than that of the pure AESO polymer ($T_{dec\,-10\%}$ = 340 °C) [33] and AESO polymers with varying amounts of VDM ($T_{dec\,-10\%}$ = 268–340 °C) [34] (Figure 5). The polymer VS also demonstrated higher thermal stability than the pure VDM polymer and the VDM and thiol copolymer [15,35]. The glass transition temperature (T_g) of the polymer VS was 9 °C. The low value of T_g is due to the high amount of AESO in the polymer. The T_g of the pure AESO polymer was reported to be −4.1 °C and the addition of VDM could increase it to 102.9 °C [34] (Figure 4). In this study, the addition of VDM increased T_g; however, the addition of PETMP contributed to a decrease, which resulted in a T_g value of the polymer VS which was close to room temperature, making it both rigid and flexible at this temperature.

(**a**)

(**b**)
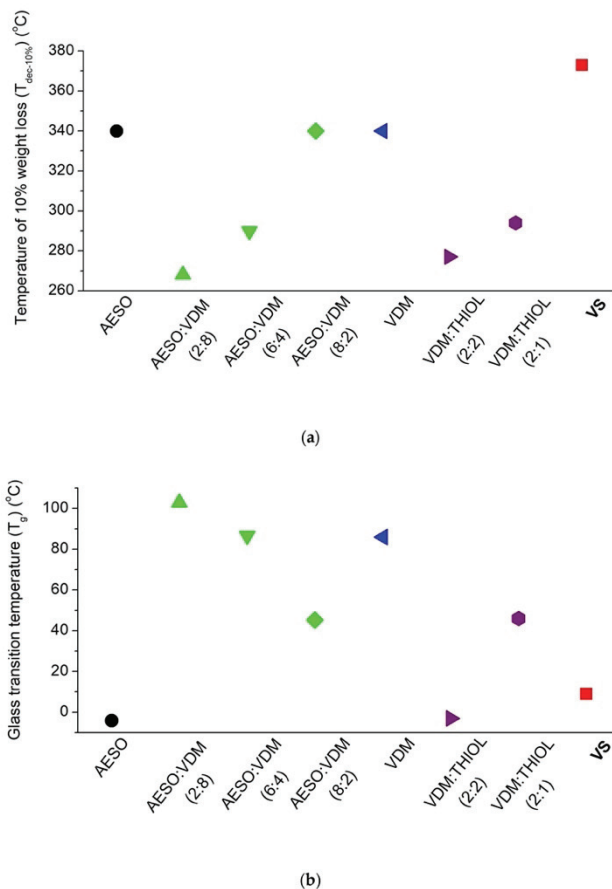
Figure 5. Comparison of the temperature of the 10% weight loss (**a**) and the glass transition temperature (**b**) of the polymer VS and the polymers of AESO [33], VDM [35], AESO and VDM [34], VDM and THIOL [15]. The molar ratio of the monomers is presented in parentheses.

3.5. Mechanical Characteristics of Cross-Linked Polymers

The most commonly-used tensile and compression tests were performed to determine the mechanical characteristics of the polymer VS for the evaluation of its mechanical strength, stiffness, and brittleness. The results are presented in Table S1 and Figure S3. The high value of Young's modulus and the low value of elongation at break show that the polymer VS is a rigid and stiff material (Table S1). Compared to other vanillin dimethacrylate- and thiol-based polymer VDM/THIOL, the polymer VS is more rigid and less flexible, as the other polymer based on VDM reached a lower Young's modulus value (3952.3 MPa)

161

and a higher elongation at break value (9.7%) [15] (Figure 6). The polymer VS is also mechanically stronger than the pure AESO polymer, which demonstrated a lower value of Young's modulus. The compression test confirmed that the polymer VS was a less brittle material. The compression modulus reached 1633.72 MPa and was much higher than that of the other vanillin dimethacrylate- and thiol-based polymer VDM/THIOL [39], the pure AESO polymer, and the polymer AESO/VDM [40]. These results show that the polymer VS can be used in applications that require mechanically-strong polymers.
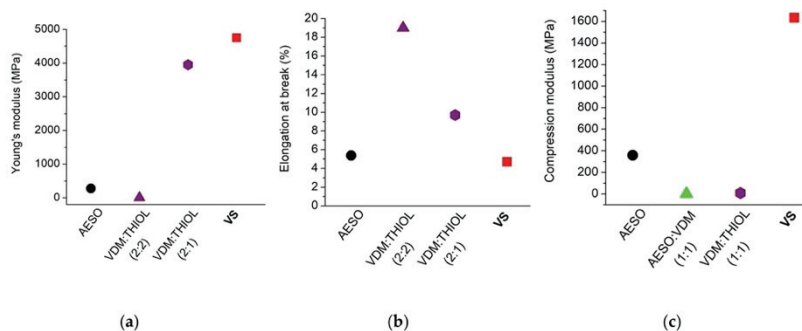
Figure 6. Comparison of Young's modulus (**a**), elongation at break (**b**), and compression modulus (**c**) of the polymer VS and the polymers of AESO [33], AESO and VDM [40], VDM and THIOL [15,39]. The molar ratio of the monomers is presented in parentheses.

3.6. SLA 3D Printing

The composed resin VS was successfully applied in the SLA 3D printing technology. Complex shape structures were printed with high accuracy and a smooth surface finish, confirming the suitability of this biobased resin for the SLA 3D printing technology. The images of the 3D printed 'Ameralabs Town' are presented in Figure 7.
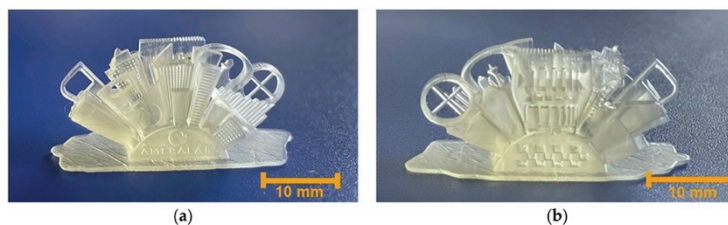
Figure 7. Images of SLA 3D printed polymer structures. The front side is on the left (**a**), and the back side is on the right (**b**).

The main limitation of the application of the VS resin in SLA 3D printing was the high viscosity, which resulted in a relatively slow 3D printing process at room temperature due to the necessary long wait period to recoat a new layer [41]. However, a high viscosity of the photocurable resin is preferred in laser direct writing technology, as it limits the mobility of oxygen and radicals that terminate the propagation, resulting in a decrease in polymerization thresholds and an increased dynamic range (difference between polymer-

ization and optical damage thresholds) [42]. Moreover, the results of the 2-BIT experiment showed that high viscosity can be overcome by using a 3D printer with a heating function, as increasing the temperature also increases the rate of photopolymerization.

3.7. Determination of the Polymerization Threshold Using the 2-BIT Method

The results of the 2-BIT experiment are provided in Figure 8. The normalized power of beam 2 vs the normalized power of beam 1 is depicted. Normally, it is expected that, when decreasing the power of beam 2, beam 1 should be proportionally increased to observe the polymerized features. Eventually, when beam 2 is close to the value of 0, beam 1 should reach the value of 1, which is determined as the polymerization threshold when a single beam was used. In this study, this value was P_{single} = 6.4 mW for beam 1 and P_{single} = 6.6 mW for beam 2. This did not allow for direct assessment of n_{eff} in the used photocurable resin but provided some interesting and useful data while varying sample preheating conditions.
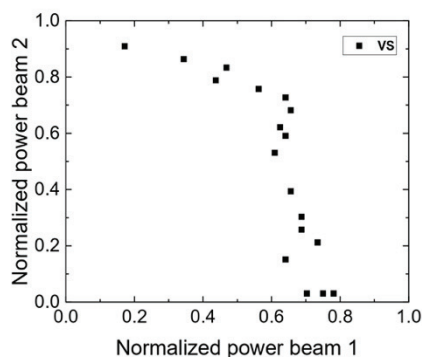
Figure 8. 2-BIT data for the polymer VS prepared at room temperature.

In this case, the power of beam 1 converged to 0.8 when beam 2 was close to 0. During the duration of the experiment of approximately 1 h, a noticeable decrease of 33% was determined when P_{single} was reduced from 6.4–6.6 mW to 4.3–4.4 mW. This prohibits the determination of effective order or nonlinearity due to the variable photopolymerization threshold, which might be attributed to thermal effects under ambient conditions. To confirm that the threshold was changing specifically due to thermal effects (Brownian motion of molecules that increase photopolymerization efficiency), the resin was placed on the hot plate for 2 h at 65 °C. In this case, P_{single} was recorded to be 0.8 mW and 2.8 mW for beam 1 and beam 2, respectively, resulting in a decrease which was significant more than 50% in used laser power. This is an important material feature for reducing the required laser energy consumption in the industrial applications context. A liquid form of the TPO (TPO-L) photoinitiator was used in the resist composed of tris (2-hydroxy ethyl) isocyanurate triacrylate and dipentaerythritol pentaacrylate for the 2-BIT experiment by the authors of reference [24]. The resist was excited with a laser generating 800 nm wavelengths and n_{eff} was determined to be equal to 2, resulting in the absorption of two photons at 400 nm. As both TPO and TPO-L have identical absorption spectra, a similar result was expected in this work.

163

4. Conclusions

A novel stable high biorenewable carbon content photopolymerizable resin was developed from acrylated epoxidized soybean oil, vanillin dimethacrylate, and pentaerythritol tetrakis(3-mercaptopropionate)-based polymer and was successfully applied in SLA 3D printing technology. The calculated biorenewable carbon content of the synthesized polymer was 76.45%. The resin demonstrated rapid photocuring without an induction period and reached a rigidity of 317.66 MPa, which was more than 20 times higher than that of the other vanillin-based polymers. The polymer with a high crosslinking density ($127,825 \pm 206$ mol/m^3) showed excellent mechanical properties (Young's modulus was 4753 MPa and the compression modulus was 1634 MPa) and great thermal stability (the temperature of 10% weight loss was 373 °C). The developed stable dual-cure photopolymerizable system is suitable for light-based 3D structuring of objects with complex shapes. Based on the 2-BIT experiment, it was determined that the polymerization threshold of the investigated polymer can be controlled by sample temperature and was reduced to the lower values by a f mW ($\approx$50% of the total laser power > 6 mW needed to induce photocuring). This is a great advantage, as it opens up the employment of dual-cure resins for low-power laser systems in LDW, making the footprint of the workstations cheaper, faster, and more reliable.

References

1. Skliutas, E.; Lebedevaite, M.; Kabouraki, E.; Baldacchini, T.; Ostrauskaite, J.; Vamvakaki, M.; Farsari, M.; Juodkazis, S.; Malinauskas, M. Polymerization mechanisms initiated by spatio-temporally confined light. *Nanophotonics* **2021**, *10*, 1211–1242. [CrossRef]
2. Jonušauskas, L.; Gailevičius, D.; Rekštytė, S.; Baldacchini, T.; Juodkazis, S.; Malinauskas, M. Mesoscale laser 3D printing. *Opt. Express* **2019**, *27*, 15205–15221. [CrossRef] [PubMed]
3. Raza, S.; Zhang, J.; Ali, I.; Li, X.; Liu, C. Recent trends in the development of biomass-based polymers from renewable resources and their environmental applications. *J. Taiwan Inst. Chem. Eng.* **2020**, *115*, 293–303. [CrossRef]
4. Silva, J.; Grilo, L.; Gandini, A.; Lacerda, T. The Prospering of Macromolecular Materials Based on Plant Oils within the Blooming Field of Polymers from Renewable Resources. *Polymers* **2021**, *13*, 1722. [CrossRef]
5. Zhanga, C.; Xuea, J.; Yanga, X.; Kea, Y.; Oua, R.; Wanga, Y.; Madboulyc, S.A.; Wang, Q. From plant phenols to novel bio-based polymers. *Prog. Polym. Sci.* **2022**, *125*, 101473. [CrossRef]
6. Huang, X.; Ding, Z.; Wang, W.; Yan, X.; Zhou, Y.; Cai, Z. Synthesis and properties of porous materials from polymeric acrylated epoxidized soybean oil via an emulsion template. *Ind. Crops Prod.* **2022**, *188*, 115662. [CrossRef]

7. Lebedevaite, M.; Gineika, A.; Talacka, V.; Baltakys, K.; Ostrauskaite, J. Development and optical 3D printing of acrylated epox-idized soybean oil-based composites with functionalized calcium silicate hydrate filler derived from aluminium fluoride pro-duction waste. *Compos. Part A Appl. Sci. Manuf.* **2022**, *157*, 106929. [CrossRef]

8. Skliutas, E.; Lebedevaite, M.; Kasetaite, S.; Rekštytė, S.; Lileikis, S.; Ostrauskaite, J.; Malinauskas, M. A Bio-Based Resin for a Multi-Scale Optical 3D Printing. *Sci. Rep.* **2020**, *10*, 9758. [CrossRef]

9. Chen, Z.; Wu, J.F.; Fernando, S.; Jagodzinski, K. Soy-based, high biorenewable content UV curable coatings. *Prog. Org. Coat.* **2011**, *71*, 98–109. [CrossRef]

10. La Scala, J.; Wool, R.P. Property analysis of triglyceride-based thermosets. *Polymer* **2004**, *46*, 61–69. [CrossRef]

11. Fache, M.; Boutevin, B.; Caillol, S. Vanillin, a key-intermediate of biobased polymers. *Eur. Polym. J.* **2015**, *68*, 488–502. [CrossRef]

12. Mohanraj, D.G.R.; Alagumuthu, M.; Subramaniam, P.; Bakthavachalam, D.; Arumugam, S.; Chellam, S. Antimicrobial effects of vanillin-based pyridyl-benzylidene-5-fluoroindolins. *J. Heterocycl. Chem.* **2021**, *58*, 1515–1524. [CrossRef]

13. Polo, L.; de Greñu, B.D.; Della Bella, E.; Pagani, S.; Torricelli, P.; Vivancos, J.-L.; Ruiz-Rico, M.; Barat, J.M.; Aznar, E.; Martínez-Máñez, R.; et al. Antimicrobial activity of commercial calcium phosphate based materials functionalized with vanillin. *Acta Biomater.* **2018**, *81*, 293–303. [CrossRef]

14. Grauzeliene, S.; Navaruckiene, A.; Skliutas, E.; Malinauskas, M.; Serra, A.; Ostrauskaite, J. Vegetable Oil-Based Thiol-Ene/Thiol-Epoxy Resins for Laser Direct Writing 3D Micro-/Nano-Lithography. *Polymers* **2021**, *13*, 872. [PubMed]

15. Navaruckiene, A.; Bridziuviene, D.; Raudoniene, V.; Rainosalo, E.; Ostrauskaite, J. Vanillin acrylate-based thermo-responsive shape memory antimicrobial photopolymers. *Express Polym. Lett.* **2022**, *16*, 279–295. [CrossRef]

16. Roig, A.; Ramis, X.; De la Flor, S.; Serra, À. Dual-cured thermosets from glycidyl methacrylate obtained by epoxy-amine reaction and methacrylate homopolymerization. *React. Funct. Polym.* **2021**, *159*, 104822. [CrossRef]

17. Liu, J.; Miao, P.; Zhang, W.; Song, G.; Feng, J.; Leng, X.; Li, Y. Synthesis and characterization of interpenetrating polymer networks (IPNs) based on UV curable resin and blocked isocyanate/polyols. *Polymer* **2022**, *256*, 125254. [CrossRef]

18. Konuray, O.; Fernández-Francos, X.; Ramis, X.; Serra, À. State of the Art in Dual-Curing Acrylate Systems. *Polymers* **2018**, *10*, 178. [CrossRef]

19. Nair, D.P.; Cramer, N.B.; Gaipa, J.C.; McBride, M.K.; Matherly, E.M.; McLeod, R.R.; Shandas, R.; Bowman, C.N. Two-Stage Reactive Polymer Network Forming Systems. *Adv. Funct. Mater.* **2012**, *22*, 1502–1510. [CrossRef]

20. Green, W.A. *Industrial Photoinitiators, A Technical Guide*, 2nd ed.; CRC Press: Boca Raton, FL, USA, 2010.

21. Ladika, D.; Noirbent, G.; Dumur, F.; Gigmes, D.; Mourka, A.; Barmparis, G.D.; Farsari, M.; Gray, D. Synthesis and application of triphenylamine-based aldehydes as photo-initiators for multi-photon lithography. *Appl. Phys. A* **2022**, *128*, 745. [CrossRef]

22. Williams, H.E.; Diaz, C.; Padilla, G.; Hernandez, F.E.; Kuebler, S.M. Order of multiphoton excitation of sulfonium photo-acid generators used in photoresists based on SU-8. *J. Appl. Phys.* **2017**, *121*, 223104. [CrossRef]

23. Yang, L.; Münchinger, A.; Kadic, M.; Hahn, V.; Mayer, F.; Blasco, E.; Barner-Kowollik, C.; Wegener, M. On the Schwarzschild Effect in 3D Two-Photon Laser Lithography. *Adv. Opt. Mater.* **2019**, *7*, 1901040. [CrossRef]

24. Liaros, N. Far-field lithography through saturated resonance energy transfer. *Opt. Lett.* **2022**, *47*, 3327. [CrossRef] [PubMed]

25. Tomova, Z.; Liaros, N.; Razo, S.A.G.; Wolf, S.M.; Fourkas, J.T. In situ measurement of the effective nonlinear absorption order in multiphoton photoresists. *Laser Photon.-Rev.* **2016**, *10*, 849–854. [CrossRef]

26. Nguyen, D.T.T.; Tong, Q.C.; Ledoux-Rak, I.; Lai, N.D. One-step fabrication of submicrostructures by low one-photon absorption direct laser writing technique with local thermal effect. *J. Appl. Phys.* **2016**, *119*, 013101. [CrossRef]

27. Zyla, G.; Surkamp, N.; Gurevich, E.L.; Esen, C.; Klehr, A.; Knigge, A.; Hofmann, M.R.; Ostendorf, A. Two-photon polymerization with diode lasers emitting ultrashort pulses with high repetition rate. *Opt. Lett.* **2020**, *45*, 4827. [CrossRef]

28. Somers, P.; Liang, Z.; Johnson, J.E.; Boudouris, B.W.; Pan, L.; Xu, X. Rapid, continuous projection multi-photon 3D printing enabled by spatiotemporal focusing of femtosecond pulses. *Light. Sci. Appl.* **2021**, *10*, 1–11. [CrossRef]

29. Kiefer, P.; Hahn, V.; Nardi, M.; Yang, L.; Blasco, E.; Barner-Kowollik, C.; Wegener, M. Sensitive Photoresists for Rapid Multiphoton 3D Laser Micro- and Nanoprinting. *Adv. Opt. Mater.* **2020**, *8*, 2000895. [CrossRef]

30. Hahn, V.; Rietz, P.; Hermann, F.; Müller, P.; Barner-Kowollik, C.; Schlöder, T.; Wenzel, W.; Blasco, E.; Wegener, M. Light-sheet 3D microprinting via two-colour two-step absorption. *Nat. Photon.* **2022**, *16*, 784–791. [CrossRef]

31. Flory, P.J. *Principles of Polymer Chemistry*, 1st ed.; Cornell University Press: Ithaca, NY, USA, 1953.

32. Ladika, M.; Farsari, M.; Gray, D. Two beam initiation threshold measurements of photo-initiators for laser writing of biocompatible 3D structures. In Proceedings of the 2019 Conference on Lasers and Electro-Optics Europe and European Quantum Electronics Conference, Munich, Germany, 23–27 June 2019.

33. Lebedevaite, M.; Ostrauskaite, J. Influence of photoinitiator and temperature on photocross-linking kinetics of acrylated epoxi-dized soybean oil and properties of the resulting polymers. *Ind. Crops Prod.* **2021**, *161*, 113210. [CrossRef]

34. Zhang, C.; Yan, M.; Cochran, E.W.; Kessler, M.R. Biorenewable polymers based on acrylated epoxidized soybean oil and methacrylated vanillin. *Mater. Today Commun.* **2015**, *5*, 18–22. [CrossRef]

35. Navaruckiene, A.; Skliutas, E.; Kasetaite, S.; Rekštytė, S.; Raudoniene, V.; Bridziuviene, D.; Malinauskas, M.; Ostrauskaite, J. Vanillin Acrylate-Based Resins for Optical 3D Printing. *Polymers* **2020**, *12*, 397. [CrossRef]

36. Xie, R.; Weisen, A.R.; Lee, Y.; Aplan, M.A.; Fenton, A.M.; Masucci, A.E.; Kempe, F.; Sommer, M.; Pester, C.W.; Colby, R.H.; et al. Glass transition temperature from the chemical structure of conjugated polymers. *Nat. Commun.* **2020**, *11*, 893. [CrossRef] [PubMed]

165

37. Mezger, T.G. *The Rheology Handbook*, 3rd ed.; Vincentz Network: Hanover, Germany, 2011.
38. Gurr, M.; Mülhaupt, R. Rapid prototyping. In *Polymer Science: A Comprehensive Reference*, 1st ed.; Matyjaszewski, K., Möller, M., Eds.; Elsevier: Edinburgh, UK, 2012; Volume 1, pp. 77–99.
39. Navaruckiene, A.; Kasetaite, S.; Ostrauskaite, J. Vanillin-based thiol-ene systems as photoresins for optical 3D printing. *Rapid Prototyp. J.* **2019**, *26*, 402–408. [CrossRef]
40. Lebedevaite, M.; Ostrauskaite, J.; Skliutas, E.; Malinauskas, M. Photocross-linked polymers based on plant-derived monomers for potential application in optical 3D printing. *J. Appl. Polym. Sci.* **2019**, *137*, 48708. [CrossRef]
41. Vyas, A.; Garg, V.; Ghosh, S.B.; Bandyopadhyay-Ghosh, S. Photopolymerizable resin-based 3D printed biomedical composites: Factors affecting resin viscosity. *Mater. Today Proc.* **2022**, *62*, 1435–1439. [CrossRef]
42. Zandrini, T.; Liaros, N.; Jiang, L.J.; Lu, Y.F.; Fourkas, J.T.; Osellame, R.; Baldacchini, T. Effect of the resin viscosity on the writing properties of two-photon polymerization. *Opt. Mater. Express* **2019**, *9*, 2601–2616. [CrossRef]

166

RESEARCH ARTICLE

Applied Polymer WILEY
JOURNAL OF SCIENCE

Antimicrobial dual-cured photopolymers of vanillin alcohol diglycidyl ether and glycerol dimethacrylate

Greta Motiekaityte[1] | Aukse Navaruckiene[1] | Vita Raudoniene[2] |
Danguole Bridziuviene[2] | Justinas Jaras[1] | Kristina Kantminiene[3] |
Jolita Ostrauskaite[1]

[1]Department of Polymer Chemistry and Technology, Kaunas University of Technology, Kaunas, Lithuania

[2]Biodeterioration Research Laboratory, Nature Research Center, Vilnius, Lithuania

[3]Department of Physical and Inorganic Chemistry, Kaunas University of Technology, Kaunas, Lithuania

Correspondence
Jolita Ostrauskaite, Department of Polymer Chemistry and Technology, Kaunas University of Technology, Radvilenu Rd. 19, Kaunas LT-50254, Lithuania.
Email: jolita.ostrauskaite@ktu.lt

Funding information
European Social Fund, Grant/Award Number: 09.3.3-LMT-K-712-22-0011; Lietuvos Mokslo Taryba, Grant/Award Number: S-MIP-20-17

Abstract

Considering the current efforts for to develop new antimicrobial polymers from renewable resources suitable for application in environmentally friendly light-based technologies, novel dual-cured photopolymers of vanillin alcohol diglycidyl ether and glycerol dimethacrylate are developed. The kinetics of the sequential and simultaneous dual-curing processes, combining free radical and cationic photopolymerizations, is investigated by real-time photorheometry. Comparison of dual-curing systems with different ratios of biobased epoxy and acrylate monomers revealed that the increase in the acrylate content increases the photocuring rate and improves the mechanical performance (Young's modulus increases from 76.64 to 190.71 MPa) and thermal stability (the 10% weight loss increases from 227 to 274°C) of the polymers, while the increase in the vanillin epoxy content results in better antimicrobial activity. Developed photopolymers create unfavorable conditions for the growth of microorganisms and reduce their population by up to 0% in 24 h. The excellent antibacterial and antifungal activity of new photopolymers allows them to be considered as biobased alternatives to petroleum-based antimicrobial coatings, films, or optical 3D printed objects.

KEYWORDS

antimicrobial activity, biobased, dual-curing, photopolymerization, vanillin

1 | INTRODUCTION

Microbes are part of our daily life, they grow in our surroundings and can cause microbial infections to humans, animals, and plants, the spoilage of food and textiles.[1] Microbial infections are the major issue in the environment of medicine and food storage. Therefore, antimicrobial polymers are receiving great attention as they can prevent infections during surgeries, protect food from spoiling quickly and reduce the spreading of dangerous microorganisms. The use of antimicrobial coatings also

reduces the need for disinfectants in homes and public places.[2] In addition to natural antimicrobial polymers, such as chitosan, the most commonly used methods to impart antimicrobial properties to polymeric materials are chemical modification of polymers or incorporation of inorganic particles into the polymer network.[3] Antimicrobial composites are mostly created by combining synthetic polymers with antimicrobial properties and natural polymers,[4] for example, polyurethanes with zinc oxide nanoparticles were used to create composite films with antibacterial properties,[5] zwitterionic copolymers

1 of 13

synthesized with 3-dimethyl (methacyloyloxyethyl) ammonium propane sulfonate and acrylic acid also demonstrated antimicrobial properties. However, antimicrobial polymers or composites are usually obtained by thermal polymerization.[6] An environmentally friendly photopolymerization method has been used very rarely to obtain antimicrobial polymeric materials.[7] Among them, only in a few cases biobased monomers were used for the synthesis of antimicrobial photopolymers.[8]

Dual cure is a process defined as a combination of two curing reactions taking place simultaneously or sequentially[9] that result in interpenetrating polymer networks or semiinterpenetrating polymer networks.[10] Dual curing allows the creation of polymers with unique properties, such as high mechanical strength and thermal stability.[11] Both curing reactions can be of the same type (e.g., thermal curing at two different temperatures or photocuring at different wavelengths) or of a different type (e.g., photocuring and thermal curing).[12] Dual-curing process is a fairly new tool to synthesize polymers with high mechanical strength and thermal stability, which could not be obtained using other polymerization reactions.[13] UV/UV photocuring has been used successfully in the production of adhesives, and only a small residue of monomers remained in the samples after the second curing, suggesting that they had completely hardened.[14] UV/UV photocuring has also been used in the creation of pressure-sensitive acrylic adhesives.[15] However, this method has not yet been used in biobased epoxy systems.

Photo-photo dual-curing has a huge advantage over photo-thermal dual-curing as it does not require two separate devices, a UV chamber with controlled wavelength or light filters can be used for this process.[16] Furthermore, this process can be carried out at room temperature or lower temperatures, which simplifies the requirements for polymer production. Another advantage of photo-photo dual cure is the reaction rate; photopolymerization starts rapidly after irradiation and takes only seconds or minutes until the polymer is fully cured.[17] Therefore, it is not necessary to keep samples in the chamber for hours or days, as in the case of thermal polymerization.[18] Moreover, it is an easily controlled process, as it only starts in irradiated areas.[19] This allows the use of photo-photo dual-curing compositions as resins for optical 3D printing,[20] which is a much more accurate technique than thermal 3D printing.[21] Due to the advantages mentioned above, a photo-photo dual-curing process was chosen for this study.

In this work, new antimicrobial photopolymers have been developed, creating unfavorable conditions for the growth of microorganisms and reducing their population by up to 0% in 24 h. These polymers have great potential in the medical field as coatings or for the production of medical devices and instruments that can stop the growth of disease causing microorganisms.[22] Optical 3D printing can be used to rapidly produce complex and precise shaped components and devices from the developed polymers.[23,24] Moreover, these polymers can also help solve environmental problems, as they are synthesized from biobased monomers by an environmentally friendly photocuring process.

2 | EXPERIMENTAL

2.1 | Materials

Vanillin alcohol diglycidyl ether (VDGE, Specific Polymers), glycerol dimethacrylate mixture of isomers (GDMK, ALFA Chemistry), triarylsulfonium hexafluorophosphate salt mixture (TASHFF), and phenylbis (2,4,6-trimethylbenzoyl) phosphine oxide (BAPO) (both Merck) (Figure 1), dichloromethane (DCM, Eurochemicals), chitosan and hydroxyethyl starch (both Merck) were used as received.

2.2 | Preparation of photopolymer samples

The initial mixtures containing 1 or 0.5 mol of VDGE, 1 or 0.5 mol of glycerol dimethacrylate (GDMK), 3 mol% of TASHFF (calculated from the molar amount of VDGE) and 3 mol% of BAPO (calculated from the molar amount of GDMK) were stirred with a magnetic stirrer at room temperature (25°C) for 5 min. VDGE was dissolved in a small amount of DCM before mixing with other resin components (0.1 g of DCM for 1 g of VDGE). The homogeneous resins were then poured into Teflon molds of different dimensions for different tests and cured for 2–4 min (until the samples have hardened) under a UV/Vis lamp (Helios Italquartz, model GR.E 500 W, Milan, Italy) with an intensity of 310 mW/cm^2. All molds have the ability to change their depth to prepare specimens of desired thickness as different thicknesses of the specimens are needed for different experiments. The composition of the resins is presented in Table 1.

2.3 | Real-time photorheometry

The UV/Vis cure tests of the resins (Table 1) were performed on an MCR302 rheometer (Anton Paar, Graz, Austria) equipped with the plate/plate measuring system. The Peltier-controlled temperature chamber with the
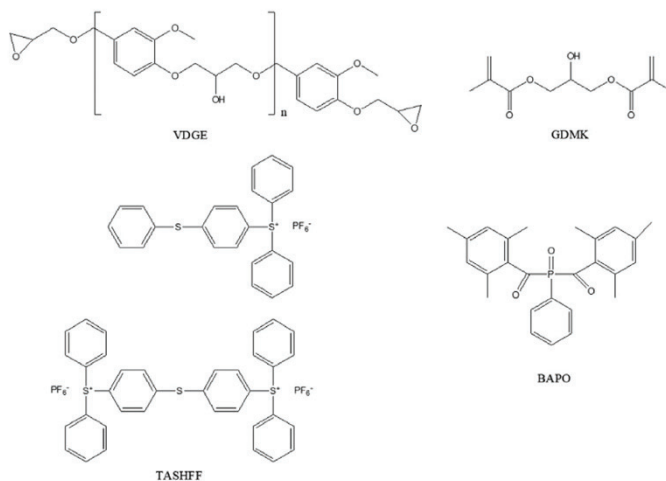
FIGURE 1 Chemical structure of vanillin alcohol diglycidyl ether, $n = 0.0–0.2$ (VDGE), glycerol dimethacrylate mixture of isomers (GDMK), triarylsulfonium hexafluorophosphate salts (TASHFF), and phenylbis (2,4,6-trimethylbenzoyl) phosphine oxide (BAPO).

TABLE 1 Composition of resins

Resin	Amount of VDGE, mol	Amount of GDMK, mol	Amount of TASHFF, mol%	Amount of BAPO, mol%	Amount of DCM, mol
C1	1	0.5	3	3	0.4
C2	1	1	3	3	0.4
C3	0.5	1	3	3	0.2
VDGE	1	0	3	0	0.4
GDMK	0	1	0	3	0

glass plate (diameter 38 mm) and the PP15 top plate (diameter 15 mm) was used. The measurement gap was set to 0.1 mm and the samples were irradiated with UV/Vis light in a wavelength range of 250–450 nm through the glass plate using the OmniCure S2000 UV/Vis spot curing system (Lumen Dynamics Group Inc., Mississauga, ON, Canada). The light filter, which only allows for the transmission of light 400–450 nm to the sample, was used to manipulate the initiation of photocuring. Two different curing routes, sequential and simultaneous, were used. At the first stage of the sequential route, the samples were irradiated by UV/Vis light in a wavelength range of 400–450 nm for 240 s using a light filter, and at the second step the filter was removed, and they were irradiated by UV/Vis light in a wavelength range of 250–450 nm for 760 s. During the simultaneous route, the samples were irradiated by UV/Vis light in a wavelength range of 250–450 nm for 1000 s. The temperature was 25°C. In all cases, the shear mode was used with a frequency of 10 Hz and a shear strain of 0.1%. The storage modulus (G'), the loss modulus (G''), and the complex viscosity (η^*) were recorded as a function of the irradiation time. The gel point (t_{gel}) was calculated as an intersection point of the G' and G'' curves. The induction period was measured as the onset of the increase in G'. The shrinkage was calculated from the reduction of the height of the sample during the photocuring process. The normal force was set to 0 N during the measurement of the sample shrinkage. Five measurements of each resin were used to obtain the mean value and standard deviation.

169

2.4 | Characterization techniques

Fourier transformation infrared (FT-IR) spectra were recorded using a Spectrum BX II FT-IR spectrometer (Perkin Elmer, Llantrisant, UK). Reflection was measured during the test. The range of wavenumbers was 500–4000 cm^{-1}.

The Soxhlet extraction was used to determine the yield of the insoluble fraction. 0.4 g polymer samples were extracted with acetone for 24 h. After 24 h, the insoluble fractions were dried under vacuum until no weight changes were observed. The yield of the insoluble fraction was calculated as the difference between weight before and after extraction and drying.

The swelling value of the crosslinked polymer samples was obtained by measuring the volume of the samples swollen in acetone and toluene at room temperature (25°C). The initial volume of the polymer specimen was measured before placing it into the measuring container, which was connected with the graduated tube used to indicate the reduction of the solvent. The experiment was carried out in the hermetic container to avoid the risk of solvent evaporation. The change in solvent volume was measured every 5 min until no change was observed. The swelling value was calculated according to the following equation:

$$\alpha = \frac{V - V_0}{V_0} \cdot 100,$$ (1)

where α is a swelling value (%); V is a volume of swollen sample (ml); V_0 is an initial volume of sample (ml).

Thermogravimetrical analysis (TGA) was performed on a TGA 4000 apparatus (Perkin Elmer, Llantrisant, UK). A heating rate of 20°C/min was chosen in a nitrogen atmosphere (100 ml/min). The temperature range of (10–800)°C was used. Aluminium oxide pans were used.

Dynamical mechanical thermal analysis (DMTA) was performed on an MCR302 rheometer (Anton Paar, Graz, Austria) equipped with the plate/plate measuring system. The Peltier-controlled temperature chamber with the metal plate (diameter 38 mm) and the PP08 top plate (diameter 8 mm) was used. The temperature was increased from 0 to 120°C. The normal force was set at 5 N during the measurement. In all cases, the shear mode was used with a frequency of 10 Hz and a shear strain of 0.1%. The storage modulus (G'), the loss modulus (G''), and the loss factor (tanδ) were recorded as a function of temperature.

The mechanical properties of the polymers were determined by tensile, compression, and bending tests. The tensile test was performed on a Testometric M500-50CT testing machine (Testometric Co Ltd, Rochdale, UK) with flat-face grips at room temperature (25°C). A rectangular mold with internal dimensions of 50 ($\pm$0.00) × 5.00 ($\pm$0.00) mm and depth set to 1 mm was used for the tension test specimens

(UV curing time 2 min). The dimensions of the test specimens were 50 ($\pm$0.00) × 5.00 ($\pm$0.00) × 1 ($\pm$0.15) mm (Figure 2a). The gap between the grips was set to 20 mm and the test was performed at a speed of 5 mm/min until the specimen broke. Young's modulus, tensile strength, and elongation at break were determined.

The compression test was performed on a Testometric M500-50CT testing machine (Testometric Co Ltd, Rochdale, UK) with HDGG100 grips at room temperature (25°C). The cylindrical mold with internal diameter of 30 mm and depth set to 3 mm was used for preparation of round tablets (UV curing time 4 min). The dimensions of the round tablets used for the test were 30 ($\pm$0.00) × 3 ($\pm$0.30) mm (Figure 2b). The test was carried out at a speed of 5 mm/min until the sample broke. The compression modulus and the force needed to break the specimen during compression were determined.

The bending test was performed on an RSA-G2 Solids Analyzer (TA Instruments, New Castle, Delaware, USA). A rectangular mold with internal dimensions of 40 ($\pm$0.00) × 5.00 ($\pm$0.00) mm and depth set to 1.7 mm was used for the tension test specimens (UV curing time 3 min). The size of the samples was 1.7 ($\pm$0.1) × 5.00 ($\pm$0.00) × 40.00 ($\pm$0.00) mm (Figure 2c). The test was carried out at 20°C. The bending speed was 0.1 mm/s. Three-point contact bending geometry with a 25 mm gap between end contacts was used. The specimen bend force of 30% and the bending modulus were determined. The bending modulus was calculated using the following equation:

$$\delta = \frac{3 \cdot F \cdot L}{2 \cdot w \cdot d^2},$$ (2)

where δ is the bending modulus (Pa); F is the maximum force applied to the sample (N); L is the length of the sample (m); w is the width of the sample (m); and d is the thickness of the sample (m).[25]

The crosslinking density was calculated by the theory of rubber elasticity using the following equation:

$$G' = \nu \cdot R \cdot T,$$ (3)

where G' is the steady-state value of the storage modulus taken from the photorheometry measurement curve after 1000 s (Pa); ν is a crosslinking density (mol/m^3); R is the universal gas constant (8.314 J/mol·K); T is the temperature (K).[26]

2.5 | Antimicrobial test

The study of the antimicrobial (antibacterial and antifungal) activity of polymers was carried out using two strains

FIGURE 2 Specimens used for tension (a), compression (b), and bending (c) tests. [Color figure can be viewed at wileyonlinelibrary.com]

of bacteria, Gram-negative bacterium *Escherichia coli* ATCC 25922 (*E. coli*) and Gram-positive bacteria *Staphylococcus aureus* ATCC 29213 (*S. aureus*), and two fungal strains, *Aspergillus niger* 0999-14 (*A. niger*) and *Aspergillus flavus* 1087-03 (*A. flavus*). Microorganism suspensions were prepared from fully mature cultures. The concentration of suspensions was determined by measuring the optical density with a spectrophotometer (Evolution 60 S, Thermo Fisher Scientific, Waltham, MA, USA) and then corrected by plating on nutrient medium. The final inoculum concentrations were 2.22×10^5 for *E. coli*, 1.95×10^5 for *S. aureus*, 6.85×10^6 for *A. niger* and 4.70×10^6 colony forming units/ml (CFU/ml) for *A. flavus*. The test films (10×10 mm) were placed in empty Petri dishes. Then 10 µl of the bacterial or fungal suspension was applied to its surface. For comparison, chitosan and hydroxyethyl starch films were infected in the same manner. Plates with infected films were incubated for 24 h in a humid chamber (90% relative humidity) at 37°C for those infected with bacteria and at 26°C for those infected with the fungi. After 2, 6, and 24 h of incubation, 2 ml of saline was applied to each film to remove the spores. The resulting suspensions were seeded in nutrient medium (bacteria on Mueller Hinton Agar [Liofilmchem, Italy] and microscopic fungi on Malt Extract Agar [Liofilmchem, Italy]) and incubated at 37°C with bacteria and at 26°C with fungi. After 1–2 days of incubation, the grown bacterial colonies were counted, and after 5–6 days, the fungal colonies were counted and the percent and logarithmic reduction of the spores was calculated. The percentage reduction was calculated according to the formula: $(a-b)/a \times 100\%$ and the lg reduction of the viable spores was calculated according to the formula: $\lg(a) - \lg(b)$, where a is the concentration of colonies-forming units (CFU/ml) in inoculum suspension; b is the mean viable spores (CFU/ml) in samples from experiments in triplicate after incubation.

2.6 | Statistical analysis

The data collected were statistically analyzed using ANOVA for the Microsoft Excel programme. All experiments were carried out three times and the results were assumed as the average values $\pm$ standard deviation. The estimated *p*-value was below 0.05 within the groups.

3 | RESULTS AND DISCUSSION

3.1 | Photocuring kinetics

The photocuring of VDGE and glycerol dimethacrylate (GDMK) based resins was studied by real-time photorheometry. The amounts of VDGE and GDMK in the resins were changed to manipulate the ratio of the two interpenetrating networks. A light filter, narrowing the wavelength to 400–450 nm, was used to manipulate the initiation of photocuring in sequential dual-curing, as the radical photoinitiator BAPO absorbs light up to 435 nm,[27] while TASHFF absorbs it only up to 350 nm.[28] In this work, two different types of polymerization were combined, free-radical and cationic.[29,30]

It has been determined that the ratio of monomers in the resin has a huge influence on the reaction speed and rigidity of the polymers. Real-time photorheometry data for all resins are summarized in Table 2. The dependence of the storage modulus G' on the irradiation time of all resins, prepared sequentially, is presented in Figure 3. The increase in GDMK content in the resin led to a faster photocuring process and a higher rigidity of the resulting polymers. As a result of a higher amount of GDMK in the resin, the gel point was reduced from 15.5 to 12.5 s and the rigidity increased from 22.63 to 25.56 MPa. Resins with higher amounts of GDMK produce more reactive radicals that compete with each other in the photopolymerization initiation step by reacting with the double bond of the unsaturated monomer[31] and that leads to a higher reaction speed. The increase in GDMK also increased the shrinkage of polymers, as it is well known that acrylates shrink more than epoxides during the polymerization process.[32] As expected, the highest difference in the rigidity of the polymer after the first and second curing stages was demonstrated by the resin **C1***, which was prepared with the highest amount of VDGE. The rigidity of this resin increased almost twice from 11.50 to 22.63 MPa. The shrinkage of resins **C1***–**C3*** also increased after the second stage of photocuring, although

TABLE 2 Rheological characteristics of resins

Resin	Storage modulus G', MPa	Loss modulus G'', MPa	Complex viscosity η, mPa, s	Gel point t_{gel}, s	Induction period, s	Shrinkage, %
Sequential process (400–450 nm for 240 s and 250–450 nm for 760 s)						
C1*	22.63 ± 0.13	12.17 ± 0.61	360.47 ± 18.02	15.5 ± 0.24	7.6 ± 0.24	8.5 ± 0.43
C2*	24.55 ± 0.23	2.15 ± 0.11	393.31 ± 19.67	15.0 ± 0.36	9.6 ± 0.36	9.5 ± 0.48
C3*	25.56 ± 0.28	1.8 ± 0.09	407.8 ± 20.39	12.5 ± 0.19	9.6 ± 0.19	12.7 ± 0.64
VDGE*	7.48 ± 0.28	0.079 ± 0.08	118.4 ± 8.07	300 ± 0.65	275 ± 0.65	2.8 ± 0.13
GDMK*	50.50 ± 0.93	16.99 ± 0.78	827.39 ± 37.6	8.8 ± 0.48	7.0 ± 0.48	12.4 ± 0.50
Simultaneous process (250–450 nm for 1000 s)						
C1	17.97 ± 0.90	1.15 ± 0.06	291.9 ± 14.60	12.5 ± 0.24	9.6 ± 0.24	7.5 ± 0.38
C2	28.23 ± 0.41	2.5 ± 0.13	451.09 ± 22.55	12.0 ± 0.36	9.6 ± 0.36	12.2 ± 0.61
C3	27.51 ± 0.38	3.0 ± 0.15	440.65 ± 22.03	12.5 ± 0.24	9.6 ± 0.24	10.0 ± 0.50
VDGE	7.59 ± 0.38	0.081 ± 0.01	121.6 ± 6.08	64.0 ± 0.60	36.0 ± 0.60	3.0 ± 0.15
GDMK	50.56 ± 2.52	17.12 ± 0.86	839.38 ± 41.97	9.2 ± 0.27	7.2 ± 0.27	13.0 ± 0.65
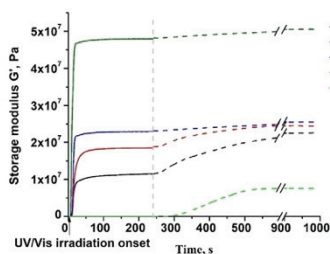
FIGURE 3 Dependence of the storage modulus G' of the resins on the irradiation time (sequential photocuring). Solid line—Wavelength range of 400–450 nm, split line—wavelength range of 250–450 nm. [Color figure can be viewed at wileyonlinelibrary.com]

FIGURE 4 Dependence of the storage modulus G' of the resins on the irradiation time (simultaneous photocuring). [Color figure can be viewed at wileyonlinelibrary.com]

the difference was in the range of 1%–1.5% for all resins. The induction period of all resins **C1*–C3*** was very similar (7.6–9.6 s), indicating a much lower onset of resin cure compared with VDGE (275 s) and only slightly higher than that of GDMK (7.0 s). The reason for this is the difference between processes, since free-radical photopolymerization is much faster than cationic photopolymerization.[33]

The influence of the resin composition on the photocuring kinetics was also investigated during the simultaneous process (Figure 4). In this process, samples were irradiated by UV/Vis light in a wavelength range of 250–450 nm for 1000 s. In this case, no control over the initiation was applied, allowing the initiation of both free-radical and cationic photopolymerizations. During
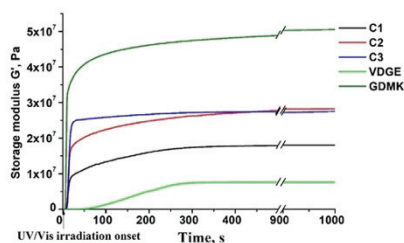
this process, the induction period of the **C1–C3** resins was the same (9.6 s) and was intermediate between the VDGE (36.0 s) and GDMK (7.2 s) resins. The gel point of the **C1–C3** resins was also very similar and was in the range of 12.0–12.5 s. The main difference between polymers **C1–C3** was rigidity, indicated by storage modulus. The highest rigidity was shown by polymer **C2**, although it was very similar to that of polymer **C3**. The lowest rigidity was demonstrated by polymer **C1** with the highest amount of VDGE.

The results of the simultaneous process were compared with those of the sequential process. A similar trend was observed in the rigidity, gel point, and shrinkage of the polymers; however, the rigidity of polymer **C1** was lower during the simultaneous process. The reason could be the higher amount of solvent DCM in this resin compared with **C2** and **C3** resins. DCM acts as a chain

transfer agent that slows the photocuring process.[34] In all cases, slightly more rigid polymers were obtained when photocuring was performed simultaneously. The reason might be spatial hindrances of the dense network structure, which occur in both simultaneous and sequential processes. The growing polymer chains cannot pass through each other during the photopolymerization process and become separated, resulting in a less crosslinked and thus less rigid polymer.[35] However, during the sequential process, only free-radical photopolymerization is activated in the first part of the process, creating a GDMK-based polymer network that acts as spatial hindrances and VDGE-based polymer chains that cannot pass through that network during the second stage of photocuring. As a result, less rigid polymers were formed during the sequential process. The only exception was polymers **C1** and **C1***. In this case, the more rigid polymer was **C1***, prepared by a sequential dual-curing process. This resin has the lowest amount of GDMK compared with other resins. Because of that, the GDMK-based polymer network, formed during the first stage of photocuring, is not dense enough to form spatial hindrances; moreover, there are many VDGE monomer molecules, mixed around the GDMK-based polymer network. These VDGE monomers can form their own polymer network more easily in this case. As a result, two interpenetrating polymer networks are formed during the sequential process and the polymer **C1*** obtained is more rigid than **C1**. This leads to the conclusion that the most often simultaneous process results in more rigid polymers with a similar reaction rate, allowing this process to be chosen for further investigation of the designed polymers.

3.2 | Characterization of photocrosslinked polymer structure

The chemical structure of photocrosslinked polymers was confirmed by FT-IR spectroscopy. The signals of the C=C group which were present at 1637 cm^{-1} and the signals of the C=O group which were present at 1720 cm^{-1} in the FT-IR spectra of GDMK were reduced in their polymer spectra. The signals of epoxy group that were present at 796, 908, and 1264 cm^{-1} in the spectra of VDGE were also reduced in the polymer spectra. The other characteristic group signals were also visible in the spectra: OH at 3384–3474 cm^{-1}, C—O—C at 1129–1151 cm^{-1}, CH^2 at 685–755 cm^{-1}, aromatic C—H at 3001–3106 cm^{-1}, and aliphatic C—H at 2929–2957 cm^{-1}. As an example, the FT-IR spectra of VDGE, GDMK and the crosslinked polymer **C1** are presented in Figure 5.
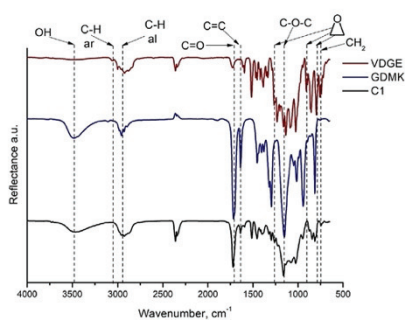

FIGURE 5 FT-IR spectra of VDGE, GDMK, and the crosslinked polymer **C1**. [Color figure can be viewed at wileyonlinelibrary.com]

The Soxhlet extraction was performed to confirm the crosslinked structure of the polymers. The yield of the insoluble fraction of the polymers was in the range of 34%–60% (Table 3). The low value of the yield of the insoluble fraction is due to a large amount of soluble linear or branched polymer fragments. These fragments were formed due to spatial hindrances, the inability of chains to pass through each other during the photopolymerization process.[32] The highest amount of insoluble fraction was in the **C3** polymer, which was prepared with the highest amount of GDMK. When a higher amount of GDMK was used in the resin, a denser polymer network was formed, and a lower amount of linear and branched polymer fragments were obtained. Acrylates polymerize faster than epoxides and form a polymer network inside the resin, leading to spatial hindrances and a large amount of linear polymer fragments. The amount of these fragments increases with increasing VDGE content, which is slower to polymerize and cannot pass through GDMK chains.[32] These results are correlated with the crosslinking density and the swelling value of the polymers (Table 3).

Two different solvents, acetone and toluene, were used to investigate the swelling of the polymers. The swelling values of the polymers are presented in Figure 6. In all cases, the polymers were more swollen when the yield of the insoluble fraction and the crosslinking density were lower. The higher swelling values showed that longer chains were formed between the crosslinking points in the polymer structure when the higher amount of VDGE was used.[36] VDGE is a longer molecule compared with GDMK and leads to the formation of longer chains in the polymer structure.[37] Swelling in acetone

TABLE 3 Characteristics of simultaneously crosslinked polymers **C1–C3**

Polymer	Yield of the insoluble fraction, %	Swelling value in acetone, %	Swelling value in toluene, %	Crosslinking density, mol/m^3
C1	34 ± 1.5	330 ± 12	360 ± 14	7503 ± 243
C2	51 ± 2.0	280 ± 10	300 ± 12	11,089 ± 395
C3	60 ± 2.5	230 ± 6	240 ± 6	11,487 ± 427
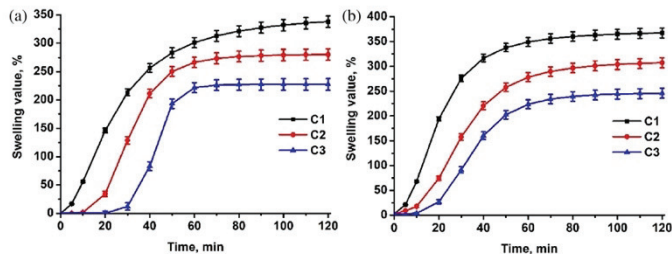
FIGURE 6 Dependence of the swelling values of vanillin-based polymers **C1–C3** on the duration of swelling in acetone (a) and toluene (b). [Color figure can be viewed at wileyonlinelibrary.com]
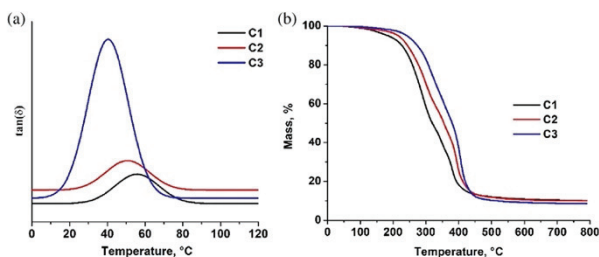
FIGURE 7 DMTA thermograms (a) and thermogravimetric curves (b) of crosslinked polymers **C1–C3**. [Color figure can be viewed at wileyonlinelibrary.com]

began rapidly for polymer **C1** with the lowest crosslinking density. The swelling became slower with increasing crosslinking density, since polymer **C3**, which crosslinking density is the highest, started to swell only after 20 min in acetone. The reason for this is polymer structure, a higher crosslinking density showing that polymer has a more dense inner structure, which makes it harder for solvent molecules to penetrate into polymer. The same tendency was observed in the other solvent, toluene. However, polymers started to swell twice faster in toluene than in acetone. The swelling of all polymers was slightly greater in the nonpolar solvent toluene compared with that in the polar solvent acetone, although they were still quite similar for the same polymer samples.

3.3 | Thermal properties

DMTA was used to determine the glass transition temperature of the polymers. The DMTA curves of the crosslinked polymers are presented in Figure 7a. The glass transition temperature of all synthesized polymers was in the range of 41–57°C. The highest glass transition temperature value was shown by polymer **C1** with the highest amount of VDGE (57°C). When the amount of GDMK was increased, lower values of the glass transition temperature were obtained for polymers **C2** (51°C) and **C3** (41°C). TGA was used to determine the thermal stability of polymers. Thermogravimetric curves of the crosslinked polymers are presented in Figure 7b. The temperature of 10% weight loss ($T_{dec.-10\%}$) of all
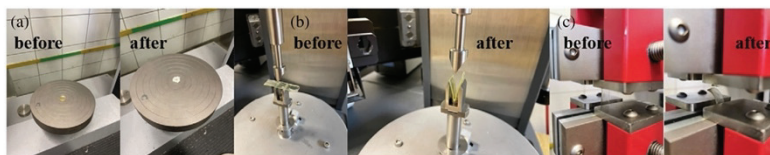
FIGURE 8 Photos of polymer specimens before mechanical testing and after it: (a) compression test, (b) bending test, (c) tensile test. [Color figure can be viewed at wileyonlinelibrary.com]

TABLE 4 Mechanical characteristics of simultaneously crosslinked polymers **C1–C3**

Polymer	C1	C2	C3
Elongation at break, %	4.75 ± 1,02	3.95 ± 0.12	3.41 ± 0.07
Young's modulus, MPa	76.64 ± 15.24	108.45 ± 14.34	190.71 ± 14.39
Tensile strength, MPa	15.56 ± 0.41	17.58 ± 2.92	21.74 ± 4.22
Bending modulus, MPa	15.78 ± 0.92	18.49 ± 0.87	27.36 ± 1.32
Specimen bend force of 30%, N	0.112 ± 0.05	0.167 ± 0.10	0.187 ± 0.05
The force needed to break the specimen during compression, kN	330 ± 0.01	820 ± 0.06	860 ± 0.07
Compression modulus, kPa	6.78 ± 1.63	12.23 ± 2.29	38.78 ± 1.96

synthesized polymers was in the range of 227–274°C. The higher decomposition temperatures were shown by the polymers with the higher yield of insoluble fraction and crosslinking density.[38] Polymer **C3** 41 ($T_{\text{dec.}-10\%} = 274°C$), prepared with the highest amount of GDMK, was more thermally stable than polymers **C1** 57 ($T_{\text{dec.}-10\%} = 227°C$) and **C2** 52 ($T_{\text{dec.}-10\%} = 244°C$). The temperature of 10% weight loss of these polymers is similar to vanillin acrylate and GDMK based polymers, used for additive manufacturing ($T_{\text{dec.}-10\%} = 250–280°C$).[39]

3.4 | Mechanical characteristics

Tensile, compression, and bending tests were performed to determine the mechanical characteristics of the photocrosslinked polymers. The photos of the polymer samples before and after the experiments are presented in Figure 8. The results are presented in Table 4. Young's modulus and tensile strength values were determined to increase with increasing GDMK content in the polymer specimen. The same tendency was visible in the bending and compression tests. The compression modulus, the force needed to break the sample during compression, the bending modulus, and the specimen bend force of 30% increased with increasing amount of GDMK. These results are correlated with the yield of the insoluble fraction because polymers with higher yield and crosslinking density are

mechanically stronger.[40] The bending modulus shows that polymer **C3**, which has a higher amount of GDMK, is more resistant to bending than polymers **C1** and **C2**. These results show that polymers with higher amounts of VDGE are more flexible compared with polymers with higher amounts of GDMK. The reason for this is the structure of VDGE, as it is a longer molecule compared with GDMK, leading to the formation of longer chains in the polymer structure, as mentioned earlier.[34]

3.5 | Antimicrobial activity of polymers

The antibacterial and antifungal activity of the polymer films was investigated during direct contact of the bacterial or fungal suspension with the samples by calculating the log reduction and the percent reduction of viable microbial spores. Two reference polymer films of chitosan, which is a well-known antibacterial polymer, and hydroxyethyl starch, which does not possess such activity, were used. The results are presented in Tables 5 and 6.

After 2 h of exposure, the viability of *E. coli* was reduced to 98.6%, while the viability of *St. aureus* was reduced to 74.6% by polymer films (Figure 9). Grampositive *St. aureus* viability was significantly weaker than that of Gram-negative *E. coli*, since *St. aureus* is more resistant to antibiotics and other antibacterial agents and

TABLE 5 Characteristics of antibacterial activity of polymer films

Polymer film	Escherichia coli		Staphylococcus aureus	
	Lg reduction after 24 h	Percent reduction after 24 h, %	Lg reduction after 24 h	Percent reduction after 24 h, %
C1	5.35 ± 0.00	100 ± 0.00	5.29 ± 0.00	100 ± 0.00
C2	5.35 ± 0.00	100 ± 0.00	5.29 ± 0.00	100 ± 0.00
C3	5.35 ± 0.00	100 ± 0.00	5.29 ± 0.00	100 ± 0.00
Chitosan	5.35 ± 0.00	100 ± 0.00	5.29 ± 0.00	100 ± 0.00
Hydroxyethyl starch	0.00 ± 0.00	0.00 ± 0.00	0.48 ± 0.02	66.6 ± 0.02

TABLE 6 Characteristics of antifungal activity of polymer films

Polymer film	Aspergillus flavus		Aspergillus niger	
	Lg reduction after 24 h	Percent reduction after 24 h, %	Lg reduction after 24 h	Percent reduction after 24 h, %
C1	3.37 ± 0.01	99.9 ± 0.01	6.84 ± 0.00	100 ± 0.00
C2	1.77 ± 0.02	98.3 ± 0.02	6.84 ± 0.00	100 ± 0.00
C3	2.07 ± 0.02	99.1 ± 0.02	1.50 ± 0.05	96.8 ± 0.05
Chitosan	1.34 ± 0.04	95.4 ± 0.04	2.38 ± 0.02	99.6 ± 0.02
Hydroxyethyl starch	1.89 ± 0.02	98.7 ± 0.02	2.02 ± 0.01	99.7 ± 0.01
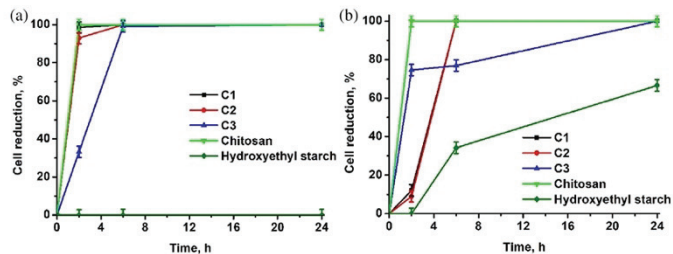
FIGURE 9 Reduction of *E. coli* (a) and *S. aureus* (b) cells during 24 h of contact time with films of vanillin-based polymers, chitosan, and hydroxyethyl starch. [Color figure can be viewed at wileyonlinelibrary.com]

needs a longer contact time for the spores to lose viability compared with *E. coli*.[41] After 6 h of exposure, the viability of the bacteria tested on the **C1** and **C2** films was completely inhibited. Compared with chitosan films, a longer exposure time was required for complete inhibition of bacterial viability on the tested films, as a 100% reduction in bacteria cells was observed after 2 h of exposure to chitosan. That confirms the fact that chitosan is a well-known antimicrobial agent and has better antimicrobial properties compared with the investigated polymers **C1–C3**. After 6 and 24 h of exposure, a reduction in

St. aureus cells was also observed on the hydroxyethyl starch films, but was 2.9- and 1.5- times weaker, respectively, than on the **C1** and **C2** films, as hydroxyethyl starch does not have antimicrobial properties. Polymer **C1** was prepared with the highest amount of VDGE compared with **C2** and **C3** polymers. That explains why polymer **C1** reached a 100% reduction the fastest.

After inoculation of test films with suspensions of *A. niger* and *A. flavus* spores, the percentage reduction was slightly reduced after 6 h of exposure compared with 2 h of exposure on some polymer films, which could be
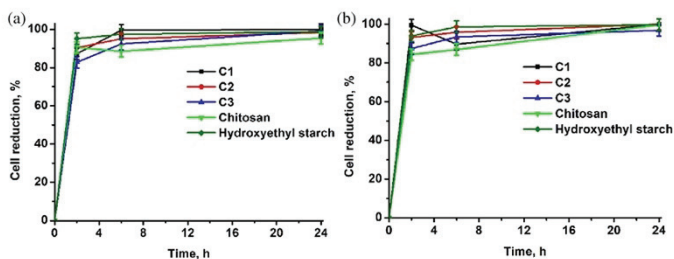
FIGURE 10   Reduction of *A. flavus* (a) and *A. niger* (b) cells during 24 h of contact time with specimens of the polymers, chitosan, and hydroxyethyl starch. [Color figure can be viewed at wileyonlinelibrary.com]

FIGURE 11   Photos of the resulting suspensions plated on nutrient media after 24 h: (a) *Escherichia coli*, (b) *Staphylococcus aureus*, (c) *Aspergillus flavus*, and (d) *Aspergillus niger*; photos of the microorganisms used for specimen inoculation: (e) *Escherichia coli*, (f) *Staphylococcus aureus*, (g) *Aspergillus flavus*, and (h) *Aspergillus niger*. [Color figure can be viewed at wileyonlinelibrary.com]
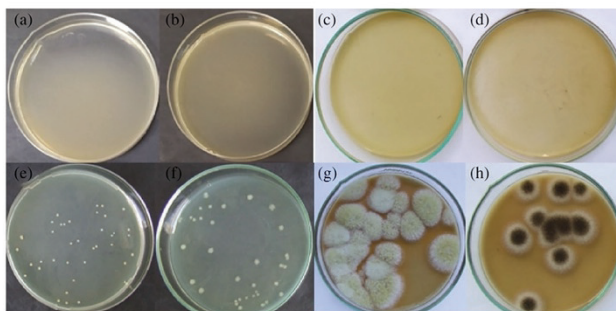
explained by spore germination (formation of vegetative cells from spores under favorable conditions) (Figure 10). However, after 24 h, the viability of *A. niger* and *A. flavus* decreased due to the unfavorable conditions for the development of the fungus and the percent reduction increased. The highest reduction of *A. flavus* spores after 24 h was obtained on the **C1** polymer film (99.9%), while the highest reduction of *A. niger* was obtained on the **C1** and **C2** polymer films (both 100%). The reason for this is the large amount of VDGE, as it has been proven previously that polymers, prepared with vanillin and its derivatives, have high antifungal activity.[42] However, the relatively high reduction rate (more than 90%) on the reference films has shown that the conditions for the growth of the microscopic fungus were unfavorable on both the vanillin-based and reference films.

The photos of the resulting suspensions plated on nutrient media when cell reduction is in the range of 70%–100% with no visible bacteria or fungi are presented in Figure 11a–d. The photos of the microorganisms used for specimen inoculation, showing how the suspensions

would look like if polymer antimicrobial activity was 0% are presented in Figure 11e–h.

4 | CONCLUSION

Novel antimicrobial biobased photopolymers have been developed and investigated. A dual-curing process, combining free radical and cationic photopolymerization, was used for their synthesis. The simultaneous process resulted in more rigid polymers with a similar reaction rate. The increase in the acrylate content increased the rate of photocuring, improved the mechanical properties of the polymers, and improved their thermal stability. However, the increase in vanillin epoxy content resulted in higher antimicrobial activity. All vanillin-based polymer films showed significant antibacterial activity against *E. coli* and *S. aureus* (cell reduction reached 100% after 24 h for all polymers), which was similar to that of the chitosan film. Vanillin-based polymer films also showed antifungal activity against *A. flavus* (cell reduction

reached 98.3%–99.9% after 24 h) and *A. niger* (cell reduction reached 96.8%–100% after 24 h). The photopolymers developed have great potential as biobased alternatives to petroleum-based photopolymers for optical 3D printing or as antimicrobial films or coatings to prevent the spread of infections. Considering the different characteristics, of which the most important for successful optical 3D printing are curing time and mechanical characteristics, the resin **C3** is the most promising for this application.

AUTHOR CONTRIBUTIONS

Greta Motiekaityte: Investigation (lead). **Aukse Navaruckiene:** Formal analysis (lead); methodology (equal); writing – original draft (equal). **Vita Raudoniene:** Investigation (equal). **Danguole Bridziuviene:** Formal analysis (equal); investigation (equal); methodology (equal); writing – original draft (equal). **Justinas Jaras:** Investigation (supporting). **Kristina Kantminiene:** Writing – review and editing (equal). **Jolita Ostrauskaite:** Conceptualization (lead); project administration (lead); supervision (lead); writing – review and editing (lead).

ACKNOWLEDGMENTS

DATA AVAILABILITY STATEMENT

The data that support the findings of this study are available from the corresponding author upon reasonable request.

ORCID

Jolita Ostrauskaite https://orcid.org/0000-0001-8600-7040

REFERENCES

[1] A. Nagaraja, M. D. Jalageri, Y. M. Puttaiahgowda, K. R. Reddy, A. V. Raghu, *J. Microbiol. Methods.* **2019**, *163*, 105650.

[2] A. Jain, L. S. Duvvuri, S. Farah, N. Beyth, A. J. Domb, W. Khan, *Adv. Healthc. Mater.* **2014**, *3*, 1969.

[3] H. Sun, Y. Wang, J. Song, *Polymer.* **2021**, *13*, 2903.

[4] M. Bil, *Mater. Lett.* **2021**, *284*, 129007.

[5] Z. Liu, C. Chen, R. Jiang, J. Zhao, L. Ren, *Mater. Lett.* **2021**, *286*, 129186.

[6] S. Chen, Z. Mei, H. Ren, H. Zhuo, *Mater. Lett.* **2017**, *189*, 74.

[7] Z. Li, C. Wang, W. Qiu, R. Liu, *Photochem. Photobiol.* **2019**, *95*, 1219.

[8] A. Navaruckiene, D. Bridziuviene, V. Raudoniene, E. Rainosalo, J. Ostrauskaite, *Materials.* **2021**, *14*, 653.

[9] A. Roig, X. Ramis, S. De la Flor, À. Serra, *React. Funct. Polym.* **2021**, *159*, 104822.

[10] Y. S. Ye, J. Rick, B. J. Hwang BJ, *Polymer.* **2012**, *4*, 913.

[11] J. P. Fouassier, J. Lalevée, *Polymer.* **2014**, *6*, 2588.

[12] Y. S. Ye, J. Rick, B. J. Hwang, *Polymer.* **2012**, *4*, 913.

[13] C. M. Roland, in *Encyclopedia of Polymeric Nanomaterials*, Vol. 1 (Eds: S. Kobayashi, K. Muller), Springer-Verlag, Berlin Heidelberg **2013**.

[14] J. S. Kim, G. S. Shim, D. Baek, J. H. Back, S. W. Jang, H. J. Kim, J. S. Choi, J. S. Yeom, *Express. Polym. Lett.* **2019**, *9*, 794.

[15] G. S. Shim, J. S. Kim, J. H. Back, S. W. Jang, J. W. Park, H. J. Kim, J. S. Choi, J. S. Yeom, *Int. J. Adhes. Adhes.* **2020**, *96*, 102445.

[16] W. A. Green, *Industrial Photoiniciators*. A Technical Guide, Taylor and Francis Group, London, UK **2001**.

[17] S. Shi, C. Croutxé-Barghorn, X. Allonas, *Prog. Polym. Sci.* **2017**, *65*, 007.

[18] R. Yan, Y. Liu, B. Liu, Y. Zhang, Q. Zhao, Z. Sun, W. Hu, N. Zhang, *Compos. Commun.* **2018**, *10*, 52.

[19] M. Sangermano, I. Roppolo, A. Chiappone, *Polymer*, **2018**, *10*, 136.

[20] A. Bagheri, J. Jin, *ACS Appl. Polym. Mater.* **2019**, *1*, 4.

[21] J. Zhang, P. Xiao, *Polym. Chem.* **2018**, *9*, 1530.

[22] R. Sasi, S. L. Sreejith, G. Ramesh, D. R. Sherin, J. E. Kaviyil, W. Paul, R. Joseph, *Surf. Interfaces.* **2021**, *5*, 100026.

[23] W. Xu, S. Jambhulkar, Y. Zhu, D. Ravichandran, M. Kakarla, B. Vernon, D. G. Lott, J. L. Cornella, O. Shefi, G. Miquelard-Garnier, Y. Yang, K. Song, *Compos. Part B: Eng.* **2021**, *223*, 109102.

[24] H. Quan, T. Zhang, H. Xu, S. Luo, J. Nie, X. Zhu, *Bioact. Mater.* **2020**, *5*, 110.

[25] J. J. Licari, D. W. Swanson, *Adhesives Technology for Electronic Applications*, Elsevier Science Publishers, Amsterdam **2011**.

[26] P. J. Flory, *Principles of Polymer Chemistry*, Cornell University Press, Ithaca **1953**.

[27] L. Tang, J. Nie, X. Zhu, *Polym. Chem.* **2020**, *11*, 2855.

[28] B. Gachet, M. Lecompere, C. Croutxe-Barghorn, D. Burr, G. L'Hostis, X. Allonas, *RSC Adv.* **2020**, *10*, 41915.

[29] O. Konuray, X. Fernández-Francos, X. Ramis, À. Serra, *Polymer*, **2018**, *10*, 178.

[30] Q. Michaudel, V. Kottisch, B. P. Fors, *Polym. Chem.* **2017**, *56*, 9670.

[31] L. Macarie, G. Ilia, *Open. Chem.* **2005**, *3*, 721.

[32] Y. Jian, Y. He, T. Jiang, C. Li, W. Yang, J. Nie, J. Coat. *Technol. Res.*, **2013**, *10*, 231.

[33] K. Matyjaszewski, in *Ionic Polymerizations and Related Processes*, Vol. 1 (Eds: J. E. Puskas, A. Michel, S. Barghi), Springer, Dordrecht **2009**, Ch. 5.

[34] D. P. Nair, M. Podgórski, S. Chatani, T. Gong, W. Xi, C. R. Fenoli, C. N. Bowman, *Chem. Mater.* **2014**, *26*, 724.

[35] M. V. Imakaev, K. M. Tchourine, S. K. Nechaev, L. A. Mirny, *Soft. Matter.* **2015**, *11*, 665.

[36] K. Saalwächter, W. Chassé, J. U. Sommer, *Soft. Matter.* **2013**, *9*, 6587.

[37] T. Buruiana, V. Melinte, L. Stroea, E. Buruiana, *Polym. J.*, **2009**, *41*, 978.

[38] Y. Guo, K. Ruan, X. Shi, X. Yang, J. Gu, *Compos. Sci. Technol.* **2020**, *193*, 108134.

[39] A. W. Bassett, A. E. Honnig, C. M. Breyta, I. C. Dunn, J. J. La Scala, J. F. Stanzione, *ACS Sustain. Chem. Eng.* **2020**, *8*, 5626.

[40] M. R. M. Asyraf, M. R. Ishak, A. Syamsir, N. M. Nurazzi, F. A. Sabaruddin, S. S. Shazleen, M. N. F. Norrrahim, M. Rafidah, R. A. Ilyas, M. Z. Abd Rashid, M. R. Razman, *J. Mater. Res. Technol.* **2022**, *17*, 23.

[41] J. T. Poolman, A. S. Anderson, *Expert Rev. Vaccines.* **2018**, *17*, 607.

[42] A. Navaruckiene, D. Bridziuviene, V. Raudoniene, E. Rainosalo, J. Ostrauskaite, *Express Polym. Lett.* **2022**, *16*, 279.

179

10. APPENDIX

10.2. MB "AmeraLabs" Trial production act

AMERALABS

TRIAL PRODUCTION ACT

SLA 3D printing of vanillin dimethacrylate-based resin in the MB "AmeraLabs" production line

In 2022 years, a novel vanillin dimethacrylate (VDM)-based resin has been applied in stereolithography (SLA) 3D printing by the company "AmeraLabs". The 3D printing parameters have been validated, and the 3D polymeric objects have been SLA 3D printed according to the standardized company procedure.

The VDM-based resin was composed of VDM, acrylated epoxidized soybean oil, pentaerythritol tetrakis(3-mercaptopropionate), diphenyl(2,4,6-trimethylbenzoyl) phosphine oxide and 2,5-bis(5-tert-butyl-2-benzoxazolyl)thiophene. VDM-based polymer was 3D printed using a custom AmeraLabs SLA 3D printer equipped with an Acer H6518BD projector 400-600 nm. The 3D printing parameters are presented in Table 1. After printing, the objects were soaked in isopropanol for 15 min and postcured under LED light ($\lambda = 400$-405 nm, 50 W) for 2 h at room temperature.

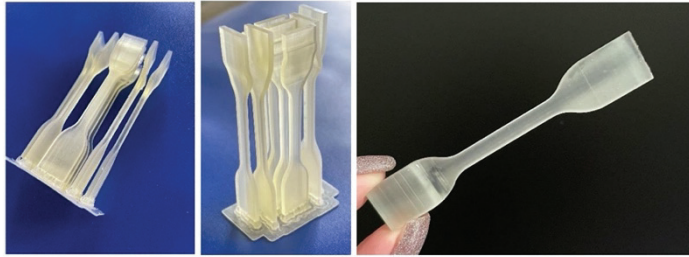**Table 1.** 3D printing parameters with custom 3D printer

Parameter	Value
Building volume	134 x 75 x 130 mm
XY resolution	35 µm
Layer thickness	50 µm
Exposure time	12 s

3D printed objects are presented in Figures 1 and 2.
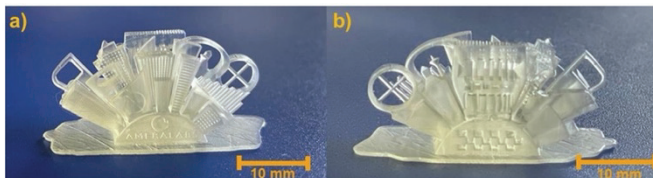
Figure 1. The front side (a) and back side (b) of SLA 3D printed objects of VDM-based resin.

Figure 2. SLA 3D printed bone-shaped specimens of VDM-based resin.

Conclusions

Vanillin dimethacrylate-based resin has been applied in stereolithography (SLA) 3D printing by the company "AmeraLabs". 3D printed polymeric objects showed high printing accuracy with smooth surface finishing.

MB "AmeraLabs" representative:

        Co-funder
        V. Talačka   2022-06-17

KTU representatives:

        Prof. dr. J. Ostrauskaitė   2022-06-17

        PhD student A. Navaruckienė   2022-06-17

11. ACKNOWLEDGEMENT